Host-guest complexation integrated in chemical reaction networks

Li, G.

Citation (APA)
Li, G. (2022). *Host-guest complexation integrated in chemical reaction networks*. [Dissertation (TU Delft), Delft University of Technology]. https://doi.org/10.4233/uuid:31c7c7ec-a510-424e-a6af-24e2d6d00433

Important note
To cite this publication, please use the final published version (if applicable).
Please check the document version above.

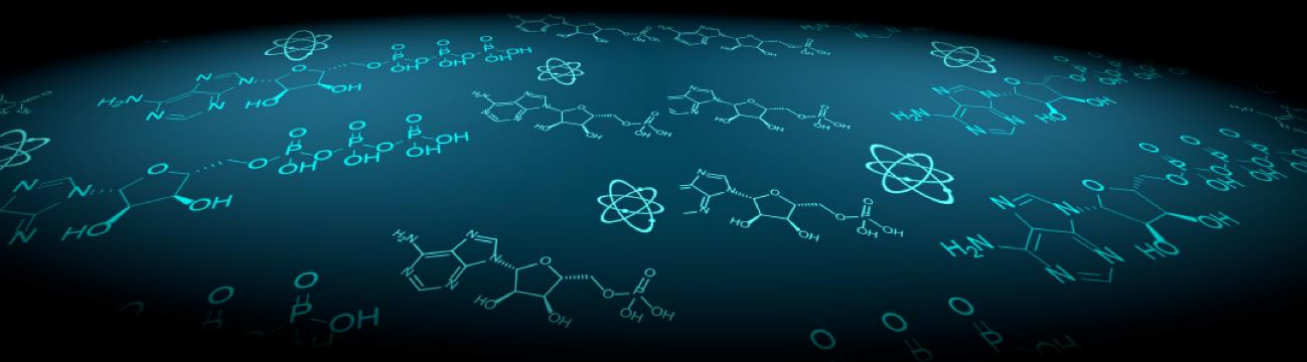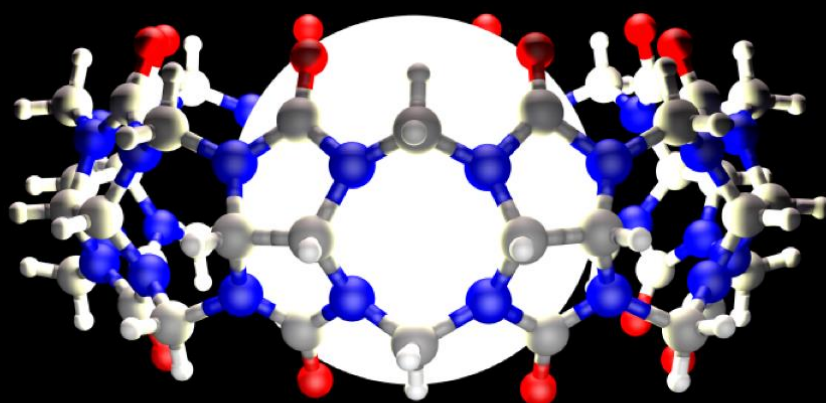# Host-guest Complexation Integrated in Chemical Reaction Networks

Guotai Li

Propositions

Belonging to the thesis:

Host-guest complexation integrated in Chemical reaction networks

By Guotai Li

1. Science sometimes gives the answer before stating the question.

2. As a researcher, it is not often that one can make great progress, but even a tiny step forward is a success to extend human knowledge.

3. Slow but steady wins the race, since correcting mistakes wastes more time.

4. Control experiments take extra time and work, but it is always necessary to avoid controversial mistakes.

(chapter 4 of this thesis)

5. Like much in chemistry, CB[8] solubility is mysterious, and careful attention has to be paid to what exactly happens.

(chapter 4–6 of this thesis)

6. Compared to biological systems, man-made out-of-equilibrium chemical systems are still in their infancy, but considering more than 4 billion years spent by natural evolution to achieve this, we are doing a good job.

7. The design of specific organic reactions in water is essential to make chemistry in water a reality, not just simply changing the solvents of a reaction.

(*Chem. Sci.*, 2021, 12, 4237-4266)

8. Supramolecular chemistry had been used and studied long before its definition.

(chapter 1 in this thesis & Supramolecular Chemistry–Fundamentals and Applications)

9. Research in different disciplines is more and more closely linked together, as for example supramolecular encapsulation can be used to control the activity of organocatalysts.

(chapter 3 of this thesis)

10. "Small molecule, big effects" continues to play a big role in chemistry and molecular materials research.

These propositions are regarded as opposable and defendable, and have been approved as such by promoter Dr. R. Eelkema and Prof. Dr. J. H. van Esch.

Host-guest complexation integrated in chemical reaction networks

Dissertation

for the purpose of obtaining the degree of doctor

at Delft University of Technology

by the authority of the Rector Magnificus, Prof.dr.ir. T.H.J.J. van der Hagen,

chair of the Board of Doctorates

to be defended publicly on

Wednesday 16 November 2022 at 17:30 o'clock

by

Guotai LI

Master of Science in Chemistry,

East China University of Science and Technology, China

Born in Qingdao, China

This dissertation has been approved by the promotors.

Composition of the doctoral committee:

Rector Magnificus	Chairperson
Dr. R. Eelkema	Delft University of Technology, promotor
Prof. dr. J.H.van Esch	Delft University of Technology, promotor

Independent members:

Prof.dr. X. Zhang	Tsinghua University
Prof.dr. T. Kudernac	University of Groningen
Prof.dr. M.J. Webber	University of Notre Dame
Prof.dr. A. Urakawa	Delft University of Technology
Prof.dr. J. Boekhoven	Technical University of Munich
Prof.dr. E.A. Pidko	Delft University of Technology, reserve member

TUDelft

An electronic version of the dissertation is available at TU Delft library.

Table of Contents

Chapter 1

Introduction

Chemistry is moving fast from the study of isolated and static structures to the investigation of multicomponent responsive systems over the last decades.[1] This evolution is inspired by nature's dynamic features with sophisticated functionality by changing the structures of building blocks to control their assembly/disassembly through all kinds of chemical reactions.[2] Mimicking nature, scientists have developed various 'life-like' self-assembling systems, responsive or adaptive to environmental variation, showing promising application in drug delivery[3,4], sensing, molecular imaging[5] and so on.[6] More recently, out-of-equilibrium assembly is increasingly attracting researchers' attention since these systems possess the functions of self-replication, feedback, self-healing and signals amplification in a higher dynamic level as reported.[7–9] However, despite these elegant works, our ability to spatiotemporally control assembly processes is still in the infancy.[10] Therefore, in this thesis, we aim to investigate and explore possibilities and potential of supramolecular systems under control of chemical reaction networks, with a focus on host-guest complexation.

1.1 Host-guest complexation

Long before the field of supramolecular chemistry was initiated, host-guest chemistry was known for its molecular recognition properties,[11] which can date back to 1967 with the discovery of crown ethers able to bind certain metallic ions. The Nobel Prize in Chemistry 1987 was awarded jointly to Cram, Lehn and Pedersen for their "development and use of molecules with structure-specific interactions of high selectivity" in this area. Regarded as molecular recognition which can be widely found in bio-recognition processes, such as enzyme-substrates (Figure 1.1a) and antigen-antibody interactions, host-guest interaction has enormous value in both biological and chemical applications. Beside crown ethers, various macrocyclic host molecules and their derivatives have been developed including calixarenes, cyclodextrins, cyclophanes, cucurbit[n]urils (CB[n]), pillar[n]arenes etc. Among them, CB[n] family is young but promising one since the guest binding affinity and selectivity of CB[n] are generally higher than those of many other synthetic receptors (Figure 1.1c).[12] Because of this, we mainly use CB[7] and CB[8] in this thesis. Furthermore, CB[n] shows strong affinity toward cationic guests, moderate to neutral guests, and very little to anionic guests. We used this as a the basic principle

for selecting guest molecules and designing chemical reactions to tune assembly. Encapsulated by CB[*n*], guest molecules can have enhanced stability, solubility, lower cytotoxicity, increased optical properties or catalytic activities, enabling application in drug delivery, molecular sensing and catalysis. Moreover, based the host-guest interaction, materials such as hydrogel, micelles, framework and so on can be constructed.
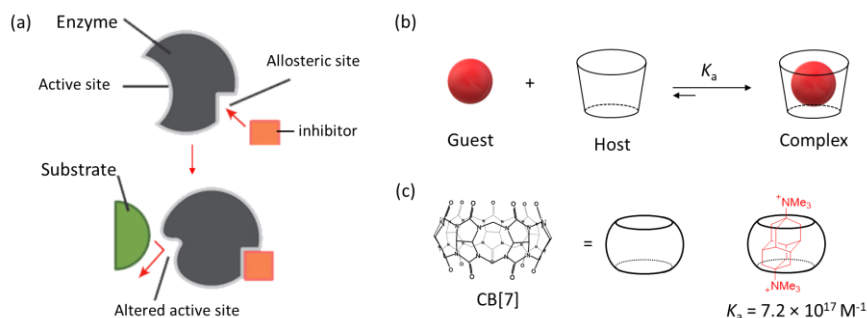
Figure 1.1 Schematic representation of allosteric regulation of enzyme by an inhibitor, adapted from Ref [13] (a); Dynamic host-guest complex assembly with their binding constant K_a (b); Structure of CB[7] and an ultrastable guest pair[14] with $K_a = 7.2 \times 10^{17}$ M^{-1} (c).

1.2 Chemical reaction networks in supramolecular chemistry

Signalling cascades are essential to the processes in living cells, regulating specific cellular functionalities and biological events. Signalling cascades are a series of chemical reactions, where each step is involved to respond effectively to environmental changes. On the other hand, supramolecular polymers are sensitive to external stimuli due to the dynamic nature of noncovalent interactions including hydrogen bonding, π−π stacking, and electrostatic interactions in their building blocks. Any chemical reactions influencing the strength of these noncovalent bonds can result in the assembly/disassembly of supramolecular materials. Recently, chemical reaction networks (CRN) are applied to designing out-of-equilibrium supramolecular assembly[7,15,16] (Figure 1.2). A typical chemical reaction network driving a supramolecular system out-of-equilibrium consists of at least two competing reactions: activation of precursor to form building blocks by molecular fuels and depletion of building blocks through reaction with environmental substrates. By controlling the reaction rate of activation and deactivation, life time of supramolecular materials can thus be regulated accordingly.
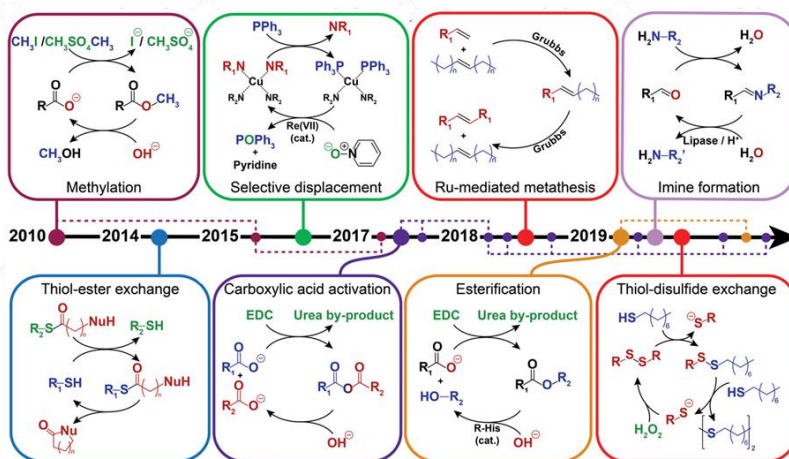
Figure 1.2 Timeline of various chemical reaction cycles developed to control the assembly and disassembly of supramolecular system. Adapted from ref.15.

In turn, the kinetics of reactions can be tuned by supramolecular assembly involved with their reactants, catalysts, intermediates and products. An important example in nature is in enzymatic reactions, where small molecules can bind to the enzyme, causing changes of the enzymatic activity and regulating the reaction rate.[17] Macrocycles have also proven to be promising in controlling chemical reactions by use as nano-reactors, for transition-state stabilization, catalysis inhibition and enhancement.[18] Moreover, out-of-equilibrium system recently are engaged into the control of reaction rate by affecting catalytic properties. [19–21]

1.3 Main research goals

Currently most of the host-guest assembly studies concern thermodynamic equilibrium states, seldomly coupled to chemical reactions to regulate their properties. Their combination could help to acquire more advanced functionality.

Therefore, in this thesis we hope to integrate chemical reaction networks with host-guest complexation. By this, the properties of materials based on host-guest interactions can be regulated by chemical signals, and the rates of chemical reactions can be tuned by host-guest complexation. Ultimately it would pave the way for designing advanced artificial responsive and functional materials.

1.4 Thesis outline

This thesis reports on the relationship between host-guest complexation and chemical reactions with different research aims in each chapter. After this general introductory chapter, the second chapter provides a literature overview on out-equilibrium system based on host-guest interaction. The third chapter describes a host-guest strategy for the tuneable control of organocatalysts. The fourth chapter describes an attempt to build a new out-of-equilibrium system based on host-guest interaction by chemical fuels. The fifth chapter presents work where host-guest aggregation is triggered by biological signals through cascade reactions. In the sixth chapter, we applied the chemical signals into the release of drug guest molecules from macrocyclic encapsulation. We finish this thesis with a summary of the work.

1.5 Reference

(1)   Mattia, E.; Otto, S. Supramolecular Systems Chemistry. *Nat. Nanotechnol.* **2015**, *10* (2), 111–119.

(2)   Goodsell, D. S. Molecular Machines. In *The Machinery of Life*; Springer New York: New York, NY, 2009; Vol. 47, pp 8–26.

(3)   Zhang, A.; Jung, K.; Li, A.; Liu, J.; Boyer, C. Recent Advances in Stimuli-Responsive Polymer Systems for Remotely Controlled Drug Release. *Prog. Polym. Sci.* **2019**, *99*, 101164.

(4)   Braegelman, A. S.; Webber, M. J. Integrating Stimuli–Responsive Properties in Host–Guest Supramolecular Drug Delivery Systems. *Theranostics* **2019**, *9* (11), 3017–3040.

(5)   Shi, X.; Zhang, X.; Ni, X. L.; Zhang, H.; Wei, P.; Liu, J.; Xing, H.; Peng, H. Q.; Lam, J. W. Y.; Zhang, P.; Wang, Z.; Hao, H.; Tang, B. Z. Supramolecular Polymerization with Dynamic Self-Sorting Sequence Control. *Macromolecules* **2019**, *52* (22), 8814–8825.

(6)   Kolesnichenko, I. V.; Anslyn, E. V. Practical Applications of Supramolecular Chemistry. *Chem. Soc. Rev.* **2017**, *46* (9), 2385–2390.

(7)   Van Rossum, S. A. P.; Tena-Solsona, M.; Van Esch, J. H.; Eelkema, R.; Boekhoven, J. Dissipative Out-of-Equilibrium Assembly of Man-Made Supramolecular Materials. *Chem. Soc. Rev.* **2017**, *46* (18), 5519–5535.

(8)   Sharko, A.; Livitz, D.; De Piccoli, S.; Bishop, K. J. M.; Hermans, T. M. Insights into Chemically Fueled Supramolecular Polymers. *Chem. Rev.* **2022**, *122* (13), 11759–11777.

(9)   Das, K.; Gabrielli, L.; Prins, L. J. Chemically Fueled Self-Assembly in Biology and Chemistry. *Angew. Chem. Int. Ed.* **2021**, *60* (37), 20120–20143.

(10)   te Brinke, E.; Groen, J.; Herrmann, A.; Heus, H. A.; Rivas, G.; Spruijt, E.; Huck, W. T. S. Dissipative Adaptation in Driven Self-Assembly Leading to Self-Dividing Fibrils. *Nat. Nanotechnol.* **2018**, *13* (9), 849–855.

(11)   Ariga, K.; Kunitake, T. The Chemistry of Molecular Recognition — Host Molecules and Guest Molecules. In *Supramolecular Chemistry — Fundamentals and Applications*; Springer-Verlag: Berlin/Heidelberg, 2006; pp 7–44.

(12)   Shetty, D.; Khedkar, J. K.; Park, K. M.; Kim, K. Can We Beat the Biotin–Avidin Pair?:

Cucurbit[7]Uril-Based Ultrahigh Affinity Host–Guest Complexes and Their Applications. *Chem. Soc. Rev.* **2015**, *44* (23), 8747–8761.

(13) Enzyme regulation https://www.khanacademy.org/science/ap-biology/cellular-energetics/environmental-impacts-on-enzyme-function/a/enzyme-regulation (accessed Jun 23, 2022).

(14) Cao, L.; Šekutor, M.; Zavalij, P. Y.; Mlinarič-Majerski, K.; Glaser, R.; Isaacs, L. Cucurbit[7]Uril×guest Pair with an Attomolar Dissociation Constant. *Angew. Chem. Int. Ed.* **2014**, *53* (4), 988–993.

(15) Rieß, B.; Grötsch, R. K.; Boekhoven, J. The Design of Dissipative Molecular Assemblies Driven by Chemical Reaction Cycles. *Chem* **2020**, *6* (3), 552–578.

(16) Singh, N.; Formon, G. J. M.; De Piccoli, S.; Hermans, T. M. Devising Synthetic Reaction Cycles for Dissipative Nonequilibrium Self-Assembly. *Adv. Mater.* **2020**, *32* (20), 1906834.

(17) Goodey, N. M.; Benkovic, S. J. Allosteric Regulation and Catalysis Emerge via a Common Route. *Nat. Chem. Biol.* **2008**, *4* (8), 474–482.

(18) Pemberton, B. C.; Raghunathan, R.; Volla, S.; Sivaguru, J. From Containers to Catalysts: Supramolecular Catalysis within Cucurbiturils. *Chem. - A Eur. J.* **2012**, *18* (39), 12178–12190.

(19) Chen, R.; Neri, S.; Prins, L. J. Enhanced Catalytic Activity under Non-Equilibrium Conditions. *Nat. Nanotechnol.* **2020**, *15* (10), 868–874.

(20) van der Helm, M. P.; Li, G.; Hartono, M.; Eelkema, R. Transient Host–Guest Complexation To Control Catalytic Activity. *J. Am. Chem. Soc.* **2022**, *144* (21), 9465–9471.

(21) Biagini, C.; Fielden, S. D. P.; Leigh, D. A.; Schaufelberger, F.; Di Stefano, S.; Thomas, D. Dissipative Catalysis with a Molecular Machine. *Angew. Chem. Int. Ed.* **2019**, *58* (29), 9876–9880.

Chapter 2

Out-of-equilibrium Assembly Based on Host-guest Interactions

Abstract: The field of supramolecular chemistry is moving fast from building thermodynamically stable systems residing in (global) minima on the free-energy landscape, to out-of-equilibrium systems where energy conversion is needed to create and maintain their structures. A wide variety of artificial out-of-equilibrium systems in various areas of supramolecular chemistry have been developed during the last decade, many of which have been extensively reviewed. An area that has received little attention so far, is the use of out-of-equilibrium processes to control host-guest interactions, which is the subject of this mini-review. Construction of out-of-equilibrium systems based on host-guest complexation should share many common strategies with analogous noncovalent interactions, which is accordingly summarized at the start. Next, representative publications that demonstrate these strategies are discussed and categorized with regards to which component is modulated, either host, guest or competitive molecules. With this, we aim to shed light on the design of out-of-equilibrium systems based on host-guest interactions, and provide insights into preparation strategies for various transient materials.
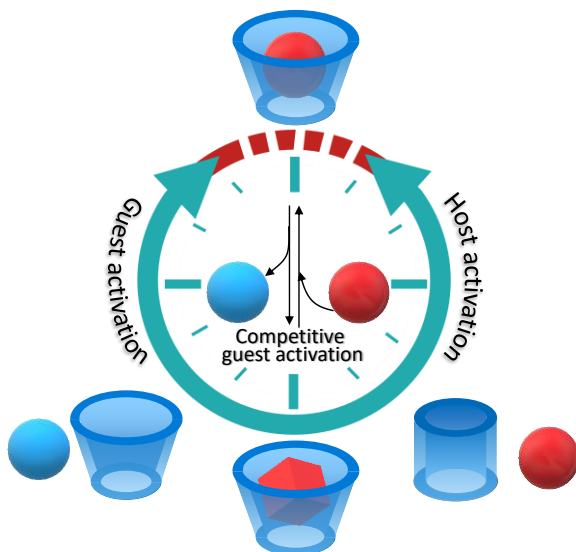
2.1 Introduction

The research of supramolecular chemistry is often inspired by biological entities such as proteins, lipids and their multi-molecular complexes. Studying their non-covalent interactions is crucial and beneficial to understand biological processes that rely on these forces for structure and function.[1] Inspired by living systems in nature, where assembled structures reside in out-of-equilibrium state, non-equilibrium self-assembly systems have started to absorb researchers' attention. This began with the pioneering work of van Esch, Eelkema and co-workers developing an artificial chemical-fuel-driven system in 2010,[2] with the field seeing explosive development in recent years. Different from the predominantly reported self-assembly systems staying in thermodynamic equilibrium, out-of-equilibrium assembled structures need continuous consumption of energy to maintain their state and to prevent degradation into their stable chemical elements. The dependence on continuously supplied energy endows out-of-equilibrium supramolecular systems with highly dynamic properties such as self-replication, internal feedback, stimuli-responsiveness, self-adaptation, self-healing and signal amplification. The concepts, terminologies and design principles of out-of-equilibrium systems have been thoroughly introduced and discussed in an assortment of comprehensive tutorial reviews,[3–14] which is not our focus in this chapter. Instead, we will focus on classifying and summarizing the multitude of different areas where out-of-equilibrium assembly and host guest chemistry come together.

As one of the earliest studied branches of supramolecular chemistry, host-guest complexation has tremendous value in both biological and chemical systems. Regarded as molecular recognition, this type of interaction is widely found in physiological processes, such as enzyme-substrate and antigen-antibody interactions. The past decades have witnessed the rapid development of artificial host-guest systems, expanding the toolbox available to chemists and enriching the knowledge of supramolecular chemistry. Various macrocyclic host molecules and their derivatives have been developed including calixarenes (CAs), crown ethers, cyclodextrins (CDs), cyclophanes, cucurbit[n]urils (CBs), pillar[n]arenes (PAs) etc. Based on these hosts; materials such as gels, micelles, vesicles and nanoparticles can be prepared, showing promising applications in the areas of molecular sensors, drug delivery,[15] nanomedicines,[16] fluorescence probes, catalysis[17–19] and so on.[20] Currently man-made host-guest pairs can even possess higher affinity (7.2×10^{17} M^{-1})[21] than the strongest and best known natural noncovalent interaction pair of biotin-streptavidin (10^{13}–10^{15} M^{-1}).[22] Although closely similar to biological molecular recognition, most studies of host-guest assembly are still conducted with thermodynamic equilibrium states.

Since 2015, a handful of out-of-equilibrium self-assembly systems based on transient host-guest complexation have been published. In this chapter, we collect these examples, summarizing and analysing the strategies used in these works. We hope this

can provide helpful guidance in the design of more non-equilibrium host-guest systems, while also bringing inspiration to other supramolecular systems which may not have been noticed before. At beginning, we briefly introduce the generic methods in making an artificial out-of-equilibrium supramolecular system, targeted to the feasibility for use in a host-guest system. Next, corresponding examples of these publications will be explained and discussed in detail. We then conclude with a discussion and perspective around how these systems can be improved and better applied in the future, with improvements towards more life-like features and properties.

2.1 General Strategies

In this section, we summarise the strategies of making a supramolecular system far from equilibrium which are also applicable to the cases of host-guest system.
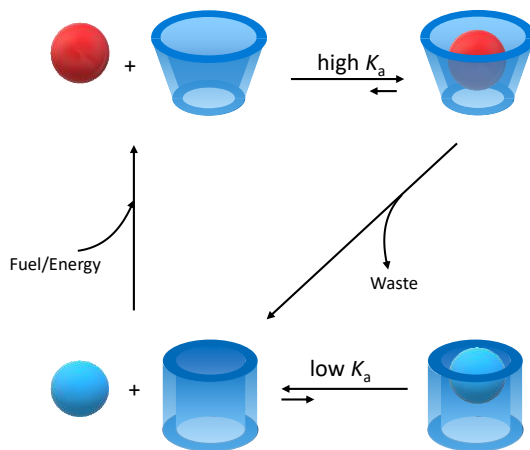
Scheme 2.1. A general reaction cycle of out-of-equilibrium host-guest complexation driven by energy or fuels.

Central to the design of a non-equilibrium system is an energy source which can elevate non-assembling building blocks into a species capable of assembly. Reported in 2010 as the first artificial out-of-equilibrium system, methyl iodide (MeI) was introduced as a chemical fuel to activate the hydrogelator precursor dibenzoyl-(L)-cystine by esterification to form a hydrogel.[2] This self-assembly is not stable at pH 7, and subsequent ester hydrolysis later leads to collapse of the hydrogel after all of the chemical fuel is consumed. Regarded as a high-energy chemical, here MeI is the energy input to drive transient self-assembly. Another common energy source is light, which can be complementary with chemical fuels on several levels; including in methods of activation, diversity of fuels and precursors, efficiency of generating the activated state and and multifactorial control over the lifetime of assembly.[6] Usually the term "chemical fuel" includes transient acids/bases to regulate pH and the behaviour of pH-responsive

groups,[12] however, from experience, designing a system based on the direct activation of building blocks via chemical reactions generally has different considerations with that in pH-responsive systems. As such, we have separated pH changes through transient acids / bases as an independent method to other chemical reaction cycles.

It is essential that the reaction consuming the energy source is able to adjust host-guest interactions for the construction of an out-of-equilibrium host-guest assembly (Scheme 2.1). There are several factors that can influence host-guest affinity, such as size and shape, polarity, charge, hydrophobicity and hydrophilicity. Any strategy to achieve control of these properties with either the host or guest molecule can efficiently switch the state of host-guest assembly. Moreover, disassembly of a host-guest complex is well-known to be easily achieved by competitive binding by another guest molecule with higher affinity to the host.[23] Thus, the structural properties of a competitive guest can also have a significant impact on the stability of a host-guest system. In summary, three key components: host, guest, and competitive guest, have to be considered for activation/de-activation during a system design.

Scheme 2.2 Host-guest competitive binding and the chemical structures reported in various fuelling systems.

2.2.1 Chemical reaction cycles

As we introduced in the general strategies, the chemical fuel MeI was applied in the first synthetic example to drive a supramolecular system far from equilibrium. Later on, the stronger methylating agent dimethylsulfate was reported to get faster cycles of the sol-

gel-sol transition.[24] After these pioneering works, more chemical fuels were reported to drive systems far from equilibrium, among which, adenosine triphosphate (ATP)[14] and carbodiimide reagents such as EDC[25], are the most widely used (Scheme 2.2, 2nd line). As summarized by Boekhoven and coworkers, the minimal requirement of chemical reaction cycles to drive out-of-equilibrium self-assembly involves two chemical reactions, an activation and a deactivation reaction.[5] The activation reaction has to be converting a precursor into building blocks, while the deactivation is spontaneous, reverting the product back to the precursor. The strategies of chemical reaction cycles are also applicable to host-guest systems. So far, ATP[26] and EDC[27] have indeed been reported as chemical fuels for driving host-guest systems far from equilibrium, however their roles may be quite different with what they played in other systems. For example, while chemical fuels would conventionally activate either a host, guest, or competitive guest molecule, they can also directly act as a transient host, guest, or competitive guest molecule to achieve a non-equilibrium assembly.

2.2.2 pH control

The use of pH changes to regulate supramolecular forces including electrostatic attraction/repulsion and hydrophobic interactions with pH responsive building block is one of the most general approaches to affect self-assembly. To achieve an out-of-equilibrium system controlled by pH, energy sources that can induce a transient pH change have to be introduced; these include ester derivatives,[28] urea/urease,[29–31] 2-cyano-2-phenylpropanoic acid,[32] or the combination of them[33,34] (Scheme 2.2, 3rd line). Usually these species are used in combination with another acid/base, with their addition first leading to a rapid pH change, and the decomposition of transient acids/bases later in specific conditions (e.g. base, enzymes) results in gradual reverting of pH back to the original value. The use of two temporary species to regulate the pH is also possible, often leading to more programmability of the change.[33,34] Host-guest binding profiles are well known to be modulated by pH as studied in various examples of equilibrium complexation.[35] In a system with pH mediated by temporary acids/bases, a transient host-guest complex can be achieved when a pH responsive functional group is incorporated into either the guest or host structures.

2.2.3 Light control

Light as a clean and widely used energy source to drive a system far from equilibrium has the advantages of (typically) less waste generation compared to chemical fuels, ability of remote control, easy operation in a chemically closed system, and the precise control of lifetime.[6,36] A requirement for light-driven assemblies is the incorporation of a photoswitchable moiety, such as azobenzene,[37,38] spiropyran,[39,40] dithienylethenes (DTEs),[41] viologen and many others (Scheme 2.2, 4th line).[36,42] To be noted here, in the case of spiropyran, light is also able to adjust the environmental pH by releasing a proton

from its ring-opening reaction,[43] with which a pH-responsive system can be modulated by light, as discussed in Section 2.2. While photoswitchable molecules are usually applied as guest molecules in a photo-responsive host-guest system,[44] they can also be incorporated into macrocyclic structures resulting in photo-active host molecules by rational synthesis.[45]

2.3 Specific strategies on host-guest system

In this section, strategies of making a host-guest self-assembly an out-of-equilibrium process will be discussed in detail with reported examples. These strategies are sorted by which component the fuel consuming reaction exerts control over, these being: host molecules, guest molecules and competitive guest molecules. We believe this is the most intuitive way to see key changes in a system between equilibrium and non-equilibrium states.

2.3.1 Based on guest control

Structural design of guest molecules to affect host-guest binding is the most intuitive way, since typically a wider variety of guest molecules can be chosen and their sites for chemical modification are more accessible than that for macrocycles. While macrocyclic encapsulation has a highly selective recognition on the structures of guest molecules, the binding strength can be readily modulated by activation/deactivation of guest molecules through the methods introduced in Section 2 (Figure 2.1a).
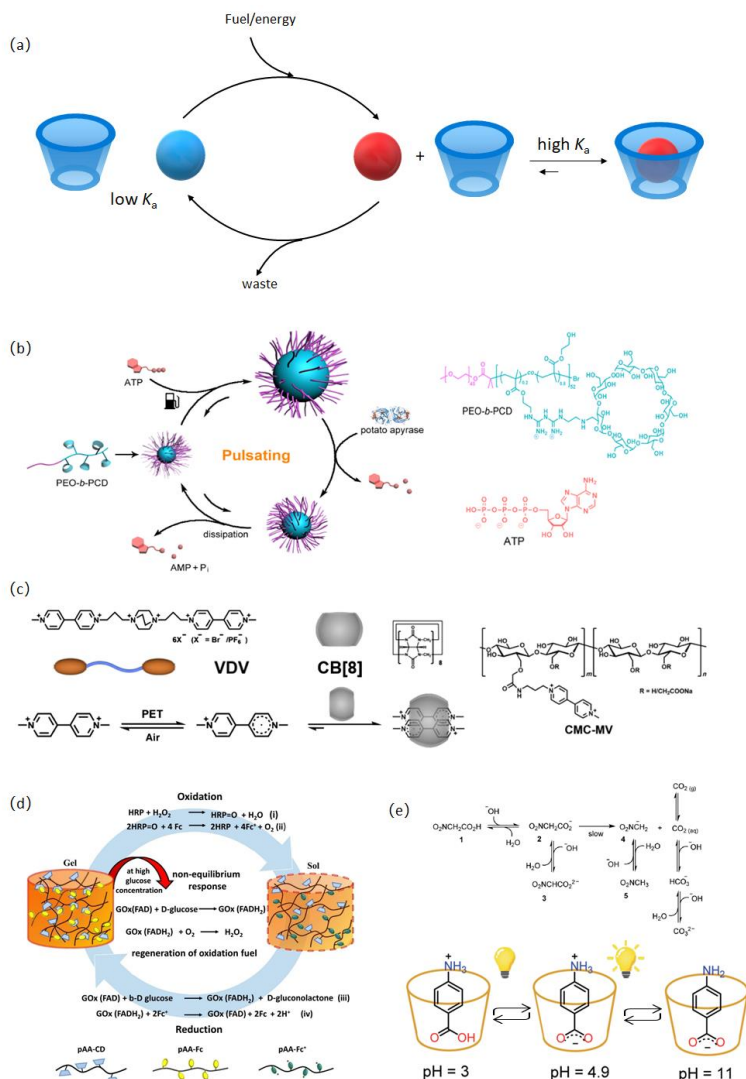
Figure 2.1. Examples of transient host-guest complex by guest control. (a) Schematic representation of the strategy based on guest activation. (b) Illustration of the pulsating polymer micelle in dissipative self-assembly process, adapted from ref [46], copyright 2017 ACS publications (c) Dissipative supramolecular polymerization powered by light, adapted from ref [47], copyright 2019 Chinese Chemical Society (d) Fuel-driven and enzyme-regulated redox-responsive supramolecular hydrogels, adapted from ref [48], copyright 2021 John Wiley & Sons, Inc. (e) Time-programmable pH by decarboxylation of nitroacetic acid allows time-controlled

complexation, reproduced from ref [49], copyright 2021 Royal Society of Chemistry.

In 2017, Yan et al. observed periodic and self-adaptive pulsating motion in a polymer micellar system controlled by adenosine triphosphate (ATP) (Figure 2.1b).[46] An amphiphilic block-copolymer composed of a poly(ethylene oxide) (PEO) block and functionalised cyclodextrin as host receptor of ATP was synthesised. This PEO-b-PCD copolymer forms small micellar nanoparticles (16 ± 3 nm). Upon adding ATP, cyclodextrin in the micelle core binds with ATP resulting in an increase of micellar hydrophobic domains and micellar expansion (55 ± 9 nm). Meanwhile, potato apyrase as a phosphatase in the solution decomposes ATP to phosphate (Pi) and adenosine monophosphate (AMP). The formed AMP would not associate with the receptors in copolymer due to a significant lower affinity of AMP with positive charged cyclodextrin compared to ATP ($K_B = 7.52 \times 10^7$ M^{-1} *vs* $K_B < 10^2$ M^{-1}).[50] As a consequence, the swelled micelles underwent a spontaneous shrinking stage, reverting to their initial state (18 ± 4 nm). This process can be repeated by continuous ATP supply over five cycles. The periodicity and amplitude of micellar pulsation can be tuned by the concentration of ATP and potato apyrase enzyme. Furthermore, periodic and controlled release of doxorubicin (Dox) was achieved in this system. As a brief summary, the high-energy chemical ATP was applied directly as a guest molecule on the building blocks stabilizing the expanded micellar nanoparticles through the host-guest interaction.

Out-of-equilibrium host-guest assembly driven by light was reported by Zhang, Xu and co-workers in 2019 (Figure 2.1c).[47] They designed a bifunctional monomer, containing two viologen moieties as end groups and a 1,4-diazabi-cyclo[2.2.2]octane (DABCO) moiety as a rigid linker (VDV). In an aqueous solution of VDV and cucurbit[8]uril (CB[8]), no supramolecular polymers could be formed because of the 1:1 host-guest complexation between dicationic viologen moiety and CB[8]. However, under irradiation of light at 254 nm, the viologens could be reduced to viologen cation radicals (V$^{+\bullet}$) via photoinduced electron transfer (PET). As the viologen cation radicals can form a stable dimer inside the cavity of CB[8], the 1:1 complexation between viologen and CB[8] could be converted to a 2:1 complex. In this way, non-equilibrium supramolecular polymers could be formed which are powered by light through activation of VDV. After that, this far-from-equilibrium system returned to equilibrium in air and dark environment, since the viologen radicals are unstable in air and can be oxidized back to viologen cations by oxygen. Consequently, the complexation reverted to 1:1, leading to supramolecular polymer disassembly and recovery of its original state. Moreover, the light-powered strategy is not only applied to linear supramolecular polymerization, but also to dissipative cross-linked supramolecular polymerization by introducing methyl viologens into sodium carboxymethylcellulose (0.75%, w/w). This modified polymer can form transient hydrogels through supramolecular cross-links in a far-from-equilibrium state under UV irradiation, which after removing the light source gradually returned to

solution in 9 hours. This sol-gel-sol transition could occur at least three times indicating a good reversibility of the dissipative cross-linked supramolecular polymerization.

Ravoo and Jain presented a work In 2021,[48] integrating chemical reaction networks (CRNs) regulated by enzymes and host-guest molecular recognition on a typical pair of β-cyclodextrin (CD) and ferrocene (Fc) (Figure 2.1d). In aqueous solution Fc has a high affinity to CD, with binding constant about 4800 M^{-1}, while its oxidized species ferrocenium ion (Fc^+) has no affinity to CD. In the presence of horseradish peroxidase (HRP) and H_2O_2, Fc is oxidized to Fc^+. which can later be reduced by glucose oxidase (GOx) and D-glucose. Very interestingly in this work, a re-oxidation of Fc was observed without further addition of H_2O_2, where only D-glucose additions were needed for 4 additional cycles. The mechanism of this autonomous re-oxidation was through the regeneration of H_2O_2 from O_2 and GOx[$FADH_2$]—an intermediate product from the reaction of GOx and D-glucose. After investigating the redox properties of Fc in the presence of the enzyme couples, they applied it to prepare responsive supramolecular hydrogels by host-guest interaction between both Fc and CD functionalized to polyacrylic acid (pAA). The pAA-CD/pAA-Fc hydrogel was observed to disassemble to sol by addition of oxidation catalyst HRP and H_2O_2, which was later reassembled to gel by reduction catalyst GOx and fuel D-glucose. The reformed gels were unstable and reverted to sol without any further oxidant addition. As detected by 2,2'-azino-bis(3-ethylbenzothiazoline)-6-sulfonic acid (ABTS), this gel-sol transformation was due to the reformation of H_2O_2 from O_2 and GOx[$FADH_2$].

Transient pH changes on a guest molecule to form an out-of-equilibrium system were studied by Di Stefano, Ercolani et al. in 2021 (Figure 2.1e).[49] A time-programmable sequence of pH variation ($pH_{1(high)}$–$pH_{2(low)}$–$pH_{3(high)}$) was achieved by using nitroacetic acid and a starting basic aqueous solution (NaOH). Adding nitroacetic acid into the solution of NaOH (0.01 M) in water results in rapid pH changes from basic to acidic, and subsequent decomposition reactions of nitroacetic acid raise the pH back to a basic value. The pH jump ($pH_{1(high)}$–$pH_{2(low)}$) and time of pH rising from acidic to basic value ($pH_{2(low)}$–$pH_{3(high)}$) can be predictably controlled by the concentration of base and acid. As a proof of concept, they successfully applied this pH programmable system to a pH dependent host-guest complex of α-cyclodextrin and *p*-aminobenzoic acid. Fluorescence was monitored as an indication of host-guest binding extent, with higher fluorescence emission indicating stronger binding. Starting at pH 11 in the solution, very low fluorescence emission (λ_{exc} = 282 nm, λ_{em} = 338 nm) was observed. Addition of nitroacetic acid resulted in a pH drop to 3.0, and also caused an immediate strong enhancement of fluorescence emission. After that, the pH started to increase since decarboxylation of the acid proceeded, but the fluorescence continued to increase until pH 4.9. Here, the zwitterionic form of guest molecule is predominant and strongly binds to cyclodextrin. The pH continued to rise past 4.9, where the guest molecule was

gradually transformed to negative charge where it only weakly binds to cyclodextrin. Consequently, the fluorescence started to decrease again.

2.3.2 Based on host control

Macrocyclic molecules including crown ethers, calixarenes, cucurbiturils, pillararenes, and cyclodextrins are intuitively stable, but there are still many ways to either synthesize a transient host molecule, by making it hydrolysable involving an enzymatic reaction, or pH control if a pH responsive group is incorporated into the host (Figure 2.2a).

In 2017, Hartley, Kariyawasam et al. reported transient formation of host molecules by a chemical fuel (EDC) (Figure 2.2b).[27] When oligo(ethylene glycol) diacids were treated with EDC, hydrolytically unstable cyclic anhydrides were formed, which are analogues of crown ethers (18-crown-6 or 21-crown-7). In the presence of ions (Li^+, Na^+, K^+, Cs^+), the hydrolysis rate of the cyclic anhydrides is slower, indicating a host-guest binding effect. Moreover, the ions affected the net yield of anhydride, falling in the order of Li^+ > Na^+ > Cs^+ > K^+, which is surprisingly the exact opposite of the known cation affinities of crown ethers. This effect was proposed by the authors as "negative templation", where the matched cations suppress the formation of anhydride, but the molecular-level mechanism for this process is unclear. In another publication, temporary macrocyclic molecules were also achieved by EDC, however very limited work relating to the host-guest interaction was introduced based on the transiently formed macrocycles.[51,52]
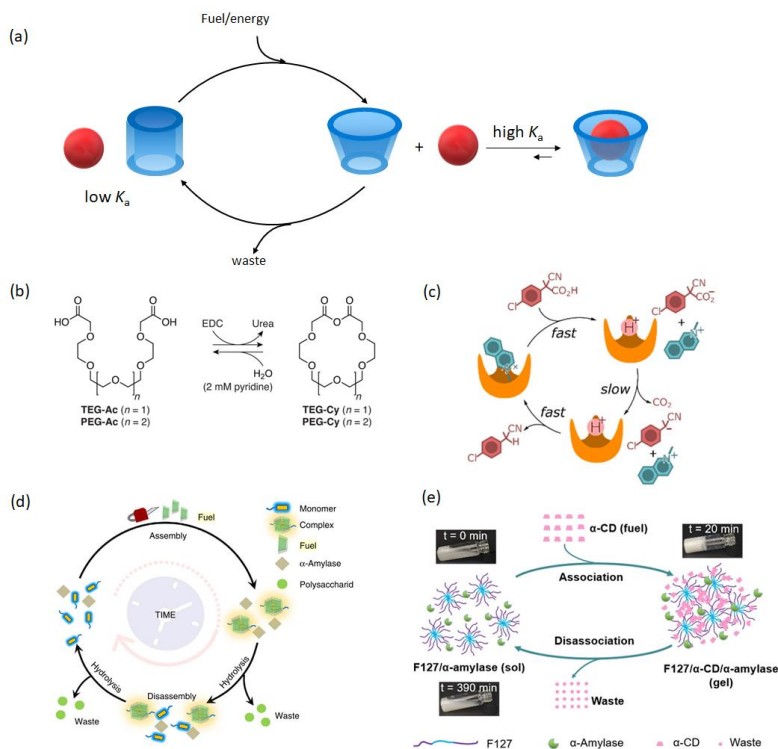
Figure 2.2 Examples of transient host-guest complex by control on host. (a) Schematic representation of the strategy based on host activation. (b) Formation of macrocyclic anhydrides treated with carbodiimide EDC, adapted from ref [27], copyright 2017 ACS publications (c) Schematic representing the release-reuptake controlled by programmable pH , adapted from ref [53], copyright 2022 ACS publications. (d) Schematic representation of the transient assembly cycle of color-tunable fluorescence system controlled by γ-cyclodextrins, adapted from ref [54], copyright 2020 Springer Nature Limited. (e) Schematic representation of transient supramolecular hydrogels based host-guest interaction with hydrolysable α-CD, adapted from ref [55], copyright 2022 John Wiley & Sons, Inc.

Using the hydrolysable host molecule γ-cyclodextrin (γ-CD) in the presence of α-amylase, in 2020, Qu and Tian et al reported an out-of-equilibrium host-guest assembling system (Figure 2.2d), resulting in multicolor switchable and transient fluorescence.[54] The system is initiated with pyrene units in aqueous solution which will act as guest molecules with a blue fluorescence. Addition of γ-CD resulted in the formation of 2:2 host-guest complexes, enabling a red-shift in the fluorescence and a yellow luminescence was observed. The enzyme α-amylase was introduced to hydrolyze γ-CD, and as a

consequence, host-guest complexes were disassembled resulting in a return to blue fluorescence. The chemically fuelled out-of-equilibrium system could be driven over three cycles. Moreover, based on the multicolour fluorescent control, a self-erasable message was written in a fluorescent gel where the write-erase process could be repeated four times.

Very similarly, in a recent publication, Wang and co-workers presented a work utilizing hydrolysable host molecules drive the system to a non-equilibrium state (Figure 2.2e).[55] In their work, α-cyclodextrin (α-CD) was used as the host molecule which is hydrolysable in the presence of α-amylase. In their system, a triblock copolymer Pluronic F127 ($PEO_{100}PPO_{100}PEO_{100}$) was used as the guest, where the PEO chain can penetrate the cavity of α-CD, forming a host-guest polymeric gel. In the presence of α-amylase, α-CD underwent hydrolysis leading to the collapse of the hydrogel network, with maltose formed as a waste. In an optimized condition, addition of α-CD (80 mg/mL) to F127 (100 mg/mL) containing α-amylase (50 mg/mL) leads to the formation of opaque hydrogels in 20 min, which slowly transferred to liquid in 390 min. The process can sustain multiple cycles but with a prolonged gelation lifetime and reduced maximum G′ in the latter cycles. Other Pluronic polymers are also able to achieve this gel-sol transition, where higher PEO content leads to longer gel lifetimes.

A pH control strategy was also applied to modulate host molecule structure and build a transient host-guest complex with temporal pH sources. In 2022, Baldini, Di Stefano et al, extended their previously developed locked/unlocked method[56] on a macrocyclic calix[4]arene scaffold to transient host-guest interaction. Using 2-cyano-2-phenylpropanoic acid as a transient acid to protonate two amino groups on the upper rim of calix[4]arene, a closed pinched cone conformation or "locked" state for calix[4]arene is obtained. Subsequent decarboxylation of the transient acid results in deprotonation of the calix[4]arene amino groups and regeneration of the native "unlocked" state. Specifically, in this work (Figure 2.2c),[53] guest molecule *N*-methylisoquinolinium with a binding constant K_{ass} of 500 ± 30 M^{-1} with calix[6]arene is applied, while the protonated calix[6]arene has no affinity to the positively charged *N*-methylisoquinolinium. By introducing a transient acid to temporally program the pH, release-reuptake of guest was achieved as indicated by chemical shifts in ^{1}H NMR. Moreover, the amount of released guest and the duration of the unloaded state can be controlled by modulation of the quantity of temporary acid added.

2.3.3 Control on the competitive guest molecules

Host-guest interactions are featured with high recognition and selectivity and a competitive guest molecule can have a dramatic influence on the original binding (Figure 2.3a). This offers a unique approach to take host-guest supramolecular systems out-of-equilibrium.

In 2021, Yan, Hao et al, developed an approach for temporal control over the host-guest process,[53] based on their previous work[46] of gel swelling induced by ATP as introduced in Section 3.1 (Figure 2.3b). In this work, macrogels were obtained by combining β-cyclodextrin (host) and adamantine (guest) functionalized polymers, which are cross-linked by host-guest interactions. ATP, which has a higher affinity for β-cyclodextrin than adamantine, can thus be added as a competitive guest to destroy the supramolecular crosslinks. When ATP was added into the hydrogel pre-embedded with potato apyrase (which catalyses the hydrolysis of ATP to weakly binding AMP), a transition of gel-sol-gel was observed. The cycle could be repeated more than 10 times, indicating minimal effect on the cycle from waste accumulation. Furthermore, they also extended this approach to fabricate chemo-mechanochromic microgels with spiropyran as a force-responsive cross-link in the polymer. Here, the ATP added causes the temporary swelling of microgels, straining the force-responsive crosslinks which triggers a color change due to the force induced spiropyran-to-merocyanine transition.
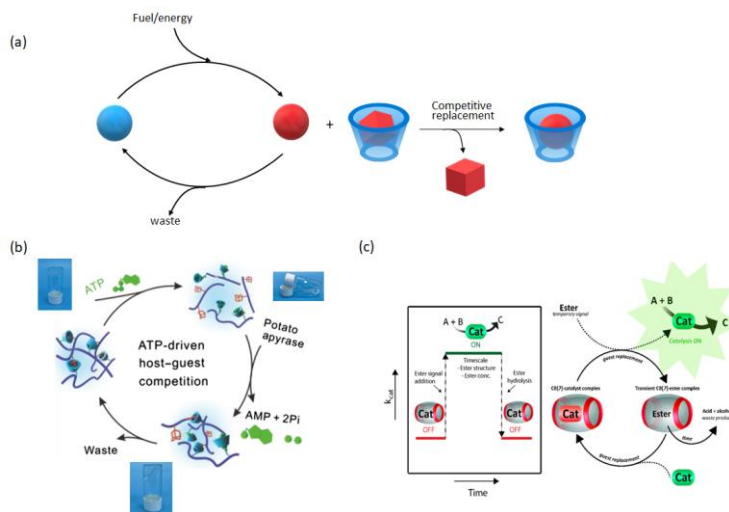
Figure 2.3 Examples of transient host-guest complexation by competitive guest control.(a) Schematic representation of the strategy based on competitive guest activation; (b) Schematic representation of dynamic macro/microgels driven by APT-induced competitive host-guest interaction, adapted from ref 26, copyright 2021 Chinese Chemical Society. (c) Transient host–guest complexation to control catalytic activity by temporary signals of hydrolytically unstable esters, adapted from ref [57], copyright 2022 ACS publications.

Just recently, based on a previously reported strategy of catalytic control by host-guest chemistry,[19] our group presented a work[57] incorporating hydrolytically unstable

competitive guests to temporarily activate an organocatalyst (Figure 2.3c). Glycine betaine esters bearing a quaternary ammonium bind highly with CB[7] and form a transient host-guest complex able to replace an originally bound aniline as catalyst, which when released restores properties such as fluorescent emission and catalytic activity. The esters, acting as competitive guest molecules, are unstable and are hydrolysed in basic conditions (pH 7.5), leading to guest reuptake. This concept was first demonstrated in a temporary dye release and reuptake, and was further used to tune the reaction rate of aniline catalysed hydrazone formation. The ester signals were effectively applied for *in situ* catalyst activation and allowed for at least 3 consecutive cycles of signal-controlled transient catalysis demonstrated by multiple signal additions. Moreover, the experimental data were supported by a kinetic model. This work shows a promising application of catalysis control by constructing a non-equilibrium CRN.

2.3.4 Other

Although most of the reported examples can be assigned to one of the three categories, there is one example which falls outside the categories defined above.

In 2019, a transient crystallization of CB[8] based host-guest complex was reported (Figure 2.4). Upon addition of trichloroacetic acid (TCA), L-tryptophan methyl ester (TrpE) formed rhombohedral-shaped crystals with CB[8] (TrpE@CB[8]) as indicated from single crystal X-ray diffraction.[58] Unlike conventional pH-controlled protonation/deprotonation on specific molecular structures, here the authors found that the extensive hydrogen-bonding network between complexes by addition of trichloroacetic acid facilitated the formation of TrpE@CB[8] crystals. After that, thermal decarboxylation of TCA by trimethylamine (TEA) and heating at 75 °C for a day resulted in the dissolution of microcrystals. By re-feeding TCA, microcrystals were quickly formed again. In addition, the lifetime of the microcrystals can be tuned by varying the temperature for the decarboxylation or by changing the amount of TCA. They then built an out-of-equilibrium system by adding TCA to a solution of TrpE@CB[8] and TEA under continuous heating to maintain the solution temperature at 75 °C. The durability of the transient crystallization process was tested by consecutive feeding of TCA every 24 h for 18 days. Turbidity of the mixture solution was monitored for these processes, revealing a good reproducibility of the transient crystallization for 18 cycles without significant damping. The remarkable durability comes from bare accumulation of wastes, since the generated volatile chemical wastes (CO_2 and $CHCl_3$) are spontaneously removed from the solution.
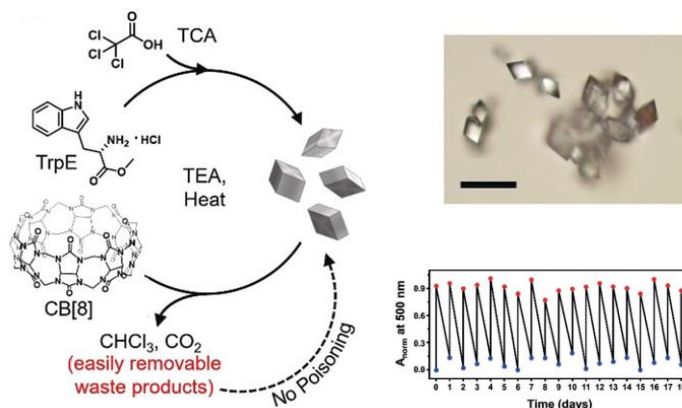
Figure 2.4. TCA-driven transient crystallization of TrpE@CB[8] without the accumulation of wastes, adapted from ref [58], copyright 2019 John Wiley & Sons, Inc.

2.4 Conclusion and outlook

In summary, we have introduced some representative examples of out-of-equilibrium supramolecular systems based on host-guest interactions. General strategies and considerations have been discussed with specific examples in the categories of control using host, guest, and competitive guest molecules. Complementary to other supramolecular systems, non-equilibrium host-guest systems can easily achieve properties such as temporal control over fluorescent emission and catalytic activities. As illustrated by a variety of examples, the main difficulty in designing an out-of-equilibrium system is related to the selection of activation/deactivation pathways with respect to the strength of the non-covalent interaction,[4,5] meanwhile some features specific to host-guest chemistry should be highlighted here: (i) All structures involved should be carefully inspected since unnecessary binding may result in a bad reversibility and durability in a system, especially with waste products; (ii) Bio-catalytic reactions with enzymes can achieve unique regulation such as a negative feedback response, and enable a wider range of possibilities such as hydrolysable host molecules; (iii) Competitive guest control is an efficient way to switch between equilibrium and non-equilibrium states, and can often be more convenient since no direct chemical conversion on the initial building blocks is required.

Despite these impressive examples introduced above, we can see that this field is still in its infancy compared to biological systems. While more efforts will be put into exploring the spatiotemporal control of supramolecular structures, we believe the following optimisations are required to further advance non-equilibrium host-guest assemblies: reduce the amount of fuel while still having an efficient activation, minimize the

poisoning effect of accumulative wastes, and develop more methods to regulate assembly lifetime beside fuel concentration. For these, we could take advantage of elegant thermodynamic equilibrium self-assembly systems already developed. For example, using only 0.6 wt% of a photoresponsive comonomer, Meijer's group was able to achieve a photoactivated gel-sol transformation.[59] Furthermore, there is also a need to expand to real life applications beside the currently reported functions.[60] More appealing and promising applications could be in energy storage,[61,62] drug delivery,[63] tissue engineering[64] and many others which are well-established in conventional supramolecular materials. Moreover, as introduced in previous publication, enzymes, ATP and other biological species have been involved in the construction of artificial out-of-equilibrium systems, a promising direction could be that these transient materials are formed *in vivo* for curing disease, and then later automatically degrade. In the end, more efforts in supramolecular systems both in- and out-of-equilibrium are required to make artificial life-like materials with sophisticated functions.

2.5 Reference

(1)   Uhlenheuer, D. A.; Petkau, K.; Brunsveld, L. Combining Supramolecular Chemistry with Biology. *Chem. Soc. Rev.* **2010**, *39* (8), 2817–2826.

(2)   Boekhoven, J.; Brizard, A. M.; Kowlgi, K. N. K.; Koper, G. J. M.; Eelkema, R.; Van Esch, J. H. Dissipative Self-Assembly of a Molecular Gelator by Using a Chemical Fuel. *Angew. Chem. Int. Ed.* **2010**, *49* (28), 4825–4828.

(3)   Mattia, E.; Otto, S. Supramolecular Systems Chemistry. *Nat. Nanotechnol.* **2015**, *10* (2), 111–119.

(4)   Van Rossum, S. A. P.; Tena-Solsona, M.; Van Esch, J. H.; Eelkema, R.; Boekhoven, J. Dissipative Out-of-Equilibrium Assembly of Man-Made Supramolecular Materials. *Chem. Soc. Rev.* **2017**, *46* (18), 5519–5535.

(5)   Rieß, B.; Grötsch, R. K.; Boekhoven, J. The Design of Dissipative Molecular Assemblies Driven by Chemical Reaction Cycles. *Chem* **2020**, *6* (3), 552–578.

(6)   Weißenfels, M.; Gemen, J.; Klajn, R. Dissipative Self-Assembly: Fueling with Chemicals versus Light. *Chem* **2021**, *7* (1), 23–37.

(7)   Krabbenborg, S. O.; Veerbeek, J.; Huskens, J. Spatially Controlled Out-of-Equilibrium Host-Guest System under Electrochemical Control. *Chem. - A Eur. J.* **2015**, *21* (27), 9638–9644.

(8)   Van Ravensteijn, B. G. P.; Voets, I. K.; Kegel, W. K.; Eelkema, R. Out-of-Equilibrium Colloidal Assembly Driven by Chemical Reaction Networks. *Langmuir* **2020**, *36* (36), 10639–10656.

(9)   Mattia, E.; Otto, S. Supramolecular Systems Chemistry. *Nat. Nanotechnol.* **2015**, *10* (2), 111–119.

(10)   Ragazzon, G.; Prins, L. J. Energy Consumption in Chemical Fuel-Driven Self-Assembly. *Nat. Nanotechnol.* **2018**, *13* (10), 882–889.

(11)   Das, K.; Gabrielli, L.; Prins, L. J. Chemically Fueled Self-Assembly in Biology and Chemistry. *Angew. Chem. Int. Ed.* **2021**, *60* (37), 20120–20143.

(12)   Wang, Q.; Qi, Z.; Chen, M.; Qu, D. Out-of-equilibrium Supramolecular Self-assembling Systems Driven by Chemical Fuel. *Aggregate* **2021**, *2* (5), e110.

(13)   De, S.; Klajn, R. Dissipative Self-Assembly Driven by the Consumption of Chemical Fuels. *Adv. Mater.* **2018**, *30* (41), 1706750.

(14)   Deng, J.; Walther, A. ATP-Responsive and ATP-Fueled Self-Assembling Systems and Materials. *Adv. Mater.* **2020**, *32* (42), 2002629.

(15)   Braegelman, A. S.; Webber, M. J. Integrating Stimuli–Responsive Properties in Host–Guest Supramolecular Drug Delivery Systems. *Theranostics* **2019**, *9* (11), 3017–3040.

(16)   Geng, W. C.; Sessler, J. L.; Guo, D. S. Supramolecular Prodrugs Based on Host-Guest Interactions. *Chem. Soc. Rev.* **2020**, *49* (8), 2303–2315.

(17)   Tang, B.; Zhao, J.; Xu, J. F.; Zhang, X. Cucurbit[n]Urils for Supramolecular Catalysis. *Chem. - A Eur. J.* **2020**, *26* (67), 15446–15460.

(18)   Tehrani, F. N.; Assaf, K. I.; Hein, R.; Jensen, C. M. E.; Nugent, T. C.; Nau, W. M. Supramolecular Catalysis of a Catalysis-Resistant Diels-Alder Reaction: Almost Theoretical Acceleration of Cyclopentadiene Dimerization inside Cucurbit[7]Uril. *ACS Catal.* **2022**, *12* (4), 2261–2269.

(19)   Li, G.; Trausel, F.; Helm, M. P.; Klemm, B.; Brévé, T. G.; Rossum, S. A. P.; Hartono, M.; Gerlings, H. H. P. J.; Lovrak, M.; Esch, J. H.; Eelkema, R. Tuneable Control of Organocatalytic Activity through Host–Guest Chemistry. *Angew. Chem. Int. Ed.* **2021**, *60* (25), 14022–14029.

(20)   Ma, X.; Zhao, Y. Biomedical Applications of Supramolecular Systems Based on Host-Guest Interactions. *Chem. Rev.* **2015**, *115* (15), 7794–7839.

(21)   Cao, L.; Šekutor, M.; Zavalij, P. Y.; Mlinarič-Majerski, K.; Glaser, R.; Isaacs, L. Cucurbit[7]Uril×guest Pair with an Attomolar Dissociation Constant. *Angew. Chem. Int. Ed.* **2014**, *53* (4), 988–993.

(22)   Shetty, D.; Khedkar, J. K.; Park, K. M.; Kim, K. Can We Beat the Biotin–Avidin Pair?: Cucurbit[7]Uril-Based Ultrahigh Affinity Host–Guest Complexes and Their Applications. *Chem. Soc. Rev.* **2015**, *44* (23), 8747–8761.

(23)   Pluth, M. D.; Raymond, K. N. Reversible Guest Exchange Mechanisms in Supramolecular Host–Guest Assemblies. *Chem. Soc. Rev.* **2007**, *36* (2), 161–171.

(24)   Boekhoven, J.; Hendriksen, W. E.; Koper, G. J. M.; Eelkema, R.; van Esch, J. H. Transient Assembly of Active Materials Fueled by a Chemical Reaction. *Science* **2015**, *349* (6252), 1075–1079.

(25)   Tena-Solsona, M.; Rieß, B.; Grötsch, R. K.; Löhrer, F. C.; Wanzke, C.; Käsdorf, B.; Bausch, A. R.; Müller-Buschbaum, P.; Lieleg, O.; Boekhoven, J. Non-Equilibrium Dissipative Supramolecular Materials with a Tunable Lifetime. *Nat. Commun.* **2017**, *8* (1), 15895.

(26)   Hao, X.; Wang, H.; Zhao, W.; Wang, L.; Peng, F.; Yan, Q. Dynamic Macro- and Microgels Driven by Adenosine Triphosphate-Fueled Competitive Host–Guest Interaction. *CCS Chem.* **2022**, *4* (3), 838–846.

(27)   Kariyawasam, L. S.; Hartley, C. S. Dissipative Assembly of Aqueous Carboxylic Acid Anhydrides Fueled by Carbodiimides. *J. Am. Chem. Soc.* **2017**, *139* (34), 11949–11955.

(28)   Heuser, T.; Steppert, A. K.; Molano Lopez, C.; Zhu, B.; Walther, A. Generic

Concept to Program the Time Domain of Self-Assemblies with a Self-Regulation Mechanism. *Nano Lett.* **2015**, *15* (4), 2213–2219.

(29)   Che, H.; Cao, S.; Van Hest, J. C. M. Feedback-Induced Temporal Control of "Breathing" Polymersomes to Create Self-Adaptive Nanoreactors. *J. Am. Chem. Soc.* **2018**, *140* (16), 5356–5359.

(30)   Hao, X.; Yang, K.; Wang, H.; Peng, F.; Yang, H. Biocatalytic Feedback-Controlled Non-Newtonian Fluids. *Angew. Chem. Int. Ed.* **2020**, *59* (11), 4314–4319.

(31)   Heuser, T.; Weyandt, E.; Walther, A. Biocatalytic Feedback-Driven Temporal Programming of Self-Regulating Peptide Hydrogels. *Angew. Chem. Int. Ed.* **2015**, *54* (45), 13258–13262.

(32)   Berrocal, J. A.; Biagini, C.; Mandolini, L.; Di Stefano, S. Coupling of the Decarboxylation of 2-Cyano-2-Phenylpropanoic Acid to Large-Amplitude Motions: A Convenient Fuel for an Acid-Base-Operated Molecular Switch. *Angew. Chem. Int. Ed.* **2016**, *55* (24), 6997–7001.

(33)   Dowari, P.; Das, S.; Pramanik, B.; Das, D. PH Clock Instructed Transient Supramolecular Peptide Amphiphile and Its Vesicular Assembly. *Chem. Commun.* **2019**, *55* (94), 14119–14122.

(34)   Heinen, L.; Heuser, T.; Steinschulte, A.; Walther, A. Antagonistic Enzymes in a Biocatalytic Ph Feedback System Program Autonomous DNA Hydrogel Life Cycles. *Nano Lett.* **2017**, *17* (8), 4989–4995.

(35)   Paul, T. J.; Vilseck, J. Z.; Hayes, R. L.; Brooks, C. L. Exploring PH Dependent Host/Guest Binding Affinities. *J. Phys. Chem. B* **2020**, *124* (30), 6520–6528.

(36)   Bian, T.; Chu, Z.; Klajn, R. The Many Ways to Assemble Nanoparticles Using Light. *Adv. Mater.* **2020**, *32* (20).

(37)   Bandara, H. M. D.; Burdette, S. C. Photoisomerization in Different Classes of Azobenzene. *Chem. Soc. Rev.* **2012**, *41* (5), 1809–1825.

(38)   Vapaavuori, J.; Bazuin, C. G.; Priimagi, A. Supramolecular Design Principles for Efficient Photoresponsive Polymer-Azobenzene Complexes. *J. Mater. Chem. C* **2018**, *6* (9), 2168–2188.

(39)   Moncelsi, G.; Ballester, P. Photoswitchable Host-Guest Systems Incorporating Hemithioindigo and Spiropyran Units. *ChemPhotoChem* **2019**, *3* (6), 304–317.

(40)   Klajn, R. Spiropyran-Based Dynamic Materials. *Chem. Soc. Rev.* **2014**, *43* (1), 148–184.

(41)   Fredrich, S.; Göstl, R.; Herder, M.; Grubert, L.; Hecht, S. Switching Diarylethenes Reliably in Both Directions with Visible Light. *Angew. Chem. Int. Ed.* **2016**, *55* (3), 1208–1212.

(42)   Kathan, M.; Hecht, S. Photoswitchable Molecules as Key Ingredients to Drive Systems Away from the Global Thermodynamic Minimum. *Chem. Soc. Rev.* **2017**, *46* (18), 5536–5550.

(43)   Wimberger, L.; Prasad, S. K. K.; Peeks, M. D.; Andréasson, J.; Schmidt, T. W.; Beves, J. E. Large, Tunable, and Reversible PH Changes by Merocyanine Photoacids. *J. Am. Chem. Soc.* **2021**, *143* (49), 20758–20768.

(44)   Tian, F.; Jiao, D.; Biedermann, F.; Scherman, O. A. Orthogonal Switching of a Single Supramolecular Complex. *Nat. Commun.* **2012**, *3*, 1–8.

(45)   Vlasceanu, A.; Cacciarini, M.; Nielsen, M. B. Photo/Thermochromic Macrocycles

Based on Dihydroazulenes, Dithienylethenes, and Spiropyrans. *Tetrahedron* **2018**, *74* (46), 6635–6646.

(46)   Hao, X.; Sang, W.; Hu, J.; Yan, Q. Pulsating Polymer Micelles via ATP-Fueled Dissipative Self-Assembly. *ACS Macro Lett.* **2017**, *6* (10), 1151–1155.

(47)   Yin, Z.; Song, G.; Jiao, Y.; Zheng, P.; Xu, J.-F.; Zhang, X. Dissipative Supramolecular Polymerization Powered by Light. *CCS Chem.* **2019**, *1* (4), 335–342.

(48)   Jain, M.; Ravoo, B. J. Fuel-Driven and Enzyme-Regulated Redox-Responsive Supramolecular Hydrogels. *Angew. Chem. Int. Ed.* **2021**, *60* (38), 21062–21068.

(49)   Del Giudice, D.; Spatola, E.; Valentini, M.; Bombelli, C.; Ercolani, G.; Di Stefano, S. Time-Programmable PH: Decarboxylation of Nitroacetic Acid Allows the Time-Controlled Rising of PH to a Definite Value. *Chem. Sci.* **2021**, *12* (21), 7460–7466.

(50)   Yan, Q.; Zhao, Y. ATP-Triggered Biomimetic Deformations of Bioinspired Receptor-Containing Polymer Assemblies. *Chem. Sci.* **2015**, *6* (7), 4343–4349.

(51)   Zong, Z.; Zhang, Q.; Qiu, S. H.; Wang, Q.; Zhao, C.; Zhao, C. X.; Tian, H.; Qu, D. H. Dynamic Timing Control over Multicolor Molecular Emission by Temporal Chemical Locking. *Angew. Chem. Int. Ed.* **2022**, *61* (13), 1–5.

(52)   Hossain, M. M.; Atkinson, J. L.; Hartley, C. S. Dissipative Assembly of Macrocycles Comprising Multiple Transient Bonds. *Angew. Chem. Int. Ed.* **2020**, *59* (33), 13807–13813.

(53)   Rispoli, F.; Spatola, E.; Del Giudice, D.; Cacciapaglia, R.; Casnati, A.; Baldini, L.; Di Stefano, S. Temporal Control of the Host–Guest Properties of a Calix[6]Arene Receptor by the Use of a Chemical Fuel. *J. Org. Chem.* **2022**, *87* (5), 3623–3629.

(54)   Wang, Q.; Zhang, Q.; Zhang, Q.-W.; Li, X.; Zhao, C.-X.; Xu, T.-Y.; Qu, D.-H.; Tian, H. Color-Tunable Single-Fluorophore Supramolecular System with Assembly-Encoded Emission. *Nat. Commun.* **2020**, *11* (1), 158.

(55)   Lu, H.; Hao, J.; Wang, X. Host-Fueled Transient Supramolecular Hydrogels. *ChemSystemsChem* **2022**, *4* (3).

(56)   Del Giudice, D.; Spatola, E.; Cacciapaglia, R.; Casnati, A.; Baldini, L.; Ercolani, G.; Di Stefano, S. Time Programmable Locking/Unlocking of the Calix[4]Arene Scaffold by Means of Chemical Fuels. *Chem. – A Eur. J.* **2020**, *26* (65), 14954–14962.

(57)   van der Helm, M. P.; Li, G.; Hartono, M.; Eelkema, R. Transient Host–Guest Complexation To Control Catalytic Activity. *J. Am. Chem. Soc.* **2022**, *144* (21), 9465–9471.

(58)   Choi, S.; Mukhopadhyay, R. D.; Kim, Y.; Hwang, I.; Hwang, W.; Ghosh, S. K.; Baek, K.; Kim, K. Fuel-Driven Transient Crystallization of a Cucurbit[8]Uril-Based Host–Guest Complex. *Angew. Chem. Int. Ed.* **2019**, *58* (47), 16850–16853.

(59)   Weyandt, E.; ter Huurne, G. M.; Vantomme, G.; Markvoort, A. J.; Palmans, A. R. A.; Meijer, E. W. Photodynamic Control of the Chain Length in Supramolecular Polymers: Switching an Intercalator into a Chain Capper. *J. Am. Chem. Soc.* **2020**, *142* (13), 6295–6303.

(60)   Rieß, B.; Boekhoven, J. Applications of Dissipative Supramolecular Materials with a Tunable Lifetime. *ChemNanoMat* **2018**, *4* (8), 710–719.

(61)   Dumele, O.; Chen, J.; Passarelli, J. V.; Stupp, S. I. Supramolecular Energy Materials. *Adv. Mater.* **2020**, *32* (17).

(62)   Kwon, T. woo; Choi, J. W.; Coskun, A. Prospect for Supramolecular Chemistry in High-Energy-Density Rechargeable Batteries. *Joule* **2019**, *3* (3), 662–682.

(63)   Webber, M. J.; Langer, R. Drug Delivery by Supramolecular Design. *Chem. Soc. Rev.* **2017**, *46* (21), 6600–6620.

(64)   Zhao, Y.; Song, S.; Ren, X.; Zhang, J.; Lin, Q.; Zhao, Y. Supramolecular Adhesive Hydrogels for Tissue Engineering Applications. *Chem. Rev.* **2022**, *122* (6), 5604–5640.

Chapter 3

Tuneable Control of Organocatalytic Activity through Host–Guest Chemistry

Abstract: Dynamic regulation of chemical reactivity is important in many complex chemical reaction networks, such as cascade reactions and signal transduction processes. Signal responsive catalysts could play a crucial role in regulating these reaction pathways. Recently, supramolecular encapsulation was reported to regulate the activities of artificial catalysts. We present a host-guest chemistry strategy to modulate the activity of commercially available synthetic organocatalysts. The molecular container cucurbit[7]uril was successfully applied to change the activity of four different organocatalysts and one initiator, enabling up- or down-regulation of the reaction rates of four different classes of chemical reactions. In most cases CB[7] encapsulation results in catalyst inhibition, however in one case catalyst activation by binding to CB[7] was observed. The mechanism behind this unexpected behavior was explored by NMR binding studies and pKa measurements. The catalytic activity can be instantaneously switched during operation, by addition of either supramolecular host or competitive binding molecules, and the reaction rate can be predicted with a kinetic model. Overall, this signal responsive system proves a promising tool to control catalytic activity.
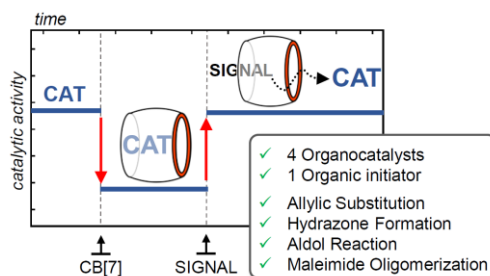
This chapter is mainly based on:

Li, G., Trausel, F., van der Helm, M. P., Klemm, B., Brevé, T. G., van Rossum, S. A. P., Hartono, M., Gerlings, H. H. P. J., Lovrak, M., van Esch, J. H., Eelkema, R. Tuneable Control of Organocatalytic Activity through Host–Guest Chemistry. *Angew. Chem. Int. Ed.* **2021**, *60*, 14022–14029.

3.1 Introduction

Dynamic regulation of chemical reactivity is important in many complex chemical reaction networks such as cascade reactions and signal transduction processes.[1,2] In nature, these processes are heavily regulated by enzymatic catalysis, where the activity of these catalysts themselves are modulated to render such reaction networks responsive to external signals, changes in substrate levels or changes in the environment.[3] Responsive artificial catalysts could play similar roles in chemical reaction networks, where regulation of catalytic activity is crucial to achieve efficient temporal and spatial control over chemical transformations without unnecessary waste or off-cycle reaction pathways. Furthermore, the reversible de-activation/re-activation of catalysts by external signals can make such artificial systems highly responsive to environmental stimuli, analogous to signal-responsive enzyme catalysis in nature [2,4]. Still, to this date such responsive catalysts remain very rare, have a narrow application scope or rely on extensive synthetic efforts.[5] Recently, there have been reports of regulation of the activity of synthetic catalysts[6] by supramolecular encapsulation including rotaxanes [7–9], resorcin[4]arene [10–12], cyclodextrin [13] and cucurbit[7]uril [14–18] which is of high interest because it enables precise, reversible and responsive control over reaction rates by adjusting the amount of available catalyst *in-situ*. Among them, cucurbit[7]uril (CB[7]) is a widely applied molecular container, a cyclic glycoluril heptamer that binds strongly to small neutral and cationic compounds. [19–21] CB[7] is commercially available, non-toxic and relatively soluble in water, which makes it possible to be used in aqueous environments or even biological systems. Examples of CB[7] catalytic activity regulation include the regulation of transition metal catalysts embedded in gold nanoparticles in cells, [14] the enhancement of photocatalytic H_2 evolution,[15] promotion of the Fenton oxidation through supramolecularly modulated ferrocene catalysts,[16] and control over copper catalyzed alkyne azide click chemistry [17]. Most of these examples focus on transition metal catalysis. To date, only Leigh and coworkers reported a switchable secondary amine catalyst based on a rotaxane [7–9], but that system has a highly specialized design to enable complex formation between host and catalyst. As of now no generic method is available for tuneable catalytic activity regulation of common simple, commercially available organocatalysts. Since organocatalysis is emerging as one of the main branches of synthetic science,[22] we hypothesize that the exploration of CB to control readily accessible and widely used organocatalysts, would highly broaden the application scope of this method.

Herein we report a strategy to change and tune the catalytic activity *in-situ* of diverse, widely applied organocatalysts by host-guest encapsulation in aqueous environment. Specifically, with supramolecular encapsulation we can control the catalytic activity of four different organocatalysts in various bond forming reactions: primary amine (**C1**: aniline and **C5**: benzimidazole-amine) catalyzed hydrazone formation, tertiary amine (**C2**: DABCO) catalyzed allylic substitution, secondary amine (**C3**: prolinol) catalyzed aldol

formation, as well as the oligomerization of maleimide initiated by an amine initiator (**C4**: nornicotine) (Scheme 3.1c). These reactions all proceed in aqueous media under biologically relevant conditions[23]. In most of the cases, reaction rates can be down- and upregulated by binding the catalyst to CB[7] and subsequently releasing it by adding a competitive strong binder for CB as a chemical signal.
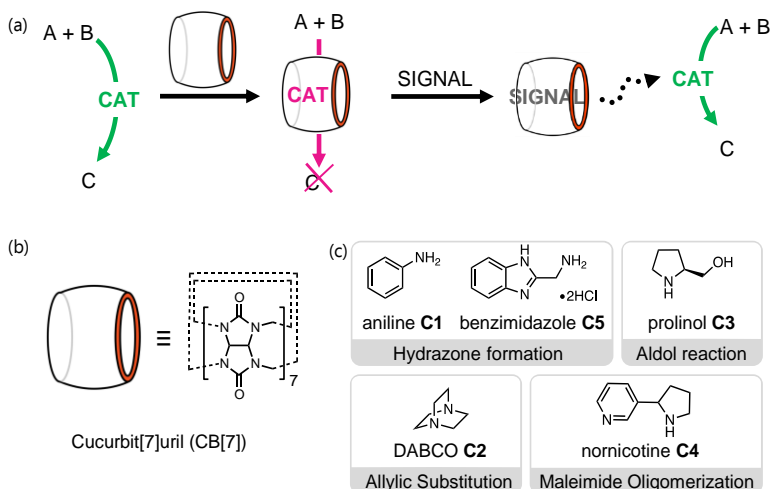
Scheme 3.1. The concept of using host-guest chemistry to control the activity of organocatalysts. (**a**) Schematic representation of CB[7] binding to the organocatalyst (CAT), hindering its catalytic activity. Addition of the stronger binding signal leads to the release of the catalyst and restores its catalytic activity; (**b**) Structure of CB[7]; (**c**) Organocatalysts **C1**-**C5** and their associated reactions.
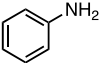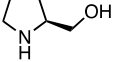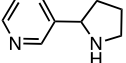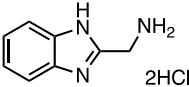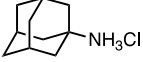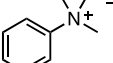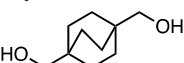
3.2 Results and Discussion

3.2.1 System design considerations and organocatalysts selection

The applied catalysts (Scheme 3.1c) were first selected based on the binding affinity with CB[7]. CB[7] binds strongly to somewhat hydrophobic, positively charged molecules with an appropriate size for the CB[7] cavity.[12] To be able to use CB[7] to modify catalyst activity by encapsulation, it is essential that the catalyzed reaction works in aqueous environments, and that the affinity of the catalysts with CB[7] is high enough to ensure that the majority of catalyst is encapsulated at the operational concentrations. Meanwhile, the substrates and products should not bind to CB[7]. On the other hand, the signal molecules should have a much larger affinity for CB[7] than the catalyst, to allow efficient liberation of the catalyst through competitive binding, analogous to the indicator displacement assay (IDA)[24]. From this principle, four organocatalysts and one

organic initiator: aniline **C1**, DABCO **C2**, L-prolinol **C3**, nornicotine **C4** (an initiator for maleimide oligomerization), 1*H*-benzimidazole-2-methanamine **C5**, and three signal molecules (**SG1**-**3**) were selected and used separately in a range of reactions. NMR binding studies of these catalysts and initiator also indicated their affinity to CB[7] (Figures S3.5-S3.10). Table 3.1 summarizes the binding constants of CB[7] with **C1-5** and **SG1-3**. Generally, the binding constants of the catalysts are in the range of ~10^3-10^5 M^{-1} and the signal molecules are ~10^8-10^{12} M^{-1}, while the reaction substrates and products are chosen such that they bind with $K_a <$ 10 M^{-1}. (Supporting information Table S3.5).

Table 3.1. Binding constants of organocatalysts and signal molecules with CB[7].

Compound	Structure	K_a (M^{-1})
C1		$(1.3 \pm 0.038) \times 10^5$ [a]
C2		$(3.6 \pm 0.032) \times 10^5$ [b]
C3		$(5.75 \pm 0.16) \times 10^3$ [b]
C4		$(4.6 \pm 0.035) \times 10^4$ [b]
C5		$(2.8 \pm 0.20) \times 10^5$ [a]
SG1		$(4.2 \pm 1.0) \times 10^{12}$ [c]
SG2		$(2.5 \pm 0.6) \times 10^8$ [d]
SG3		$(6.1 \pm 0.5) \times 10^9$ [e]

[a] Measured by ITC in 10 mM sodium phosphate buffer pH 6.0, 25 °C, ; [b] Measured by ITC in 100 mM sodium phosphate buffer pH 7.4, 25 °C; [c] Values from Ref [19], measured by NMR in NaO$_2$CCD$_3$ (50 mM) buffer, pH 4.74; [d] Values from Ref [25], measured by NMR in D$_2$O, 25 °C; [e] Values from Ref [26], measured by ITC in H$_2$O, 25 °C.

3.2.2 Control over aniline (C1) catalysis in hydrazone formation

We first focused on the hydrazone formation reaction, a widely applied condensation reaction between an aldehyde and a hydrazide that takes place in aqueous buffer and is accelerated by a variety of organocatalysts.[27,28] Aniline **C1** is often used as a catalyst in this reaction, although in (super)stoichiometric amounts because of its low efficiency.[29,30] The reaction between aldehyde **SM1** (0.4 mM) and hydrazide **SM2** (0.04

mM) in aqueous buffer (10 mM sodium phosphate buffer pH 6.0) leads to the formation of hydrazone product **P1** (Fig. 3.1), where both catalyzed and uncatalyzed reactions follow second-order reaction kinetics. However, under the operational conditions (with [**SM1**] >> [**SM2**]) we calculate the reaction rate constant based on the pseudo-first order assumption (Equation S1). As is apparent from Fig.3.1(a)(c) and Table S3.1, catalyst **C1** (0.4 mM) increases the reaction rate 13-fold with respect to the uncatalyzed reaction. A blank reaction with CB[7] (0.42 mM) alone increases the reaction rate 1.9-fold with respect to the uncatalyzed reaction, indicating that the macrocycle shows a small catalytic activity towards the hydrazone formation reaction.[31] Addition of CB[7] (0.42 mM) to catalyst **C1** (0.4 mM) should lead to an estimated >89% of the catalyst bound in CB[7] (Equation S10). This mixture gives a reaction rate constant of 0.28 $M^{-1}s^{-1}$, which is 3.5-fold lower than the catalyzed reaction, showing a substantial reduction of the catalytic activity of **C1**. On top of that, hydrazone formation in the presence of CB[7] (0.42 mM), catalyst **C1** (0.4 mM) and signal molecule **SG1** (0.8 mM) gives a reaction rate constant of 1.2 $M^{-1}s^{-1}$, showing that the signal molecule effectively replaces the catalyst by competitive binding with CB[7], restoring the catalytic activity of catalyst **C1**. Noteworthy, the reaction rate in the presence of CB[7], catalyst **C1** and signal molecule **SG1** is slightly higher than the reaction rate with only catalyst **C1**. A reason might be that the catalytic activity of CB[7] adds up to the catalytic activity of catalyst **C1**, leading to a higher reaction rate. Signal guest molecule **SG1** (0.8 mM) alone does not show any catalytic activity, while the reaction in the presence of CB[7] (0.42 mM) and signal guest **SG1** (0.8 mM) is 1.3-fold faster than the blank reaction, showing that a guest inside the cavity of CB[7] does not have a significant effect on the CB[7] catalytic background activity. In essence, CB[7] encapsulation thus reduces the catalytic activity of organocatalyst **C1**, which can be restored by competitive binding with a signal molecule.
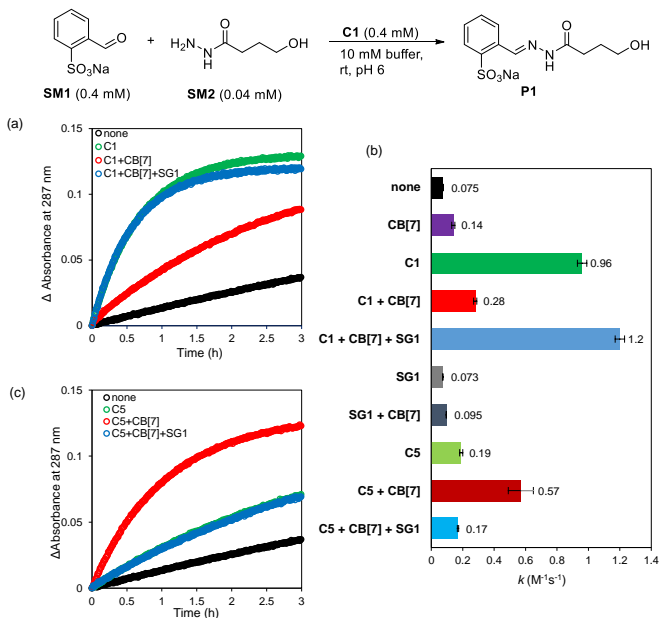
Figure 3.1. Hydrazone formation catalyzed by **C1** and **C5**: UV-absorbance changes at 287 nm of hydrazone product **P1** followed over time, catalyzed by **C1** (**a**) and **C5** (**b**), evaluation of reaction rate constants (**c**).

3.2.3 Control over DABCO (C2) catalysis in allylic substitution

The successful control of the hydrazone formation reaction rate via CB[7] catalyst encapsulation encouraged us to extend the application of this strategy to other organocatalysts. 1,4-Diazabicyclo[2.2.2]octane (DABCO, **C2**) is a widely used catalyst in many organic reactions.[32] From ITC, we learned that the binding constant of DABCO (**C2**) with CB[7] is 3.6×10^5 M^{-1} (Table 3.1), which is in a similar range as **C1** and a suitable value for reaction rate control. Moreover, DABCO was reported to accelerate the allylic substitution reaction between diethyl(α-acetoxymethyl) vinylphosphonate **SM3** and nitrogen-based nucleophiles in aqueous solvents.[33,34] Hence, we used glycine (**SM4**; 100 mM) as nucleophile in phosphate buffer (100 mM, pH 7.4) to react with **SM3** (10 mM), giving the double substituted compound as the major product (Fig. 3.2). Similar to the hydrazone reaction, with [**SM4**]>>[**SM3**] in this substitution reaction, we measured a pseudo-first order reaction rate by ^{1}H NMR following the consumption of **SM3** (Fig. S3.2). With 20 mol% of DABCO (2 mM), the **SM3** consumption is 13-fold faster than the uncatalyzed reactions conditions (15.86 M^{-1}h^{-1} *vs*. 1.19 M^{-1}h^{-1}; Fig. 3.2(a)(b)). Addition of 3.5 mM CB[7], encapsulating about 99.8% of the present DABCO, decreased the reaction constant to 1.23 M^{-1}h^{-1}, giving a similar rate constant as the blank reaction. To avoid any side-reactions of the substrate with **SG1** (a primary amine) signal molecule, **SG2** was

used in this particular system to release the catalyst. In the presence of CB[7] (3.5 mM), catalyst **C2** (2 mM, 20%) and signal molecule **SG2** (6 mM), the reaction rate is accelerated again, about 11.4-times faster than the blank reaction, although slightly lower than the catalytic reaction which may be cause by the slight inhibitory effect of CB[7] itself on this reaction (Fig.3.2b). Neither the signal molecule **SG2** (6 mM), or CB[7] (3.5 mM) separately or together show any catalytic activity. This demonstrates a successful re-activation of the substitution reaction through the release of catalyst **C2** from the CB cavity by competitive binding of the signal molecule. From these results, we prove that the catalytic activity of DABCO can be tuned by CB[7] encapsulation and competitive binding of a signal molecule.
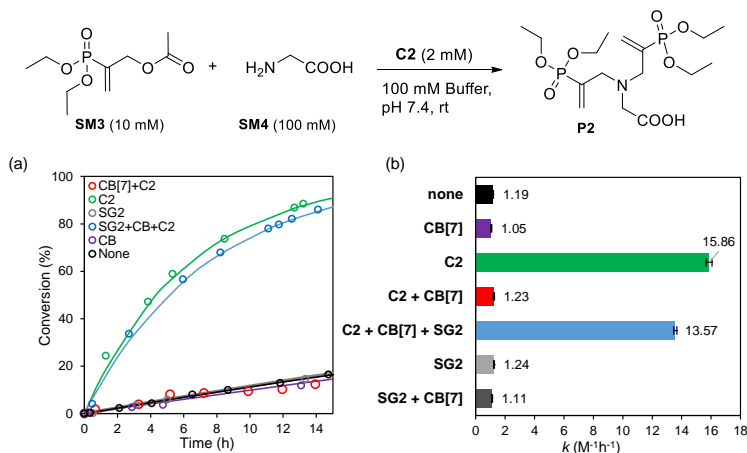

Figure 3.2. Allylic substitution catalyzed by **C2**: **SM3** conversion followed by ^{1}H NMR (**a**), evaluation of reaction rate constants (**b**). Markers indicate experimental data, lines indicate fitted kinetic models.

3.2.4 Control over prolinol catalysis in aldol reaction

Host-guest regulation of catalytic activity is also applicable to the aldol reaction, one of the most popular synthetic and biochemical means to construct carbon-carbon bonds. The aldol reaction can be catalyzed by a variety of organocatalysts in aqueous media.[35–37] We selected a water-soluble aldehyde substrate (**SM5**) as aldol acceptor that with acetone as aldol donor generates aldol product **P3** (Fig. 3.3). This reaction is catalyzed by L-prolinol (**C3**), which has a moderate binding affinity towards CB[7] (Table 3.1). Without the catalyst, the aldehyde substrate **SM5** (20 mM) with acetone (600 mM, 30 eq.) in phosphate buffer (100 mM, pH 7.4) shows almost no conversion to **P3** (Fig. 3.3a). However, L-prolinol catalysis (**C3**, 6 mM, 30 mol%) gives a reaction rate constant of 3.17 $\times 10^{-3}$ $M^{-1}h^{-1}$, a 12.7-fold increase relative to the uncatalyzed reaction, under the pseudo-first order conditions ([acetone]>>[**SM5**]). Addition of CB[7] (7 mM) to the catalyzed reaction results in a 36% decrease in the reaction rate. The only moderate rate decrease

for this reaction by addition of CB[7] might be caused by the comparably low binding constant of **C3** to CB[7] (5.75×10^3 M^{-1}) and from the unexpectedly high affinity of acetone with CB[7] (592 M^{-1})[38]. In addition, CB[7] itself also has some catalytic activity for this aldol reaction, shown in Fig.3.3(a)(b). Remarkably, addition of signal molecules does not result in restoration of catalytic activity of **C3** as would be expected, no matter if the signal molecules are charged (**SG2**) or neutral (**SG3**). The origin of this unexpected result remains unclear, as ^{1}H-NMR did not show unforeseen binding of reaction products or intermediates to CB[7] or the catalyst, which might interfere with catalyst reactivation.
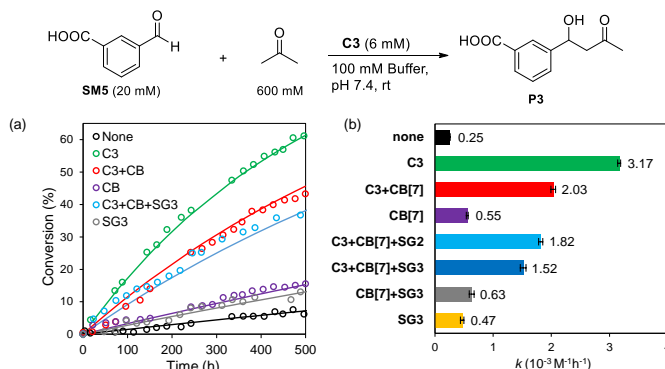

Figure 3.3 Aldol reaction catalyzed by **C3**: **SM5** conversion followed by ^{1}H NMR (a) and evaluation of reaction rate constants (b). Markers indicate experimental data, lines indicate fitted kinetic models.

3.2.5 Control over nornicotine in maleimide oligomerization

After demonstrating the capability of CB[7] to control the activity of organocatalysts, we wondered whether the same strategy can be used for the regulation of other organic molecules, such as an organic initiator for polymerization, in order to extend the scope of our strategy. In that context, we used CB[7] to control the oligomerization of a maleimide derivative. Maleimide is a widely used functional building block in polymer materials.[39] The homo-polymerization of maleimide can be initiated through an anionic mechanism by a base initiator, such as an organic pyridine base in aqueous solution.[40,41] As the initiator we used nornicotine **C4**, which has a binding constant of 4.6×10^4 M^{-1} for CB[7] (Fig. 3.4). Moreover, to avoid maleimide *N*-additions as side reactions, *N*-acetic acid maleimide (**SM6**) was synthesized, which also increased substrate solubility and removed any affinity for CB[7]. In the presence of **C4**, the substrate consumption was accelerated (>90% conversion in 50 h) compared to the initiator-free blank reaction, resulting in a 5.9-fold faster reaction (5.29 h^{-1} *vs.* 0.89 h^{-1}, Fig. 3.4(b)). Addition of 7 mM CB[7] into the reaction mixture slowed down the rate to 1.27 h^{-1}. Analogous to the organocatalyzed reactions above, addition of signal molecule **SG2** (12 mM) leads to

recovery of the reaction rate back to the same level as with only nornicotine present, while the signal molecule and CB[7] alone did not show any activity.
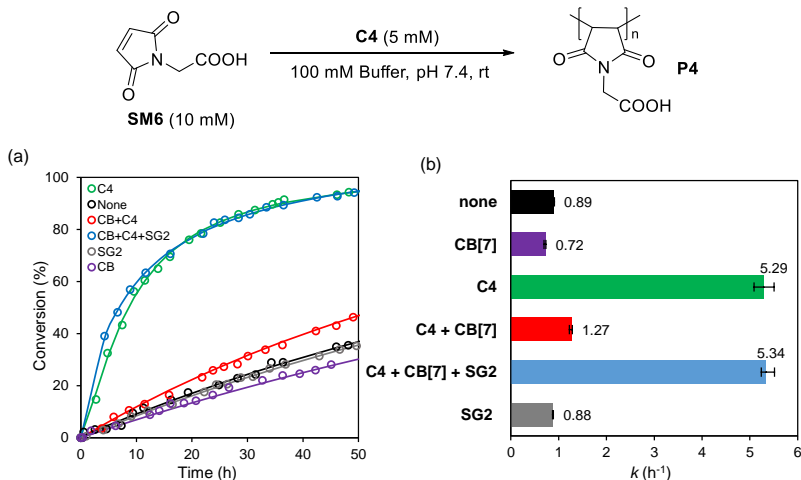

Figure 3.4 Maleimide oligomerization initiated by **C4**: Conversion of **SM6** followed by ^{1}H NMR (a), evaluation of reaction rate constants (b). Markers indicate experimental data, lines indicate fitted kinetic models.

3.2.6 Catalysis enhancement (C5)

So far, we have demonstrated the inhibiting effect of CB[7] on the activity of organocatalysts **C1**, **C2**, **C3** and initiator **C4**. Yet, CB[7] can also be used to increase organocatalytic activity. 1*H*-benzimidazole-2-methanamine **C5** (0.4 mM) is a catalyst for the same hydrazone formation reaction as shown in Fig.3.1(b)(c). Addition of CB[7] (0.42 mM) to that reaction leads to a 3-fold higher reaction rate than the reaction rate with only **C5** (0.57 vs 0.19 $M^{-1}s^{-1}$). CB[7] encapsulation in this case increased the catalytic activity of **C5**, which is an opposite effect compared to what we observe for catalyst **C1** in the same reaction. Next, addition of signal molecule **SG1** (0.8 mM) to the reaction with catalyst **C5** (0.4 mM) and CB[7] (0.42 mM) gives a reaction rate of 0.17 $M^{-1}s^{-1}$, thus restoring the catalytic activity of catalyst **C5** to its original value. As such, in this opposite activation model the catalyst release from CB[7] with a signal molecule also works effectively. We were interested in exploring the mechanism behind the unexpected inverse effect of CB[7] encapsulation on the two catalysts. ^{1}H-NMR binding studies (Fig. S3.5) indicate that catalyst **C1** is fully sequestered inside the CB[7] host. For catalyst **C5**, ^{1}H-NMR shows that only the aromatic part is inside the host but the aliphatic amine sticks out beyond the CB[7] carbonyl rim (Fig. S3.9,S3.10). To further elucidate the mechanism, the pK_a of the two catalysts was measured in the absence and presence of CB[7] by pH dependent UV absorbance experiments (Fig. S3.17).[42] Without CB[7], pK_a

values are 4.7 for **C1**, and 3.0 (benzimidazole unit), 7.8 (primary amine unit) for **C5**, which has a good agreement with earlier reports (Table S3.6). [37,38] Macrocyclic encapsulation is well known to influence the pK_a of the guest molecules inside.[45] In our measurement, the presence of CB[7] increases all the pK_a values of **C1** (4.7 to 6.5) and **C5** (3.0 to 4.8, 7.8 to 8.9, Fig. S19,20). Next, we tested **C5** analogs without benzimidazole unit, (1*H*-indol-2-yl)methanamine and benzylamine. Although their pK_a values also increased upon CB[7] binding, these two molecules did not show any catalytic activity enhancement (Fig. S21,22). Kool postulates that the proton donating ability of the benzimidazole unit in the transition state of the rate determining step is crucial for catalytic activity. (Scheme S3.1, **TS1**).[27–29] We now see that CB[7] encapsulation can further enhance the protonation ability of benzimidazole, bringing the pK_a from 3.0 to 4.8 and thus closer to the solvent pH (pH 6.0). Binding to CB[7] increased the pK_a of the benzimidazole ring and thus its protonation equilibrium, enhancing catalytic activity of **C5**.

3.2.7 *In-situ* control over catalytic activity

Using this supramolecular encapsulation strategy, we hypothesized that we should be able to change the reaction rate at any given moment of time during the reaction, by adding CB[7] to encapsulate the catalyst or by releasing the catalyst with addition of a signal molecule. We performed these *in-situ* control experiments with CB[7] for the organocatalysts in the allylic substitution reaction and the hydrazone formation reaction (Fig. 3.5). In the allylic substitution reaction with catalyst **C2** (2 mM), adding CB[7] (3.5 mM) after 5 h caused an immediate flattening of the conversion curve (Fig. 3.5a), demonstrating that the host molecule can very rapidly change the activity of the catalyst by encapsulating it. Subsequent addition of signal molecule **SG2** after 10 h shifted the curve back to a higher rate. The decrease of the reaction rate constant after CB[7] addition at 5 h and re-initialization with **SG2** at 10 h confirms the effective regulation of the catalytic activity of DABCO (Fig. 3.5b). Similarly, for catalyst **C1** in the hydrazone formation reaction, we also performed an *in-situ* (de-)activation experiment. When monitoring the reaction using catalyst **C1** (0.4 mM), upon adding CB[7] (0.42 mM) after 10 min we immediately observed a decrease in reaction rate (Fig. 3.5c). Subsequent addition of signal molecule **SG1** (0.8 mM) after 20 min resulted in an increased reaction rate, back to the original value. For the activated catalyst **C5**, *in-situ* activity control also works. As shown in Fig. 3.5d, adding CB[7] after 10 min to the reaction mixture with catalyst **C5** (0.4 mM) increases the reaction rate immediately. Addition of signal molecule **SG1** (0.8 mM) 10 min later liberated the catalyst again from the CB[7] cavity restoring the reaction rate to the original level. These results of two reaction examples with three different organocatalysts confirm successful *in-situ* control of the catalytic activity where CB[7] can thus be used to switch off the catalyst, and a signal molecule can switch the system back on again.
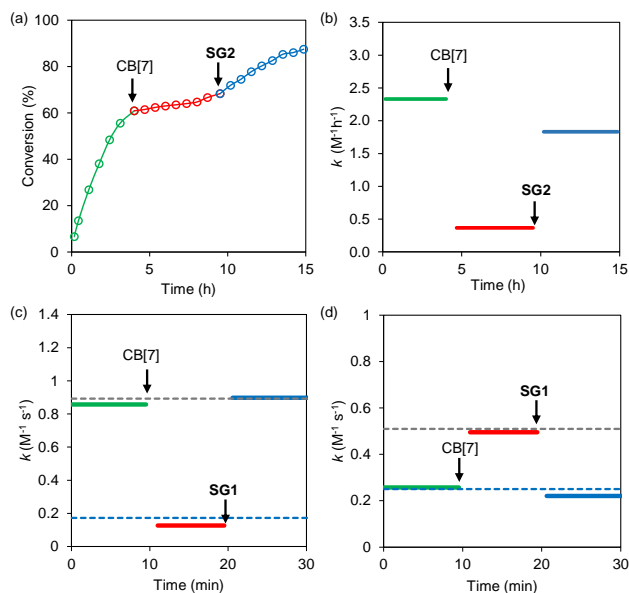
Figure 3.5 Using CB[7] to control the reaction rate by reversibly binding to the catalyst *in-situ*. (a) Conversion of **SM3** in the allylic substitution using **C2**, CB[7] is added after 5 h and **SG2** is added after 10 h; (b) Reaction rate constant as a function of time for the allylic substitution depicted in Fig. 3.5a; (c) Reaction rate constant as a function of time for the hydrazone formation reaction using catalyst **C1**, CB[7] is added after 10 min and **SG1** is added after 20 min; (d) Reaction rate constant as a function of time for the hydrazone formation reaction using catalyst **C5**, CB[7] is added after 10 min and **SG1** is added after 20 min.

3.2.8 A kinetic model to predict reaction rates based on speciation

With this CB[7] responsive catalyst systems in hand, we wondered whether we can control the rate of hydrazone formation precisely by varying the ratio of [catalyst] versus [CB[7]] and predict the reaction rate with a kinetic model. We followed the reactions with different concentrations of catalyst **C1** and CB[7] and determined the reaction rates constants experimentally (Fig. 3.6; black dots). The developed kinetic model to predict the reaction rate constants is shown in Fig. 3.6 (red lines). In the kinetic model we assumed that hydrazone formation occurred without catalyst (k_1), via organocatalysis (k_2), catalyzed by CB[7] (k_3) and catalyzed by the catalyst⊂CB[7] complex (k_4) (Equation 1). The partial reaction rate constants were determined by fitting the concentration profiles of the formation of hydrazone with the least square error method, giving: k_1 = 0.0568 $M^{-1} \cdot s^{-1}$, k_2 = 2.46 × 10^3 $M^{-2} \cdot s^{-1}$, k_3 = 150 $M^{-2} \cdot s^{-1}$, k_4 = 221 $M^{-2} \cdot s^{-1}$ (see Supplementary information).

$k_{total} = k_1 + k_2 \cdot [cat] + k_3 \cdot [CB7] + k_4 \cdot [cat \subset CB7]$ $\qquad$ Equation 1

We quantified how well the model (Fig. 3.6, red line) fits the experimental values by determining the coefficients of determination R^2 [46]. In Fig. 6a we kept the concentration of CB[7] (0.42 mM) constant and varied the concentration of catalyst **C1**. When [**C1**] < [CB[7]], the reaction rate hardly increases due to the inhibiting effect of CB[7] encapsulation, until all CB cavities are occupied and free catalysts become available to the system. When [**C1**] > [CB[7]] the reaction rate increases linearly in the measured concentration range. The highest concentration of catalyst **C1** used was 1.8 mM, where the reaction rate is 25-fold higher than without catalyst **C1**. The reaction rates are predicted well by the linear kinetic model of Equation 1 with an R^2 value of 0.990. In Fig. 3.6b we kept the concentration of catalyst **C1** (0.4 mM) constant and varied the concentration of CB[7]. The reaction rates decreased linearly with increasing CB[7] concentrations until the concentration of CB[7] exceeds the catalyst concentration: then the reaction rate levels off and even increase slightly again, most probably due to the catalytic activity of CB[7] itself (Figure 3.1). The model predicts the experimental data in Fig. 3.6b with an R^2 value of 0.978. Overall, the kinetic model of Equation 1 predicts the reactions rates well, indicating that the reaction rate constants are a linear combination of all processes taking place, which are in turn proportional to the concentrations (speciation, Fig. 3.6) of all catalytic species involved. This linear relationship allows for precise control over catalytic activity through CB[7] complexation.

In Figure 3.6c,d we varied the CB[7] to catalyst **C5** ratio. The reaction rates increases dramatically when we keep the concentration of CB[7] (0.42 mM) constant and increase the concentration of catalyst **C5**, up to 39-fold higher with [**C5**] = 1.8 mM than without catalyst (Fig. 3.6c). Similarly, in Fig. 3.6d, the reaction rate also shows a stark increase with increasing excess of CB[7] when the concentration of catalyst **C5** (0.4 mM) is kept constant. These activities are among the highest recorded for hydrazone formation using small molecule catalysts.[27,28,47] The linear kinetic model (eq. 1) used before does not describe the measurements (R^2 values of -0.372 and 0.210). When comparing the host-guest-complex speciation (free CB[7], free catalyst **C5,** the **C5**⊂CB[7] complex) at varying ratios of CB[7] and catalyst **C5** to the observed rates, a correlation appears to exist between the rate and the product of the complex and excess species concentrations. Such a correlation suggests the existence of a synergistic effect between the excess species (either free CB[7] or free catalyst **C5**) and the **C5**⊂CB[7] complex that leads to a higher catalytic activity than all species separately. In an attempt to incorporate this synergistic effect into the kinetic model, we extended our existing model with two more extra partial rate constants (Equation 2), and adjust this formulation for second-order influence (Equation 3). The new model prediction of the reaction rates in both Figure 3.6c and 3.6d is in much better agreement with the experimental data with R^2 values of respectively 0.856 and 0.997 (purple line), which suggests that there is indeed a synergistic effect and a second-order influence of catalyst

C5. Nevertheless, the mechanism behind this synergistic behavior remains unclear, as eq. 2 and 3 indicate that a large number of catalytic species is involved in the rate determining step, which has a reduced likelihood with increasing complexity.
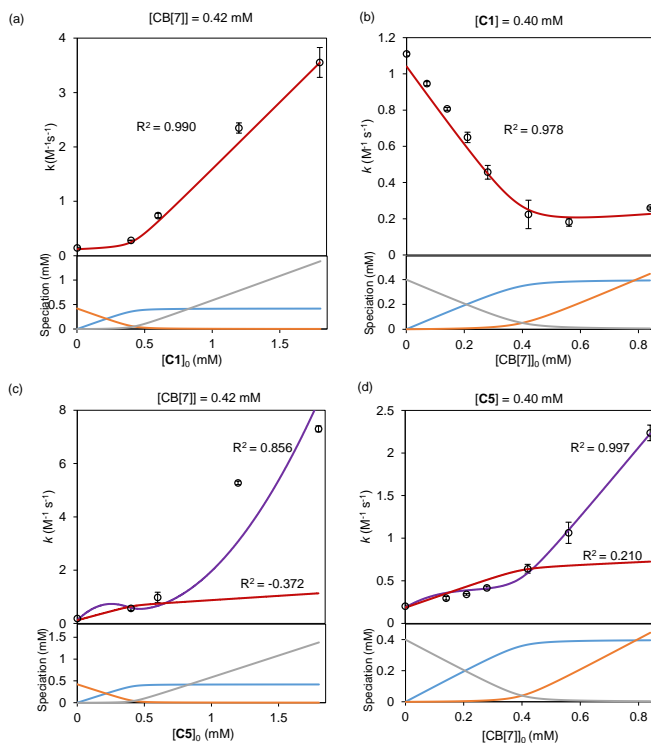

Figure 3.6 The reaction rate can be controlled precisely by adjusting the ratio of CB[7] and catalyst. The upper graphs show the rate constants for hydrazone formation for varying concentrations of added catalyst and CB[7]. Experimentally determined reaction rate constants are shown as markers and the line represents the kinetic model (see SI). The lower graphs show the varying concentrations of different species in the system depending on the catalyst (**C1** or **C5**) and CB[7] concentration, blue = [Catalyst⊂CB7] (mM), orange = [CB7]$_{free}$ (mM), grey = [catalyst]$_{free}$ (mM). (a) The concentration of CB[7] is kept constant at 0.42 mM while the concentration of **C1** is varied between 0–1.8 mM, R^2 = 0.990; (b) The concentration of **C1** is kept constant at 0.4 mM whereas the concentration of CB[7] is varied between 0–0.84 mM, R^2 = 0.978. (c) The concentration of CB[7] is kept constant at 0.42 mM whereas the concentration of **C5** is varied between 0–1.8 mM, R^2(eq. 1) = -0.372 (red line), R^2(eq. 3) = 0.856 (purple line). (d) The concentration of **C5** is kept constant at 0.4 mM

whereas the concentration of CB[7] is varied between 0–0.84 mM, R^2(eq. 1) = 0.210 (red line), R^2(eq. 3) = is 0.997 (purple line).

$$k_{total} = k_1 + k_2 \cdot [\text{cat}] + k_3 \cdot [\text{CB7}] + k_4 \cdot [\text{cat} \subset \text{CB7}] + k_5 \cdot [\text{CB7}] \cdot [\text{cat} \subset \text{CB7}] + k_6 \cdot [\text{cat}] \cdot [\text{cat} \subset \text{CB7}]$$

Equation 2

$$k_{total} = k_1 + k_2 \cdot [\text{cat}] + k_3 \cdot [\text{CB7}] + k_4 \cdot [\text{cat} \subset \text{CB7}] + k_5 \cdot [\text{CB7}] [\text{cat} \subset \text{CB7}] + k_6 \cdot [\text{cat}]^2 \cdot [\text{cat} \subset \text{CB7}]$$

Equation 3

3.3 Conclusions

In this work, we show that supramolecular encapsulation of organocatalysts with CB[7] is a powerful tool to control and tune catalytic activity. Addition of stoichiometric amounts of CB[7] to the catalysts or initiator leads to an immediate reaction rate decrease for catalysts **C1** to **C4**, where CB[7] acts as an inhibitor, and an rate increase for **C5**, where CB[7] acts as an activator. Addition of a stronger binding signal molecule restores the reaction rate back to the original value. These events can be carried out *in situ*, leading to an immediate response. On top of that, we show that adjusting the ratio of catalyst to CB[7] allows precision control over the reaction rate. The experimental data were supported by a kinetic model that accurately predicts the rate of hydrazone formation with catalyst **C1**. For catalyst **C5**, we discovered a disproportionally high increase in reaction rate in non-equimolar mixtures of CB[7] and catalyst **C5**. Fitting this data to a quadratic model suggests a synergistic effect between CB[7], catalyst **C5** and the **C5**⊂CB[7]-complex. Altogether, by using a variety of common, simple, commercially available organocatalysts and different reactions we demonstrated that this strategy is broadly applicable for signal-responsive control of organocatalyst activity. This responsive catalyst system is a step forward in the development of man-made chemical reaction networks and cascades that respond to chemical changes in the environment, as ubiquitously present in nature.

3.4 References

(1)   Ashkenasy, G.; Hermans, T. M.; Otto, S.; Taylor, A. F. Systems Chemistry. *Chem. Soc. Rev.* **2017**, *46* (9), 2543–2554.
(2)   van der Helm, M. P.; de Beun, T.; Eelkema, R. On the Use of Catalysis to Bias Reaction Pathways in Out-of-Equilibrium Systems. *Chem. Sci.* **2021**, *12* (12), 4484–4493.
(3)   Traut, T. W. *Allosteric Regulatory Enzymes*; Springer: New York, 2008.
(4)   Monod, J.; Changeux, J.-P.; Jacob, F. Allosteric Proteins and Cellular Control Systems. *J. Mol. Biol.* **1963**, *6* (4), 306–329.
(5)   Blanco, V.; Leigh, D. A.; Marcos, V. Artificial Switchable Catalysts. *Chem. Soc. Rev.*

2015, *44* (15), 5341–5370.

(6)   Yoon, H. J.; Kuwabara, J.; Kim, J.-H.; Mirkin, C. A. Allosteric Supramolecular Triple-Layer Catalysts. *Science* **2010**, *330* (6000), 66–69.

(7)   Blanco, V.; Carlone, A.; Hänni, K. D.; Leigh, D. A.; Lewandowski, B. A Rotaxane-Based Switchable Organocatalyst. *Angew. Chem. Int. Ed.* **2012**, *51* (21), 5166–5169.

(8)   Blanco, V.; Leigh, D. A.; Marcos, V.; Morales-Serna, J. A.; Nussbaumer, A. L. A Switchable [2]Rotaxane Asymmetric Organocatalyst That Utilizes an Acyclic Chiral Secondary Amine. *J. Am. Chem. Soc.* **2014**, *136* (13), 4905–4908.

(9)   Blanco, V.; Leigh, D. A.; Lewandowska, U.; Lewandowski, B.; Marcos, V. Exploring the Activation Modes of a Rotaxane-Based Switchable Organocatalyst. *J. Am. Chem. Soc.* **2014**, *136* (44), 15775–15780.

(10)   Jans, A. C. H.; Gómez-Suárez, A.; Nolan, S. P.; Reek, J. N. H. A Switchable Gold Catalyst by Encapsulation in a Self-Assembled Cage. *Chem. - A Eur. J.* **2016**, *22* (42), 14836–14839.

(11)   Cavarzan, A.; Scarso, A.; Sgarbossa, P.; Strukul, G.; Reek, J. N. H. Supramolecular Control on Chemo- and Regioselectivity via Encapsulation of (NHC)-Au Catalyst within a Hexameric Self-Assembled Host. *J. Am. Chem. Soc.* **2011**, *133* (9), 2848–2851.

(12)   Bianchini, G.; Scarso, A.; Sorella, G. La; Strukul, G. Switching the Activity of a Photoredox Catalyst through Reversible Encapsulation and Release. *Chem. Commun.* **2012**, *48* (99), 12082–12084.

(13)   Czescik, J.; Lyu, Y.; Neuberg, S.; Scrimin, P.; Mancin, F. Host–Guest Allosteric Control of an Artificial Phosphatase. *J. Am. Chem. Soc.* **2020**, *142* (15), 6837–6841.

(14)   Tonga, G. Y.; Jeong, Y.; Duncan, B.; Mizuhara, T.; Mout, R.; Das, R.; Kim, S. T.; Yeh, Y. C.; Yan, B.; Hou, S.; Rotello, V. M. Supramolecular Regulation of Bioorthogonal Catalysis in Cells Using Nanoparticle-Embedded Transition Metal Catalysts. *Nat. Chem.* **2015**, *7* (7), 597–603.

(15)   Song, D.; Li, B.; Li, X.; Sun, X.; Li, J.; Li, C.; Xu, T.; Zhu, Y.; Li, F.; Wang, N. Orthogonal Supramolecular Assembly Triggered by Inclusion and Exclusion Interactions with Cucurbit[7]Uril for Photocatalytic H2 Evolution. *ChemSusChem* **2020**, *13* (2), 394–399.

(16)   Tang, B.; Zhao, J.; Jiao, Y.; Xu, J.-F.; Zhang, X. Cucurbit[7]Uril Promoted Fenton Oxidation by Modulating the Redox Property of Catalysts. *Chem. Commun.* **2019**, 14127–14130.

(17)   Brevé, T. G.; Filius, M.; Araman, C.; van der Helm, M. P.; Hagedoorn, P. L.; Joo, C.; van Kasteren, S. I.; Eelkema, R. Conditional Copper-Catalyzed Azide–Alkyne Cycloaddition by Catalyst Encapsulation. *Angew. Chem. Int. Ed.* **2020**, *59* (24), 9340–9344.

(18)   Tang, B.; Zhao, J.; Xu, J.-F.; Zhang, X. Cucurbit[n]Urils for Supramolecular Catalysis. *Chem. – A Eur. J.* **2020**, *26* (67), 15446–15460.

(19)   Liu, S.; Ruspic, C.; Mukhopadhyay, P.; Chakrabarti, S.; Zavalij, P. Y.; Isaacs, L. The Cucurbit[n]Uril Family: Prime Components for Self-Sorting Systems. *J. Am. Chem. Soc.* **2005**, *127* (45), 15959–15967.

(20)   Isaacs, L. Cucurbit[n]Urils: From Mechanism to Structure and Function. *Chem. Commun.* **2009**, No. 6, 619–629.

(21)   Barrow, S. J.; Kasera, S.; Rowland, M. J.; Del Barrio, J.; Scherman, O. A. Cucurbituril-Based Molecular Recognition. *Chem. Rev.* **2015**, *115* (22), 12320–12406.

(22)   MacMillan, D. W. C. The Advent and Development of Organocatalysis. *Nature* **2008**, *455* (7211), 304–308.

(23)   van der Helm, M. P.; Klemm, B.; Eelkema, R. Organocatalysis in Aqueous Media. *Nat. Rev. Chem.* **2019**, *3*, 491–508.

(24)   Sinn, S.; Biedermann, F. Chemical Sensors Based on Cucurbit[n]Uril Macrocycles. *Isr. J. Chem.* **2018**, *58* (3), 357–412.

(25)   St-Jacques, A. D.; Wyman, I. W.; Macartney, D. H. Encapsulation of Charge-Diffuse Peralkylated Onium Cations in the Cavity of Cucurbit[7]Uril. *Chem. Commun.* **2008**, No. 40, 4936.

(26)   Moghaddam, S.; Yang, C.; Rekharsky, M.; Ko, Y. H.; Kim, K.; Inoue, Y.; Gilson, M. K. New Ultrahigh Affinity Host-Guest Complexes of Cucurbit[7]Uril with Bicyclo[2.2.2]Octane and Adamantane Guests: Thermodynamic Analysis and Evaluation of M2 Affinity Calculations. *J. Am. Chem. Soc.* **2011**, *133* (10), 3570–3581.

(27)   Crisalli, P.; Kool, E. T. Water-Soluble Organocatalysts for Hydrazone and Oxime Formation. *J. Org. Chem.* **2013**, *78* (3), 1184–1189.

(28)   Larsen, D.; Pittelkow, M.; Karmakar, S.; Kool, E. T. New Organocatalyst Scaffolds with High Activity in Promoting Hydrazone and Oxime Formation at Neutral PH. *Org. Lett.* **2015**, *17* (2), 274–277.

(29)   Kölmel, D. K.; Kool, E. T. Oximes and Hydrazones in Bioconjugation: Mechanism and Catalysis. *Chem. Rev.* **2017**, *117* (15), 10358–10376.

(30)   Trausel, F.; Fan, B.; van Rossum, S. A. P.; van Esch, J. H.; Eelkema, R. Aniline Catalysed Hydrazone Formation Reactions Show a Large Variation in Reaction Rates and Catalytic Effects. *Adv. Synth. Catal.* **2018**, *360* (13), 2571–2576.

(31)   Palma, A.; Artelsmair, M.; Wu, G.; Lu, X.; Barrow, S. J.; Uddin, N.; Rosta, E.; Masson, E.; Scherman, O. A. Cucurbit[7]Uril as a Supramolecular Artificial Enzyme for Diels–Alder Reactions. *Angew. Chem. Int. Ed.* **2017**, *56* (49), 15688–15692.

(32)   Abdel, A.; El, M. S.; Abdelhamid, A. O. 1,4-Diazabicyclo[2.2.2]Octane (DABCO) as a Useful Catalyst in Organic Synthesis. *Eur. J. Chem.* **2012**, *3* (4), 455–460.

(33)   Garzon, C.; Attolini, M.; Maffei, M. Synthesis of β-Aminovinylphosphonates by Organocatalytic Nucleophilic Displacement of Acetate with Amines. *Tetrahedron Lett.* **2010**, *51* (29), 3772–3774.

(34)   Seingeot, A.; Charmasson, Y.; Attolini, M.; Maffei, M. Organocatalyzed Synthesis of Functionalized Vinylphosphonates in Water. *Heteroat. Chem.* **2017**, *28* (1), e21352.

(35)   Dickerson, T. J.; Janda, K. D. Aqueous Aldol Catalysis by a Nicotine Metabolite. *J. Am. Chem. Soc.* **2002**, *124* (13), 3220–3221.

(36)   Mase, N.; Nakai, Y.; Ohara, N.; Yoda, H.; Takabe, K.; Tanaka, F.; Barbas, C. F. Organocatalytic Direct Asymmetric Aldol Reactions in Water. *J. Am. Chem. Soc.*

2006, *128* (3), 734–735.

(37) Raj, M.; Singh, V. K. Organocatalytic Reactions in Water. *Chem. Commun.* **2009**, No. 44, 6687–6703.

(38) Wyman, I. W.; MacArtney, D. H. Cucurbit[7]Uril Host-Guest Complexes with Small Polar Organic Guests in Aqueous Solution. *Org. Biomol. Chem.* **2008**, *6* (10), 1796–1801.

(39) Dolci, E.; Froidevaux, V.; Joly-Duhamel, C.; Auvergne, R.; Boutevin, B.; Caillol, S. Maleimides as a Building Block for the Synthesis of High Performance Polymers. *Polym. Rev.* **2016**, *56* (3), 512–556.

(40) Decker, D. Pyridine Catalyzed Polymerization of Maleimide in Water Solution. *Die Makromol. Chem.* **1973**, *168* (1), 51–58.

(41) Azechi, M.; Toyota, N.; Yamabuki, K.; Onimura, K.; Oishi, T. Anionic Polymerization of N-Substituted Maleimide with Achiral and Chiral Amines as an Initiator. *Polym. Bull.* **2011**, *67* (4), 631–640.

(42) Barooah, N.; Sundararajan, M.; Mohanty, J.; Bhasikuttan, A. C. Synergistic Effect of Intramolecular Charge Transfer toward Supramolecular p K a Shift in Cucurbit[7]Uril Encapsulated Coumarin Dyes. *J. Phys. Chem. B* **2014**, *118* (25), 7136–7146.

(43) Cordes, E. H.; Jencks, W. P. Nucleophilic Catalysis of Semicarbazone Formation by Anilines. *J. Am. Chem. Soc.* **1962**, *84* (5), 826–831.

(44) Sierra-Zenteno, A.; Galán-Vidal, C.; Tapia-Benavides, R. Acid-Base Equilibrium Studies of 2-(Aminomethyl)Benzimidazole in Aqueous Solution. *Rev. la Soc. Química México* **2002**, *46* (2), 125–130.

(45) Ghosh, I.; Nau, W. M. The Strategic Use of Supramolecular PKa Shifts to Enhance the Bioavailability of Drugs. *Adv. Drug Deliv. Rev.* **2012**, *64* (9), 764–783.

(46) Magee, L. R2measures Based on Wald and Likelihood Ratio Joint Significance Tests. *Am. Stat.* **1990**, *44* (3), 250–253.

(47) Zhou, Y.; Piergentili, I.; Hong, J.; Van Der Helm, M. P.; MacChione, M.; Li, Y.; Eelkema, R.; Luo, S. Indoline Catalyzed Acylhydrazone/Oxime Condensation under Neutral Aqueous Conditions. *Org. Lett.* **2020**, *22* (15), 6035–6040.

3.5 Supplementary Information

3.5.1 Experimental details

General methods

NMR spectra were recorded on an Agilent-400 MR DD2 (399.7 MHz for ^{1}H, 100.5 MHz for ^{13}C and 161.8 MHz for ^{31}P) at 298 K using residual protonated solvent signals as internal standard (^{13}C in D_2O was referenced to internal dioxane, δ = 67.19, ^{31}P was referenced to phosphoric acid). UV/Vis spectroscopic measurements were performed on an Analytik Jena Specord 250 spectrophotometer; quartz cuvettes with a path length of 0.2 cm (hydrazone reaction) or 1.0 cm (p*K*a measurement) were used. Measurements were carried at a controlled temperature of 25 °C. Isothermal titration calorimetry (ITC) measurements were carried out at 25 °C using a MicroCal VP-ITC. Kinetic modelling was done using Matlab 2016. LC-MS was performed on a Shimadzu Liquid Chromatograph Mass Spectrometer 2010, LC-8A pump with a diode array detector SPD-M20. The pH was recorded with the Consort C830 pH meter at room temperature. GPC was performed in a Shimadzu Prominence GPC system equipped with 2x PL aquagel-OH MIXED H columns (Agilent, 8 µm, 300 × 7.5 mm) and refractive index detector (RID). Fourier Transform Infrared Spectroscopy (FTIR) spectroscopy was performed with NicoletTM 6700 FT-IR Spectrometer from Thermo Electron Corporation equipped with OMNIC Software using the ATR method.

Materials

All compounds and solvents were used without further purification. The technical solvents were purchased from VWR and the reagent grade solvents were purchased from Sigma Aldrich. Aniline (**C1**) and (1-methyl-1H-benzo[d]imidazol-2-yl)methanamine (**C5**), DABCO (**C2**), glycine (**SM4**), 3-formylbenzoic acid (**SM5**), amantadine hydrochloride (**SG1**), acetone, sodium phosphate monobasic, benzylamine were purchased from Sigma Aldrich. 2-Formylbenzenesulfonic acid sodium salt (**SM1**) was purchased from Honeywell Fluka Fischer Scientific. Hydrazide (**SM2**), (S)-(+)-prolinol (**C3**) was purchased from Alfa Aesar. DL-nornicotine (**C4**) was purchased from Chem-Impex International. Bicyclo[2.2.2]octane-1,4-diyldimethanol (**SG3**), (1*H*-indol-2-yl)methanamine and deuterium oxide were purchased from Fluorochem ltd. Trimethylphenylammonium bromide (**SG2**) was purchased from TCI Europe. Sodium phosphate dibasic was purchased from Acros Organics. Cucurbit[7]uril was purchased from Strem Chemicals Inc., based on the kinetic model and ITC measurements we estimated that it contained about 30 wt% hydration water and acid.

Synthesis and Characterization

**Hydrazone P1 was synthesized according to the following procedure:**

Aldehyde **SM1** (200 mg, 0.961 mmol) was added to a solution of hydrazide **SM2** (114 mg, 0.961 mmol) in absolute ethanol (6 mL). Glacial acetic acid (3 drops) was added and the reaction mixture was stirred overnight at room temperature, until complete conversion of the aldehyde was confirmed by NMR. The solvent was evaporated under reduced pressure to afford the pure hydrazone **P1** product as a white powder (235 mg, 0.763 mmol, 79.4%).
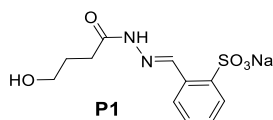
Extra splitting of the peaks in the NMR spectrum is due to cis and trans isomers. **^{1}H NMR** (400 MHz, D_2O) δ 8.95 (s, 1H), 8.14 (d, 2H, *J* = 7.5 Hz), 7.96 (d, 2H, *J* = 7.7 Hz), 7.63 (m, 2H), 3.66 (t, 2H, *J* = 6.5 Hz), 2.46 (t, 2H, *J* = 7.5 Hz), 1.92 (m, 2H). **^{13}C NMR** (100.5 MHz, D_2O) δ 178.9 (cis), 173.7 (trans), 148.2 (trans), 144.9(cis), 142.1 (trans), 141.8 (cis), 132.4 (trans), 132.3 (cis), 131.4 (cis), 131.2 (cis), 130.9 (trans), 130.8 (trans), 128.0 (trans), 127.8 (cis) 127.6 (trans), 127.5 (cis), 61.7 (cis), 61.4 (trans), 31.3 (trans), 29.5 (cis), 28.1 (trans), 27.6 (cis). **MS** (ESI Neg.) m/z: 285.0 [(M − Na$^+$)$^-$] (expected m/z = 285.05). **Extinction coefficient** in phosphate buffer (10 mM, pH 6.0): (2.03 ± 0.003) 10^4 M^{-1} cm^{-1} at 287 nm.

2-(Diethoxyphosphoryl)allyl acetate (SM3) was synthesized according to a reported procedure [1].

Allylic substitution product P2 was synthesized as follows:
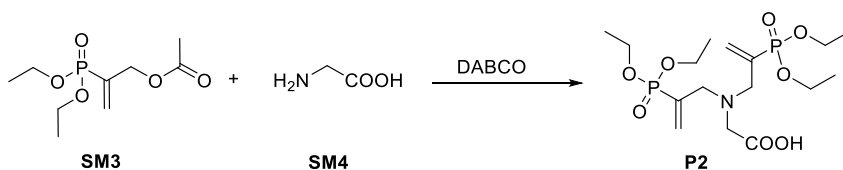
Glycine (**SM4,** 179.2 mg, 2.4 mmol) was added into a solution of **SM3** (60 mg, 0.24 mmol) in phosphate buffer (pH 7.4, 100 mM, 24 mL). DABCO (**C2**, 5.35 mg, 0.048 mM) was added and the reaction mixture was stirred for 24 hours until complete conversion of **SM3** was confirmed by NMR. The solution was acidified with 1 N HCl to pH 2. The solvent was evaporated by freeze drying. The mixture was dissolved in methanol with ultrasonication and the phosphate salts were removed by filtration. The adduct **P2** was purified by silica column chromatography with a gradient of ethyl acetate and methanol (1:10-1:4) and obtained as a white powder (36.7 mg, 0.086 mmol, 72% yield).

P2
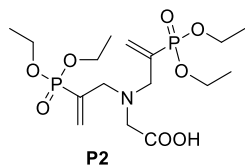
¹H NMR (400 MHz, CDCl₃) δ 6.13 – 5.99 (m, 4H), 4.10 - 4.07 (m, 8H), 3.36 (d, 2H, *J* = 12.8 Hz), 3.26 (s, 2H), 1.31 (t, 12H, *J* = 6.8 Hz). **¹³C NMR** (100 MHz, DMSO-*d₆*) δ ppm 173.97, 137.32 (d, *J* = 168.9Hz), 129.83 (d, *J* = 7.3 Hz), 61.38 (d, *J* = 5.6 Hz), 56.52, 54.53 (d, *J* = 15.2 Hz), 16.17 (d, *J* = 5.9); **³¹P NMR** (DMSO, 162 MHz): δ ppm 20.5. **FT-IR** wavenumber (cm⁻¹) = 3359, 2501, 1636, 1447, 1215, 1020, 975. **MS** (ESI Pos.) m/z: 428.70 [(M + H)]⁺ (expected m/z = 428.16).

Aldol reaction product (P3) was synthesized according to the following procedure:
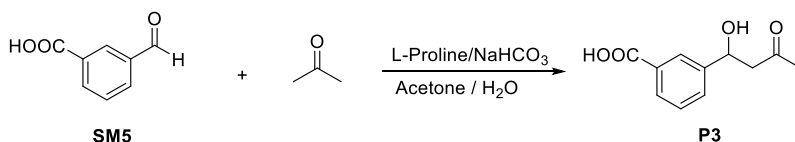
To the solution of aldehyde substrate **SM5** (200 mg, 1.33 mmol) in acetone (20 mL) and water (10 mL), was added L-proline (31 mg, 0.2 mmol, 20 mol%) and NaHCO₃ (150 mg, 1.78 mol). The resulting mixture was stirred at room temperature for 7 days. The pH of reaction solution was adjusted slowly to 2 using aq. HCl (1 M). Acetone was then evaporated under reduced pressure at room temperature. The remaining aqueous phase was extracted using ethyl acetate (3x10 mL). The organic layers were collected and further purified by column chromatography with silica gel, by a gradient of dichloromethane and methanol (1:0 - 10:1), to afford the pure product as colourless oil (131.1 mg, 47.3% yield).

P3
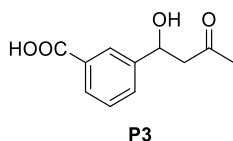
¹H NMR (400 MHz, Methanol-*d₄*) δ 8.03 (s, 1H), 7.88 (d, *J* = 7.6 Hz, 1H), 7.56 (d, *J* = 7.6 Hz, 1H), 7.39 (t, *J* = 8.0 Hz, 1H), 5.16 (dd, *J* = 9.2, 4.4 Hz, 1H), 5.08 (bs, 1H), 2.88 (dd, *J* = 16.4, 9.2 Hz, 1H), 2.75 (dd, *J* = 16.0, 4.0 Hz, 1H), 2.14 (s, 3H). **¹³C NMR** (100 MHz, Methanol-*d₄*) δ 209.57, 169.68, 146.05, 131.58, 129.76, 129.56, 128.13, 70.52, 53.23, 49.00, 30.68. **FT-IR** wavenumber (cm⁻¹) =3045, 1697, 1608, 1590, 1364, 1267, 1189, 1070, 816, 756, 696, 658. **MS** (ESI Neg.) m/z: 208.05 [(M − H)]⁻ (expected m/z = 207.07).

2-Maleimidoacetic Acid (SM6) was synthesized using a reported procedure [2]**.**

The oligomerization of 2-Maleimidoacetic Acid was performed as follows:
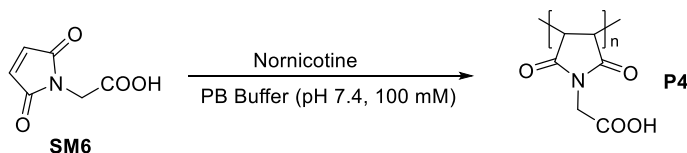
To a solution of 2-maleimidoacetic acid **SM5** (46.5 mg, 0.3 mmol) in phosphate buffer (pH 7.4, 100 mM, 30 mL), was added nornicotine **C4** (20.67 µL, 0.15 mmol). The mixture was stirred for 3 days until complete conversion of the 2-maleimidoacetic acid was confirmed by NMR. The water was evaporated by freeze drying. The mixture was washed three times with ether and acetone.

^{1}H NMR (400 MHz, D$_2$O) δ 8.23 – 7.17 (m, aromatic parts in nornicotine [3]), 6.07 and 5.66 (d, ring opening of 2-maleimidoacetic acid), 4.02-3.39 (m, terminal proton and NC*H*$_2$COO in oligomer), 2.94-2.38 (CH-CH in oligomer), 1.99-1.54 (aliphatic parts in nornicotine).

GPC: 10 µL of 10 mg/mL polymer solution (MeOH/H$_2$O=1:4) was injected and eluted with a MeOH and H$_2$O mixture (1:4) at 1 mL/min for 30 min. M$_n$ = 1425 g/mol, M$_w$ = 1524 g/mol, M$_z$ = 1628 g/mol. Đ= 1.07.

3.5.2 UV/vis measurements to follow the hydrazone reactions
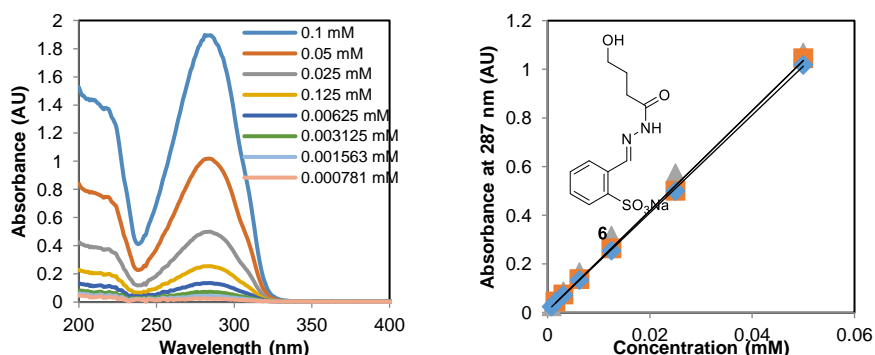
Extinction coefficient of hydrazone P1

Figure S3.1: Extinction coefficient for hydrazone **P1** at 287 nm: (2.03 ± 0.003) 10^4 M^{-1} cm^{-1}, error is the standard error of the mean (n = 3). (**a**) UV/vis spectra of hydrazone **P1** at different concentrations. (**b**)

Absorbance at 287 nm of hydrazone **P1** at different concentrations, the experimental data of 3 experiments are shown.
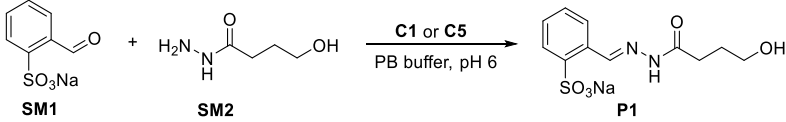
Fitting pseudo-first order reaction rate

The second-order reaction rate constants were determined by fitting the relative absorbance ($A_t - A_0$) over time with the following equation:

$$A = \frac{A_{max} \cdot e^{([H]_0 - [B]_0) \cdot kt} - A_{max}}{\frac{[H]_0}{[B]_0} \cdot e^{([H]_0 - [B]_0) \cdot kt} - 1}$$ (eq. S1) [4]

$[H]_0$ = concentration of hydrazide **SM2** at t_0, $[B]_0$ = concentration of aldehyde **SM1** at t_0, A_{max} = the maximum absorbance (when all **SM2** is converted), k is Pseudo-first order reaction rate constant ($M^{-1} s^{-1}$).

Table S3.1 Summary of the reaction rate constants of the hydrazone formation reaction[a].

Catalyst system[a]	k ($M^{-1} s^{-1}$)	k_{rel}[b]	R^2
none	0.075 ± 0.002	1.0	0.99974
cat **C1**	0.96 ± 0.03	13	0.99974
cat **C1** + CB[7]	0.28 ± 0.01	3.7	0.99916
cat **C1** + CB[7] + **SG1**	1.2 ± 0.03	15	0.99831
cat **C5**	0.19 ± 0.01	2.5	0.99959
cat **C5** + CB[7]	0.57 ± 0.08	7.5	0.99908
cat **C5** + CB[7] + **SG1**	0.17 ± 0.004	2.3	0.99957

[a]Conditions: 0.4 mM aldehyde **SM1**, 0.04 mM hydrazide **SM2**, 0.4 mM catalyst **C1**, 0.42 mM CB[7], 0.8 mM signal molecule **SG1** in 10 mM sodium phosphate buffer pH 6.0, 25 °C. [b] k_{rel} is the ratio of the rate constant of the reaction in the presence of catalyst, host and/or guest, and the rate constant of the uncatalyzed reaction: $k_{rel} = k_{cat} / k_{uncat}$.

3.5.3 NMR measurements to follow the allylic substitution reaction

General procedure to follow the allylic substitution reaction

The reaction solution was prepared from dilution of a concentrated stock solution (in pH 7.4 100 mM phosphate buffer) to make a 1 mL solution in pH 7.4 100 mM phosphate buffer containing 10 mM **SM3,** 100 mM **SM4,** 5 mM DMSO, 2 mM DABCO (**C2**), 6 mM

SG2 and 10% D_2O. CB[7] (5.82 mg, 3.5 mM) was added as a solid. The conversion of **SM3** was determined by ^1H NMR analysis over time.
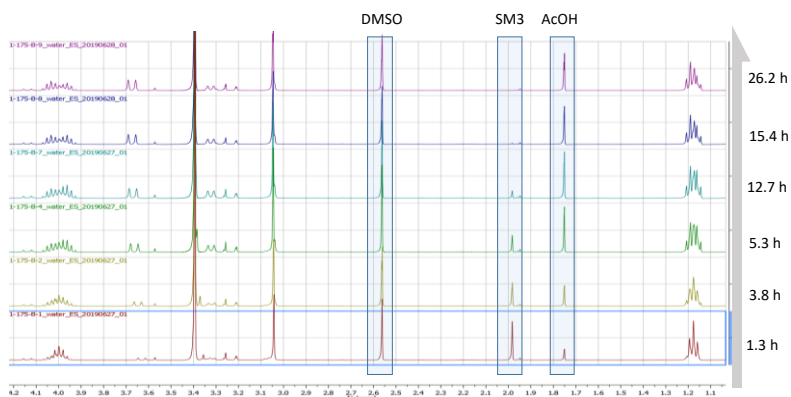

Figure S3.2 NMR spectra overlay to follow the allylic substitution reaction over time.

Fitting pseudo-first order reaction rate

The pseudo-first order reaction rate constants were determined by fitting the conversion of **SM3** ($[B]_t$) over time with the following equation:

$$\ln\left\{\frac{[B]_t}{[B]_0}\right\} = -k[A]_0 t \qquad \text{(eq. S2)}$$

$[B]_0$ = initial concentration of **SM3** at t_0, 0.01 M; $[B]_t$ = the concentration of **SM3** at every specified time obtained from ^1H NMR (Figure S2), with DMSO as the standard; k is the pseudo-first order reaction rate constant (M^{-1} h^{-1}), $[A]_0$ = initial concentration of **SM4**, 0.1 M.

Table S3.2 Summary of the reaction rate constants of the allylic substitution reaction.

Catalyst system	k (M^{-1} h^{-1})	k_{rel}	R^2
none	1.19 ± 0.0144	1.0	0.9988
CB[7]	1.05 ± 0.0289	0.9	0.9955
cat **C2**	15.86 ± 0.2	13.3	0.9990
cat **C2** + CB[7]	1.23 ± 0.0441	1.0	0.98478

cat **C2** + CB[7] + **SG2**	13.57 ± 0.105	11.4	0.99916
SG2	1.24 ± 0.0103	1.0	0.99958
SG2 + CB[7]	1.11 ± 0.0312	0.9	0.99603

[a]Conditions: 10 mM aldehyde **SM3**, 100 mM **SM4**, 2 mM catalyst **C2**, 3.5 mM CB[7], 6 mM signal molecule **SG2** in 100 mM sodium phosphate buffer pH 7.4, 25 °C.[b] k_{rel} is the ratio of the rate constant of the reaction in the presence of catalyst, host and/or guest, and the rate constant of the uncatalyzed reaction: $k_{rel} = k_{cat}/ k_{uncat}$.

3.5.4 NMR measurements to follow the aldol reaction

General procedure to follow the aldol reaction:

The reaction solution was prepared from dilution of a concentrated stock solution (in pH 7.4, 100mM phosphate buffer) to make a 0.7 mL solution in pH 7.4 100 mM phosphate buffer containing 20 mM **SM5,** 600 mM Acetone**,** 6 mM Prolinol (**C3**), 12 mM **SG2** or **SG3** and 10% D_2O. CB[7] (8.148 mg, 7 mM) was added as a solid. The conversion of **SM5** was determined by ^1H NMR analysis as a function of time.
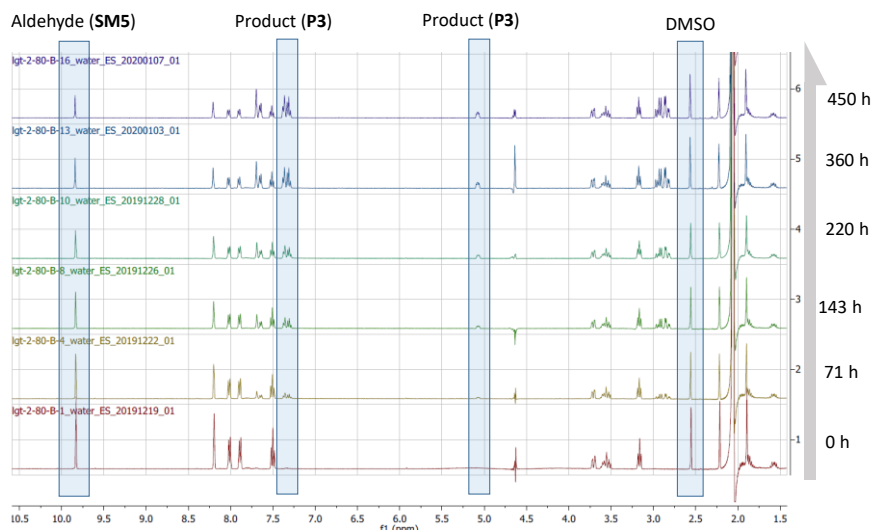

Figure S3.3 NMR spectra overlay to follow the aldol reaction over time.

Fitting pseudo-first order reaction rate

The pseudo-first order reaction rate constants were determined by fitting the conversion of **SM5** ([B]$_t$) over time with the following equation:

$$\ln\left\{\frac{[B]_t}{[B]_0}\right\} = -k[A]_0 t \qquad\qquad\qquad\text{(eq. S3)}$$

$[B]_0$ = initial concentration of **SM5** at t_0, 0.02 M; $[B]_t$ = the concentration of **SM5** at every specified time obtained from ^{1}H NMR (Figure S3), with DMSO as the standard; k is the pseudo-first order reaction rate constant (M^{-1} h^{-1}), $[A]_0$ = initial concentration of acetone, 0.6 M.

Table S3.3 Summary of the reaction rate constants of aldol the reaction.

Catalyst system	k ($10^{-3}M^{-1}$ h^{-1})	k_{rel}	R^2
none	0.25 ± 0.0126	1	0.95382
CB[7]	0.55 ± 0.0165	2.21	0.98432
C3	3.17 ± 0.0265	12.67	0.99889
C3 + CB[7]	2.03 ± 0.0394	8.13	0.99328
C3 + CB[7] + **SG2**	1.82 ± 0.0358	7.26	0.99419
C3 + CB[7] + **SG3**	1.52 ± 0.0482	6.06	0.98406
SG3	0.47 ± 0.0294	1.87	0.94392
CB[7] + **SG3**	0.63 ± 0.0415	2.52	0.94257

[a]Conditions: 20 mM aldehyde **SM5**, 600 mM acetone, 6 mM catalyst **C3**, 7 mM CB[7], 12 mM signal molecule **SG2** or **SG3** in 100 mM sodium phosphate buffer pH 7.4 containing 10% D_2O, 25 °C.[b] k_{rel} is the ratio of the rate constant of the reaction in the presence of catalyst, host and/or guest, and the rate constant of the uncatalyzed reaction: $k_{rel} = k_{cat}/ k_{uncat}$.

3.5.5 NMR measurements to follow the oligomerization reaction of 2-Maleimidoacetic Acid

General procedure to follow the oligomerization reaction

The reaction solution was prepared from dilution of a concentrated stock solution to make a 0.7 mL solution in pH 7.4 100 mM phosphate buffer containing 10 mM **SM6,** 1 mM Dimethylmalonic acid (as NMR standard), 5 mM Nornicotine (**C4**), 12 mM **SG2** and 10% D_2O. CB[7] (8.148 mg, 7 mM) was added as a solid. The conversion of **SM6** was determined by ^{1}H NMR analysis over time.
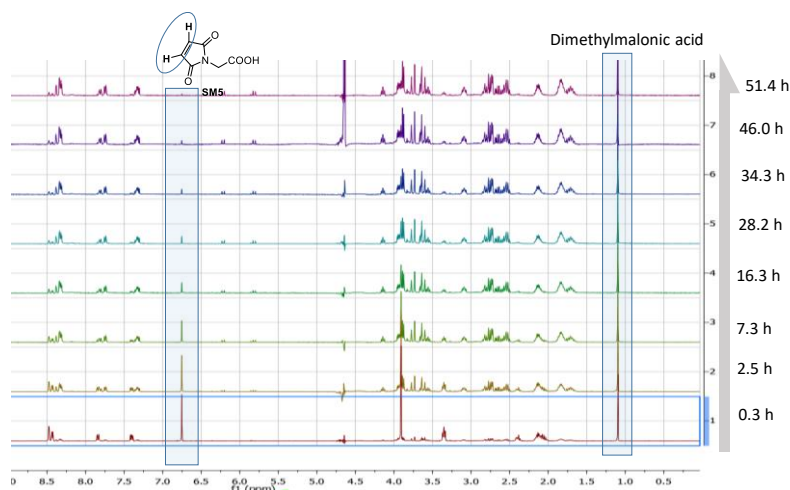
Figure S3.4 NMR spectra overlay to follow the oligomerization of 2-Maleimidoacetic Acid over time.

Fitting first order reaction rate

The first order reaction rate constants were determined by fitting the concentration of **SM6** ($[A]_t$) over time with the following equation:

$$\ln\left\{\frac{[A]_t}{[A]_0}\right\} = -kt$$

(eq. S4)

$[A]_0$ = initial concentration of **SM6** at t_0, 0.01 M; $[A]_t$ = the concentration of **SM6** at every specified time obtained from ^{1}H NMR (Figure S3.4), with Dimethylmalonic Acid as the standard; k is the first order reaction rate constant (h^{-1}).

Table S3.4 Summary of the reaction rate constants of the oligomerization reaction of Maleimide.

Catalyst system	k (h^{-1})	k_{rel}	R^2
none	0.89 ± 0.0158	1.0	0.99501
CB[7]	0.72 ± 0.0146	0.8	0.99426
Cat **C4**	5.29 ± 0.219	5.9	0.96988
Cat **C4** + CB[7]	1.27 ± 0.0182	1.4	0.99712

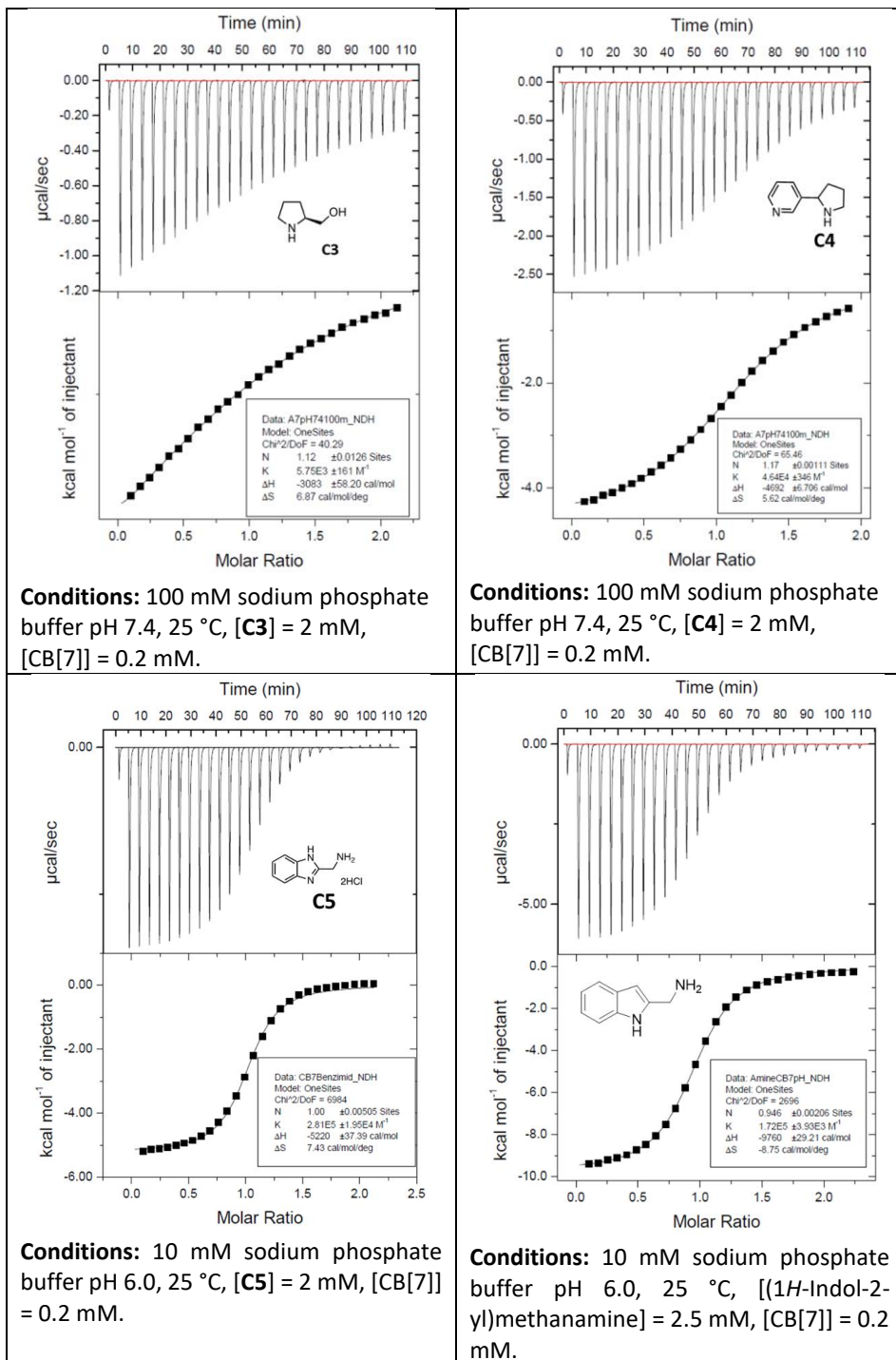|			
Cat **C4** + CB[7] + **SG2**	5.34 ± 0.174	6.0	0.98442
SG2	0.88 ± 0.0085	1.0	0.99843

[a]Conditions: 10 mM **SM6**, 5 mM catalyst **C4**, 7 mM CB[7], 12 mM signal molecule **SG2** in 100 mM sodium phosphate buffer pH 7.4, 25 °C.[b] k_{rel} is the ratio of the rate constant of the reaction in the presence of catalyst, host and/or guest, and the rate constant of the uncatalyzed reaction: k_{rel} = k_{cat}/ k_{uncat}.
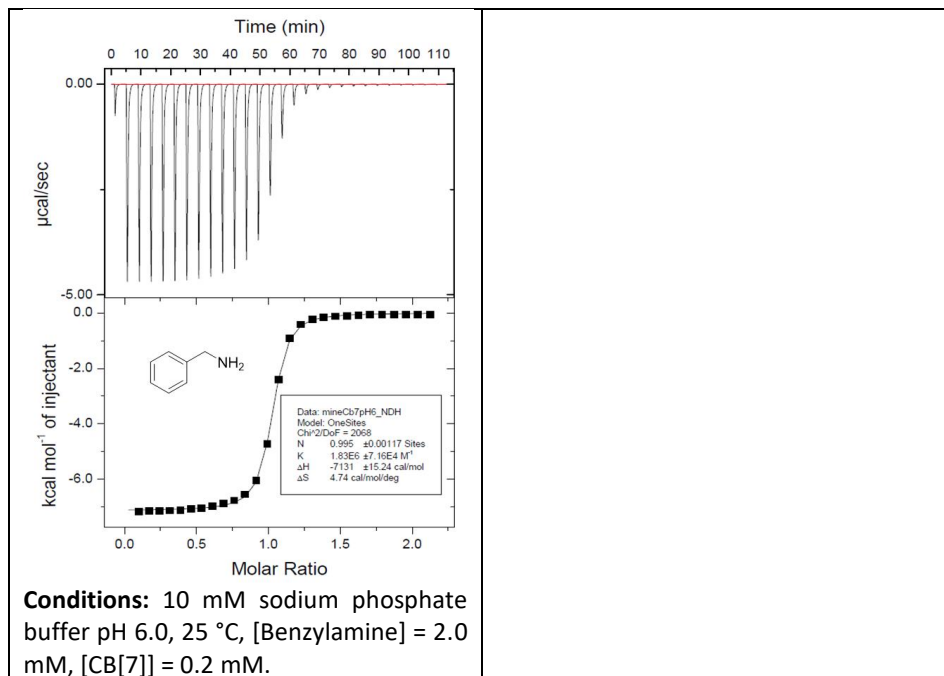
3.5.6 Isothermal titration calorimetry results

General procedure: a solution of guest molecule was titrated to a CB[7] solution at 25 °C, both in 10 or 100 mM sodium phosphate buffer. The first titration point of each ITC measurement was omitted. Binding constants were fitted with Microcal LLC ITC Origin 7 software.
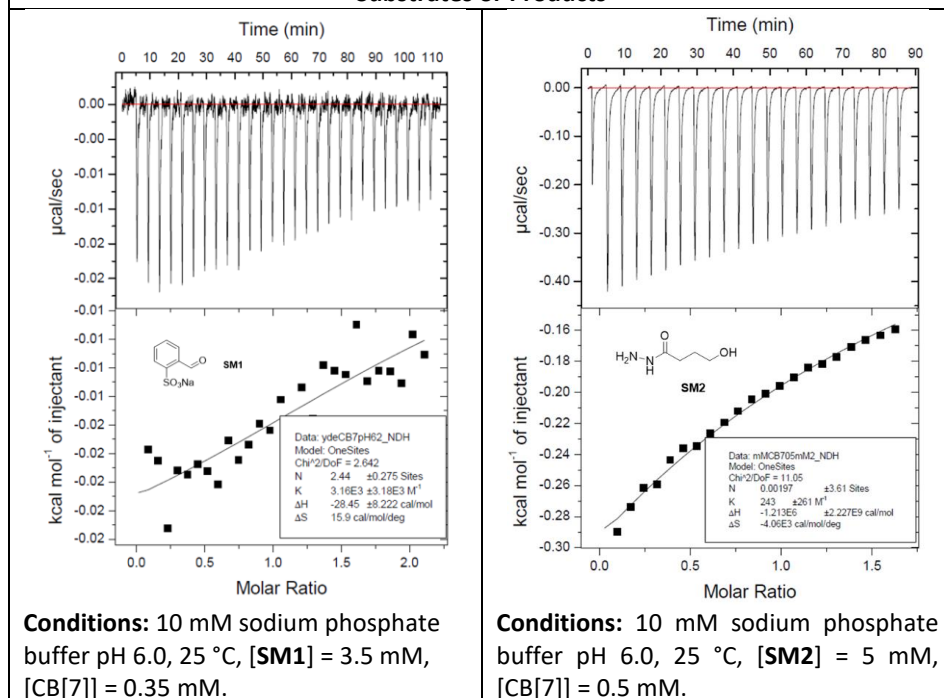
Table S3.5 Overview of all the ITC Binding constants of compounds measured in this work.
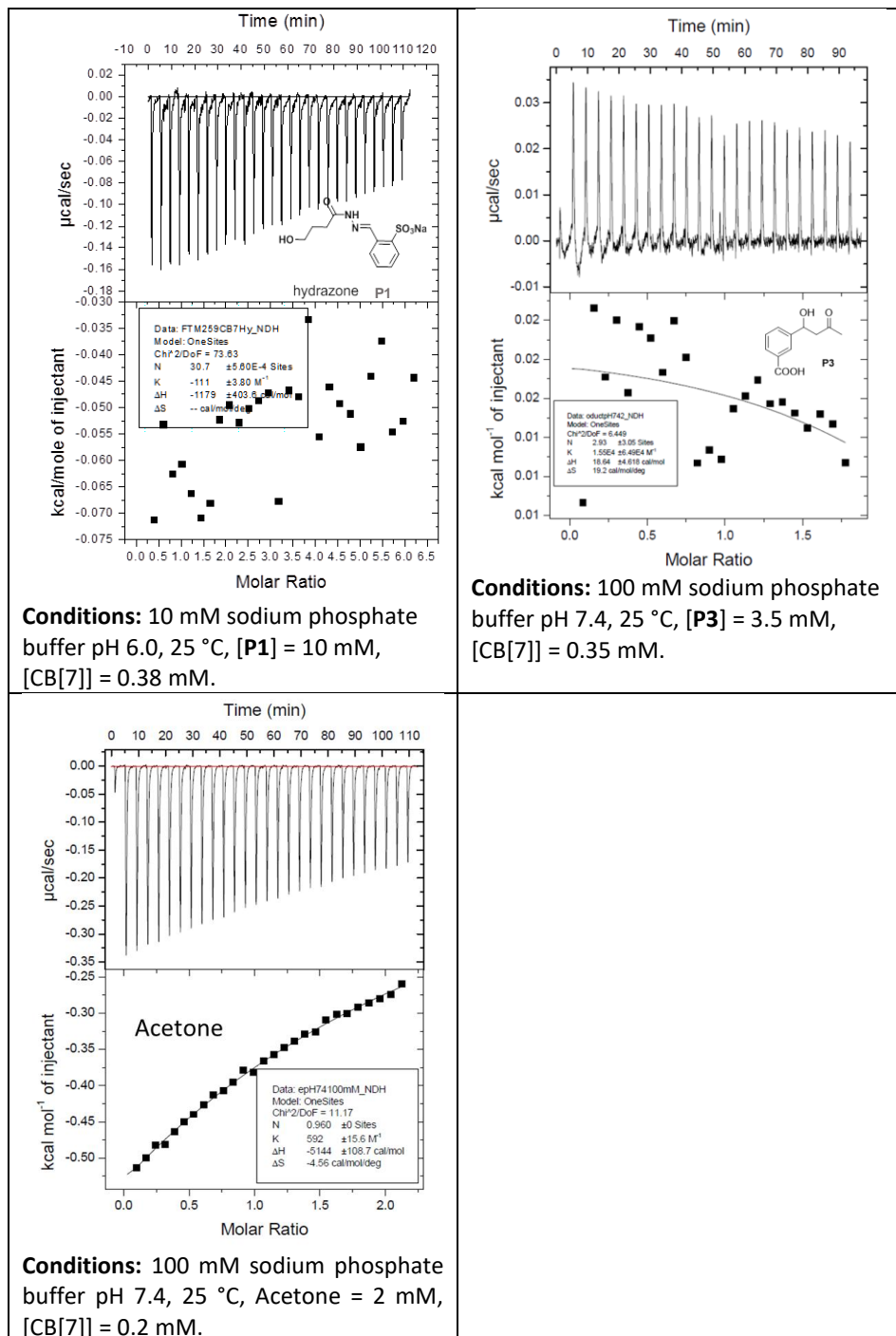

Conditions: 10 mM sodium phosphate buffer pH 6.0, 25 °C, [**C1**] = 2 mM, [CB[7]] = 0.2 mM.

Conditions: 100 mM sodium phosphate buffer pH 7.4, 25 °C, [**C2**] = 2 mM, [CB[7]] = 0.2 mM.

Conditions: 100 mM sodium phosphate buffer pH 7.4, 25 °C, [**C3**] = 2 mM, [CB[7]] = 0.2 mM.

Conditions: 100 mM sodium phosphate buffer pH 7.4, 25 °C, [**C4**] = 2 mM, [CB[7]] = 0.2 mM.

Conditions: 10 mM sodium phosphate buffer pH 6.0, 25 °C, [**C5**] = 2 mM, [CB[7]] = 0.2 mM.

Conditions: 10 mM sodium phosphate buffer pH 6.0, 25 °C, [(1*H*-Indol-2-yl)methanamine] = 2.5 mM, [CB[7]] = 0.2 mM.

Conditions: 10 mM sodium phosphate buffer pH 6.0, 25 °C, [Benzylamine] = 2.0 mM, [CB[7]] = 0.2 mM.

Substrates or Products

Conditions: 10 mM sodium phosphate buffer pH 6.0, 25 °C, [**SM1**] = 3.5 mM, [CB[7]] = 0.35 mM.

Conditions: 10 mM sodium phosphate buffer pH 6.0, 25 °C, [**SM2**] = 5 mM, [CB[7]] = 0.5 mM.

Conditions: 100 mM sodium phosphate buffer pH 7.4, 25 °C, [**SM3**] = 3.5 mM, [CB[7]] = 0.35 mM.

Conditions: 100 mM sodium phosphate buffer pH 7.4, 25 °C, [**SM4**] = 10 mM, [CB[7]] = 0.35 mM.

Conditions: 100 mM sodium phosphate buffer pH 7.4, 25 °C, [**SM5**] = 10 mM, [CB[7]] = 0.35 mM.

Conditions: 100 mM sodium phosphate buffer pH 7.4, 25 °C, [**SM6**] = 10 mM, [CB[7]] = 0.35 mM.

Conditions: 10 mM sodium phosphate buffer pH 6.0, 25 °C, [**P1**] = 10 mM, [CB[7]] = 0.38 mM.

Conditions: 100 mM sodium phosphate buffer pH 7.4, 25 °C, [**P3**] = 3.5 mM, [CB[7]] = 0.35 mM.

Conditions: 100 mM sodium phosphate buffer pH 7.4, 25 °C, Acetone = 2 mM, [CB[7]] = 0.2 mM.

3.5.7. NMR binding experiments

Structure of the complexes between catalyst **C1**-**C5**, and CB[7] was determined using ^{1}H-NMR binding studies (Figures S3.5-S3.8). Generally, addition of CB[7] to a solution of catalysts resulted in an upfield shift of the protons on the catalysts, indicative of being inside the CB cavity [5]. Addition of CB[7] to a solution of catalysts resulted a downfield shift for the protons, indicating of being at the port of CB[7] cavity. Spectra were mostly taken both in phosphate buffer, but in D_2O for cases that the catalyst (**C5**) would overlap with the water peak in phosphate buffer.
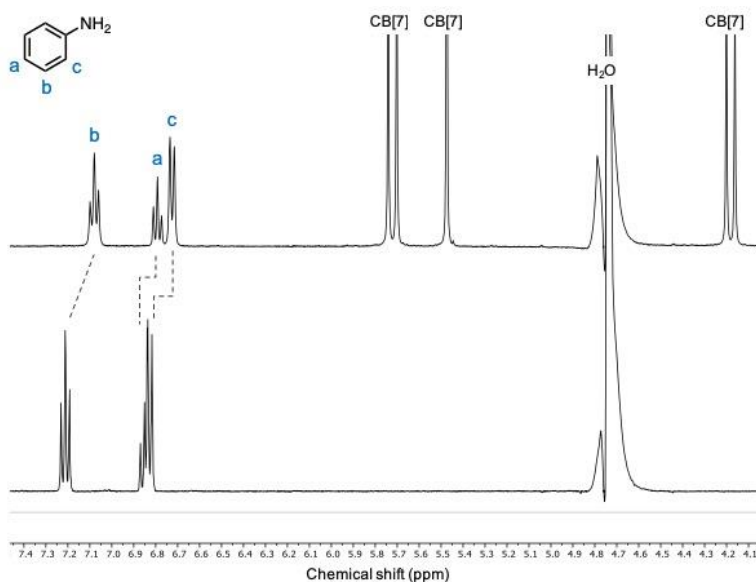
Figure S3.5 ^{1}H NMR (PRESAT) spectra of catalyst **C1** (lower spectrum) and catalyst **C1**⊂CB[7] (upper spectrum) in 10 mM sodium phosphate buffer pH 6.0. [catalyst **C1**] = 6 mM, [CB[7]] = 6.3 mM.
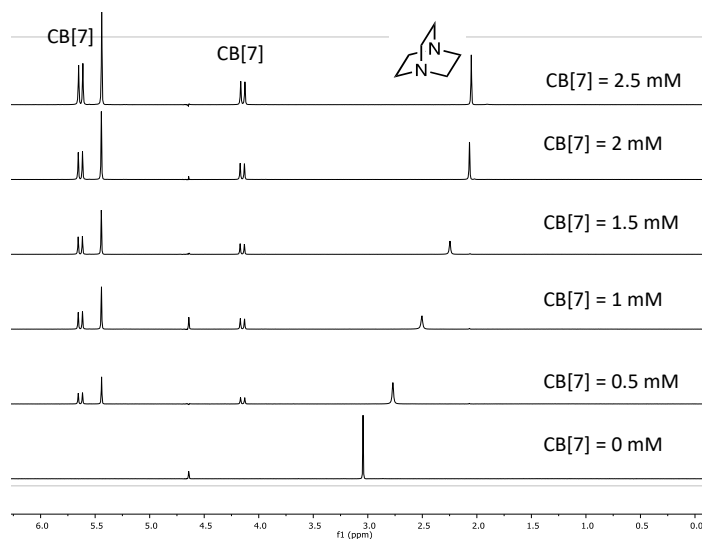
Figure S3.6 ^{1}H NMR (water suppression) spectra of catalyst **C2** (2 mM) and with increasing concentration of CB[7] (0~2.5 mM) in 100 mM sodium phosphate buffer pH 7.4.
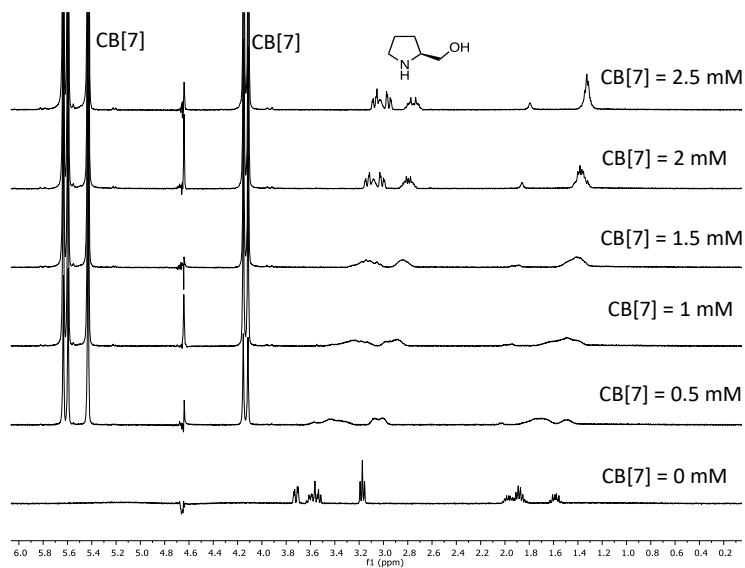
Figure S3.7 ^{1}H NMR (water suppression) spectra of catalyst **C3** (2 mM) and with increasing concentration of CB[7] (0~2.5 mM) in 100 mM sodium phosphate buffer pH 7.4.
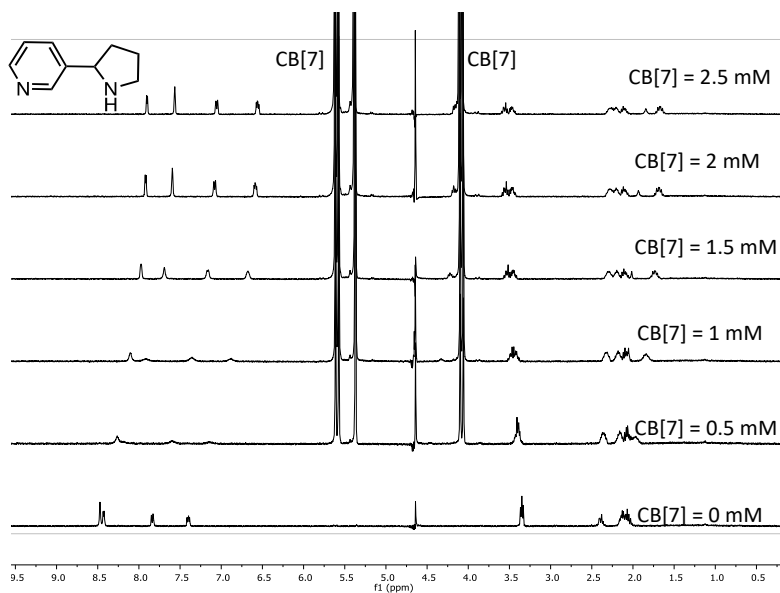
Figure S3.8 ^{1}H NMR (water suppression) spectra of catalyst **C4** (2 mM) and with increasing concentration of CB[7] (0~2.5 mM) in 100 mM sodium phosphate buffer pH 7.4.
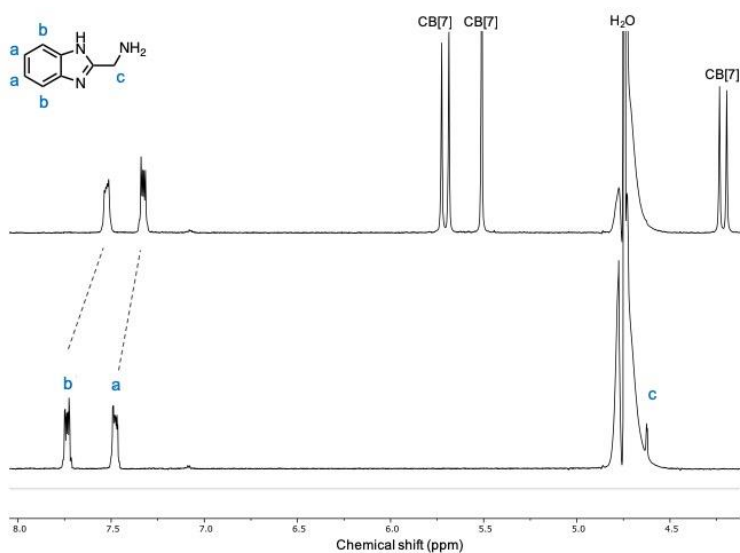
Figure S3.9 ^{1}H NMR spectra of catalyst **C5** (lower spectrum) and catalyst **C5**⊂CB[7] (upper spectrum) in 10 mM sodium phosphate buffer pH 6.0. [catalyst **C5**] **=** 6 mM, CB[7] = 6.3 mM.
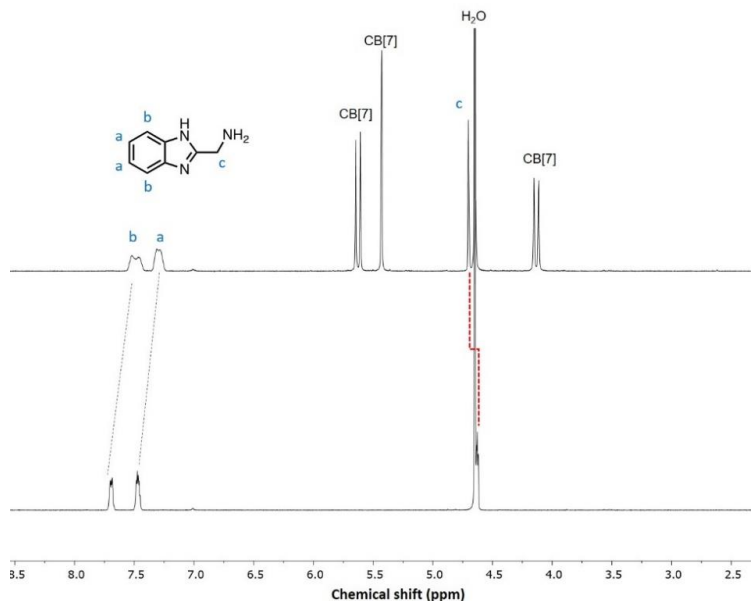
Figure S3.10 ^{1}H NMR spectra of catalyst **C5** (lower spectrum) and catalyst **C5**⊂CB[7] (upper spectrum) in D_2O. [catalyst **C5**] **=** 6 mM, [CB[7]] = 6.3 mM. The downfield shift of protons c is indicated in red.

^{1}H-NMR of **SM1** to **SM6** substrate solutions were measured with and without CB[7], showing no peak shifts, demonstrating very low binding affinity to CB[7] (Figure S3.11 to S3.15). But Acetone peak shifts in the presence of CB[7] (Figure S3.16).
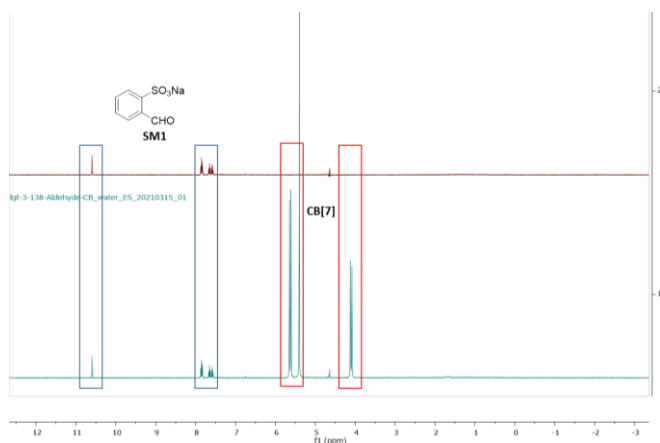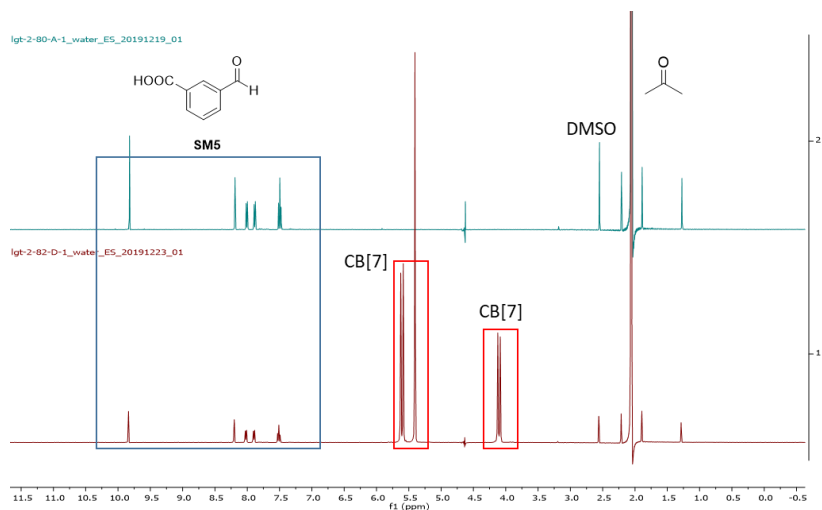

Figure S3.11 ^{1}H NMR spectra (water suppression) of the substrates **SM1** (upper), and in the presence of CB[7] (lower spectrum) in 10 mM sodium phosphate buffer pH 6.0. [**SM1**] **=** 2 mM, [CB[7]] = 2 mM.
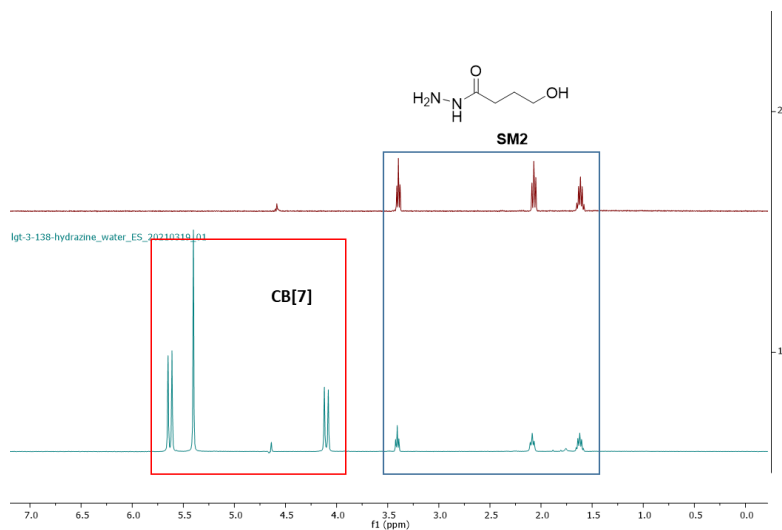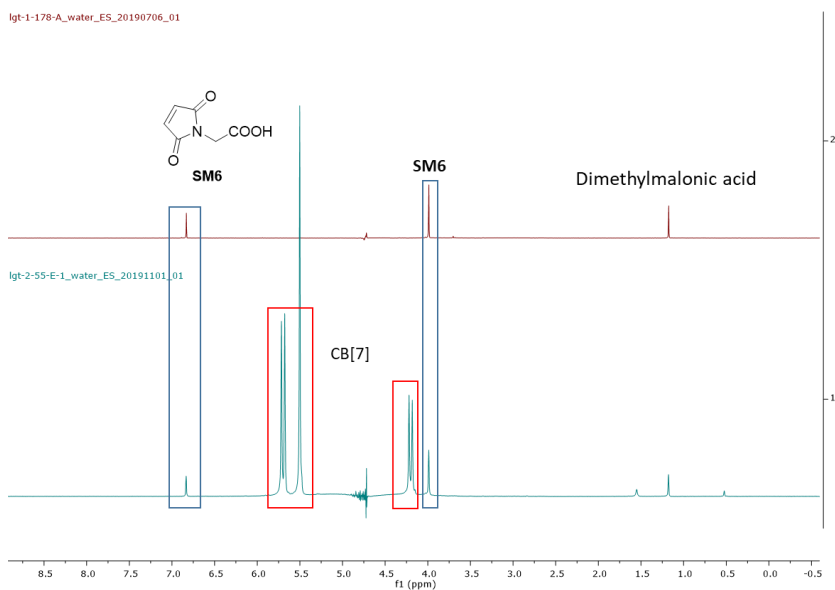
Figure S3.12 ^{1}H NMR spectra (water suppression) of the substrates **SM2** (upper), and in the presence of CB[7] (lower spectrum) in 10 mM sodium phosphate buffer pH 6.0. [**SM2**] = 2 mM, [CB[7]] = 1 mM.
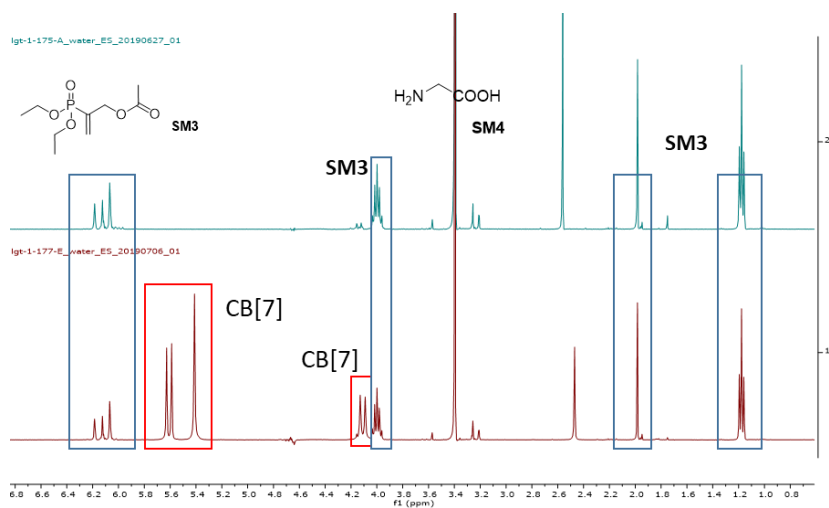
Figure S3.13 ^{1}H NMR spectra (water suppression) of the substrates **SM3** and **SM4** (upper spectrum), and in the presence of CB[7] (lower spectrum) in 100 mM sodium phosphate buffer pH 7.4. [**SM3**] = 10 mM, [**SM4**] = 100 mM. [CB[7]] = 3.5 mM
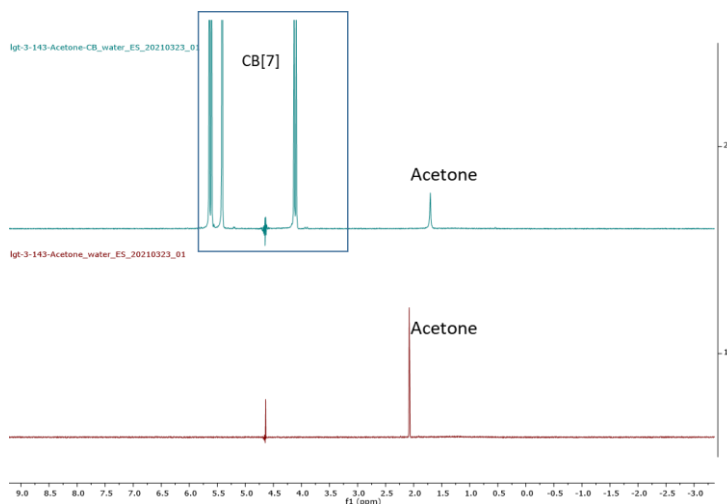
Figure S3.14 ^{1}H NMR spectra (water suppression) of the substrates **SM5** and acetone (upper spectrum), and in the presence of CB[7] (lower spectrum) in 100 mM sodium phosphate buffer pH 7.4. [**SM5**] **=** 20 mM, acetone = 600 mM. [CB[7]] = 7.0 mM.

Figure S3.15 ^{1}H NMR spectra (water suppression) of the substrates **SM6** (upper spectrum), and in the presence of CB[7] (lower spectrum) in 100 mM sodium phosphate buffer pH 7.4. [**SM6**] **=** 10 mM, [CB[7]] = 7.0 mM.

Figure S3.16 ^{1}H NMR spectra (water suppression) of acetone (lower spectrum), and in the presence of CB[7] (upper spectrum) in 100 mM sodium phosphate buffer pH 7.4. [acetone] = 2 mM. [CB[7]] = 2 mM.

3.5.8. Estimation of pK_a of catalysts in absence and presence of CB[7]

The pK_a value of catalysts **C1**, **C5**, benzylamine and (1*H*-indol-2-yl)methanamine in absence or presence of CB[7] were estimated according to a reported method. [6]

Generally, 0.1 mM free catalyst was dissolved in pH 2 aqueous solution. The solution pH was carefully increased by adding 1-2 µL aliquots of NaOH (1 M) solution containing 0.1 mM catalyst. Following that, pH and UV absorbance was measured at room temperature. The pK_a were estimated by following the absorption with respect to solution pH as shown in the Figure S3.17. The optical absorbance measured at a particular wavelength is related to the pK_a of the absorbing species as shown in the equation S5. The absorbance at that wavelength are plotted against the solution pH and the pK_a values are obtained from the best fit model by nonlinear curve fitting of equation S5 (Figure S3.18).

$$OC_\lambda = \frac{OC_{CH+}^{\infty}}{1+10^{pH-pK_a}} + \frac{OC_C^{\infty}}{1+10^{pK_a-pH}} \qquad\qquad \text{Eq S5}$$

Where OC_{CH+}^{∞} is the highest optical density of the acid form and OC_C^{∞} is the highest optical density of the neutral form at the specific wavelength.
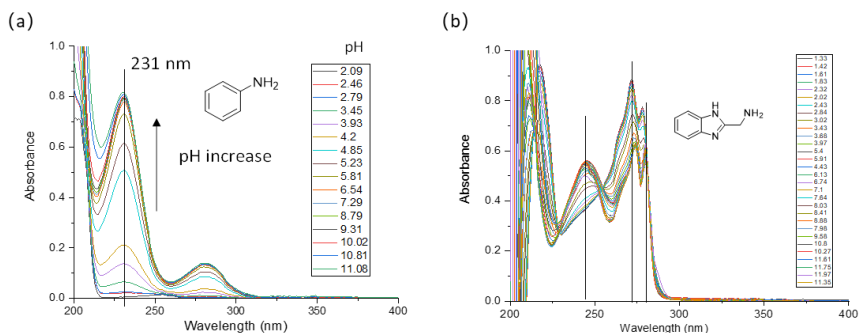
Figure S3.17 Absorption spectra of **C1** (a) and **C5** (b) at different pH. [catalyst **C1**] = 0.1 mM, [catalyst **C5**] = 0.1 mM.
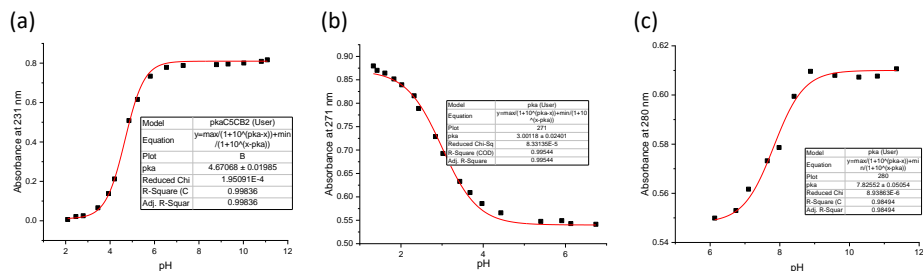

Figure S3.18 pK_a titration curves at specific wavelength to estimate pK_a of **C1** and **C5**. (a) Absorbance of **C1** at 231 nm was plotted against pH, pK_a was estimated as 4.67 ± 0.0199; (b) Absorbance of **C5** at 271 nm was plotted against pH, pK_{a1} was estimated as 3.00 ± 0.0240; (c) Absorbance of **C5** at 280 nm was plotted against pH, pK_{a2} was estimated as 7.82 ± 0.0505. Markers indicate experimental data, lines indicate fitted curve.

The pK_a values of the catalysts in the presence of CB[7] were estimated by the same method described above, where the concentration of catalysts **C1** and **C5** were 0.1 mM and CB[7] is 0.11 mM.
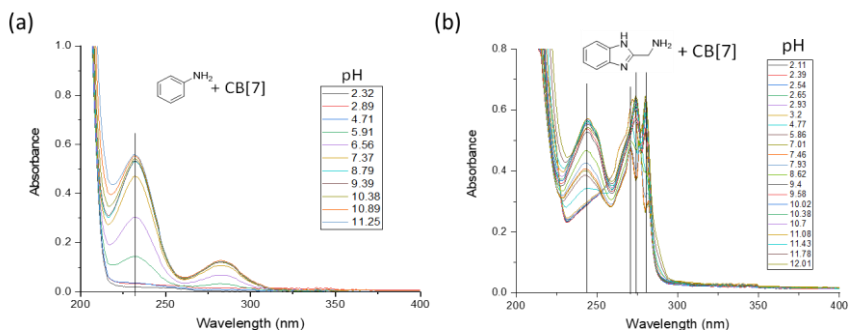
Figure S3.19 Absorption spectra of **C1+**CB[7] (a) and **C5+**CB[7] (b) at different pH. [catalyst **C1**] **=** 0.1 mM, [CB[7]]=0.11 mM; [catalyst **C5**] = 0.1 mM, [CB[7]]=0.11 mM.
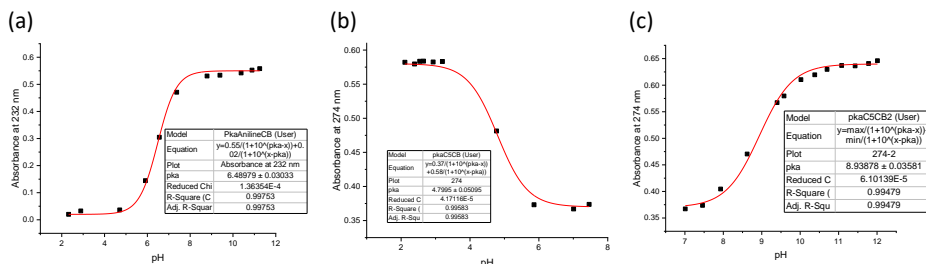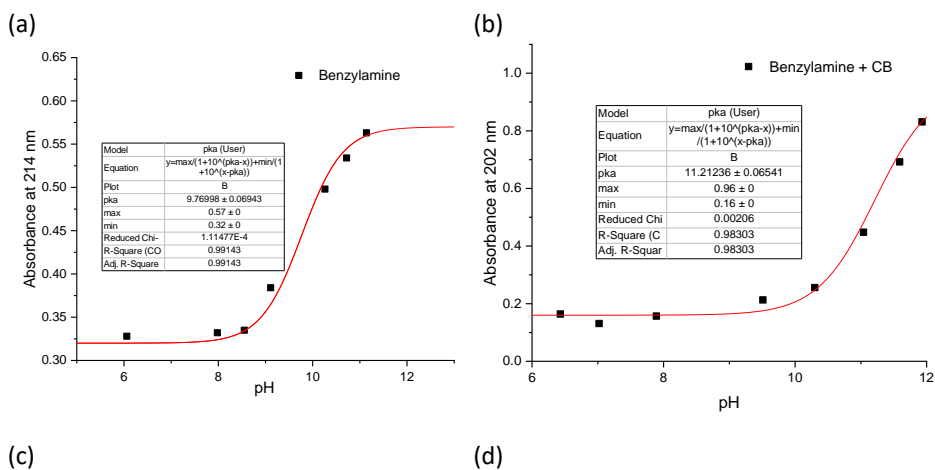
(a)   (b)   (c)

Figure S3.20 p*K*a titration curves at specific wavelength to estimate pKa. (a) Absorbance of **C1+**CB[7] at 232 nm was plotted against pH, p*K*a was estimated as 6.49 ± 0.0303; (b) Absorbance of **C5** +CB[7] at 274 nm was plotted against pH, p*K*a1 was estimated as 4.80 ± 0.0510; (c) p*K*a2 was estimated as 8.94 ± 0.0358. Markers indicate experimental data, lines indicate fitted curve.

Similarly, the p*K*a values of benzylamine and (1*H*-indol-2-yl)methanamine themselves and in the presence of CB[7] were estimated by the method described above, where the concentration of these two molecules is 0.1 mM and CB[7] is 0.11 mM.
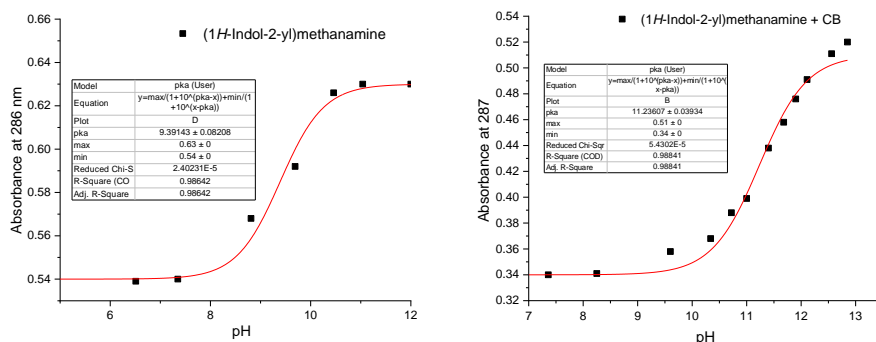
(a)   (b)

(c)   (d)

Figure S3.21 pK_a titration curves at specific wavelength to estimate pK_a of of benzylamine and (1*H*-indol-2-yl)methanamine or in the presence of CB[7]. (a) Absorbance of benzylamine (0.1 mM) at 214 nm was plotted against pH, pK_a was estimated as 9.77 ± 0.0694; (b) Absorbance of benzylamine (0.1 mM) + CB[7] (0.11 mM) at 202 nm was plotted against pH, pK_a was estimated as 11.21 ± 0.0654; (c) Absorbance of (1*H*-indol-2-yl)methanamine (0.1 mM) at 286 nm was plotted against pH, pK_a was estimated as 9.39 ± 0.0821; (d) Absorbance of (1*H*-indol-2-yl)methanamine (0.1 mM) + CB[7] (0.11 mM) at 287 nm was plotted against pH, pK_a was estimated as 11.24 ± 0.0394. Markers indicate experimental data, lines indicate fitted curve.

Table S3.6 Summary and comparison of the estimated pK_a.

Compound	pK_a	
	This work	**Literature**
Aniline (**C1**)	4.67 ± 0.0199	4.6 [7]
Aniline (**C1**) + CB[7]	6.49 ± 0.0303	--
C5-1	3.00 ± 0.0240	3.103 ± 0.079 [8]
(**C5**+CB[7])-1	4.80 ± 0.0510	--
C5-2	7.82 ± 0.0505	7.624 ± 0.063 [8]
(**C5**+CB[7])-2	8.94 ± 0.0358	--
Benzylamine	9.77 ± 0.0694	9.34 [9]
Benzylamine +CB[7]	11.21 ± 0.0654	--
(1*H*-Indol-2-yl)methanamine	9.39 ± 0.0821	--
(1*H*-Indol-2-yl)methanamine + CB	11.24 ± 0.0394	--

3.5.9. Discussion of the catalytic activity enhancement of C5 by CB[7] binding

The mechanism of **C5** catalysis in hydrazone formation is described below. As explored by Kool et al., the dehydration from the transition state **TS1** is the rate-determining step. The benzimidazole unit as a proton donor in **C5** is beneficial to form **TS1** and to accelerate the reaction. When binding to CB[7], the proton donating ability of

benzimidazole unit on **C5** is enhanced (**TS1***), as indicated from the pK_a value from 3.0 to 4.7, closer to the solvent pH (Figure S3.20, Table S3.6), and thus the reaction rate is increased.
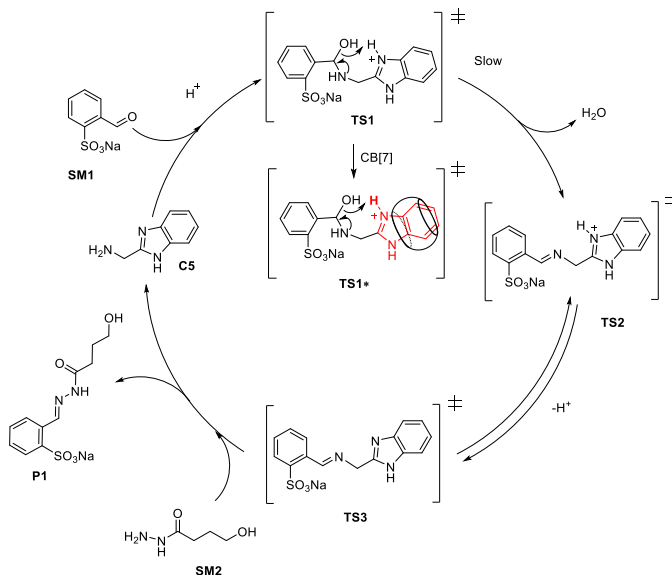
Scheme S3.1 Graphic explanation of the catalytic mechanism of **C5** on hydrazone formation reaction and the catalytic enhancement by CB[7] binding on the transition state (**TS1***).

To support this mechanism, we tested two analogs to **C5**, but lacking the benzimidazole unit entirely (benzylamine) or with an indole instead of the benzimidazole ((1*H*-Indol-2-yl)methanamine). These two molecules also bind strongly with CB[7] (ITC, Table S3.5) and have an increased pK_a on the aliphatic amine by CB[7] binding (Figure S3.21). But they did not show any catalytic activity on the reaction either with or without CB[7] added (Figure S3.22), demonstrating the crucial role of the benzimidazole unit in catalysis.
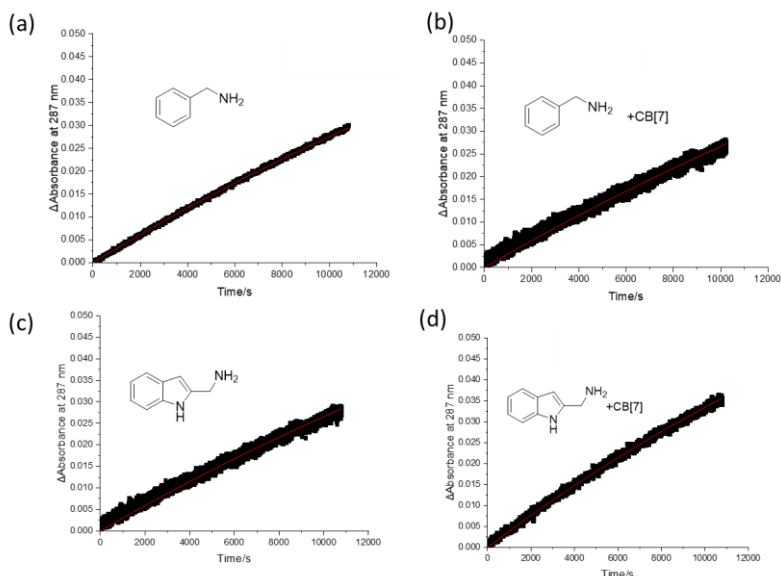
Figure S3.22 Fits of absorbance change at 287 nm of hydrazone reaction with benzylamine and (1*H*-indol-2-yl)methanamine. Reaction conditions: 0.4 mM aldehyde **SM1**, 0.040 mM hydrazide **SM2** in 10 mM phosphate buffer pH 6.0, 25 °C. (**a**) Reaction with benzylamine (0.4 mM), k = 0.066 ± 0.000043 M^{-1} s^{-1} (**b**) reaction with benzylamine (0.4 mM) and CB[7] (0.42 mM), k = 0.063 ± 0.000028 M^{-1} s^{-1} (**c**) reaction with (1*H*-Indol-2-yl)methanamine (0.4 mM) k = 0.063 ± 0.000026 M^{-1} s^{-1}; (**d**) reaction with (1*H*-Indol-2-yl)methanamine (0.4 mM) and CB[7] (0.42 mM), k = 0.083 ± 0.000063 M^{-1} s^{-1}.

3.5.10. Kinetic model for hydrazone formation

Explanation kinetic model

We assumed that the hydrazone formation reaction between hydrazide **SM2** and aldehyde **SM1** to form hydrazone **P1** is first order in each reactant. We took into account the catalytic influence of the catalyst, of CB[7] and of the catalyst⊂CB[7]-complex. Therefore we proposed the following rate equations for the reactions with catalyst and CB[7]:

$$\frac{d[A]}{dt} = -k_1[A][H] - k_2[A][H][cat] - k_3[A][H][CB7] - k_4[A][H][cat \subset \text{CB7}] \qquad \text{(eq. S6)}$$

$$\frac{d[H]}{dt} = -k_1[A][H] - k_2[A][H][cat] - k_3[A][H][CB7] - k_4[A][H][cat \subset \text{CB7}] \qquad \text{(eq. S7)}$$

$$\frac{d[P]}{dt} = k_1[A][H] + k_2[A][H][cat] + k_3[A][H][CB7] + k_4[A][H][cat \subset \text{CB7}] \qquad \text{(eq. S8)}$$

Here, $[P]$ is the concentration of hydrazone product **P1**, $[A]$ is the concentration of aldehyde **SM1**, $[H]$ is the concentration of hydrazide **SM2**, $[cat]$ is the concentration of catalyst **C1** free in solution (not bound to CB[7]), $[CB7]$ is the concentration CB[7] free in solution (not bound to the catalyst) and $[cat \subset CB7]$ is the concentration of the catalyst⊂CB[7]-complex, which was determined using the binding constant of the catalyst with CB[7], k_1 is the rate constant of the uncatalysed reaction, k_2 the rate constant for the reaction catalysed by catalyst **C1**, k_3 is the rate constant for the reaction catalysed by CB[7] and k_4 is the rate constant for the reaction catalysed by the catalyst⊂CB[7]-complex.

The equilibrium concentrations of CB[7], catalyst and the catalyst⊂CB[7]-complex were calculated using the initial, change and equilibrium Table S3.7.

Table S3.7 Initial, change and equilibrium table to calculate the concentration of CB[7] free in solution, catalyst free in solution and catalyst⊂CB[7]-complex.

	[CB[7]]	**[Cat]**	**[cat ⊂ CB[7]]**
Initial	*a*	*b*	0
Change	−*x*	−*x*	*x*
Equilibrium	*a−x*	*b−x*	*x*

$$K_a = \frac{[cat \subset CB7]}{[CB7][cat]}$$

(eq. S9)

we substituted (S8) with the results from table S3.7: $c \, \dfrac{x}{(a-x)(b-x)}$

(eq. S10)

Here, *a* = [CB[7]]$_0$ (concentration of CB[7] that was added to the reaction mixture), *b* = [Cat] (concentration of catalyst **C1** that was added to the reaction mixture), *c* = K_a (binding constant of catalyst **C1** to CB[7], *x* = [catalyst⊂CB[7]].

Solving (S9) for *x* gives the concentration of [catalyst⊂CB[7]]:

$$[cat \subset CB7] = \frac{a \cdot c + b \cdot c + 1 - \sqrt{a^2 \cdot c^2 - 2 \cdot a \cdot b \cdot c^2 + b^2 \cdot c^2 + 2 \cdot a \cdot c + 2 \cdot b \cdot c + 1}}{2 \cdot c}$$ (eq. S11)

$$[CB7] = [CB7]_0 - [cat \subset CB7]$$ (eq. S12)

$$[cat] = [cat]_0 - [cat \subset CB7]$$ (eq. S13)

Here $[CB7]$ is again the concentration CB[7] free in solution (not bound to the catalyst), $[cat]$ is the concentration of catalyst free in solution (not bound to CB[7]).

Because we followed the reaction by measuring the absorbance of the reaction mixture over time, we had to calculate the concentrations of the product using the following equation:

$$[P] = \frac{A - \varepsilon_A \cdot l \cdot [A]_0 - \varepsilon_{cat} \cdot l \cdot [cat]}{\varepsilon_P \cdot l - \varepsilon_A \cdot l} \qquad \text{(eq. S14)}$$

Here, $[P]$ is the concentration of hydrazine product **P1**, A is the absorbance of the reaction mixture, ε_A is the extinction coefficient at the rate analysis wavelength of 287 nm of aldehyde **SM1** (1423.6 (± 5.5) M^{-1} cm^{-1}), ε_{cat} is the extinction coefficient of the catalyst (for catalyst **C1** 1081.5 (± 50) M^{-1} cm^{-1}) ε_P is the extinction coefficient of hydrazone **P1** (20296 (±301) M^{-1} cm^{-1}), l is the path length (0.2 cm).

We found k_1 using the uncatalysed hydrazone reaction and performing a least-square error analysis in Matlab to find the best fit for k_1. Similarly, k_2 was found by fitting the reaction in the presence of catalyst, k_3 was found using the reaction in the presence of CB[7] and k_4 was found for the reactions with CB[7] and catalyst.

Results for catalyst C1

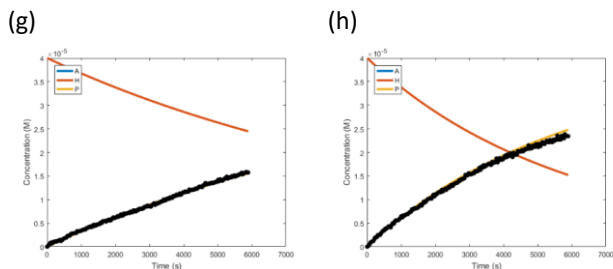(g)   (h)
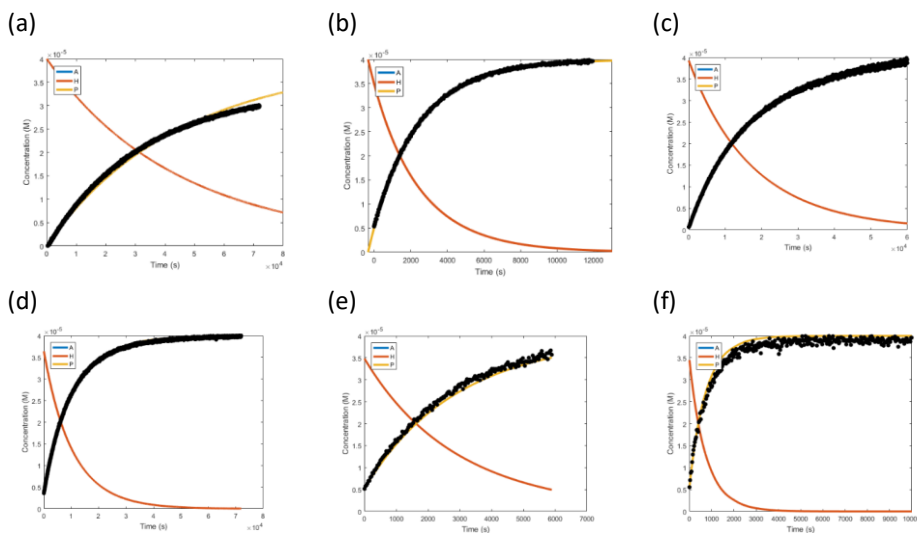
Figure S3.23 Best fits found with a least square error fit with Matlab for the concentration profiles of the formation of hydrazone **P1** (black dots) compared with the kinetic model (product **P1**: yellow line, aldehyde **SM1**: blue line (not visible because of the scale), hydrazide **SM2**: red line). Reaction conditions: 0.4 mM aldehyde **SM1**, 0.040 mM hydrazide **SM2** in 10 mM phosphate buffer pH 6.0, 25 °C. (**a**) Uncatalysed reaction, (**b**) reaction with catalyst **C1** (0.4 mM) , (**c**) reaction with CB[7] (0.42mM), (**d**) reaction used to fit k_4 with CB[7] (0.84 mM) and catalyst **C1** (0.4 mM), (**e**) with CB[7] (0.07 mM) and catalyst **C1** (0.4 mM), (**f**) with CB[7] (0.42 mM) and catalyst **C1** (1.8 mM), (**g**) with CB[7] (0.42 mM) and catalyst **C1** (0.4 mM), (**h**) with CB[7] (0.28 mM) and catalyst **C1** (0.4 mM).

Table S3.8 Partial reaction rate constants found with least-square error optimization fits in Matlab for catalyst **C1**.

Catalyst system	Rate constant	Best fit for
None	k_1	0.0568 M^{-1} s^{-1}
Catalyst **C1**	k_2	2.46×10^3 M^{-2} s^{-1}
CB[7]	k_3	150 M^{-2} s^{-1}
[**C1**⊂CB[7]]	k_4	221 M^{-2} s^{-1}

The resulting values that were found for k_1, k_2, k_3 and k_4 were used to calculate the total reaction rate constants:

$$k_{total} = k_1 + k_2 \cdot [cat] + k_3 \cdot [CB7] + k_4 \cdot [cat \subset CB7] \qquad \text{(Equation 1)}$$

To evaluate how well the model fits the experimental values, we measured and calculated the reaction constants at different concentrations of CB[7] and **C1** by the same method as in **Section 2.2**.
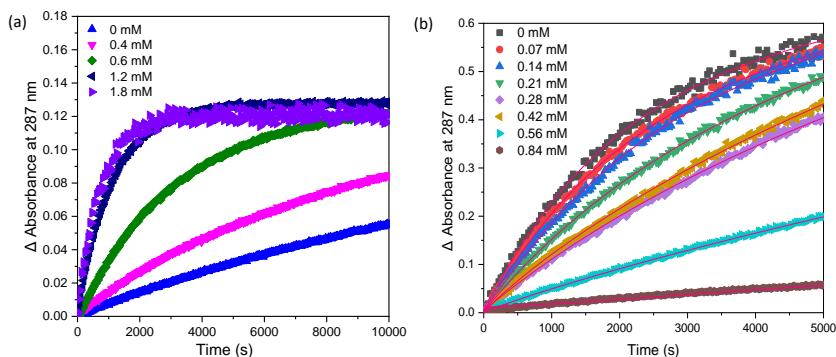

Figure S3.24 Determination of reaction constants at different concentrations of **C1** and CB[7] by measuring the absorbance changes at 287 nm of hydrazone product **P1**. Reaction conditions: 0.4 mM aldehyde **SM1**, 0.040 mM hydrazide **SM2** in 10 mM phosphate buffer pH 6.0, 25 °C. (a) The concentration of CB[7] was kept constant at 0.42 mM whereas the concentration of **C1** is varied between 0-1.8 mM; (b) The concentration of **C1** was kept constant at 0.4 mM whereas the concentration of CB[7] is varied between 0-0.84 mM.

Table S3.9 Summary of the reaction rate constants at different concentration of C1 and CB[7].

Entry	Conditions		k (M^{-1}s^{-1})
	C1 (mM)	CB[7] (mM)	
1	0	0.42	0.1437 ± 0.0108
2	0.4	0.42	0.2819 ± 0.0054
3	0.6	0.42	0.7390 ± 0.0416
4	1.2	0.42	2.3478 ± 0.0944
5	1.8	0.42	3.5534 ± 0.2748
6	0.4	0	1.1093 ± 0.0110
7	0.4	0.07	0.9455 ±0.0110
8	0.4	0.14	0.8065 ± 0.0074
9	0.4	0.21	0.6493 ± 0.0290
10	0.4	0.28	0.4569 ± 0.0375
11	0.4	0.42	0.2239 ± 0.0786

| 12 | 0.4 | 0.56 | 0.1817 ± 0.0227 |
| 13 | 0.4 | 0.84 | 0.2596 ± 0.0060 |

When [CB[7]] is kept constant, the model fits the experimental data with an R^2 (coefficient of determination) of 0.990. When [**C1**] is kept constant, the model fits the experimental data with an R^2 of 0.978. These high values (close to unity) imply that the model predicts the experimental data accurately.

Results for catalyst C5

For catalyst **C5** we were not able to find a k_4 that can fit the reaction for different ratios of catalyst **C5** and CB[7].
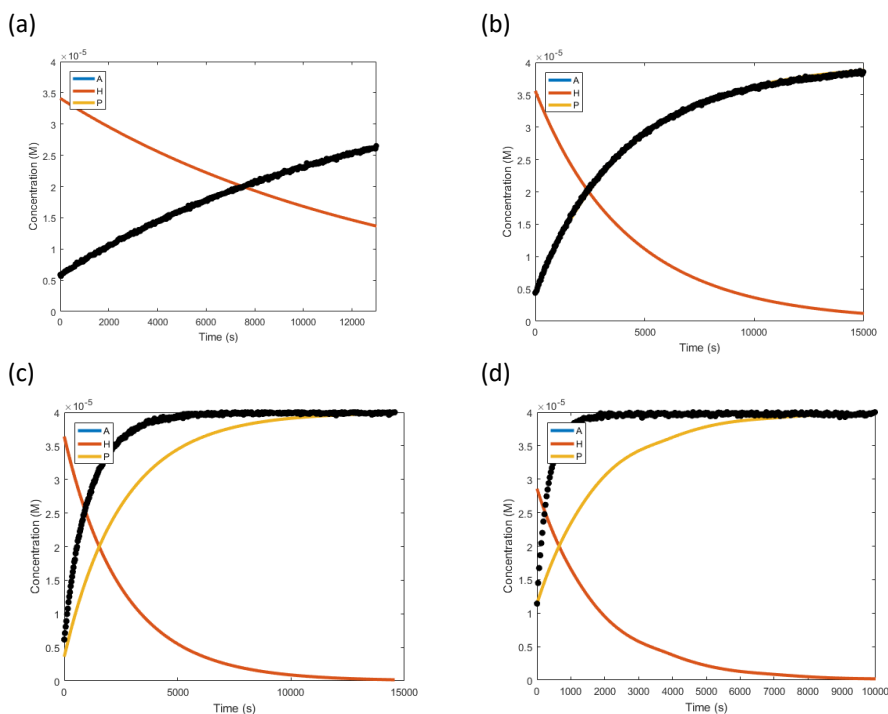
Figure S3.25 Best fits found with a least square error fit with Matlab for the concentration profiles of the formation of hydrazone **P1** (black dots) compared with the kinetic model (product **P1**: yellow line, aldehyde **SM1**: blue line (not visible because of the scale), hydrazide **SM2**: red line). Reaction conditions: 0.4 mM aldehyde **SM1**, 0.040 M hydrazide **SM2** in 10 mM phosphate buffer pH 6.0, 25 °C. (**a**) reaction with catalyst **C5**, (**b**) reaction used to fit k_4 with CB[7] (0.42 mM) and catalyst **C5** (0.4 mM), (**c**)

reaction with CB[7] (0.84 mM) and catalyst **C5** (0.4 mM), (**d**) reaction with CB[7] (0.42 mM) and catalyst **C5** (1.8 mM).

Table S3.10 Partial reaction rate constants found with least-square error optimization fits in Matlab for catalyst **C5**.

Catalyst system	Rate constant	Best fit for
None	k_1	0.0568 M^{-1} s^{-1}
Catalyst **C5**	k_2	318 M^{-2} s^{-1}
CB[7]	k_3	150 M^{-2} s^{-1}
[**C5**⊂CB[7]]	k_4	1.51 × 10^3 M^{-2} s^{-1}*

*This value is only valid when we use 0.42 mM CB[7] and 0.4 mM **C5**.

The resulting values that were found for k_1, k_2, k_3 and k_4 were again used to calculate the total reaction rate constants:

$$k_{total} = k_1 + k_2 \cdot [cat] + k_3 \cdot [CB7] + k_4 \cdot [cat \subset CB7] \qquad \text{(Equation 1)}$$

To evaluate how well the model fits the experimental values, we measured and calculated the reaction constants at different concentrations of CB[7] and **C5** by the same method as in **Section 2.2**.
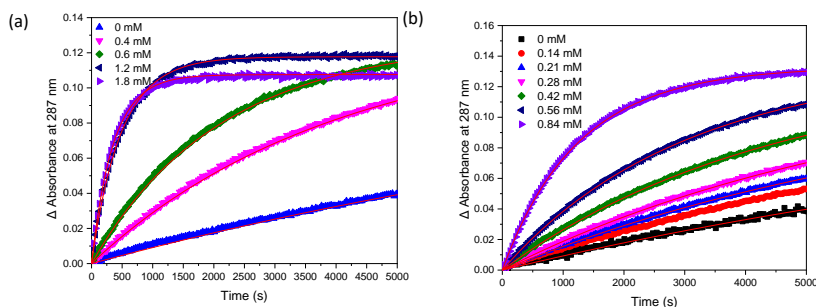

Figure S3.26 Determination of reaction constants at different concentrations of **C5** and CB[7] by measuring the absorbance changes at 287 nm of hydrazone product **P1**. Reaction conditions: 0.4 mM aldehyde **SM1**, 0.040 mM hydrazide **SM2** in 10 mM phosphate buffer pH 6.0, 25 °C. (a) The concentration of CB[7] was kept constant at 0.42 mM whereas the concentration of **C5** is varied between 0-1.8 mM; (b) The concentration of

C5 was kept constant at 0.4 mM whereas the concentration of CB[7] is varied between 0-0.84 mM.

Table S3.11 Summary of the reaction rate constants at different concentration of C5 and CB[7].

Entry	Conditions		k (M^{-1}s^{-1})
	C5 (mM)	CB[7] (mM)	
1	0	0.42	0.1859 ± 0.0137
2	0.4	0.42	0.5668 ± 0.0761
3	0.6	0.42	0.9771 ± 0.1970
4	1.2	0.42	5.2760 ± 0.0677
5	1.8	0.42	7.3012 ± 0.1094
6	0.4	0	0.2011 ± 0.0133
7	0.4	0.14	0.2951 ± 0.0209
8	0.4	0.21	0.3415 ± 0.0099
9	0.4	0.28	0.4168 ± 0.0213
10	0.4	0.42	0.6414 ± 0.0514
11	0.4	0.56	1.0637 ± 0.1243
12	0.4	0.84	2.2367 ± 0.0919

However the kinetic model-eq. doesn't fit to the experimental data, giving the R^2 value of -0.372 and 0.210. To take the synergistic effect of CB[7] with the **C5**⊂CB[7]-complex and of catalyst **C5** with the **C5**⊂CB[7]-complex into account we added k_5 and k_6 and we determined k_5 and k_6 by a least-square error fit to both sets of experimental data: (1) the rate constants with respect to the concentration of CB[7], with [**C5**] is 0.4 mM and (2) the rate constants with respect to the concentration of [**C5**], with [CB[7]] is 0.42 mM.

$$k_{total} = k_1 + k_2 \cdot [cat] + k_3 \cdot [CB7] + k_4 \cdot [cat \subset CB7] + k_5 \cdot [CB7] \cdot [cat \subset CB7] + k_6 \cdot [cat] \cdot [cat \subset CB7]$$

(Equation 2)

Table S3.12 Partial reaction rate constants found with least-square error optimization fits in Matlab for catalyst **C5**.

Catalyst system	Rate constant	Best fit for
None	k_1	0.0568 M^{-1} s^{-1}
Catalyst **C5**	k_2	318 M^{-2} s^{-1}

CB[7]	k_3	150 M^{-2} s^{-1}
C5⊂CB[7]-complex	k_4	256 M^{-2} s^{-1}
C5⊂CB[7]-complex + CB[7]	k_5	1.32 × 10^7 M^{-3} s^{-1}
C5⊂CB[7]-complex + catalyst **C5**	k_6	6.55 × 10^6 M^{-3} s^{-1}

The model fits the rate constants we find with varying [CB[7]] and keeping [**C5**] constant at 0.4 mM much better, with the R^2 of 0.948. However, it still underestimates the rate constants found with varying [**C5**] and keeping [CB[7]] constant at 0.42 mM (R^2 = 0.619). To take this nonlinear effect of [**C5**] into account we proposed the following equation to calculate the rate constants:

$$k_{total} = k_1 + k_2 \cdot [cat] + k_3 \cdot [CB7] + k_4 \cdot [cat \subset CB7] + k_5 \cdot [CB7] \cdot [cat \subset CB7] + k_6 \cdot [cat]^2 \cdot [cat \subset CB7]$$

(Equation 3)

Table S3.13 Partial reaction rate constants found with least-square error optimization fits in Matlab for catalyst **C5**.

Catalyst system	Rate constant	Best fit for
None	k_1	0.0568 M^{-1} s^{-1}
Catalyst **C5**	k_2	318 M^{-2} s^{-1}
CB[7]	k_3	150 M^{-2} s^{-1}
C5⊂CB[7]-complex	k_4	913 M^{-2} s^{-1}
C5⊂CB[7]-complex + CB[7]	k_5	9.89 × 10^6 M^{-3} s^{-1}
C5⊂CB[7]-complex + catalyst **C5**	k_6	9.32 × 10^9 M^{-4} s^{-1}

Model-eq. 3 gives the best fit for the reaction rates with different concentrations of CB[7] and **C5**, in much better agreement with the experimental data with R^2 values of respectively 0.856 and 0.997, which suggests that there is indeed a synergistic effect and a second-order influence of catalyst **C5**.
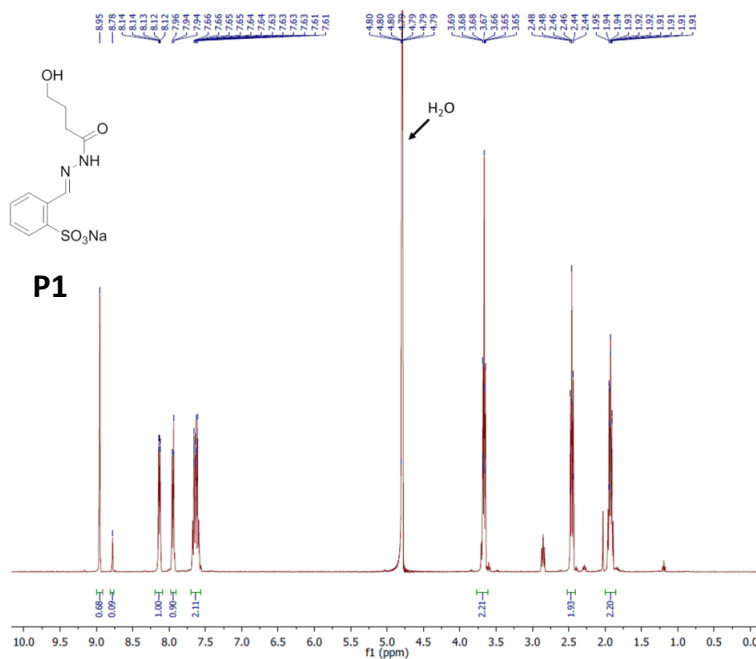
3.5.11. Spectra overview

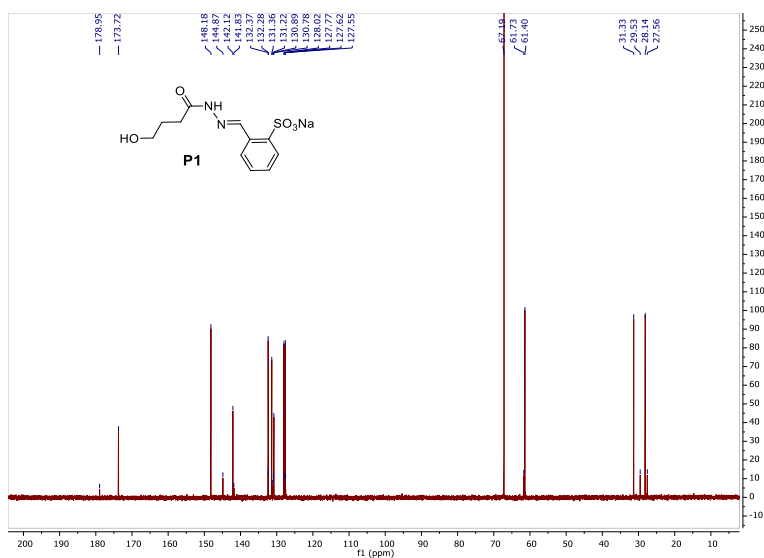**Figure S3.27** ^{1}H NMR spectrum of hydrazone **P1** in D$_2$O.

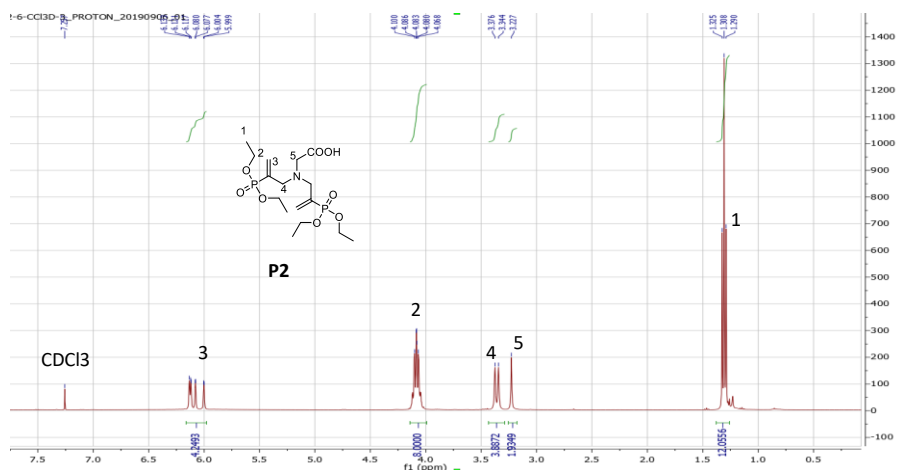**Figure S3.28** ^{13}C NMR spectrum of hydrazone **P1** in D$_2$O.

Figure S3.29 ^{1}H NMR spectrum and assignments of **P2** in CDCl₃.
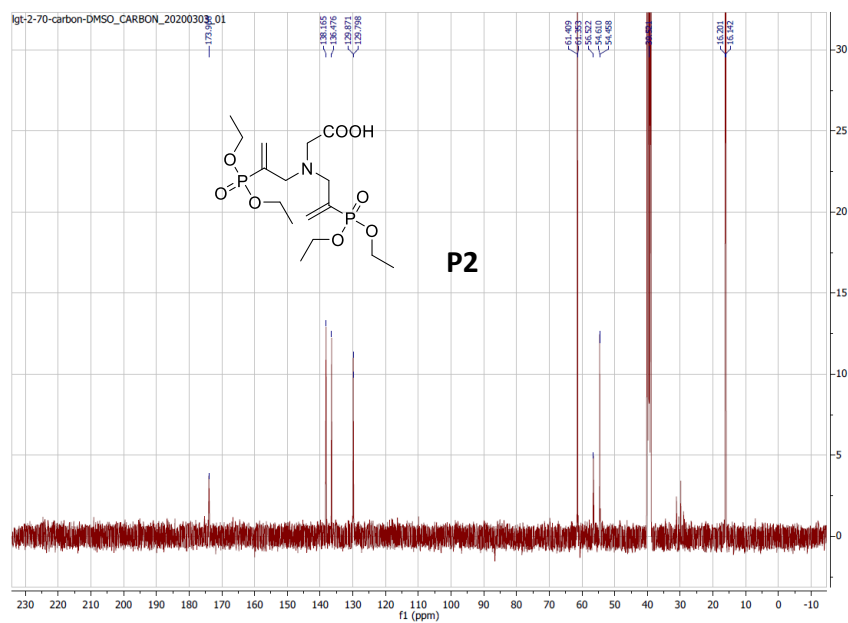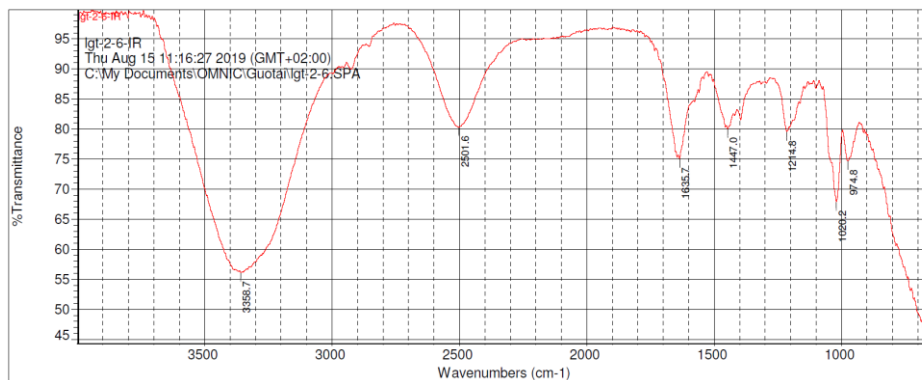

Figure S3.30 ^{13}C NMR spectrum of **P2** in DMSO-d₆.
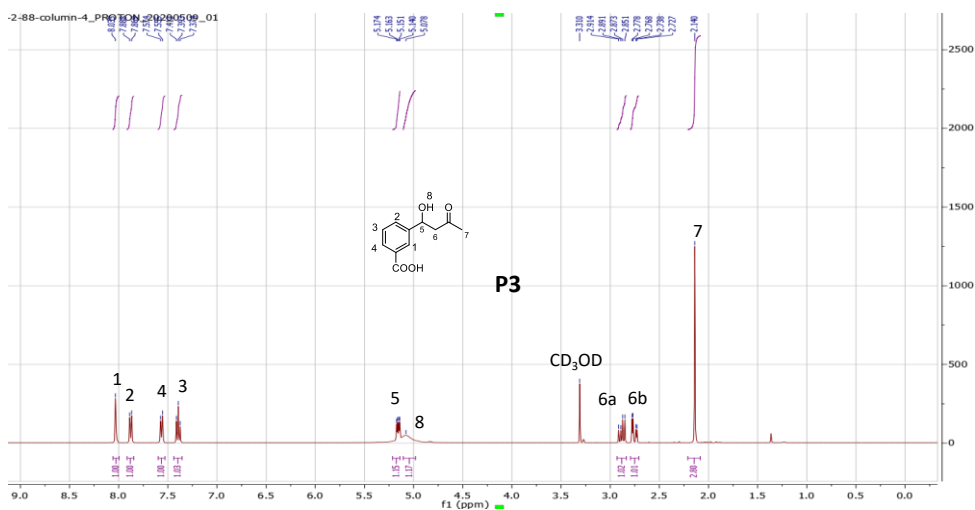
Figure S3.31 FT-IR spectrum of **P2**.

Figure S3.32 ^{1}H NMR spectrum and assignments of **P3** in CD$_3$OD.
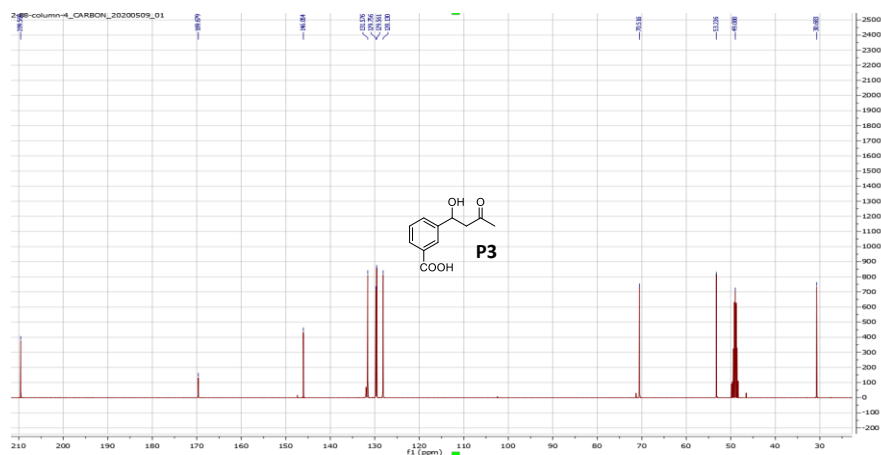
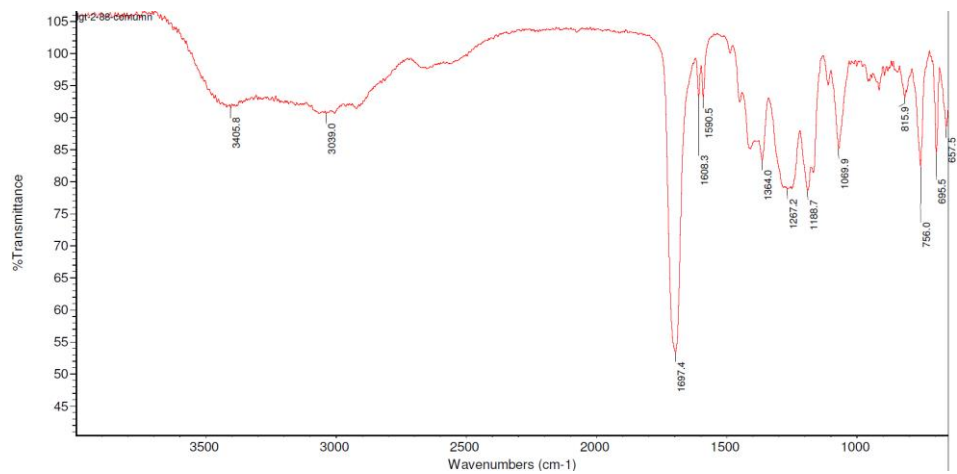**Figure S3.33** ^{13}C NMR spectrum of **P3** in CD$_3$OD.
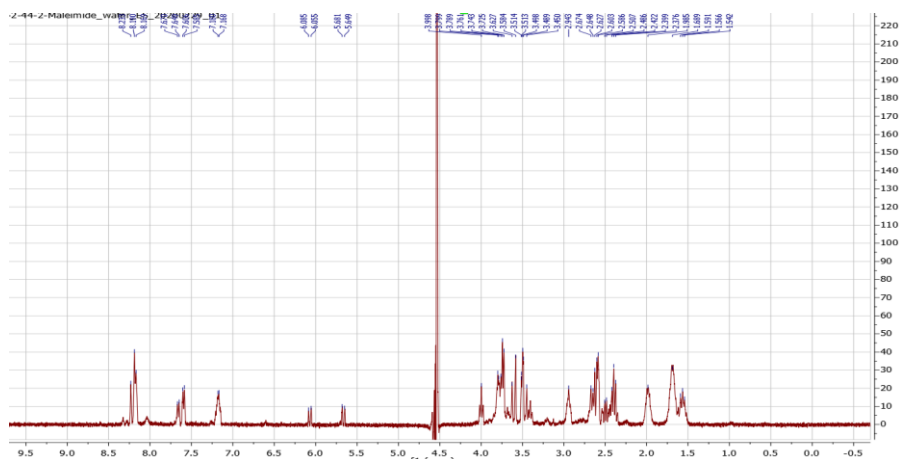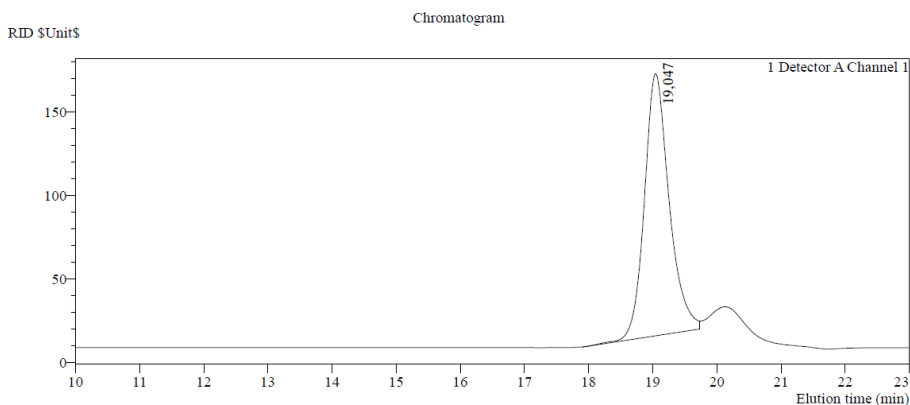

Figure S3.34 FT-IR spectrum of **P3**.

Figure S3.35 ^{1}H NMR spectrum of **P4**.

Chromatogram

RID $Unit$

1 Detector A Channel 1

GPC Summary

Chromatogram Detector 1 Ch1

Sample Name	Date Acquired	Mn	Mw	Mz	Mw/Mn
lgt-2-44-polym	3-3-2020	1425	1524	1628	1,070

Figure S3.36 GPC Spectrum of **P4** (MeOH/H_2O=1:4. The analyte peak appears at 19.047 min. The peak at 20.2 min is due to solvents (MeOH/H_2O).

3.5.12 References

[1] Fray, A.; Kraiem, J.B.; Souizi, A.; Amri, H. A Practical Synthesis of Diethyl 1-[(Alkylamino)(Cyano) Methyl] Vinylphosphonates. *Arkivoc*, **2012**, Viii, 119-127.

[2] Pearson, R.J.; Kassianidis, E.; Slawin, A.M.; Philp, D. Self-replication vs. reactive binary complexes—manipulating recognition-mediated cycloadditions by simple structural modifications. *Org. Biomol. Chem*., **2004**, *2*, 3434-3441.

[3] Azechi, M.; Toyota, N.; Yamabuki, K.; Onimura, K.; Oishi, T. Anionic Polymerization of N-Substituted Maleimide with Achiral and Chiral Amines as an Initiator. *Polym. Bull*. **2011**, *67*, 631–640.

[4] Larsen, D.; Pittelkow, M.; Karmakar, S.; Kool E.T. New Organocatalyst Scaffolds with High Activity in Promoting Hydrazone and Oxime Formation at Neutral pH. *Org. Lett*., **2015**, *17*, 274-277.

[5] Mugridge, J. S., Bergman, R. G., and Raymond, K. N.; ^{1}H NMR Chemical Shift Calculations as a Probe of Supramolecular Host Guest Geometry *J. Am. Chem. Soc.* **2011**, *133*, 11205–11212

[6] Barooah, N.; Sundararajan, M.; Mohanty, J.; Bhasikuttan, A. C. Synergistic Effect of Intramolecular Charge Transfer toward Supramolecular pKa Shift in Cucurbit[7]Uril Encapsulated Coumarin Dyes. *J. Phys. Chem. B* **2014**, *118*, 7136–7146.

[7] Cordes, E. H.; Jencks, W. P. Nucleophilic Catalysis of Semicarbazone Formation by Anilines. *J. Am. Chem. Soc.* **1962**, *84*, 826–831.

[8] Sierra-Zenteno, A.; Galán-Vidal, C.; Tapia-Benavides, R. Acid-Base Equilibrium Studies of 2-(Aminomethyl)Benzimidazole in Aqueous Solution. *Rev. la Soc. Química México* **2002**, *46*, 125–130.

[9] Hall, H. K. Correlation of the Base Strengths of Amines. *J. Am. Chem. Soc.* **1957**, *79,* 5441–5444.

Chapter 4

Towards Out-of-equilibrium Supramolecular Materials Based on Homoternary Host-guest Interactions Driven by a Chemical Reaction Network
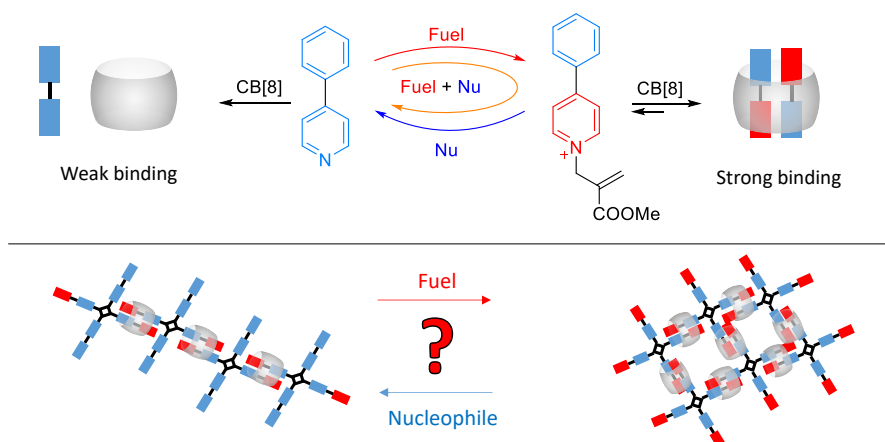
Abstract: Out-of-equilibrium supramolecular materials have attracted much attention in recent years, but systems based on host-guest interactions are still rare. In this work, we hope to realise transient host-guest interactions based assembly driven by chemical fuels. We chose cucurbit[8]uril (CB[8]) as the host molecule, as it can form homoternary complexes with 4-phenylpyridinium-based molecules. As the charge on 4-phenylpyridine can be controlled using a fuel-driven chemical reaction network, the phenylpyridinium-CB[8] interaction can be used to create temporary host-guest complexes. Using phenylpyridine as a model, the entire process of CB[8] binding and unbinding could be observed. However, when trying to create crosslinked network materials based on such temporary host-guest interactions using 4-arm guest molecules, an unexpected precipitation occurred, which turned to be precipitation of CB[8] in response to introduction of the fuel reagent. Although this approach has so far been unsuccessful in making out-of-equilibrium molecular materials, the work does offer an entry into controlling CB[8] solubility using chemical reaction networks.

4.1 Introduction

Out-of-equilibrium assembly is ubiquitous in biological living systems, contributing to sophisticated functions such as self-regulation, adaptation, evolution, self-replication, communicating, etc.[1] Inspired by nature and in the attempt to design "life-like" materials with stimuli-responsive, dynamic, adaptive, and self-regulating properties, out-of-equilibrium supramolecular polymerization has received considerable attention in recent years.[2] Unlike conventional self-assembly at or near equilibrium, out-of-equilibrium assembly of soft materials enables access to properties to be controlled over space and time, and the possibility of feedback, self-healing, and self-replication[3]. A pioneering work in this area was reported by van Esch and Eelkema in 2015[4], using methylating agents as fuels to convert a water-soluble dicarboxylate precursor into its corresponding methyl ester which is thermodynamically unstable. The ester building blocks were thus activated, prompting assembly into fibers with a network entrapping the aqueous environment to form a hydrogel, but simultaneously, ester hydrolysis take places causing collapse of the hydrogel. Crucially, these hydrogels now have a limited lifetime and many of their properties depend on the kinetics of the underlying methylation-hydrolysis chemical reaction network. After this discovery, a variety of fuel-driven out-of-equilibrium systems has been reported.[5–9] Unfortunately, the ability to spatiotemporally control out-of-equilibrium assembly processes is still in its infancy.[10] Moreover, reported examples of host-guest complex formation driven by chemical fuel are still very few, although host-guest complexation is one of the earliest studied types of self-assembly to make supramolecular materials. With the aim of extending the scope of artificial out-of-equilibrium systems and exploring more possibilities to achieve spatiotemporal control, in this work, we hope to design a host-guest assembly far from equilibrium and controlled by chemical fuels.

The design of the molecular building blocks is fundamental to constructing new functional supramolecular materials. Cucurbit[8]uril (CB[8]) is a widely used macrocyclic host to construct molecular networks, since it can simultaneously encapsulate two guest molecules and thus act as a crosslink or junction.[11] Among the guests of CB[8], phenylpyridinium moieties are well-known to form a stable 1:2 complex with CB[8] with a high association constant, through the ion-dipole interactions of pyridinium cations with the CB carbonyl rims.[12] Through complexation of phenylpyridinium and CB[8], network materials such as hydrogel[13] and molecular frameworks[14,15] have been reported. Since the cationic segment in phenylpyridinium is critical in complexing with CB[8], we hypothesized that by creating a fuel-driven switch between neutral and cationic forms, we should be able to control the formation and disassembly of the host-guest complex with CB[8], and thus the assembly and disassembly of the constructed materials would also be controlled by chemical fuels.

In recent years, the reversible allylic substitution of Michael acceptors has been reported[16] and applied to design chemoresponsive materials such as polymer hydrogels[17] and block copolymer micelle coacervates[18]. The Michael acceptors with allylic quaternary ammonium leaving group can be obtained by alkylating a tertiary amine using an acrylate electrophile with an allylic leaving group. Upon reaction with a nucleophile, the allylic quaternary ammonium group on the Michael acceptors will leave, removing the positive charge and yielding a tertiary amine product. Crucially, cationic functionalities on a guest molecule contribute strongly to their binding affinity with CB[8]. Combining these concepts, we hope to integrate the chemical reaction network of the tertiary amine alkylation and subsequent nucleophilic allylic substitution with CB[8] complexation with phenylpyridine to design an out-of-equilibrium supramolecular interaction.

4.2 Result and discussion

We first investigated the chemical reaction network that is at the basis of this concept. In this context, we looked at the reaction of 4-phenylpyridine **1** with the allylic Michael acceptors **F1** and **F2** (fuels) to form the cationic Michael acceptor **2**. Then, the cationic charge on this intermediate was removed by subsequent nucleophilic substitution. Adding chemical fuels **F1** or **F2** into a solution of 4-phenylpyridine (**1**, 0.04 mM) in 10 mM pH 7.4 phosphate buffer both resulted in the cationic 4-phenylpyridinium species (**2**) which was confirmed by characterization of the isolated pure products (**2·Br**) yielded from **1** and **F1** (SI). During the reaction, UV-Vis absorbance at 295 nm was observed to increase over time corresponding to the generation of **2**. The reaction rate can be controlled by the type of chemical fuel and its concentration. At the same fuel concentration, **F1** shows a much faster generation of **2** than fuel **F2**. The reaction rate can be further accelerated by increasing the concentration of fuels (Figure 4.1b). Similarly, the reaction rate of nucleophilic substitution of **2** back to **1** can also be tuned by using different species and concentrations of nucleophiles, 2-mercaptoethanol (**Nu1**) gives a much faster reaction than L-proline (**Nu2**), and both rates increase at higher nucleophile concentration. Interestingly, since L-proline (**Nu2**) show a relatively slow reaction rate with **2**, adding fuel ([**F1**] = 0.4 mM) to the solution of **1** (0.04 mM) and L-proline (0.96 mM) first led to the generation of **2** indicated form the increasing absorbance at 295 nm. But **2** is not stable in an environment rich in **Nu2**, causing the degradation of **2** and regeneration of **1**, observed as the absorbance at 295 nm decreasing after reaching a plateau. This progress can be repeated at least 4 times but the observed maxima are slightly lower in the later cycles. The transient formation of cationic phenylpyridinium provided the bases of designing an out-of-equilibrium system driven by chemical fuels. As discussed above, the cationic nature of the phenylpyridinium species is crucial to form a stable 1:2 complex with CB[8]. Having demonstrated that cationic phenylpyridinium (**2**) can be temporally formed, we then

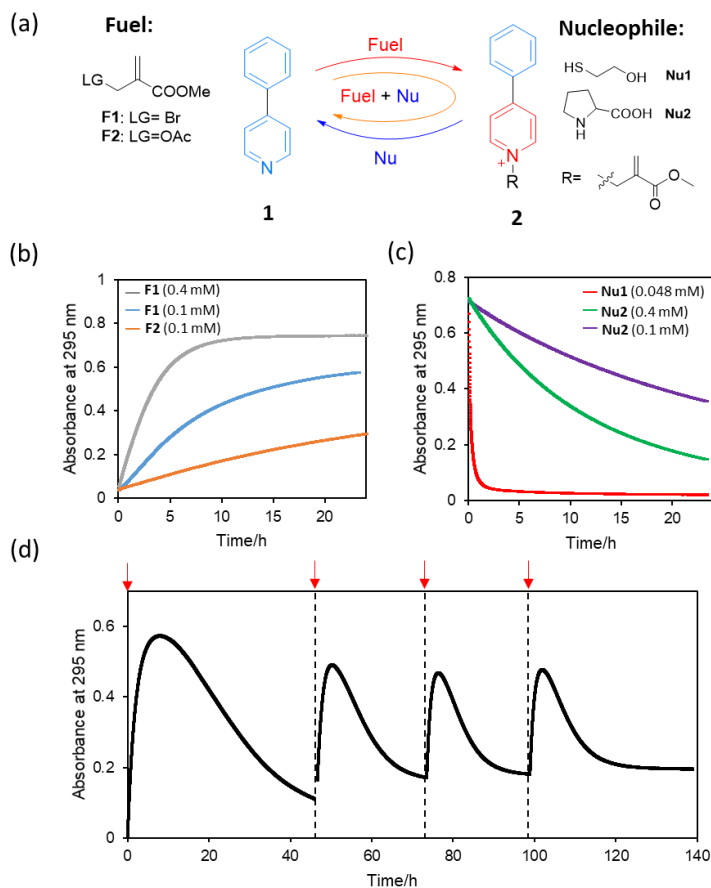moved on to using this chemical reaction network to control the time domain of CB[8] complexation.

Figure 4.1 Chemical reaction cycle driven by chemical fuels and reversed by nucleophiles. (a) Chemical structures and reactions used in this work (blue color indicates the original state and red color indicates the fuel-activated stated); (b) Uv-vis absorbance at 295 nm of **2** over time after adding chemical fuel to a solution of **1** ([**1**] = 0.04 mM, [**F1**] = 0.4 mM or 0.1 mM, [**F2**] = 0.1 mM); (c) Uv-vis absorbance at 295 nm over time after adding nucleophiles to **2** solution ([**2**] = 0.04 mM, [**Nu1**] = 0.048 mM, [**Nu2**] = 0.1 mM or 0.4 mM); (d) Multiple addition of chemical fuel ([**F1**] = 0.4 mM) into solutions of **1** (0.04 mM) and nucleophile ([**Nu2**] = 0.96 mM, complemented to maintain the concentration of 0.96 mM each time before fuelling); red arrows indicated the time of fuel injection. All samples were measured in 100 mM pH 7.4 buffer solution.

The binding affinity of CB[8] with the isolated cationic phenylpyridinium bromide (**2·Br**) was measured by isothermal titration calorimetry (ITC), showing a high binding constant and two binding sites (K_1= 1.59 × 10^5 M^{-1}, K_2= 6.82 × 10^6 M^{-1}) in 10 mM pH 7.4 phosphate buffer. ^{1}H NMR titration and Job's plot (UV) confirmed a stoichiometric ratio of CB[8]:**2** = 1:2 (SI, Figure S4.2, S4.3a,b). Unexpectedly, the neutral guest molecule 4-phenylpyridine (**1**) also showed a high binding affinity with CB[8] as measured with ITC (K_1= 1.13 × 10^5 M^{-1}, K_2= 1.46 × 10^5 M^{-1}) and two binding sites from Job's plot (Figure S4.3c,d). After testing several aqueous buffer conditions, we selected 100 mM phosphate buffer at pH 7.4 as under these conditions CB[8] has a comparatively higher binding affinity for **2** than for **1**. Moreover, under these conditions CB[8] has a very low solubility (<0.05 mM), but bound to **2** the solubility of CB[8] much improved. In contrast, guest molecule **1** did not have the capability of helping CB[8] dissolved in 100 mM pH 7.4 phosphate buffer. We hoped to demonstrate the fuel-driven host-guest interactions by monitoring CB[8] concentration in the solution. For this purpose we performed ^{1}H-NMR studies where concentration of CB[8] and guest molecules **1** and **2** were quantified by ^{1}H NMR integration. For these NMR studies, we selected the fuel **F2** and nucleophile **Nu2** to achieve a slower reaction rate that would facilitate analysis of the process. CB[8] (0.1 mM) is only partially soluble in the mixture of **1** (2 mM) in phosphate buffer (pH 7.4, 100 mM) (Figure S4.6) resulting in very small CB[8] peaks in the ^{1}H NMR spectrum (Figure 4.2a, bottom). Upon adding the chemical fuel, formation of **2** was observed, giving >98% yield in 8 hours. Simultaneously, the integrals of the CB[8] ^{1}H-NMR peaks increased, indicating an increase of the CB[8] concentration in solution. Notably, the CB[8] concentration increased by only a fraction of the concentration of **2** (Figure 4.2b). Still, 0.1 mM CB[8] is completely soluble in the presence of **2** (2 mM). When nucleophile **Nu2** was added to this mixture, reacting with **2** to form **1**, this resulted in a turbid mixture since CB[8] precipitated out. At the same time, the peaks of **2** and CB[8] disappeared from the ^{1}H-NMR spectra with the regeneration of **1** (Figure 4.3c). These results demonstrate that it is possible to overcome the poor solubility of CB[8] by temporary formation of a **2**⊂CB[8] complex driven by a chemical reaction network.
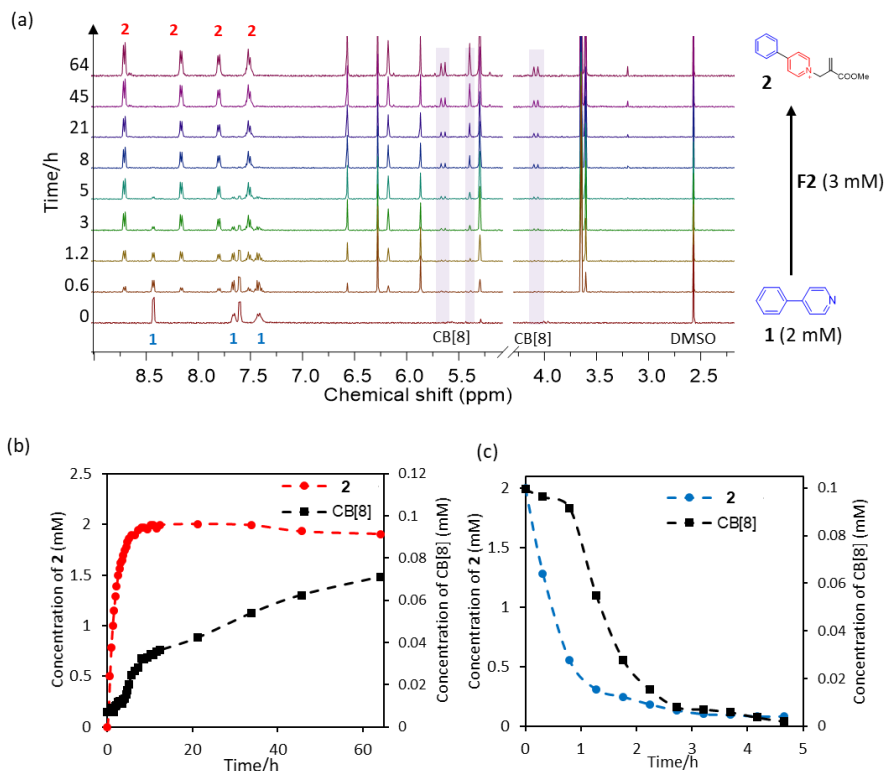
Figure 4.2 Concentration of **2** and CB[8] changed in the solution by reaction between **1** and **F2**, measured by ^{1}H NMR. (a) Overlaid ^{1}H-NMR spectra shows the growing peaks (violet hue) of CB[8] over time, after addition of **F2**. (b) Concentrations of **2** and CB[8] increased by adding chemical fuel of **F2** (3 mM) into **1** (2 mM) and CB[8] (0.1 mM) suspension. (c) Concentration of **2** (2 mM) and CB[8] (0.1 mM) decreased by adding nucleophile **Nu2** (5 mM). All samples were measured in 100 mM pH 7.4 buffer solution.

Having established the reversible formation of CB[8] host guest complexes controlled by chemical fuels and nucleophiles, we then tried to apply this interaction to achieve reversible assembly on a higher level. Cyanostilbene pyridinium derivatives have been reported to form one dimensional supramolecular polymers upon complexation with CB[8] [19–21]. Inspired by this finding, we designed a switchable linear guest molecule (**3**), having a permanent cation on one end providing a good solubility in water, and a free pyridine group on the other end that can be ionized by reaction with a chemical fuel. While guest molecule **3** was synthesized by a straightforward Knoevenagel condensation[20,21], **3** was found to be unstable in aqueous solution and decomposed in about 5 days at room temperature. The decomposition process turned out to be a

selective, light induced [2+2] cycloaddition resulting in a single isomer of the 4-arm cyclobutane **4**, having two cationic pyridinium groups. Under LED irradiation in water, this cycloaddition reaction is more efficient, giving >90% yield within 0.5 hours (SI). Again, only a single isomer was obtained indicated from NMR and the structure is equal to that formed with ambient light irradiation. Extrapolating from previous publications[22,23], the product is most probably a head-to-tail isomer, but unfortunately the absolute configuration could not be established resulting from the failure of growing single crystals. Previous publications show that guest molecules with multiple binding sites can form 2D or 3D supramolecular organic frameworks by complexation with CB[8], which may be applied in drug or DNA delivery[14,19,24–26]. Using multitopic guest **4** and the chemical reaction network developed above, we aimed to make temporary and signal responsive supramolecular organic frameworks. With guests **3** and **4** in hand, we aimed to use guests **3** and **4** to study complexation-controlled supramolecular polymerization in 1D (**3**) or 2D/3D (**4**) (Scheme 4.1). Due to the instability of **3** we mainly focused on 4-arm molecule **4**.
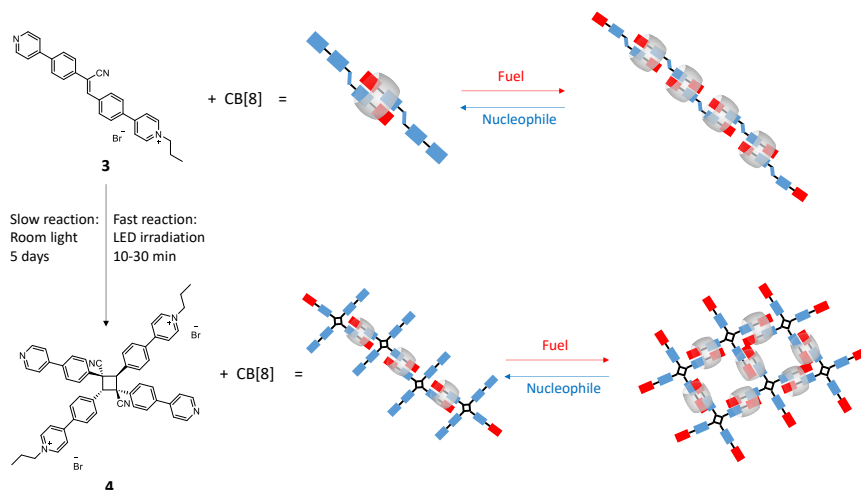
Scheme 4.1 Light-induced conversion of stilbene **3** to cyclobutane **4** (isomer structure proposed based on ref), and their proposed self-assembly with CB[8] controlled by chemical fuels and nucleophiles.

In pH 7.4 100 mM phosphate buffer solution, a mixture of 0.1 mM **4** and 0.1 mM CB[8] gave a clear solution. Note that we employed a 1:1 ratio of CB[8] and **4** to avoid unwanted binding of neutral pyridine groups with CB[8]. At these conditions, only <10 nm particles were observed using dynamic light scattering (DLS), with a very low scattering intensity that is indicative of molecularly dissolved species. Adding 1.5 equivalent **F2** (0.3 mM) caused a fast aggregation indicated by DLS, with scattering intensity reaching >2000 kcps and average particle size growing to about 6 μm in 30 min.

After addition of L-proline (**Nu2**, 0.45 mM) to the system, the aggregates gradually disappeared, observed as the scattering intensity dropping to 100 kcps in about 3 days. However, some large particles remained even on long timescales. 3 mM L-proline (10 eq.) was able to degrade the aggregates within 24 hours, showing that excess of nucleophile can accelerate the progress of disassembly. Having established a convenient processing time using excess equivalents of nucleophile, we then tried multiple fuelling in this nucleophile-rich condition. To the solution of **4** (0.1 mM), CB[8] (0.1 mM) and L-proline (100 mM), adding chemical fuel **F1** (0.3 mM) first led to a fast aggregation observed as a sharp increase in scattering count to 2500 kcps in 10 min and particles size growing to 6 μm in 30 min. After reaching a plateau, both the scattering count and particle size started to reduce, with the size reducing to ~1 μm and the scattering count dropping to <100 cps. A subsequent addition of chemical fuel gave a very similar curve, characterized by an initial fast aggregation followed by gradual reduction over the course of 24 hours. Additional fuelling cycles displayed similar behavior (Figure 4.3c). The aggregation process was followed using confocal laser scanning microscopy (CLSM) (Figure S4.8). Shortly after injecting fuel **F1** (0.45 mM) to a solution of 0.1 mM CB[8], 0.1 mM **4** and 100 mM L-proline, in 100 mM pH 7.4 phosphate buffer solution, we observed formation of small, fast moving particles, which continued to grow larger by connecting each other. In about 45 min, the amounts of particles reached the maximum. Simultaneously, slow degradation and disappearance of the particles took place, until after 20 h there were only few left. This observation of aggregate formation and autonomous degradation had a high agreement with the DLS measurement (Figure 4.3c). Surprisingly, the more reactive thiol nucleophile **Nu1** did not show a faster degradation of the formed aggregate.
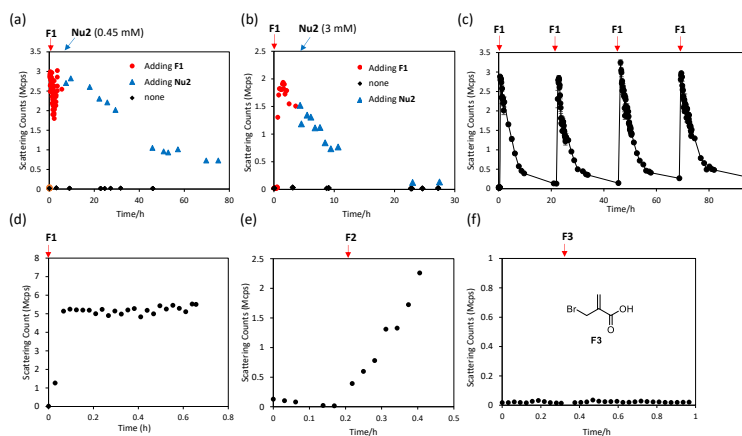

Figure 4.3 Aggregation in response to chemical fuel and nucleophile addition, measured by DLS. (a) Measurement after adding nucleophile (near stoichiometric): [**F1**] = 0.3 mM, [**Nu2**] = 0.45 mM, [**4**] = 0.1 mM, CB[8] = 0.1 mM; (b) measurement after adding nucleophile (excess): [**F1**] = 0.3

mM, [**Nu2**] = 3 mM, [**4**] = 0.1 mM, CB[8] = 0.1 mM; (c) multiple fuel injections in an excess nucleophile environment: [**F1**] = 0.3 mM × 4, [**Nu2**] = 100 mM, [**4**] = 0.1 mM, CB[8] = 0.1 mM; (d) measurement in the absence of **4**, [**F1**] = 0.02 mM, CB[8] = 0.01 mM; (e) measurement in the absence of **4**: [**F2**] = 0.02 mM, CB[8] = 0.01 mM; (f) measurement in the absence of **4** but with a chemical fuel **F3**: [**F3**] = 0.1 mM, CB[8] = 0.05 mM. All samples in sodium phosphate buffer solution 100 mM (a,b,c) or 10 mM (d,e,f).

Although these observations seemed in line with the behaviour of previously published fuel-driven processes, more characterization and control experiments did not support the formation of host-guest networks as we had designed. We isolated the formed aggregates and analysed their composition by ^{1}H-NMR spectroscopy. The precipitate was not soluble in D$_2$O, but adding the high affinity CB[8] guest *N,N,N*-trimethyl-1-adamantylammonium chloride] led to partial dissolution of the precipitate. In the ^{1}H-NMR spectrum of the obtained solution, only peaks of CB[8] and **F1** could be observed but no peaks of the 4-arm molecule **4** (Figure S4.9). DLS showed that precipitation also occurred when chemical fuel **F1** (0.02 mM) or **F2** (0.02 mM) was added to CB[8] (0.01 mM) in phosphate buffer (10 mM or 100 mM) without guest molecules **4** (Figure 4.3d,e). In contrast, addition of chemical fuel **F3** (0.1 mM), having an anionic carboxylate group which should not have any interaction with CB[8], into CB[8] (0.05 mM) solution did not cause any precipitation. Unfortunately, **F3** was not able to induce any aggregation in the presence of 4-arm guest molecule **4** and CB[8] either. Combined, we conclude that the observed aggregation was likely an insoluble complex of the chemical fuels **F1** or **F2** and CB[8]. However, we found that the precipitate had high fluorescence intensity in the solid form but solid CB[8] does not, which indicates that a small amount of 4-arm guest molecule may be present in the aggregate.

CB[8] is commonly known to be sparingly soluble in aqueous buffer, but its solubility can be increased by complexation with certain guest molecules.[27] From the results presented above, it appears that Michael acceptor fuel molecules **F1** and **F2** can decrease CB[8] solubility by complexation. Upon reaction of the fuel with a nucleophile, CB[8] solubility is restored again. In the presence of **1**, CB[8] solubility is increased upon introduction of **F1** because of the formation of **2**, which helps CB[8] solubility. In the experiments where **4** was present, CB[8] still precipitated upon addition of **F1**, likely because the concentration of **4** was much lower than in the experiments with **1**. In both systems, CB[8] solubility could be switched repeatedly by addition of fuel and/or nucleophiles.

4.3 Conclusion

In conclusion, we have developed a chemical reaction network that can control homoternary host-guest complex formation driven by chemical fuels. The reaction

network was designed based on the interaction between cationic 4-phenylpyridinium and CB[8]. 4-phenylpyridine can be quaternized by reaction with an allylic Michael acceptor fuel, leading to complex formation with CB[8]. We also developed a 2-arm and 4 arm guests with the aim of making supramolecular polymers and networks using this chemistry. Unfortunately, integrating these multitopic guests with the reaction network and CB[8] complexation did not work due to the precipitation of CB[8] in the presence of the chemical fuel. Still, the results and concept are insightful for a future design and may be applied to control temporary CB[8] solubilization.

4.4 References

(1)   Alberts, B.; Johnson, A.; Lewis, J.; Walter, P.; Raff, M.; Roberts, K. *Molecular Biology of the Cell 4th Edition: International Student Edition*; Routledge, 2002.

(2)   Sorrenti, A.; Leira-Iglesias, J.; Markvoort, A. J.; de Greef, T. F. A.; Hermans, T. M. Non-Equilibrium Supramolecular Polymerization. *Chem. Soc. Rev.* **2017**, *46* (18), 5476–5490.

(3)   Yang, S.; Schaeffer, G.; Mattia, E.; Markovitch, O.; Liu, K.; Hussain, A. S.; Ottelé, J.; Sood, A.; Otto, S. Chemical Fueling Enables Molecular Complexification of Self-Replicators. *Angew. Chem. Int. Ed.* **2021**, *60* (20), 11344–11349.

(4)   Boekhoven, J.; Hendriksen, W. E.; Koper, G. J. M.; Eelkema, R.; van Esch, J. H. Transient Assembly of Active Materials Fueled by a Chemical Reaction. *Science* **2015**, *349* (6252), 1075–1079.

(5)   De, S.; Klajn, R. Dissipative Self-Assembly Driven by the Consumption of Chemical Fuels. *Adv. Mater.* **2018**, *30* (41), 1706750.

(6)   Wang, Q.; Qi, Z.; Chen, M.; Qu, D. Out-of-equilibrium Supramolecular Self-assembling Systems Driven by Chemical Fuel. *Aggregate* **2021**, *2* (5), e110.

(7)   Van Rossum, S. A. P.; Tena-Solsona, M.; Van Esch, J. H.; Eelkema, R.; Boekhoven, J. Dissipative Out-of-Equilibrium Assembly of Man-Made Supramolecular Materials. *Chem. Soc. Rev.* **2017**, *46* (18), 5519–5535.

(8)   Rieß, B.; Grötsch, R. K.; Boekhoven, J. The Design of Dissipative Molecular Assemblies Driven by Chemical Reaction Cycles. *Chem* **2020**, *6* (3), 552–578.

(9)   Das, K.; Gabrielli, L.; Prins, L. J. Chemically Fueled Self-Assembly in Biology and Chemistry. *Angew. Chem. Int. Ed.* **2021**, *60* (37), 20120–20143.

(10)   te Brinke, E.; Groen, J.; Herrmann, A.; Heus, H. A.; Rivas, G.; Spruijt, E.; Huck, W. T. S. Dissipative Adaptation in Driven Self-Assembly Leading to Self-Dividing Fibrils. *Nat. Nanotechnol.* **2018**, *13* (9), 849–855.

(11)   Barrow, S. J.; Kasera, S.; Rowland, M. J.; Del Barrio, J.; Scherman, O. A. Cucurbituril-Based Molecular Recognition. *Chem. Rev.* **2015**, *115* (22), 12320–12406.

(12)   Zhang, Y.; Zhou, T. Y.; Zhang, K. Da; Dai, J. L.; Zhu, Y. Y.; Zhao, X. Encapsulation Enhanced Dimerization of a Series of 4-Aryl-N- Methylpyridinium Derivatives in Water: New Building Blocks for Self-Assembly in Aqueous Media. *Chem. - An Asian J.* **2014**, *9* (6), 1530–1534.

(13)   Whitaker, D. J.; Huang, Z.; Longbottom, B. W.; Sala, R. L. Supramolecular Hydrogels Prepared from Fluorescent Alkyl Pyridinium Acrylamide Monomers and CB[8].

Polym. Chem. **2021**, *12*, 519–525.

(14) Tian, J.; Zhou, T.-Y.; Zhang, S.-C.; Aloni, S.; Altoe, M. V.; Xie, S.-H.; Wang, H.; Zhang, D.-W.; Zhao, X.; Liu, Y.; Li, Z.-T. Three-Dimensional Periodic Supramolecular Organic Framework Ion Sponge in Water and Microcrystals. *Nat. Commun.* **2014**, *5* (1), 5574.

(15) Tian, J.; Xu, Z.-Y.; Zhang, D.-W.; Wang, H.; Xie, S.-H.; Xu, D.-W.; Ren, Y.-H.; Wang, H.; Liu, Y.; Li, Z.-T. Supramolecular Metal-Organic Frameworks That Display High Homogeneous and Heterogeneous Photocatalytic Activity for H_2 Production. *Nat. Commun.* **2016**, *7* (1), 11580.

(16) Zhuang, J.; Zhao, B.; Meng, X.; Schiffman, J. D.; Perry, S. L.; Vachet, R. W.; Thayumanavan, S. A Programmable Chemical Switch Based on Triggerable Michael Acceptors. *Chem. Sci.* **2020**, *11* (8), 2103–2111.

(17) Klemm, B.; Lewis, R.; Piergentili, I.; Eelkema, R. Temporally Programmed Polymer-Solvent Interactions Using a Chemical Reaction Network. **2021**. ChemRxiv. Cambridge: Cambridge Open Engage

(18) Lewis, R. W.; Klemm, B.; Macchione, M.; Eelkema, R. Fuel-Driven Macromolecular Coacervation in Complex Coacervate Core Micelles. *Chem. Sci.* **2022**, *13* (16), 4533–4544.

(19) Kim, H.-J.; Nandajan, P. C.; Gierschner, J.; Park, S. Y. Light-Harvesting Fluorescent Supramolecular Block Copolymers Based on Cyanostilbene Derivatives and Cucurbit[8]Urils in Aqueous Solution. *Adv. Funct. Mater.* **2018**, *28* (4), 1705141.

(20) Kim, H. J.; Whang, D. R.; Gierschner, J.; Park, S. Y. Highly Enhanced Fluorescence of Supramolecular Polymers Based on a Cyanostilbene Derivative and Cucurbit[8]Uril in Aqueous Solution. *Angew. Chem. Int. Ed.* **2016**, *55* (51), 15915–15919.

(21) Shi, X.; Zhang, X.; Ni, X. L.; Zhang, H.; Wei, P.; Liu, J.; Xing, H.; Peng, H. Q.; Lam, J. W. Y.; Zhang, P.; Wang, Z.; Hao, H.; Tang, B. Z. Supramolecular Polymerization with Dynamic Self-Sorting Sequence Control. *Macromolecules* **2019**, *52* (22), 8814–8825.

(22) Hu, F.; Hao, W.; Mücke, D.; Pan, Q.; Li, Z.; Qi, H.; Zhao, Y. Highly Efficient Preparation of Single-Layer Two-Dimensional Polymer Obtained from Single-Crystal to Single-Crystal Synthesis. *J. Am. Chem. Soc.* **2021**, *143* (15), 5636–5642.

(23) Wei, P.; Zhang, J. X.; Zhao, Z.; Chen, Y.; He, X.; Chen, M.; Gong, J.; Sung, H. H. Y.; Williams, I. D.; Lam, J. W. Y.; Tang, B. Z. Multiple yet Controllable Photoswitching in a Single AIEgen System. *J. Am. Chem. Soc.* **2018**, *140* (5), 1966–1975.

(24) Lee, H.-J.; Kim, H.-J.; Lee, E.-C.; Kim, J.; Park, S. Y. Highly Luminescent and Water-Soluble Two-Dimensional Supramolecular Organic Framework: All-Organic Photosensitizer Template for Visible-Light-Driven Hydrogen Evolution from Water. *Chem. - An Asian J.* **2018**, *13* (4), 390–394.

(25) Li, Y.; Qin, C.; Li, Q.; Wang, P.; Miao, X.; Jin, H.; Ao, W.; Cao, L. Supramolecular Organic Frameworks with Controllable Shape and Aggregation-Induced Emission for Tunable Luminescent Materials through Aqueous Host–Guest Complexation. *Adv. Opt. Mater.* **2020**, *8* (14), 1902154.

(26) Zhang, H.; Liang, F.; Yang, Y. W. Dual-Stimuli Responsive 2D Supramolecular Organic Framework for the Detection of Azoreductase Activity. *Chem. - A Eur. J.* **2020**, *26* (1), 198–205.

(27) Das, D.; Scherman, O. A. Cucurbituril: At the Interface of Small Molecule Host-Guest Chemistry and Dynamic Aggregates. *Isr. J. Chem.* **2011**, *51* (5–6), 537–550.

4.5 Supplementary Information

4.5.1 Experimental details

General methods

NMR spectra were recorded on an Agilent-400 MR DD2 (399.7 MHz for ^{1}H, 100.5 MHz for ^{13}C) at 298 K using residual protonated solvent signals as internal standard (^{13}C in D_2O was referenced to internal DMSO, δ = 38.69). **UV/Vis** spectroscopic measurements were performed on an Analytik Jena Specord 250 spectrophotometer; quartz cuvettes with a path length of 1.0 cm were used. **Isothermal titration calorimetry (ITC)** measurements were carried out at 25 °C using a MicroCal VP-ITC. **LC-MS** was performed on a Shimadzu Liquid Chromatograph Mass Spectrometer 2010, LC-8A pump with a diode array detector SPD-M20. **Confocal laser scanning microscopy (CLSM)** was performed in LSM 710 system using a Zeiss Observer Z.1 inverted microscope. Images were taken by an AxioCam MRm camera from Carl Zeiss MicroImaging. **Dynamic Light Scattering (DLS)** was conducted on a Malvern Zetasizer, using PMMA disposable cuvettes with a 1 cm path length, at a volume of 1.5 mL. The attenuator was set to auto during the measurement and the mean count rate was calibrated with the attenuation factor provided by the manufacturer. The temperature inside the cell was set at 25 °C for all experiments. The **pH** was recorded with the Consort C830 pH meter.

Materials

Sodium phosphate monobasic monohydrate (98%), 4-phenylpyridine (97%) 2-mercaptoethanol (99.0%), *N*-acetyl-L-proline (98%), 1-adamantanamine (97%), piperidine (99%), 2-(Bromomethyl)acrylic acid (98%), Fluorescein sodium were purchased from Sigma Aldrich. 1-bromopropane (>98.0%), methyl 2-(bromomethyl)acrylate (>97.0%), *N,N,N*-trimethyl-1-adamantylammonium hydroxide (25% in water), 1-bromopropane (>98%) were purchased from TCI Europe. Sodium phosphate dibasic salt (≥99%, analysis grade) was purchased from Acros Organics. Deuterium oxide for NMR was purchased from Euriso-top. L-proline (≥99%), 4-(4-Pyridinyl)benzaldehyde were from Fluorochem Ltd. Acetonitrile (LC/MS grade) was from Biosolve. CB[8] was obtained from Professor Oren A. Scherman's group at Cambridge University. Aqueous pH buffers were prepared by mixing the aqueous solution of sodium phosphate monobasic monohydrate salt and sodium phosphate dibasic salt at the same concentration, under the measurement of pH indicator until the required pH is achieved.

Synthesis of the guest molecules

1   **2·Br**
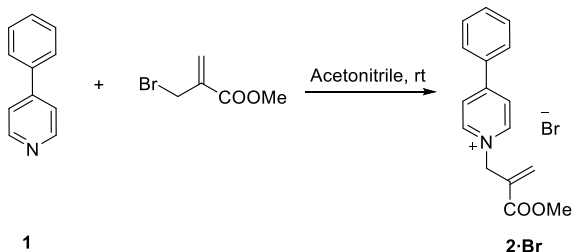
To the solution 4-phenylpyridine (1 g, 6.44 mmol) in 20 mL acetonitrile, methyl 2-(bromomethyl)acrylate (1.16 mL, 9.66 mmol, 1.5 eq) was slowly added. After stirring at room temperature for 5 hours, the solvent was evaporated out. The white solid product was obtained by precipitation and washed in ethyl acetate (2.06 g, 96% yield).

^{1}H NMR (400 MHz, D_2O) δ 8.88 (d, *J* = 7.2 Hz, 2H), 8.33 (d, *J* = 6.8 Hz, 2H), 7.97 (d, *J* = 8.0 Hz, 2H), 7.74 – 7.63 (m, 3H), 6.74 (s, 1H), 6.34 (s, 1H), 5.47 (s, 2H), 3.77 (s, 3H); ^{13}C NMR (100 MHz, D_2O) δ 166.48, 156.73, 144.33, 134.99, 133.39, 132.71, 132.25, 129.62, 127.90, 124.59, 60.63, 52.75. **MS** (ESI Pos) m/z: 254.17 [M-Br^{-}][+] (expected m/z = 254.12).

3   **4**

2-(4-(pyridin-4-yl)phenyl)acetonitrile was synthesized according to a reported procedure[1].

Synthesis of 4-(4-formylphenyl)-1-propylpyridin-1-ium bromide:

To a 100 mL flask charged with 4-(pyridin-4-yl)benzaldehyde (0.8 g, 4.36 mmol) in acetonitrile (40 mL), 1-bromopropane (3.97 mL, 43.6 mmol) was added. The solution was then stirred and heated to reflux for 24 hours. After checking by TLC (EA:PE=1:1) that the reaction had run to completion, the solvent was removed by rotary evaporator. The resulting sticky wax was dissolved again in 30 mL water and washed with ethyl acetate (20 mL) for 3 times. After removing the water by freeze drying, **4-(4-**

formylphenyl)-1-propylpyridin-1-ium bromide was obtained and used in the next step without further purification.

3 was synthesized according to a previous report using a modified procedure[2,3]:

To a dried and N_2 filled Schlenk flask, 2-(4-(pyridin-4-yl)phenyl)acetonitrile (0.35 g, 1.8 mmol), 4-(4-formylphenyl)-1-propylpyridin-1-ium bromide (0.5 g, 1.63 mmol was added and dissolved in MeOH (30 mL), after that piperidine (0.48 mL, 4.89 mmol) was added into the solution. The Schlenk flask was then sealed, and the reaction was stirred and heated to 80 °C for 24 h. After cooling to the room temperature, the solvent was removed by rotary evaporator. The product (0.51 g, 65%) was obtained as a yellow solid after washing by acetone and H_2O.

3
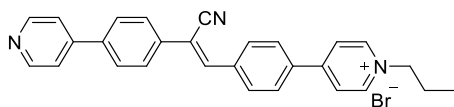
^{1}H NMR (400 MHz, methanol-d_4) δ 9.00 (d, *J* = 6.4 Hz, 2H), 8.60 (d, *J* = 5.2 Hz, 2H), 8.47 (d, *J* = 6.4 Hz, 2H), 8.17 (dd, *J* =8.0, 21.2 Hz, 4H), 8.04 (s, 1H), 7.92 (dd, *J* =8.0, 22.0 Hz, 4H), 7.76 (d, *J* = 4.8 Hz, 2H), 4.60 (t, *J* = 7.2 Hz, 2H), 2.09 (q, *J* = 7.6 Hz, 2H), 1.05 (t, *J* = 7.2 Hz, 3H); ^{13}C NMR (101 MHz, DMSO-d_6) δ 153.44, 150.39, 145.69, 144.91, 141.90, 138.15, 136.95, 135.03, 134.16, 130.20, 128.73, 127.66, 126.78, 124.62, 121.15, 117.50, 111.72, 61.35, 24.08, 10.27. **MS** (ESI Pos) m/z: 402.31 [M-Br$^-$]$^+$ (expected m/z = 402.20).

4 was synthesized using a homemade setup as shown on the right. A flask containing **3** (0.2 g) in 100 mL H_2O was irradiated with LED light (white light: 450-750 nm), under N_2 atmosphere with continuous stirring. The disappearance of a yellow color indicated that the reaction had run to completion, which was confirmed using 1H-NMR. The product was obtained as a faintly yellow solid in quantitative yield directly after removing water by freezer drying.
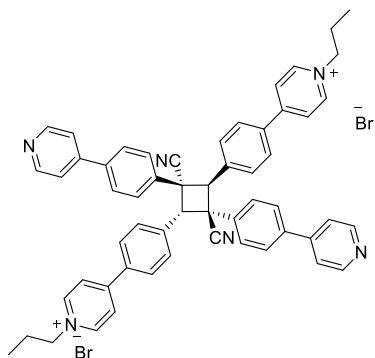
4

^{1}H NMR (400 MHz, Methanol-d_4) δ 8.94 (d, *J* = 7.2 Hz, 4H), 8.58 (d, *J* = 6.0 Hz, 4H), 8.39 (d, *J* = 6.8 Hz, 4H), 8.00 (d, *J* = 8.4 Hz, 4H), 7.86 – 7.75 (m, 8H), 7.71 (dd, *J* = 2.0, 4.8 Hz, 4H), 7.66 (d, *J* = 8.4 Hz, 4H), 5.93 (s, 2H), 4.56 (t, *J* = 7.2 Hz, 4H), 2.01 – 2.00 (m, 4H), 1.02 (t, *J* = 7.4 Hz, 6H). ^{13}C NMR (101 MHz, DMSO-d_6) δ 153.96, 150.72, 145.98, 145.23, 138.02, 137.73, 135.61, 133.95, 131.99, 129.51, 128.40, 127.60, 124.94, 121.59, 121.42, 61.67, 51.82, 47.95, 24.53, 10.66. **MS** (ESI Pos) m/z: 402.39 [(M-2Br$^-$)/2]$^+$ (expected m/z = 402.19).

4.5.2 Isothermal Titration Calorimetry

General procedure: solution of guest molecules (20 eq.) was titrated to a CB[8] solution at 25 °C, in 10 mM or 100 mM sodium phosphate buffer. CB[8] concentration was calibrated by titration with a standard solution of 1-adamantanamine. The first titration point of each ITC measurement was omitted. Binding constants were fitted with Microcal LLC ITC Origin 7 software.

Table S4.1. Overview of the ITC Binding constants measured in this work.
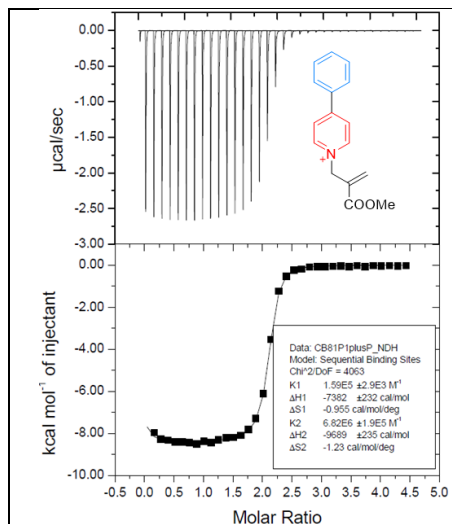
Condition: 10 mM sodium phosphate buffer pH 7.4, 25 °C, [**2**] = 0.72 mM, [CB[8]] =0.036 mM.
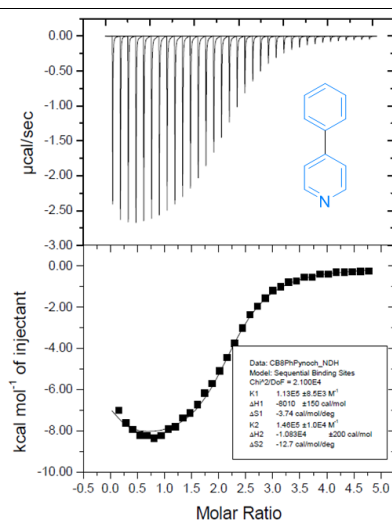
Condition: 10 mM sodium phosphate buffer pH 7.4, 25 °C, [**1**] = 0.72 mM, [CB[8]] =0.036 mM.
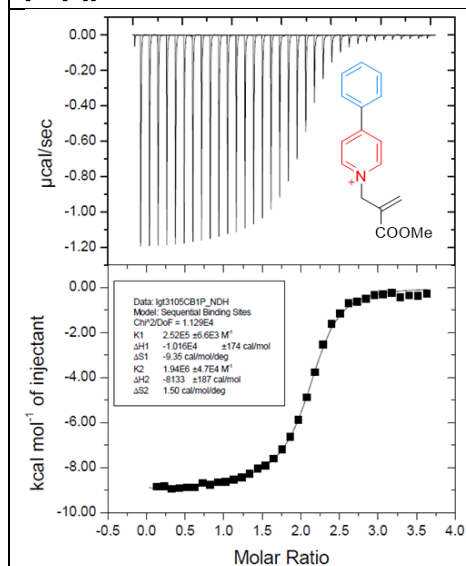
Condition: 10 mM sodium phosphate buffer pH 8.0, 25 °C, [**2**] = 0.54 mM, [CB[8]] =0.027 mM.
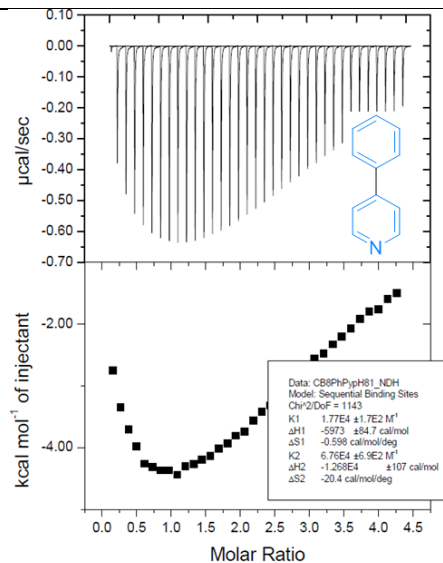
Condition: 10 mM sodium phosphate buffer pH 8.0, 25 °C, [**1**] = 0.54 mM, [CB[8]] =0.027 mM.

Condition: 100 mM sodium phosphate buffer pH 7.4, 25 °C, [**2**] = 1.17 mM, [CB[8]] =0.058 mM.

Condition: 100 mM sodium phosphate buffer pH 7.4, 25 °C, [**1**] = 1.17 mM, [CB[8]] =0.058 mM.
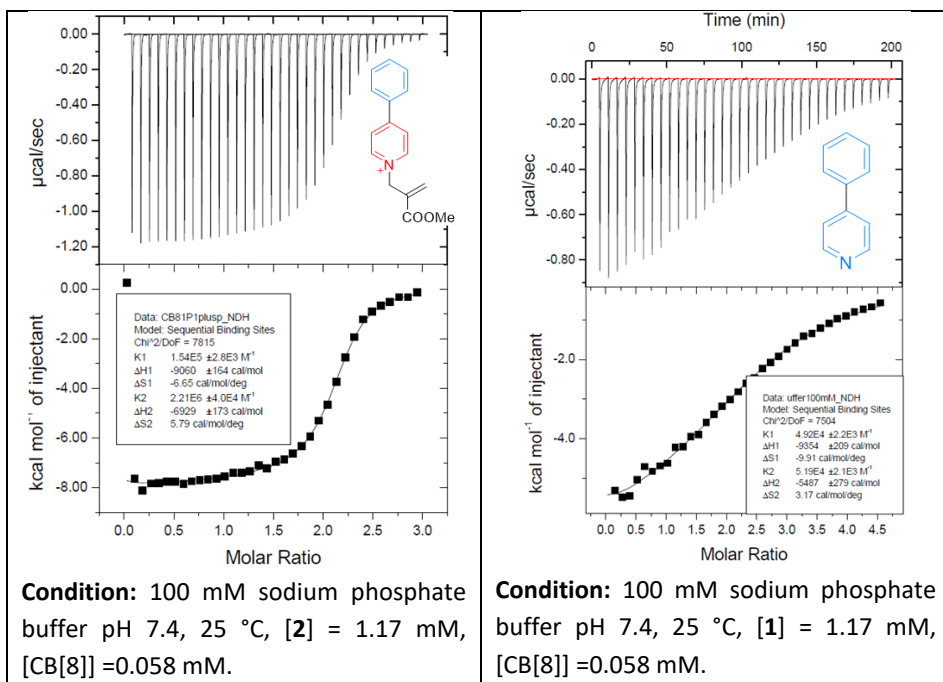
4.5.3 UV measurement to follow the reaction
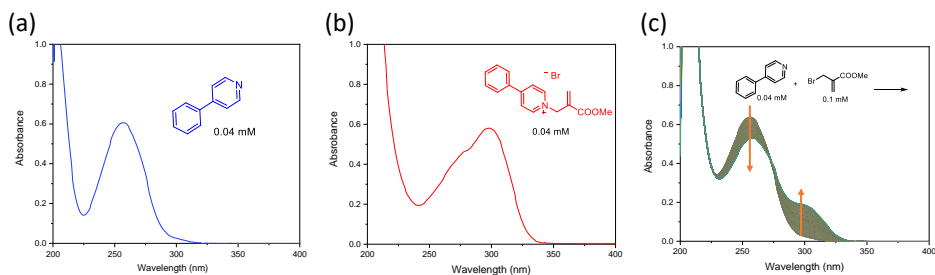
Figure S4.1 UV absorbance of the **1** (a), **2** (b) and during the fuel reaction (**c**) in pH 7.4 100 mM phosphate buffer solution.

4.5.4 NMR titration and Job's plot to show the binding process
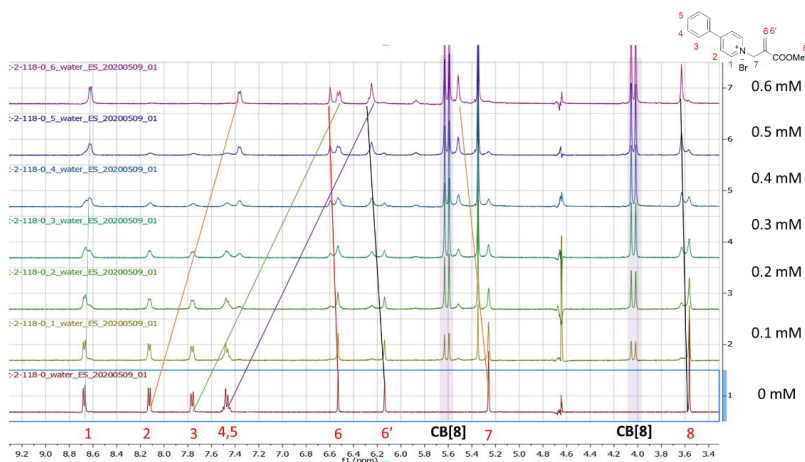
Figure S4.2 NMR titration to show the NMR peaks shift. Concentration: **2** (1 mM), CB[8] (0-0.6 mM) in 10 mM sodium phosphate pH 7.4 solution with 10% D_2O.
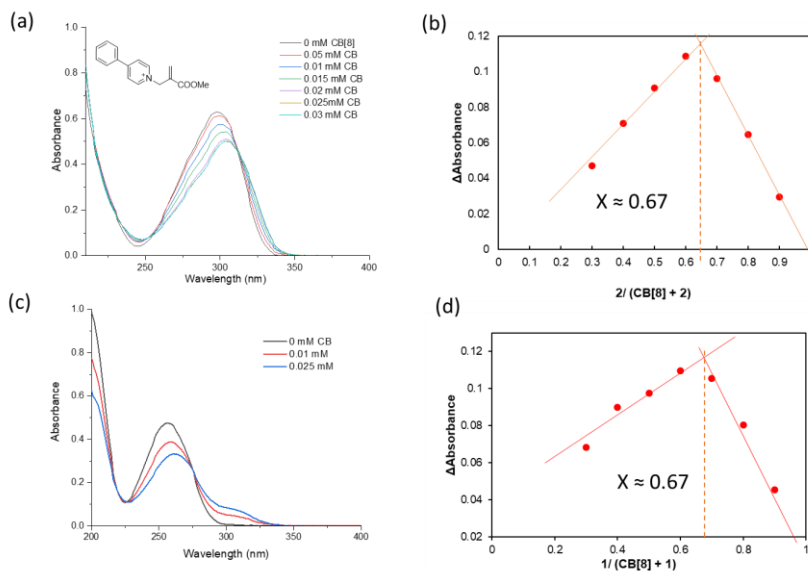
Figure S4.3 Job's plot to show the binding stoichiometry of CB[8] and guest molecules. (a) Increasing concentration of CB[8] leads to the decrease of absorbance of **2**. (b) Job's plot of CB[8] and guest molecule **2** showing a 1:2 binding stoichiometry, concentration in total is 0.04 mM. (c) Increasing concentration of CB[8] leads to the decrease of absorbance of **1**. (d) Job's plot of CB[8] and guest molecule **1** showing a 1:2 binding stoichiometry, concentration in total is 0.05 mM.

4.5.5 CB[8] solubility probed with ^{1}H-NMR spectroscopy
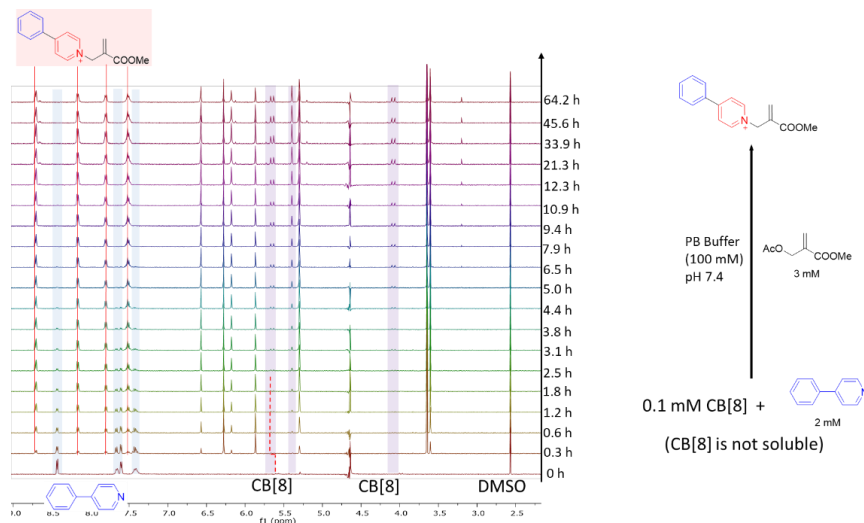
Figure S4.4 ^{1}H NMR spectra showing increasing concentration of CB[8] in solution upon reaction between **1** (2 mM) and chemical fuel **F2** (3 mM).
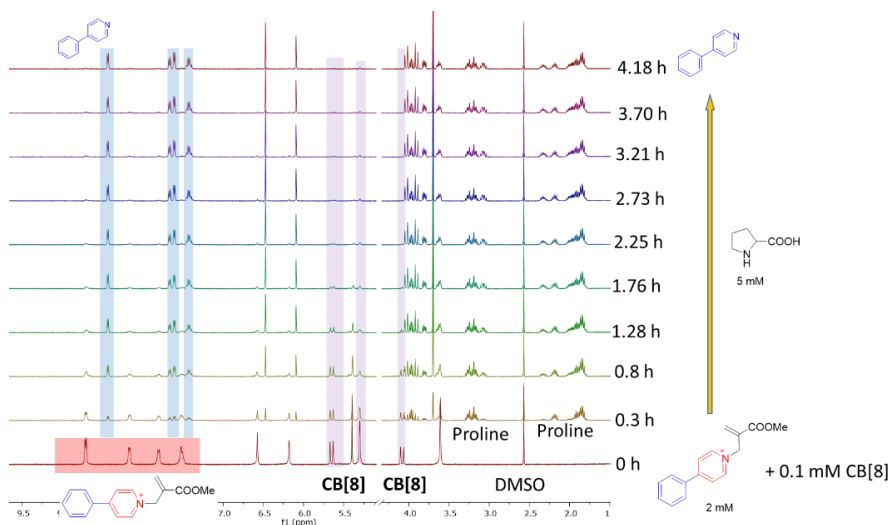
Figure S4.5 ^{1}H NMR spectra showing a decreasing CB[8] solubility upon adding L-proline (**Nu2**, 5 mM) to a mixture containing **2** (2 mM) and CB[8] (0.1 mM).
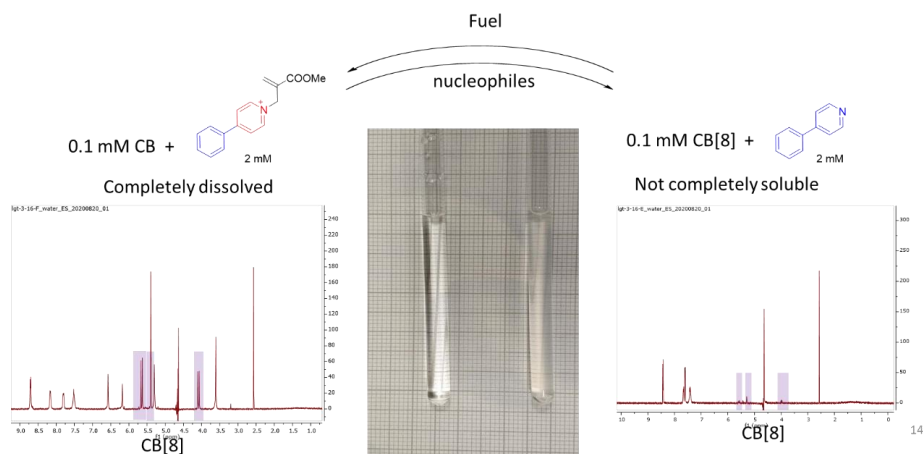
Figure S4.6 Photographs of NMR tubes containing CB[8] and **2** as a transparent solution (left) and CB[8] and **1** as suspension (right). ^{1}H-NMR spectra recorded from these tubes are shown on either side.

4.5.6 Fluorescence and continuous scanning confocal images
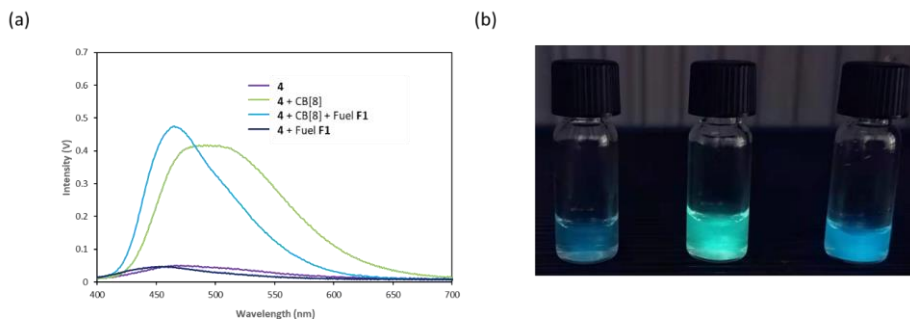
Figure S4.7 Fluorescence properties of guest molecule **4** and CB[8]. (a) Fluorescence measurement, conditions: **4** 0.1 mM, CB[8] 0.1 mM in pH 7.4 100 mM phosphate buffer solution. (b) Photograph of solution 0.1 mM **4** (left), 0.1 mM **4** + CB[8] (middle), 0.1 mM **4** + CB[8] (0.1 mM) + Fuel **F1** (0.3 mM) (right).
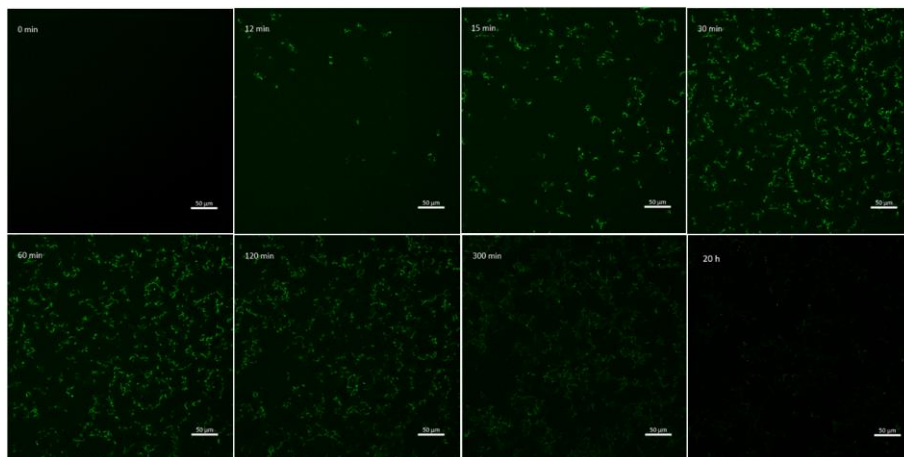
Figure S4.8 Confocal laser scanning microscopy continuous measurement. Conditions: [**4**] = 0.1 mM, [**F1**] = 0.1 mM, [**Nu2**] = 100 mM, 100 mM pH 7.4 phosphate buffer solution. Fluorescein dye (1 μM) was added as fluorescent probe, an incident laser with a wavelength of 488 nm used to excite the fluorescein probe. An interval time of 30 s was set for the continuous scanning.

4.5.7 Analysis of aggregates by ^{1}H-NMR spectroscopy

A mixture of **4** (0.5 mM) and CB[8] (1 mM) in 10 mM phosphate buffer and 10% D$_2$O was prepared by heating at 40 °C and sonication, followed by filtration using a syringe filter (450 nm) to remove insoluble particles. 1.5 mM **F1** was added to the resulting solution. The formed aggregates were isolated by centrifugation and added in D$_2$O to an NMR tube. *N,N,N*-Trimethyl-1-adamantylammonium chloride (50 mM) was added into the suspension in the NMR tube, to which sonication and heating was applied to help dissolve the precipitate. ^{1}H-NMR spectra of the solution are shown below.
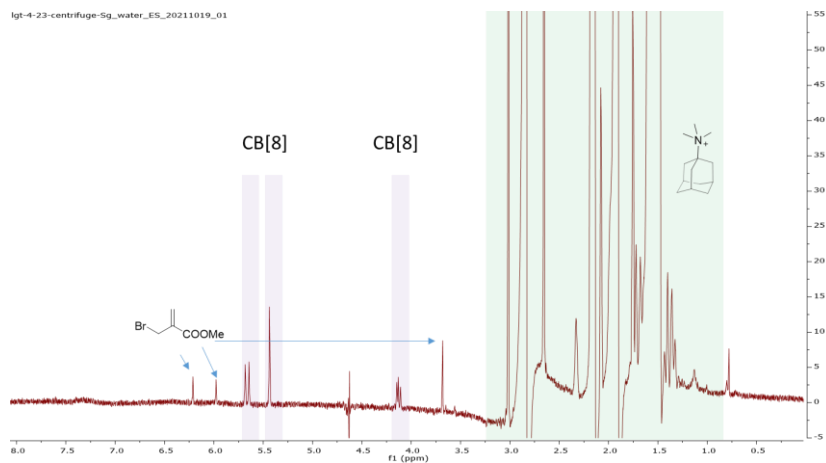
Figure S4.9 ^{1}H NMR spectrum of the precipitate after isolation by centrifugation and dissolution assisted by *N,N,N*-Trimethyl-1-adamantylammonium chloride (D$_2$O).
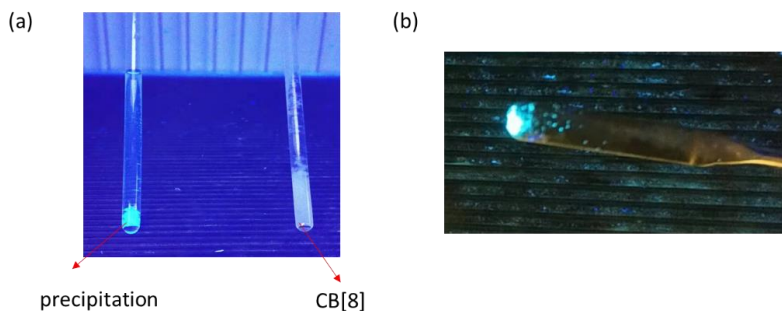

Figure S4.10 Photographs of the formed aggregate under UV lamp (375 nm). (a) Comparison of the precipitate formed by adding fuel **F1** to CB[8] and **4** (left) and CB[8] itself in phosphate buffer solution. (b) Precipitate isolated by centrifugation.
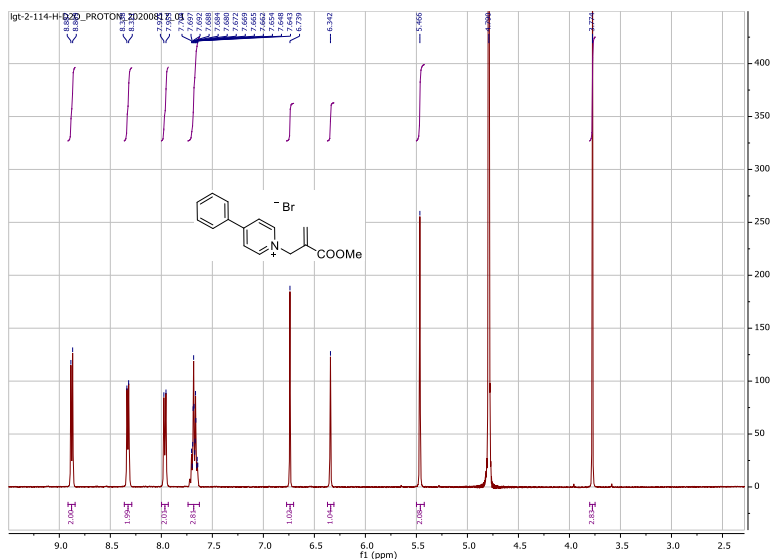
4.5.8 Spectra overview

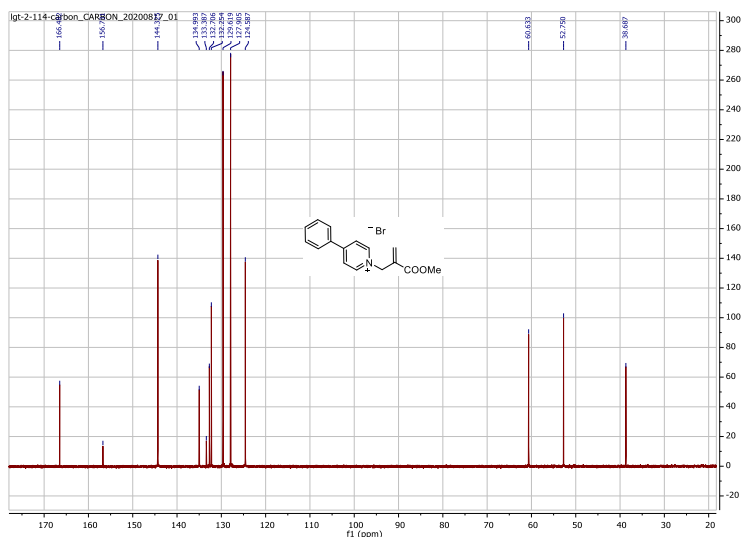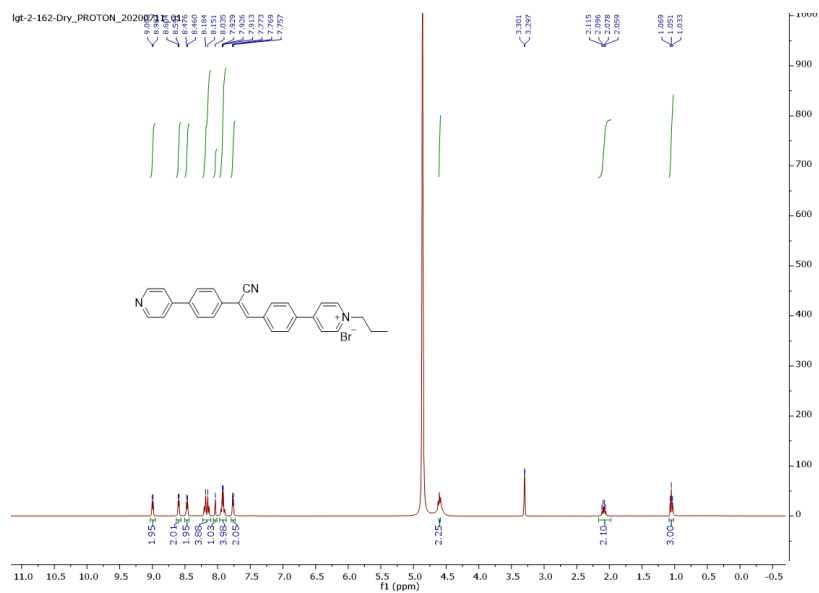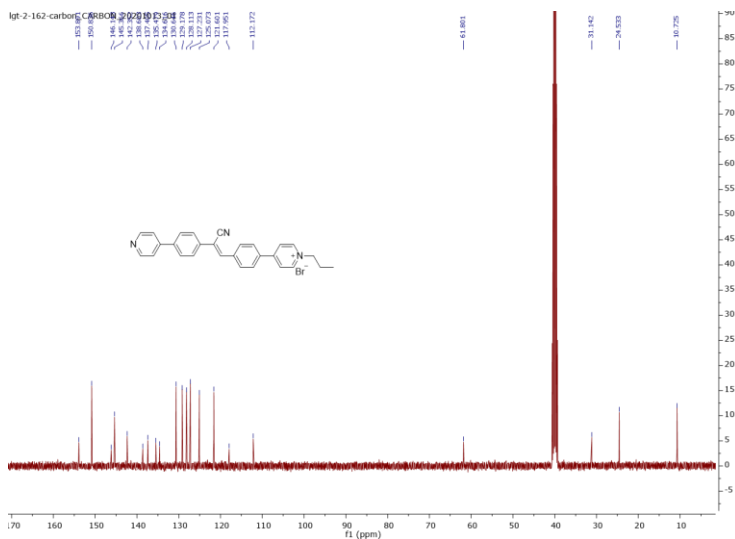**Figure S4.11** ^{1}H NMR spectrum of **2** in D_2O.

Figure S4.12 ^{13}C NMR spectrum of **2** in D_2O.

Figure S4.13 ¹H NMR spectrum of **3** in methanol-*d*₄.

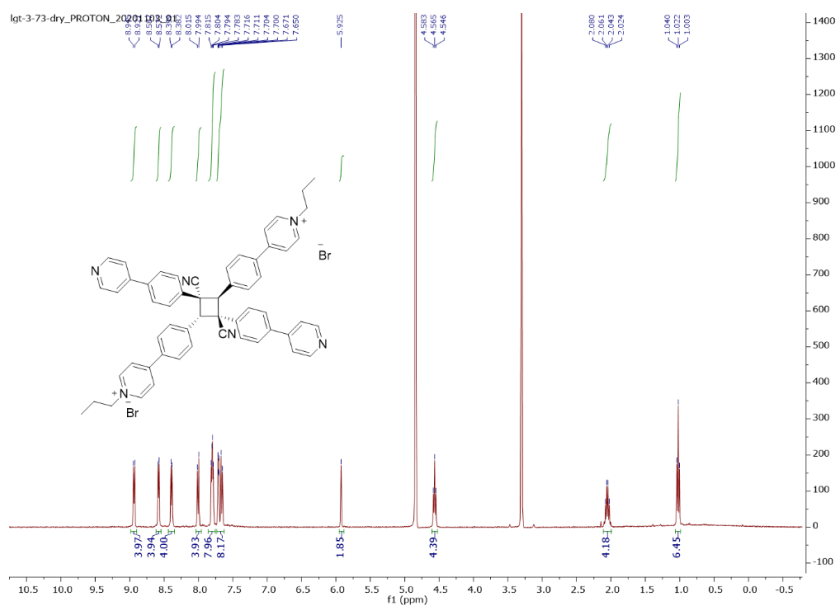**Figure S4.14** ¹³C NMR spectrum of **3** in methanol-*d*₄..

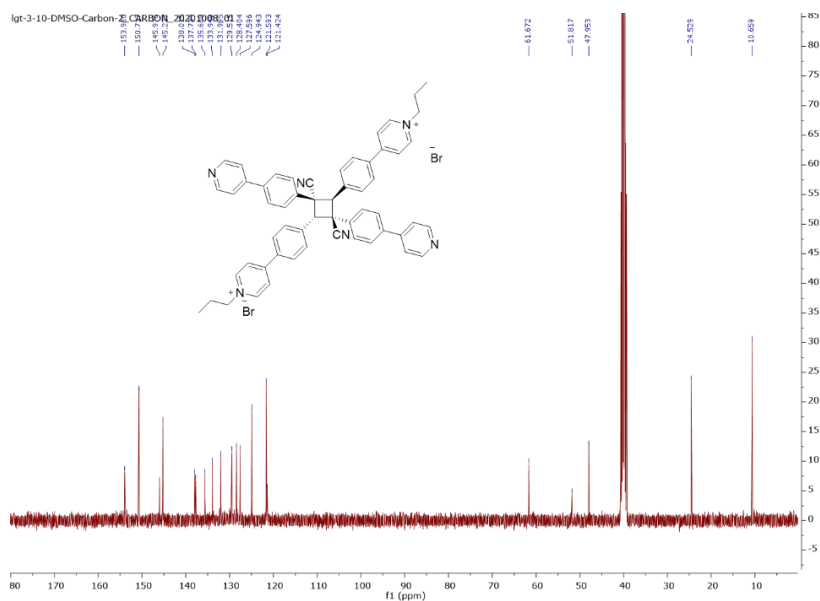**Figure S4.15** ^{1}H NMR spectrum of **4** in methanol-d_4.

Figure S4.16 ^{13}C NMR spectrum of **4** in DMSO-d_6.

4.5.9 References

(1)   Kim, J.; You, Y.; Yoon, S.-J.; Kim, J. H.; Kang, B.; Park, S. K.; Whang, D. R.; Seo, J.;
        Cho, K.; Park, S. Y. Bistable Solid-State Fluorescence Switching in
        Photoluminescent, Infinite Coordination Polymers. *Chem. - A Eur. J.* **2017**, *23*
        (42), 10017–10022.

(2)   Shi, X.; Zhang, X.; Ni, X. L.; Zhang, H.; Wei, P.; Liu, J.; Xing, H.; Peng, H. Q.; Lam,
        J. W. Y.; Zhang, P.; Wang, Z.; Hao, H.; Tang, B. Z. Supramolecular
        Polymerization with Dynamic Self-Sorting Sequence Control. *Macromolecules*
        2019, *52* (22), 8814–8825.

(3)   Kim, H. J.; Whang, D. R.; Gierschner, J.; Park, S. Y. Highly Enhanced
        Fluorescence of Supramolecular Polymers Based on a Cyanostilbene Derivative
        and Cucurbit[8]Uril in Aqueous Solution. *Angew. Chem. Int. Ed.* **2016**, *55* (51),
        15915–15919.

Chapter 5

Signal-specific Triggering of Supramolecular Aggregate Formation
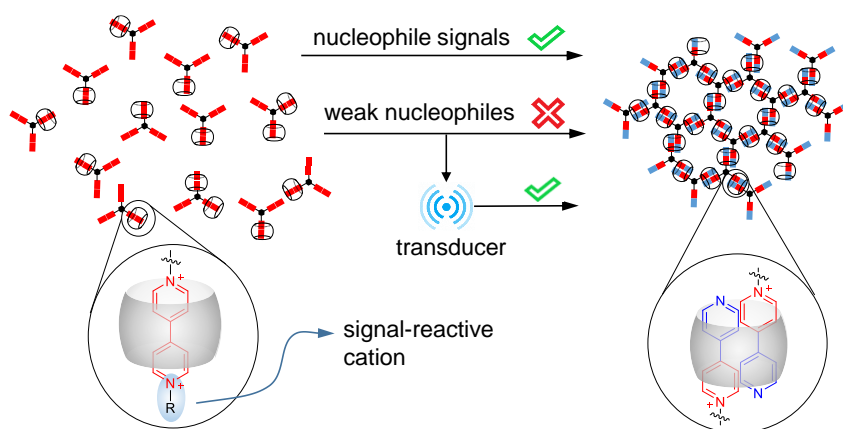
Abstract: Where biology makes extensive use of signal-responsive chemical reaction networks to regulate various biochemical and assembly processes, translation of these principles to abiotic systems is still rare. Here, we report an aggregation process of forming a supramolecular network held together by host-guest interactions, that is responsive to nucleophilic chemical signals through a chemical reaction-assembly cascade. In particular, we developed a signal induced switch between cucurbituril[8] binary and ternary complexes with cationic bipyridine derivatives, where the charge on the bipyridine can be changed through an allylic substitution reaction with the nucleophilic signal. Using a range of biologically relevant nucleophilic signals enables tuning of the reaction kinetics. We also developed a signal transducer to enable response to weakly nucleophilic signals. When applied to a multitopic bipyridine guest, reaction with the nucleophile signals leads to supramolecular network formation where the aggregation rates and final structure depend on the nucleophilicity of the signal. This work opens the door to new opportunities for signal responsive synthetic materials and interaction with biological systems.

5.1 Introduction

Processing specific signals leading to triggering of event cascades is a hallmark of living systems. Examples of such cascades are platelet aggregation and fibrin formation leading to blood coagulation, activated by agonists after vascular trauma. [1] Importantly, such cellular response is typically realized not by directly reacting to the primary stimulus, but by multiplexed signal transduction cascades transduced by receptors and switchable enzymes, causing the cell to respond to the initial stimulus. [2] In efforts to instil artificial materials with biomimetic responsivity, supramolecular materials have attracted much attention over the last two decades owning to the dynamic and reversible nature of noncovalent bonding.[3,4] These materials can have the ability to adapt to environmental stimuli[3], including physical cues (temperature[5,6], light[7–10]) or chemical signals (pH[11–13], ions[14], redox agents[15,16], and non-covalent interactions[17]). However, supramolecular assemblies that are responsive to biomolecules via chemical reaction cascades remain limited.[18]

Host-guest complexation is one of the most widely explored noncovalent interactions in the area of supramolecular materials.[19,20] A well-known host-guest pair is the viologen moiety[21] with cucurbit[8]uril (CB[8]). Viologen forms a stable, high association constant, 1:1 complex with CB[8] in aqueous media, through the ion-dipole interactions of dicationic pyridinium with the CB carbonyl rims. This complex converts to a 1:2 homoternary complex upon either direct reduction (by e.g. sodium dithionite[22]) or photoreduction[10] of viologen, from the dicationic form to the radical monocation.[23,24] The reverse process can take place through chemical[25] or electrochemical[26] oxidation. Incorporation of this reversible switch in a supramolecular material makes the material responsive to redox[27,28] or photochemical stimuli[10,28–30]. Moreover, a similar conversion between binary and homoternary complexes can also be achieved through protonation/deprotonation of bipyridine.[12,13,31,32] Nevertheless, reports of host-guest complexes that are responsive to biological signals through chemical reaction cascades remain rare.

Our work builds on a recently reported reversible allylic substitution of Michael acceptors[33] which has also been applied to design chemoresponsive materials such as polymer hydrogels[34] and block copolymer micelle coacervates[35]. When these Michael acceptors have an allylic quaternary ammonium leaving group, reaction of a nucleophile with the Michael acceptor leads to elimination of a tertiary amine and the removal of positive charge. Crucially, cationic functionalities on a guest molecule can contribute strongly to their binding affinity with CB[8].[36] Combining these concepts, we hypothesize that binding of guests to CB[8] can be controlled using the nucleophile-triggered allylic substitution. Relevant nucleophilic species such as amines (e.g. amino acids, dopamine) and thiols (e.g., glutathione (GSH)) are abundant in biological systems and also in many drugs. In this work, we want to use such biological nucleophilic species as signals to

control aggregation processes. In addition, mimicking biochemical signalling cascades, we designed a signal transducer, by which unreactive or weakly reactive signals can be applied as an effective trigger of aggregation. In this way, the range of possible signals can be broadened further.

5.2 Results and Discussion

We first studied the host-guest binding properties of CB[8] with bipyridine derivatives. Monocationic pyridinium (**1^{1+}**) was synthesized by alkylating 4,4'-bipyridine with a propyl group at one nitrogen. Further reaction with methyl 2-(bromomethyl)acrylate results in dicationic guest molecule **2^{2+}** with one permanent and one removable cation. NMR titration and isothermal titration calorimetry (ITC) showed that these two guest molecules bind with CB[8] in 2:1 and 1:1 ratios, respectively, which is in line with reported results[31]. In 50 mM sodium phosphate buffer solution, the binding constant of **1^{1+}** with CB[8] was determined by ITC as $K_1 = 8.00 \times 10^4$ M^{-1}, $K_2 = 8.59 \times 10^4$ M^{-1}, **2^{2+}** with CB[8] as $K = 1.05 \times 10^5$ M^{-1} (Figure 5.1a).

We then tested the reactivity of different nucleophiles as chemical signals to remove a charge from the dicationic guest molecule **2^{2+}**. Considering differences in structure and reactivity, we selected a thiol (Mesna[37], **Nu1**, a drug), a secondary amine (L-proline, **Nu2,** an amino acid), a hydrazide derivative (**Nu3**, hydrazides are metabolic intermediates[38]), primary amine (ethanolamine, **Nu4**, abundant in biological membranes), NH$_3$ (**Nu5**, metabolic waste) and H$_2$O$_2$ (**Nu6**, cellular reactive oxygen species) as representative nucleophiles. It should be noted that some hydrazide derivatives form as intermediates in metabolic processes, but we do not apply these specific hydrazides in this work. Instead, we use 4-hydroxybutanohydrazide (**Nu3**), which is water soluble and has low affinity for cucurbiturils.[39]

Using ^{1}H-NMR spectroscopy, we followed the conversion of **2^{2+}** (2 mM) upon reaction with 3 mM signal molecules (in 50 mM pH 7.4 sodium phosphate buffer). For Mesna, proline and ethanolamine, the reaction rates agrees very well with the reported nucleophilicity[40] as thiol> sec. amine > prim. amine (Figure 5.1b). Where Mesna gave >90% conversion in a 1 hour reaction, proline reached ~70% and ethanolamine 35% in the same time. Interestingly, 4-hydroxybutanohydrazide has a reactivity comparable with proline, reacting much faster than ethanolamine. Aqueous ammonia and hydrogen peroxide (generally considered as weak nucleophilic species) can also react with **2^{2+}**, with aqueous ammonia reacting faster than hydrogen peroxide. Both nucleophiles react faster than the non-zero background reaction.
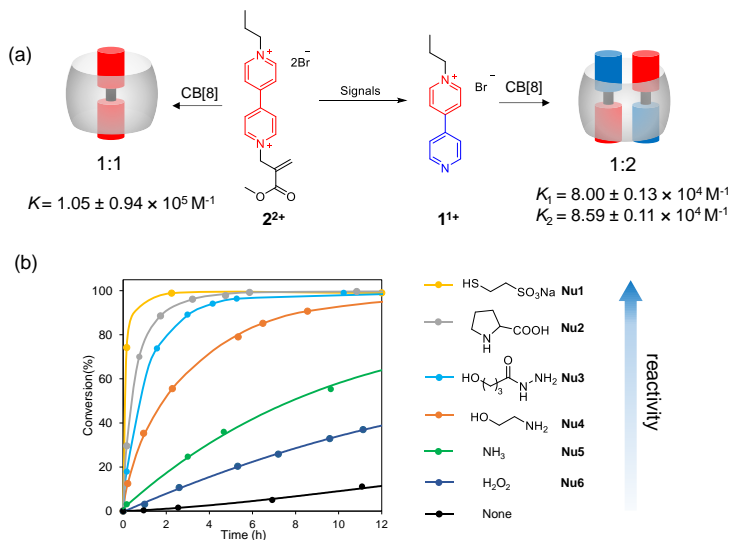
Figure 5.1 Nucleophilic Signals induced differential binding of bipyridinium derivatives to CB[8]. (a) Structures of bipyridinium derivatives and their binding affinity to CB[8] (determined by ITC, 50 mM sodium phosphate buffer, pH 7.4). (b) Conversion of **2²⁺** upon reaction with different nucleophilic signals followed by ¹H-NMR (50 mM sodium phosphate buffer with 10% D₂O), [**2²⁺**] = 2 mM, [**signals**] = 3 mM.

After exploring the CB[8] binding properties of these bipyridine derivates, and their reactivity to small molecule chemical signals, we hope to control the formation of larger supramolecular materials. 2D and 3D Supramolecular Organic Frameworks (SOF) based on cucurbituril were recently developed, showing promising application in drug[41] and DNA[42] delivery. For SOFs formed by CB[8]-dimerization of hydrophobic aromatic segments, 4-aryl-pyridinium units are the earliest and also most frequently reported binding motifs in multitopic guest molecules.[43]

As discussed above, the monocationic pyridinium (**1¹⁺**) can be generated by reaction of **2²⁺** with various signals, leading to the formation of the 2:1 complex with CB[8]. Based on this knowledge, we expected that a star-shaped tripodal guest with Michael-acceptor activated dicationic arms would form discrete monomeric complexes with CB[8]. Conversion of the dicationic arms to monocations, triggered by reaction with the nucleophile signals, would then initiate the formation of a non-covalent network by crosslinking with CB[8] (Figure 5.2a).

To test this hypothesis, we synthesized the tricationic guest **3³⁺** by alkylating 4,4'-bipyridine with 2,4,6-tribromomesitylene. Further alkylation with methyl 2-(bromomethyl)acrylate gives the **4⁶⁺** guest, having 3 pyridinium arms and 6 charges.

With these two multicationic guest molecules in hand, we first tested their complexation with CB[8]. 3^{3+} (0.1 mM) and CB[8] (0.15 mM) in 50 mM phosphate sodium buffer (pH 7.4) remain a heterogeneous mixture after sonicating and heating at 40 °C for more than 0.5 hours. After filtration with a 200 nm syringe filter at room temperature, this sample was analyzed using dynamic light scattering (DLS). Starting from a clear solution, the light scattering intensity gradually increased to 1.4 Mcps (Figure S5.16a) with particle diameters growing to 3.5 µm over the course of 20 hours (Figure S5.16b). In contrast, a solution of 4^{6+} and CB[8] under the same conditions remains transparent for over 24 hours, confirming that 3^{3+} and CB[8] will form a network but 4^{6+} and CB[8] will not. We then wanted to control this aggregation process using the signal molecules described above. As an initial estimate of aggregation, we quantified the turbidity by measuring the transmittance at 500 nm of samples made by mixing 4^{6+} (0.3 mM) and CB[8] (0.45 mM) in phosphate buffer (50 mM, pH 7.4). The 4^{6+}/CB[8] samples are transparent, but shortly after the addition of nucleophilic signals the transmittance starts to decrease sharply (Figure 5.2b,c). Notably, addition of Mesna leads to a rapid increase of turbidity (transmittance goes from 100% to <5% within 10 min (Figure 5.2c). To Figure 5. out what dominates this dramatic change, we further tested sodium vinylsulfonate and 2-mercaptoethanol (**Nu7**) as signals. While we observed no variation of turbidity after adding sodium vinylsulfonate to 4^{6+}/CB[8] (Figure S5.13a, monitored for 10 hours), addition of 2-mercaptoethanol (**Nu7**) leads to a very similar change in turbidity as observed for Mesna. This indicates that the thiol-mediated removal of the Michael acceptor indeed controls aggregation while there are only limited effects of the electrostatic interactions of the sodium salt with the multicationic guest molecule. Both for L-proline (**Nu2**) and hydrazide (**Nu3**) as signals, aggregation did not occur until much later (1.5 h after addition), which is in agreement with their reactivity in the small molecule study. The relation between signal nucleophilicity and aggregation time scale was further confirmed when using ethanolamine (**Nu4**) and NH_3 (**Nu5**), leading to aggregation time scales of 3 and 7 hours, resp. When adding either H_2O_2 (**Nu6**) or no signal, no aggregation is observed during the measurement time (>10 hr). We then further investigated the aggregation of 4^{6+} (0.1 mM) and CB[8] (0.15 mM) using dynamic light scattering (DLS). DLS shows that, in agreement with the turbidity test, aggregation immediately starts upon adding thiol signals (Mesna (**Nu1**) and 2-mercaptoethanol (**Nu7**)) with scattering counts increasing to 22 Mcps and 18 Mcps, respectively, and particle sizes increasing to 2.5 µm (Figure S5.17b). The larger scatter count observed with Mesna may be caused by a salt effect. Addition of L-proline (**Nu2**) and hydrazide (**Nu3**) give very similar aggregation profiles, both starting ~5 hours after addition, and continually increasing to 6 Mcps. With ethanolamine (**Nu4**), aggregation is observed after 14 hours. Addition of NH_3 (**Nu5**) or H_2O_2 (**Nu6**) caused much smaller increases in scatter count compared to the stronger nucleophiles, barely higher than the background scattering rate.
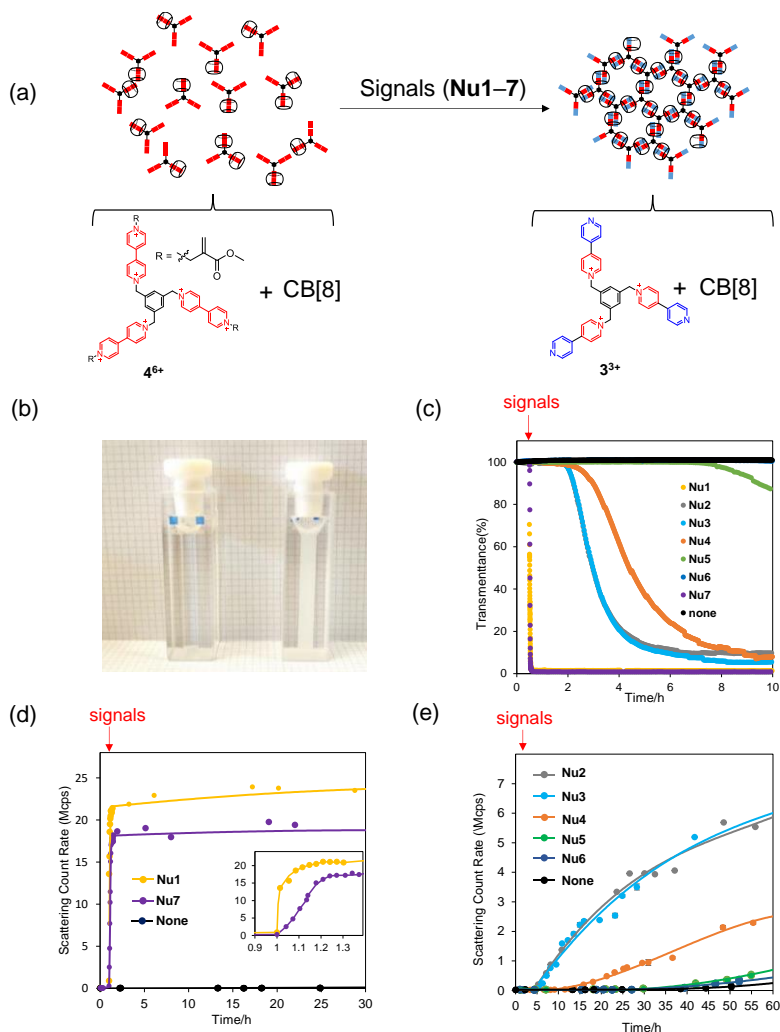
Figure 5.2 Signal-induced aggregation of a tricationic guest with CB[8]. (a) Schematic overview of the signal-induced aggregation process, Br⁻ anions are omitted; (b) Representative photographs of turbidity changes of samples ([**4⁶⁺**] = 0.3 mM, [CB[8]] = 0.45 mM) without signals (left) and 24 hours after adding proline (right, **Nu2**, 0.9 mM); (c) Turbidity measurement (transmittance at 500 nm, [**4⁶⁺**] = 0.3 mM, [CB[8]] = 0.45 mM, [**signals**] = 0.9 mM); (d,e) DLS measurements, [**4⁶⁺**] = 0.1 mM, [CB[8]] = 0.15 mM, [**signals**] = 0.3 mM in 50 mM pH=7.4 sodium phosphate buffer; The insert in (d) shows how the scattering count rate changes between t = 0.9-1.4 h.

Transmission electron microscopy (TEM) images show that the large-scale aggregates made with either 2-mercaptoethanol (**Nu7**) or proline (**Nu2**) as signals are made up from much smaller spherical nanoparticles with diameters of 20-80 nm (Figure 5.3). Aggregates generated upon reaction with 2-mercaptoethanol are much larger and have a more fractal appearance compared to the aggregates generated upon reaction with proline. Avrami analysis[44,45] (Figure S5.18) shows a significant difference in the Avrami coefficient *n* between these two samples, with *n* = 2.81 (**Nu7**) and *n* = 1.85 (**Nu2**), which indicates a higher dimensionality of the growth process in the sample triggered by 2-mercaptoethanol. This result is in line with the different degree of branching observed in the TEM images. In previously studied supramolecular gelation processes, we observed increased fiber branching at higher rates of gelator formation[44]. Analogously, the current results suggest that stronger nucleophiles lead to faster complex formation, and with that, more branching. Indicated from powder X-ray diffraction, both of the samples exhibit some crystallinity (Figure S5.19),[46] while the aggregate induced by 2-mercaptoethanol shows more crystalline characteristics than that from proline. We are unable to suggest the formation of SOFs with high regularities and periodicities on the basis of TEM and XRD results, but the shape and crystallinity of the aggregate can be likely controlled by signals with different nucleophilicity through chemical reactions. Continuous monitoring of the aggregation process (**4**$^{6+}$ (0.3 mM), CB[8] (0.45 mM), **Nu7** (0.9 mM)) by confocal laser scanning microscopy (CLSM) shows that in the beginning the aggregates are very small, fast moving particles, which over time grow and connect together to become a larger aggregate. We analysed the composition of these aggregates over the course of the process using ^{1}H-NMR (Figure s S5.13,S5.14, Scheme S5.1). A transparent solution of **4**$^{6+}$ (0.8 mM) and CB[8] (1.2 mM) in 50 mM phosphate buffer (pH 7.4, 10% D$_2$O) shows the ^{1}H-NMR peaks of the **4**$^{6+}$⊂CB[8] complex and of CB[8] itself. Addition of 2-mercaptoethanol results in immediate precipitation in the NMR tube, which leads to the complete disappearance of the NMR peaks of **4**$^{6+}$ and CB[8], indicating that they are no longer in solution (Figure S5.14). The isolated precipitates were found to be insoluble in D$_2$O. We selected *N,N,N*-trimethyl-1-adamantylammonium chloride[47] as a soluble guest molecule with very high affinity for CB[8]. This high-affinity guest is expected to break the cross-links in the aggregate by replacing **3**$^{3+}$ in the CB[8] cavity. After mixing *N,N,N*-trimethyl-1-adamantylammonium chloride (24 mM) with the **3**$^{3+}$/CB[8] precipitate in D$_2$O, we observed that part of the precipitate dissolved, and ^{1}H-NMR peaks of unbound **3**$^{3+}$ and CB[8] emerged (Figure S5.15). In this way, we demonstrate that the aggregates are indeed held together by **3**$^{3+}$ / CB[8] cross-links.
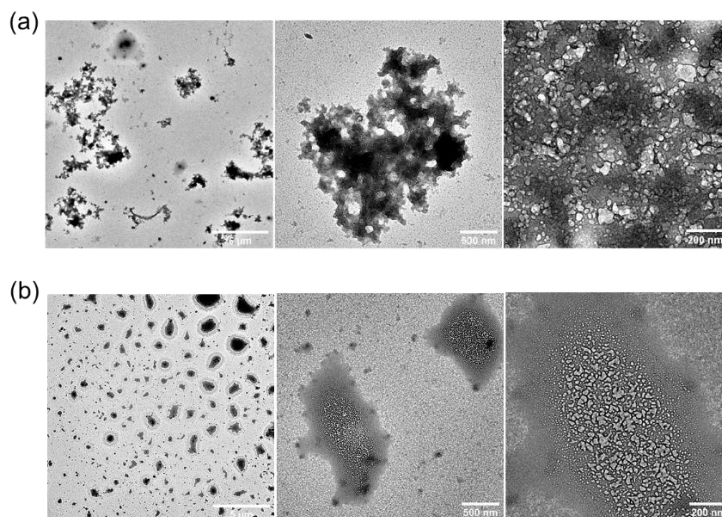
(a)

(b)

Figure 5.3 TEM images of aggregates formed using thiol and amine signals ([**4^{6+}**] = 0.1 mM, [CB[8]] = 0.15 mM). (a) Images taken 24 h after adding 2-mercaptoethanol (**Nu7**, 0.3 mM), scale bar = 5 μm (left), 500 nm (middle), 200 nm (right); (b) Images taken 72 h after adding proline (**Nu2**, 0.3 mM), scale bar = 5 μm (left), 500 nm (middle), 200 nm (right).

These results demonstrate that aggregation can be triggered by various signals, and that the aggregation rate scales with the signal nucleophilicity. However, the weak nucleophile hydrogen peroxide (**Nu6**) did not function as a signal in this cascade. H_2O_2 is generated in numerous biological systems and plays an important role in cellular processes,[48] including the role of signalling molecule to regulate a wide variety of biological responses[49] and indicating the development of diseases[50]. In an attempt to adapt hydrogen peroxide as a signal in our signalling cascade and inspired by our previous work on H_2O_2-activited organocatalysts[51,52] we designed a relayed transduction system to amend the nucleophilicity of H_2O_2. We used a blocked proline nucleophile, protected with a boronic acid responsive self-immolative group that can be oxidatively cleaved by hydrogen peroxide. This pre-proline functions as a signal-relay (Figure 5.4a), where proline released by H_2O_2 will trigger aggregation (Figure 5.3a).

Based on this design, we first tested the reactivity on small molecules. Pre-proline (**5**) is stable in the buffer solution, but adding H_2O_2 leads to >95% release of proline within 30 min (Figure 5.3b). Moreover, pre-proline shows no significant reactivity with **2^{2+}**, with a **2^{2+}** conversion rate close to the background reaction (Figure 5.3c). As discussed above, the reactivity of H_2O_2 to **2^{2+}** is low (Figure 5.1b), but in the solution of **2^{2+}** (2 mM) and pre-proline (3 mM), a high conversion rate of **2^{2+}** was observed upon adding H_2O_2. Meanwhile pre-proline **5** itself shows no affinity with CB[8] indicated by ITC (Table S1).

We subsequently moved on to applying this signalling cascade to the signal-induced aggregation process. In the turbidimetry assay, H_2O_2 or pre-proline alone added into the solution of 4^{6+} (0.3 mM) and CB[8] (0.45 mM) did not cause any changes of transmittance. Instead, H_2O_2 (0.9 mM) added to a solution of pre-proline (0.9 mM), 4^{6+} (0.3 mM) and CB[8] (0.45 mM) instantly caused a slight decrease in transmittance, with a sharp decrease observed after ~5 hours. The slower aggregation observed in this signalling cascade compared to using proline itself as a signal can be attributed to the time it takes to release proline by H_2O_2. In the DLS measurement at a lower concentration of 4^{6+} (0.1 mM) and CB[8] (0.15 mM), the aggregation process triggered by the cascade of H_2O_2 (0.3 mM) and pre-proline (0.3 mM) starts at a similar time as when using proline and hydrazide signals. Scattering counts reach 7 Mcps after 50 hours, which is slightly higher than observed for proline-triggered aggregation (Figure 5.2e). This difference may be caused by additional species created in the signal relay process.
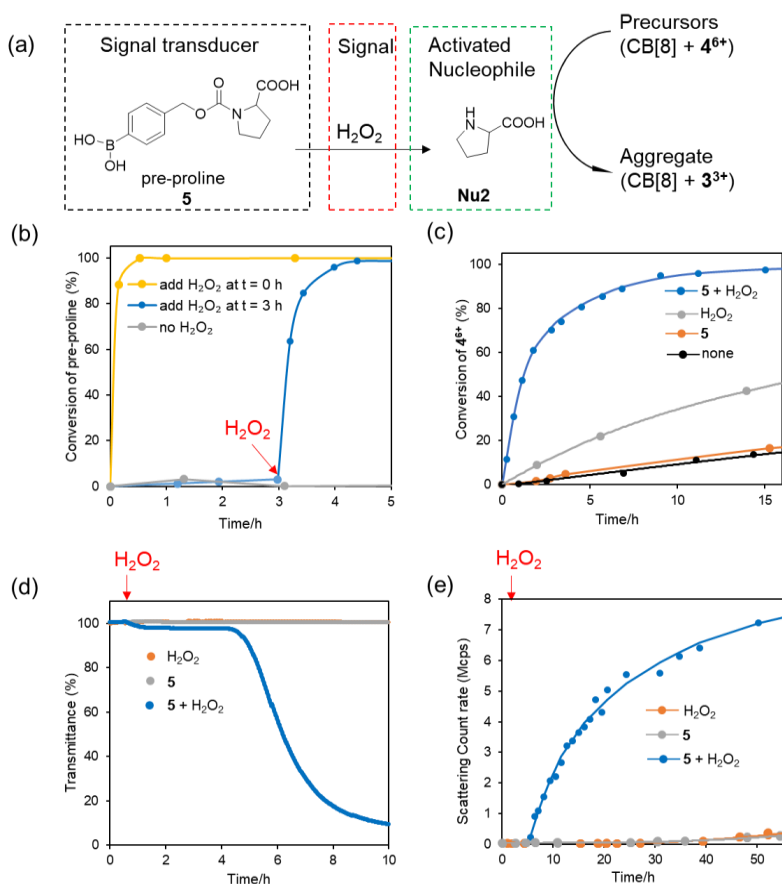

Figure 5.4 Pre-proline as a signal transducer to relay hydrogen peroxide as a nucleophilic signal. (a) Schematic description of the design. (b)

Conversion of pre-proline ([**5**] = 3 mM, H$_2$O$_2$ = 3 mM). (c) Conversion of **2^{2+}** through signalling cascade by H$_2$O$_2$ ([**2^{2+}**] = 2 mM, [**5**] = 3 mM, [H$_2$O$_2$] = 3 mM). (d) Turbidity measurement by UV-Vis transmittance at 500 nm, [**4^{6+}**] = 0.3 mM, [CB[8]] = 0.45 mM, [**5**] = 0.9 mM, [H$_2$O$_2$] = 0.9 mM; (e) DLS measurement of aggregate formation, [**4^{6+}**] = 0.1 mM, [CB[8]] = 0.15 mM, [**5**] = 0.3 mM, [H$_2$O$_2$] = 0.3 mM in 50 mM pH=7.4 sodium phosphate buffer.

5.3 Conclusions

In this work, we developed an artificial supramolecular aggregation process capable of responding to chemical signals. We demonstrate a switch between CB[8] binary and ternary host-guest complexes with charged bipyridine derivatives, where the charge on the bipyridine can be adjusted by nucleophilic signal induced removal of a pyridinium Michael acceptor. This switch is responsive to a range of biologically relevant nucleophiles such as thiols and amines. We expanded this concept to weak nucleophiles by developing a signal transducer strategy, enabling response to weakly nucleophilic hydrogen peroxide. Using a tripodal bipyridine derivative we could demonstrate signal induced supramolecular aggregate formation of CB[8]-crosslinked networks. In this process, the rate of aggregation as well as aggregate structure can be controlled with nucleophile strength. This work offers new opportunities for building more complicated signaling networks and can be expected to pave the way for construction of artificial materials that can interact with living systems through signal transduction and can realize controlled release by reacting to biomarkers.

5.4 References

(1)   Levin, J. Chapter 1 - The Evolution of Mammalian Platelets; Michelson, A. D. B. T.-P. (Third E., Ed.; Academic Press, 2013; pp 3–25.

(2)   Gomperts, B. D.; Kramer, I. M.; Tatham, P. E. R. 1 - Prologue: Signal Transduction, Origins and Personalities; Gomperts, B. D., Kramer, I. M., Tatham, P. E. R. B. T.-S. T., Eds.; Academic Press: San Diego, 2002; pp 1–17.

(3)   Yan, X.; Wang, F.; Zheng, B.; Huang, F. Stimuli-Responsive Supramolecular Polymeric Materials. *Chem. Soc. Rev.* **2012**, *41* (18), 6042–6065.

(4)   Ma, X.; Tian, H. Stimuli-Responsive Supramolecular Polymers in Aqueous Solution. *Acc. Chem. Res.* **2014**, *47* (7), 1971–1981.

(5)   Koevoets, R. A.; Versteegen, R. M.; Kooijman, H.; Spek, A. L.; Sijbesma, R. P.; Meijer, E. W. Molecular Recognition in a Thermoplastic Elastomer. *J. Am. Chem. Soc.* **2005**, *127* (9), 2999–3003.

(6)   Appel, E. A.; Biedermann, F.; Rauwald, U.; Jones, S. T.; Zayed, J. M.; Scherman, O. A. Supramolecular Cross-Linked Networks via Host-Guest Complexation with Cucurbit[8]Uril. *J. Am. Chem. Soc.* **2010**, *132* (40), 14251–14260.

(7)   Jones, C. D.; Steed, J. W. Gels with Sense: Supramolecular Materials That Respond to Heat, Light and Sound. *Chem. Soc. Rev.* **2016**, *45* (23), 6546–6596.

(8)   Del Barrio, J.; Horton, P. N.; Lairez, D.; Lloyd, G. O.; Toprakcioglu, C.; Scherman, O. A. Photocontrol over Cucurbit[8]Uril Complexes: Stoichiometry and Supramolecular Polymers. *J. Am. Chem. Soc.* **2013**, *135* (32), 11760–11763.

(9)   Zou, L.; Addonizio, C. J.; Su, B.; Sis, M. J.; Braegelman, A. S.; Liu, D.; Webber, M. J. Supramolecular Hydrogels via Light-Responsive Homoternary Cross-Links. *Biomacromolecules* **2021**, *22* (1), 171–182.

(10)   Yin, Z.; Song, G.; Jiao, Y.; Zheng, P.; Xu, J.-F.; Zhang, X. Dissipative Supramolecular Polymerization Powered by Light. *CCS Chem.* **2019**, *1* (4), 335–342.

(11)   Leung, K. C.-F.; Chak, C.-P.; Lo, C.-M.; Wong, W.-Y.; Xuan, S.; Cheng, C. H. K. PH-Controllable Supramolecular Systems. *Chem. - An Asian J.* **2009**, *4* (3), 364–381.

(12)   Yang, H.; Chen, H.; Tan, Y. Cucurbit[8]Uril Inducing Supramolecular Hydrogels by Adjusting PH. *RSC Adv.* **2013**, *3* (9), 3031–3037.

(13)   Lin, Y.; Li, L.; Li, G. A New Supramolecular Gel via Host-Guest Complexation with Cucurbit[8]Uril and N-(4-Diethylaminobenzyl)Chitosan. *Carbohydr. Polym.* **2013**, *92* (1), 429–434.

(14)   Liu, Y.; Yu, Y.; Gao, J.; Wang, Z.; Zhang, X. Water-Soluble Supramolecular Polymerization Driven by Multiple Host-Stabilized Charge-Transfer Interactions. *Angew. Chem. Int. Ed.* **2010**, *49* (37), 6576–6579.

(15)   Fukino, T.; Yamagishi, H.; Aida, T. Redox-Responsive Molecular Systems and Materials. *Adv. Mater.* **2017**, *29* (25), 1603888.

(16)   Pazos, E.; Novo, P.; Peinador, C.; Kaifer, A. E.; García, M. D. Cucurbit[8]Uril (CB[8])-Based Supramolecular Switches. *Angew. Chem. Int. Ed.* **2019**, *58* (2), 403–416.

(17)   Xu, W.; Song, Q.; Xu, J. F.; Serpe, M. J.; Zhang, X. Supramolecular Hydrogels Fabricated from Supramonomers: A Novel Wound Dressing Material. *ACS Appl. Mater. Interfaces* **2017**, *9* (13), 11368–11372.

(18)   Shigemitsu, H.; Hamachi, I. Supramolecular Assemblies Responsive to Biomolecules toward Biological Applications. *Chem. - An Asian J.* **2015**, *10* (10), 2026–2038.

(19)   Loh, X. J. Supramolecular Host-Guest Polymeric Materials for Biomedical Applications. *Mater. Horizons* **2014**, *1* (2), 185–195.

(20)   Braegelman, A. S.; Webber, M. J. Integrating Stimuli–Responsive Properties in Host–Guest Supramolecular Drug Delivery Systems. *Theranostics* **2019**, *9* (11), 3017–3040.

(21)   Correia, H. D.; Chowdhury, S.; Ramos, A. P.; Guy, L.; Demets, G. J. F.; Bucher, C. Dynamic Supramolecular Polymers Built from Cucurbit[n]Urils and Viologens. *Polym. Int.* **2019**, *68* (4), 572–588.

(22)   Zhan, T. G.; Zhou, T. Y.; Lin, F.; Zhang, L.; Zhou, C.; Qi, Q. Y.; Li, Z. T.; Zhao, X. Supramolecular Radical Polymers Self-Assembled from the Stacking of Radical Cations of Rod-like Viologen Di- and Trimers. *Org. Chem. Front.* **2016**, *3* (12), 1635–1645.

(23)   Striepe, L.; Baumgartner, T. Viologens and Their Application as Functional Materials. *Chem. - A Eur. J.* **2017**, *23* (67), 16924–16940.

(24)   Jeon, W. S.; Kim, H. J.; Lee, C.; Kim, K. Control of the Stoichiometry in Host-Guest Complexation by Redox Chemistry of Guests: Inclusion of Methylviologen in

Cucurbit[8]Uril. *Chem. Commun.* **2002**, No. 17, 1828–1829.

(25)   Zhang, Q.; Qu, D.-H.; Wang, Q.-C.; Tian, H. Dual-Mode Controlled Self-Assembly of TiO 2 Nanoparticles Through a Cucurbit[8]Uril-Enhanced Radical Cation Dimerization Interaction. *Angew. Chem. Int. Ed.* **2015**, *54* (52), 15789–15793.

(26)   Jeon, W. S.; Kim, E.; Ko, Y. H.; Hwang, I.; Lee, J. W.; Kim, S.-Y.; Kim, H.-J.; Kim, K. Molecular Loop Lock: A Redox-Driven Molecular Machine Based on a Host-Stabilized Charge-Transfer Complex. *Angew. Chem. Int. Ed.* **2005**, *44* (1), 87–91.

(27)   Zhang, L.; Zhou, T. Y.; Tian, J.; Wang, H.; Zhang, D. W.; Zhao, X.; Liu, Y.; Li, Z. T. A Two-Dimensional Single-Layer Supramolecular Organic Framework That Is Driven by Viologen Radical Cation Dimerization and Further Promoted by Cucurbit[8]Uril. *Polym. Chem.* **2014**, *5* (16), 4715–4721.

(28)   Jeon, W. S.; Ziganshina, A. Y.; Wook Lee, J.; Ko, Y. H.; Kang, J. K.; Lee, C.; Kim, K. A [2]Pseudorotaxane-Based Molecular Machine: Reversible Formation of a Molecular Loop Driven by Electrochemical and Photochemical Stimuli. *Angew. Chem. Int. Ed.* **2003**, *42* (34), 4097–4100.

(29)   Shiguo Sun,† Rong Zhang,‡ Samir Andersson,† Jingxi Pan,‡ Dapeng Zou,† Bjo1rn Åkermark, § and Licheng Sun. Host−Guest Chemistry and Light Driven Molecular Lock of Ru(Bpy)3−Viologen with Cucurbit[7–8]Urils. *J. Phys. Chem. B* **2007**, *111*.

(30)   Zhang, Q.; Qu, D.; Wang, Q.; Tian, H. Dual-Mode Controlled Self-Assembly of TiO 2 Nanoparticles Through a Cucurbit[8]Uril-Enhanced Radical Cation Dimerization Interaction. *Angew. Chem. Int. Ed.* **2015**, *54* (52), 15789–15793.

(31)   Vincil, G. A.; Urbach, A. R. Effects of the Number and Placement of Positive Charges on Viologen-Cucurbit[n]Uril Interactions. *Supramol. Chem.* **2008**, *20* (8), 681–687.

(32)   Zhang, Z. J.; Zhang, Y. M.; Liu, Y. Controlled Molecular Self-Assembly Behaviors between Cucurbituril and Bispyridinium Derivatives. *J. Org. Chem.* **2011**, *76* (11), 4682–4685.

(33)   Zhuang, J.; Zhao, B.; Meng, X.; Schiffman, J. D.; Perry, S. L.; Vachet, R. W.; Thayumanavan, S. A Programmable Chemical Switch Based on Triggerable Michael Acceptors. *Chem. Sci.* **2020**, *11* (8), 2103–2111.

(34)   Klemm, B.; Lewis, R.; Piergentili, I.; Eelkema, R. Temporally Programmed Polymer-Solvent Interactions Using a Chemical Reaction Network. **2021**.

(35)   Lewis, R. W.; Klemm, B.; Macchione, M.; Eelkema, R. Fuel-Driven Macromolecular Coacervation in Complex Coacervate Core Micelles. *Chem. Sci.* **2022**, *13* (16), 4533–4544.

(36)   Barrow, S. J.; Kasera, S.; Rowland, M. J.; Del Barrio, J.; Scherman, O. A. Cucurbituril-Based Molecular Recognition. *Chem. Rev.* **2015**, *115* (22), 12320–12406.

(37)   National Center for Biotechnology Information. PubChem Compound Summary for CID 23662354, Mesna https://pubchem.ncbi.nlm.nih.gov/compound/Mesna (accessed Jan 11, 2022).

(38)   Le Goff, G.; Ouazzani, J. Natural Hydrazine-Containing Compounds: Biosynthesis, Isolation, Biological Activities and Synthesis. *Bioorganic Med. Chem.* **2014**, *22* (23), 6529–6544.

(39)   Li, G.; Trausel, F.; van der Helm, M. P.; Klemm, B.; Brevé, T. G.; van Rossum, S. A.

P.; Hartono, M.; Gerlings, H. H. P. J.; Lovrak, M.; van Esch, J. H.; Eelkema, R. Tuneable Control of Organocatalytic Activity through Host–Guest Chemistry. *Angew. Chem. Int. Ed.* **2021**, *60* (25), 14022–14029.

(40) Brotzel, F.; Mayr, H. Nucleophilicities of Amino Acids and Peptides. *Org. Biomol. Chem.* **2007**, *5* (23), 3814–3820.

(41) Tian, J.; Zhou, T.-Y.; Zhang, S.-C.; Aloni, S.; Altoe, M. V.; Xie, S.-H.; Wang, H.; Zhang, D.-W.; Zhao, X.; Liu, Y.; Li, Z.-T. Three-Dimensional Periodic Supramolecular Organic Framework Ion Sponge in Water and Microcrystals. *Nat. Commun.* **2014**, *5* (1), 5574.

(42) Li, Y.; Qin, C.; Li, Q.; Wang, P.; Miao, X.; Jin, H.; Ao, W.; Cao, L. Supramolecular Organic Frameworks with Controllable Shape and Aggregation-Induced Emission for Tunable Luminescent Materials through Aqueous Host–Guest Complexation. *Adv. Opt. Mater.* **2020**, *8* (14), 1902154.

(43) Wang, H.; Zhang, D.; Zhao, X.; Li, Z.-T. Chapter 8. Cucurbit[8]Uril-Based 2D and 3D Regular Porous Frameworks; 2019; pp 175–192.

(44) Boekhoven, J.; Poolman, J. M.; Maity, C.; Li, F.; Van Der Mee, L.; Minkenberg, C. B.; Mendes, E.; Van Esch, J. H.; Eelkema, R. Catalytic Control over Supramolecular Gel Formation. *Nat. Chem.* **2013**, *5* (5), 433–437.

(45) Liu, X. Y.; Sawant, P. D. Mechanism of the Formation of Self-Organized Microstructures in Soft Functional Materials. *Adv. Mater.* **2002**, *14* (6), 421–426.

(46) Li, Y.; Li, Q.; Miao, X.; Qin, C.; Chu, D.; Cao, L. Adaptive Chirality of an Achiral Cucurbit[8]Uril-Based Supramolecular Organic Framework for Chirality Induction in Water. *Angew. Chem. Int. Ed.* **2021**, *60* (12), 6744–6751.

(47) Liu, S.; Ruspic, C.; Mukhopadhyay, P.; Chakrabarti, S.; Zavalij, P. Y.; Isaacs, L. The Cucurbit[n]Uril Family: Prime Components for Self-Sorting Systems. *Journal of the American Chemical Society*. 2005, pp 15959–15967.

(48) Winterbourn, C. C. The Biological Chemistry of Hydrogen Peroxide. *Methods Enzymol.* **2013**, *528*, 3–25.

(49) Veal, E. A.; Day, A. M.; Morgan, B. A. Hydrogen Peroxide Sensing and Signaling. *Mol. Cell* **2007**, *26* (1), 1–14.

(50) Pravda, J. Hydrogen Peroxide and Disease: Towards a Unified System of Pathogenesis and Therapeutics. *Mol. Med.* **2020**, *26* (1), 41.

(51) Trausel, F.; Maity, C.; Poolman, J. M.; Kouwenberg, D. S. J.; Versluis, F.; van Esch, J. H.; Eelkema, R. Chemical Signal Activation of an Organocatalyst Enables Control over Soft Material Formation. *Nat. Commun.* **2017**, *8* (1), 879.

(52) Maity, C.; Trausel, F.; Eelkema, R. Selective Activation of Organocatalysts by Specific Signals. *Chem. Sci.* **2018**, *9* (27), 5999–6005.

5.5 Supplementary Information

5.5.1 General information

General methods

NMR spectra were recorded on an Agilent-400 MR DD2 (399.7 MHz for ^{1}H, 100.5 MHz for ^{13}C) at 298 K using residual protonated solvent signals as internal standard (^{13}C in D_2O was referenced to internal 1,4-Dioxane, δ = 67.19). **UV/Vis** spectroscopic measurements were performed on an Analytik Jena Specord 250 spectrophotometer; quartz cuvettes with a path length of 1.0 cm were used. **Isothermal titration calorimetry (ITC)** measurements were carried out at room temperature using a MicroCal VP-ITC. **LC-MS** was performed on a Shimadzu Liquid Chromatograph Mass Spectrometer 2010, LC-8A pump with a diode array detector SPD-M20. The **pH** was recorded with the Consort C830 pH meter. **Fourier Transform Infrared Spectroscopy (FTIR)** spectroscopy was performed with NicoletTM 6700 FT-IR Spectrometer from Thermo Electron Corporation equipped with OMNIC Software using the ATR method. **The Dynamic Light Scattering (DLS)** test was conducted on Malvern Zetasizer, using PMMA disposable cuvettes with a 1 cm path length, a volume of 1.5 mL. The attenuator was set to be auto during the measurement and the mean count rate was calibrated with the attenuation factor provided by the manufacturer. The temperature inside the cell was set at 25°C for all experiments. **Transmission election microscopy (TEM)** were performed on a JEOLJEM-1400plus TEM operated at 120 kV. Samples were prepared by placing 3 μL of the solution onto carbon coated copper grids and incubating for 1 minute followed by blotting the excess solution onto filter paper. The samples were then washed (2×) with of milli-q water, followed by removing the excess onto filter paper. The images were analysed using Image J software. **Confocal laser scanning microscopy** (CLSM) was performed in LSM 710 system using a Zeiss Observer Z.1 inverted microscope. Images were taken by an AxioCam MRm camera from Carl Zeiss MicroImaging. **Powder Xray diffraction (PXRD)** spectra were recorded on a Bruker D8 Advance-ECO with Bragg-Brentano geometry. The source of X-ray is Cu radiation, wavelengths: Kα1(100) = 1.54060 Å, Kα2(50) = 1.54439 Å.

Materials

Sodium phosphate monobasic monohydrate (98%), 1,3,5-tris(bromomethyl)benzene (97%), , sodium 2-mercaptoethanesulfonate (Mesna, ≥98%), ammonium hydroxide (28.0-30.0% NH_3 basis), 4-hydroxybutyric acid hydrazide, 2-mercaptoethanol (99.0%), *N*-acetyl-L-proline (98%), 1-adamantanamine (97%) were purchased from Sigma Aldrich. 4,4'-bipyridine (>98.0%), 1-bromopropane (>98.0%), methyl 2-(bromomethyl)acrylate (>97.0%), ethanolamine (>99%), 4-(4,4,5,5-tetramethyl-1,3,2-dioxaborolan-2-yl)benzyl alcohol (>98%), *N,N,N*-trimethyl-1-

adamantylammonium hydroxide (25% in water), sodium vinylsulfonate (25% in water) were purchased from TCI Europe. Sodium phosphate dibasic salt (≥99%, analysis grade) was purchased from Acros Organics. Deuterium oxide for NMR was purchased from Euriso-top. L-proline (≥99%) was from Fluorochem Ltd. CB[8] was obtained from Professor Oren A. Scherman's group at Cambridge University. Aqueous pH buffers were prepared by mixing the aqueous solution of sodium phosphate monobasic monohydrate salt and sodium phosphate dibasic salt at the same concentration, under the measurement of pH indicator until the required pH is achieved.

Synthesis and characterization
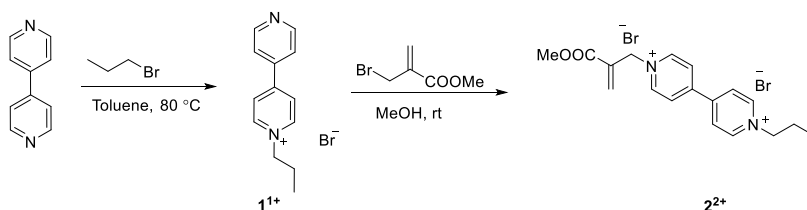
The guest molecule **1**[1+] was synthesized according to a published procedure[1] by reacting 4,4'-bipyridine with 1-bromopropane in toluene at 80 °C for 48 h. The raw product was purified by filtering off the toluene and the residue was washed with ethyl acetate to afford a brown sticky solid.

^{1}H NMR (400 MHz, Deuterium Oxide) δ 8.97 (d, J = 6.4 Hz, 2H), 8.79 (d, J = 6.4 Hz, 2H), 8.42 (d, J = 6.4 Hz, 2H), 7.92 (d, J = 6.4 Hz, 2H), 4.64 (t, J = 7.2 Hz, 2H), 2.09 (tq, J_1 = 7.2, J_2 =7.2 Hz, 2H), 0.99 (t, J = 7.2 Hz, 3H).[1]

Dicationic guest molecule **2**[2+] was synthesized by reacting 22.3 mg of guest molecule **1**[1+] (0.08 mM) and 11.9 μL methyl 2-(bromomethyl)acrylate (0.11 mmol, 1.4 eq) in 0.9 mL methanol at room temperature overnight. The solvent and unreacted methyl 2-(bromomethyl)acrylate were removed through rotary evaporation and subsequent drying under vacuum, affording the product as a yellow fine powder.

28.1 mg, yield 72%. **^{1}H NMR** (400 MHz, Deuterium Oxide) δ 9.02 (dd, J = 25.8, 6.8 Hz, 4H), 8.41 (d, J = 6.6 Hz, 4H), 6.65 (s, 1H), 6.30 (s, 1H), 5.46 (s, 2H), 4.56 (t, J = 7.2 Hz, 2H), 3.63 (s, 3H), 1.97 (tq, J_1 = 7.2, J_2 = 7.2 Hz, 2H), 0.86 (t, J = 7.2 Hz, 3H). **^{13}C NMR** (101 MHz, D_2O) δ 167.05, 151.36, 150.50, 146.56, 146.11, 136.42, 132.97, 127.61, 127.42, 64.23, 62.52, 53.43, 24.86, 10.26. **MS** (ESI Pos) m/z: 149.04 [(M-2Br⁻)/2]⁺ (expected m/z = 149.08).
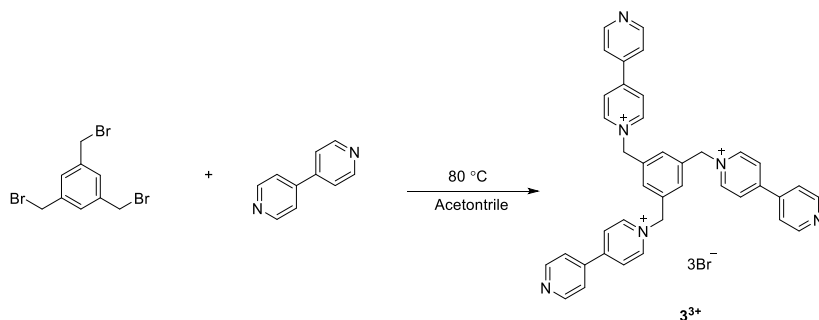
Guest molecule **3³⁺** was synthesized according to a previous publication[2,3] with modification. 5 g 4,4'-bipyridine (32 mmol, 6.4 eq.) was dissolved in 30 mL acetonitrile. A solution of 1.78 g 1,3,5-tris(bromomethyl)benzene (5 mmol, 1.0 eq.) in 20 mL acetonitrile was added dropwise to the 4,4'-bipyridine solution. The mixture was then stirred at reflux for 20 hours. The raw product was filtered off after cooling to room temperature. The filter cake was washed by dichloromethane and then dissolved in water, which was then washed with dichloromethane four times to fully remove the excess 4,4'-bipyridine. After freeze-drying, the yellow powder was dissolved into a minimum amount of methanol and diethyl ether was added to initiate precipitation. The precipitate was separated by centrifugation and dried under vacuum overnight, yielding 2.01 g yellow powder (48.7%). **¹H NMR** (400 MHz, Deuterium Oxide) δ 8.98 (d, *J* = 6.6 Hz, 6H), 8.70 (d, *J* = 6.0 Hz, 6H), 8.39 (d, *J* = 6.6 Hz, 6H), 7.80 (d, *J* = 6.0 Hz, 6H), 7.38 (s, 3H), 5.97 (s, 6H).
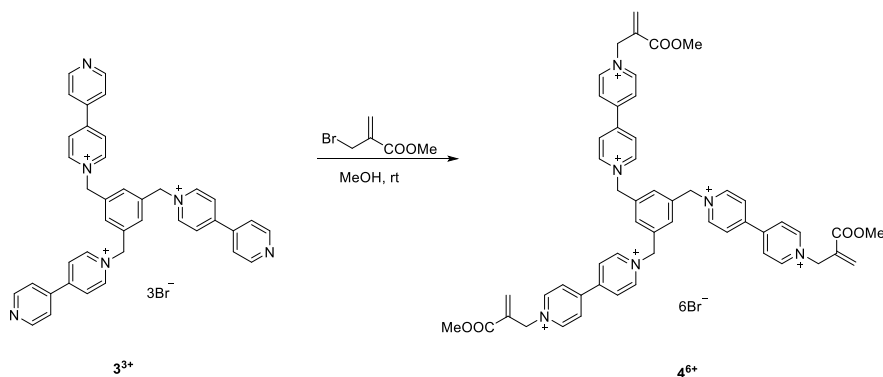
Synthesis of guest molecule **4⁶⁺** is similar to **2²⁺**. 290 mg of guest molecule **3³⁺** (0.35 mmol) and 189 μL methyl 2-(bromomethyl)acrylate (1.58 mmol) was stirred in 3.5 mL methanol overnight at room temperature. Final product was obtained by removing the solvent and unreacted methyl 2-(bromomethyl)acrylate through rotary evaporator and vacuum, as a yellow waxy solid (355 mg, yield 74%).

^{1}H NMR (400 MHz, Deuterium Oxide) δ 9.20 (d, J = 5.6 Hz, 12H), 8.60-8.55 (m, 12H), 7.82 (s, 3H), 6.79 (s, 3H), 6.45 (s, 3H), 6.03 (s, 6H), 5.60 (s, 6H), 3.76 (s, 9H). **^{13}C NMR** (101 MHz, D$_2$O) δ 167.04, 151.26, 151.07, 146.57, 146.37, 136.45, 135.67, 132.94, 132.39, 128.14, 127.56, 64.21, 62.56, 53.45. **MS** (ESI Pos) m/z: 176.33 [(M-6Br$^-$)/5]$^+$ (expected m/z = 176.48); m/z: 219.97 [(M-6Br$^-$)/4]$^+$ (expected m/z = 220.60); m/z: 293.20 [(M-6Br$^-$)/3]$^+$ (expected m/z = 294.14).
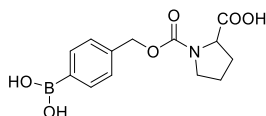
5

Pre-proline **5** was synthesized according to a previously reported procedure.[4]

^{1}H NMR (400 MHz, DMSO-d_6) δ 8.03 (d, *J* = 4.5 Hz, 2H), 7.76 (dd, *J* = 9.5, 7.8 Hz, 1H), 7.28 (dd, *J* = 21.1, 7.7 Hz, 1H), 5.10–4.99 (m, 2H), 4.28–4.11 (m, 1H), 3.36-3.46 (m, 2H), 2.18-2.23 (m, 1H), 1.80-1.95 (d, *J* = 7.7 Hz, 2H).

5.5.2 Isothermal titration calorimetry results (ITC)

ITC plots were measured by Microcal VP-ITC at 298.15 K in 50 mM pH=7.4 sodium phosphate buffer. The guest molecule solution (in the injection syringe, with a concentration of 10 (**2^{2+}**) or 20 (**1^{1+}**) times to the concentration of the CB[8]) was titrated into the CB[8] solution in the sample cell. The CB[8] concentration was calibrated by titration of a 1-adamantanamine solution. Thermodynamic data of the association were obtained by fitting the measured data point (excluding the first titration) with Microcal LLC ITC Origin 7 software.

Table S5.1. ITC plots and fitting results of guest molecules with CB[8].

(a)

Model: Sequential Binding Sites
Chi²/DoF = 1223
K1   8.00E4 ±1.3E3 M⁻¹
ΔH1   -3916 ±50.6 cal/mol
ΔS1   9.30 cal/mol/deg
K2   8.59E4 ±1.1E3 M⁻¹
ΔH2   -9213 ±63.7 cal/mol
ΔS2   -8.32 cal/mol/deg

Condition: 50 mM sodium phosphate buffer pH 7.4, 25 °C, [**1¹⁺**] = 0.52 mM, [CB[8]] = 0.026 mM.

(b)

Model: OneSites
Chi²/DoF = 4023
N   1.03   ±0.0204 Sites
K   1.05E5 ±9.38E3 M⁻¹
ΔH   -4000 ±124.2 cal/mol
ΔS   9.56 cal/mol/deg

Condition: 50 mM sodium phosphate buffer pH 7.4, 25 °C, [**2²⁺**] = 0.37 mM, [CB[8]] = 0.037 mM.

Data: preprolinet_NDH
Model: OneSites
Chi²/DoF = 1.410E4
N   8.02E3 ±4.08E9 Sites
K   0.838   ±4.26E5 M⁻¹
ΔH   -429.9 ±7525 cal/mol
ΔS   -1.79 cal/mol/deg

Condition: 10 mM sodium phosphate buffer pH 7.4, 25 °C, [**5**] = 0.44 mM, [CB[8]] = 0.044mM.

5.5.3 NMR titration to show the binding stoichiometric ratio

Solutions of 1 mM guest molecule with gradient equivalents of CB[8] (from 0 eq. to 1 eq.) were prepared in 10 mM pH=7.4 phosphate buffer solution (90%) and deuterium oxide (10%). ^{1}H NMR of these mixture were measured using a water suppression pulse sequence.
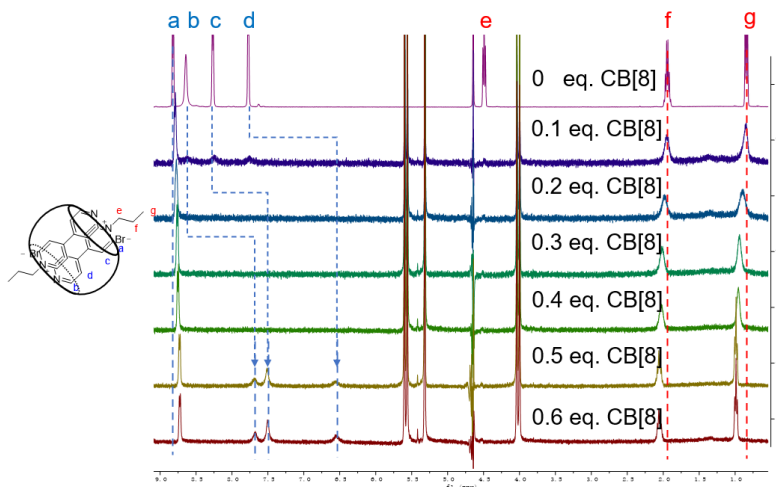
Figure S5.1 ^{1}H-NMR titration (water suppression mode, in 10 mM pH=7.4 sodium phosphate buffer) of 1 mM monocationic guest molecule **1[1+]** with different equivalents of CB[8].
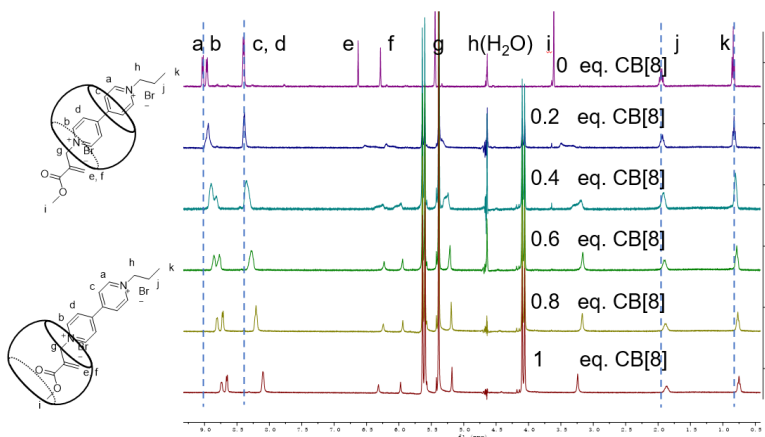
Figure S5.2 ^{1}H NMR titration (water suppression mode, in 10 mM pH=7.4 sodium phosphate buffer) of 1 mM dicationic guest molecule **2[2+]** with different equivalents of CB[8].

5.5.4 ¹H-NMR measurements to follow the triggerable Michael addition reaction

General procedure of continuous ¹H-NMR measurements of the reaction:

The reaction solution containing the substrates of **2²⁺** (2 mM) and signals molecules (3 mM), sodium trimethylsilylpropanesulfonate (**DSS**, 0.5 mM) as standard in 50 mM phosphate buffer and 10% D₂O was prepared by mixing and dilution of concentrated stock solutions. Conversion of **2²⁺** was determined by measuring ¹H-NMR (water suppression mode) over time.
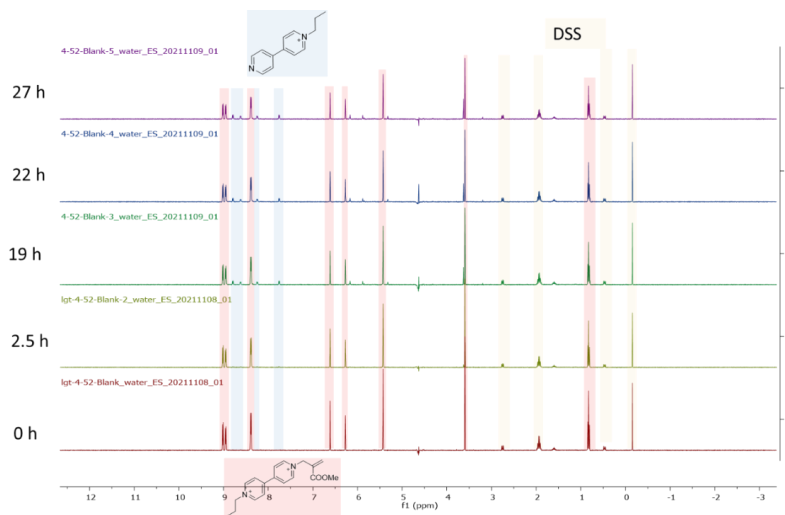
Figure S5.3 NMR spectra overlay to follow the blank reaction (**2²⁺** 2 mM) over time.
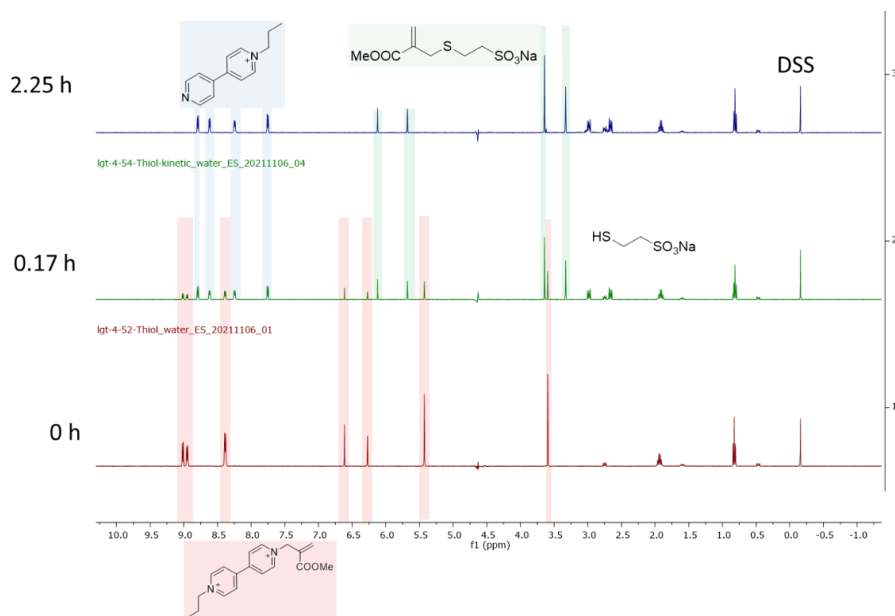
Figure S5.4 ^{1}H-NMR spectra overlay to follow the reaction of **2^{2+}** (2 mM) and Mesna (**Nu1** 3 mM) over time.
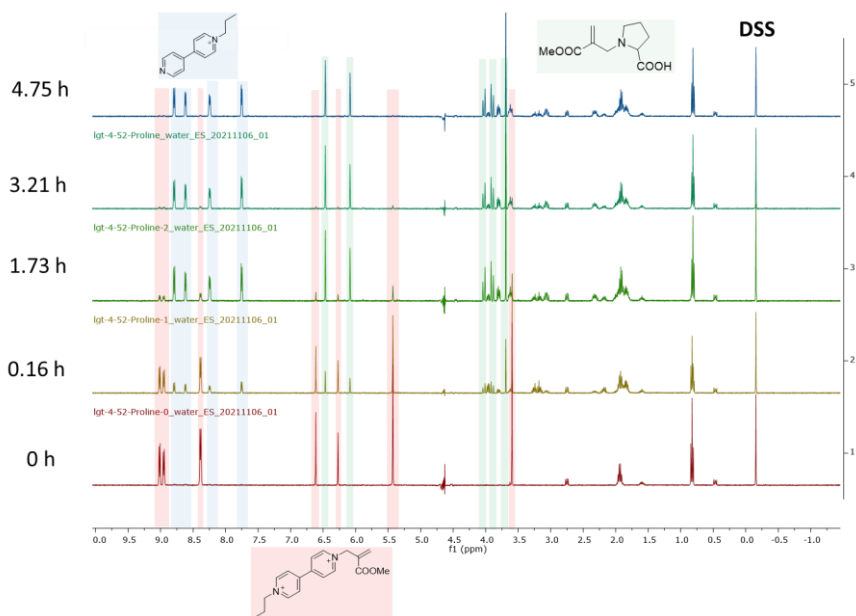
Figure S5.5 ^{1}H-NMR spectra overlay to follow the reaction of **2^{2+}** (2 mM) and proline (**Nu2**, 3 mM) over time.
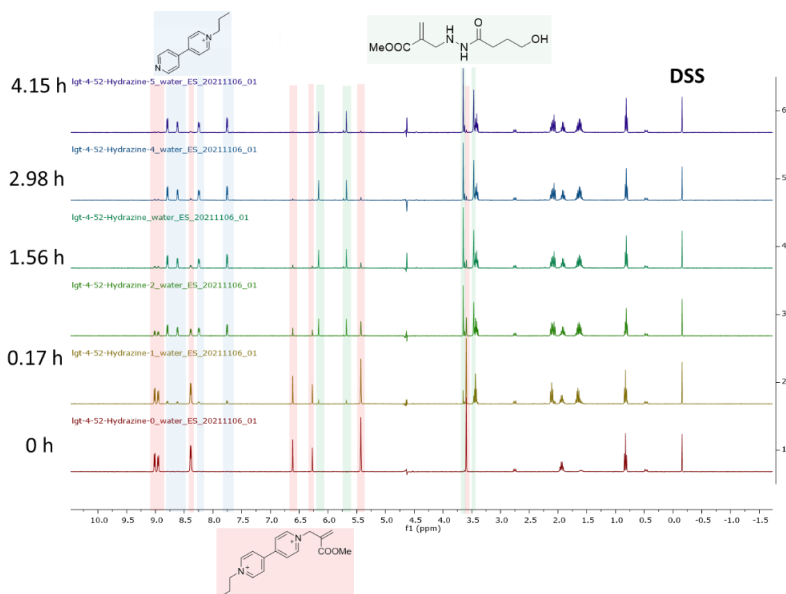
Figure S5.6 ^{1}H-NMR spectra overlay to follow the reaction of **2²⁺** (2 mM) and 4-hydroxybutanohydrazide (**Nu3**, 3 mM) over time.
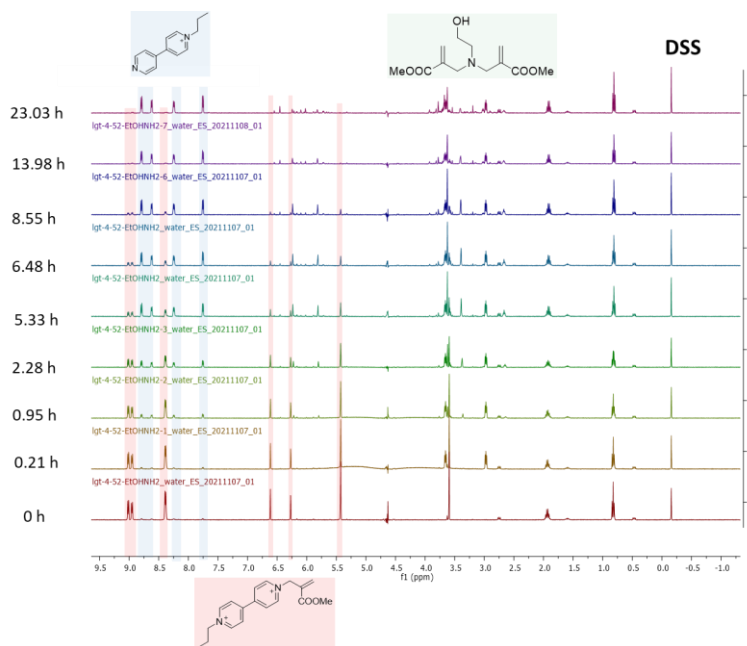
Figure S5.7 ^{1}H-NMR spectra overlay to follow the reaction of **2²⁺** (2 mM) and ethanolamine (3 mM) over time.
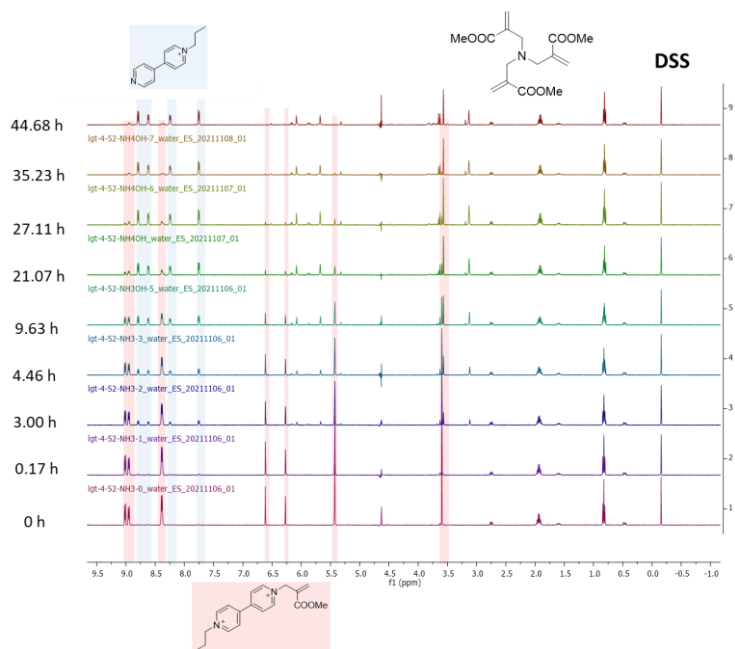
Figure S5.8 ¹H-NMR spectra overlay to follow the reaction of **2²⁺** (2 mM) and NH₃ (3 mM) over time.
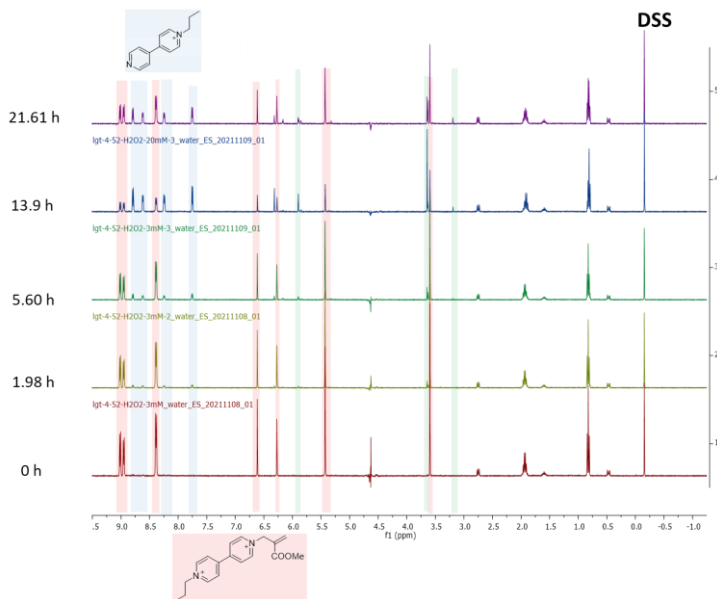
Figure S5.9 ¹H-NMR spectra overlay to follow the reaction of **2²⁺** (2 mM) and H₂O₂ (3 mM) over time.

In the series of **pre-proline** experiments, **2²⁺** (2 mM) and pre-proline (3 mM) mixed together first. ¹H-NMR (water suppression mode) was measured with or without H₂O₂.
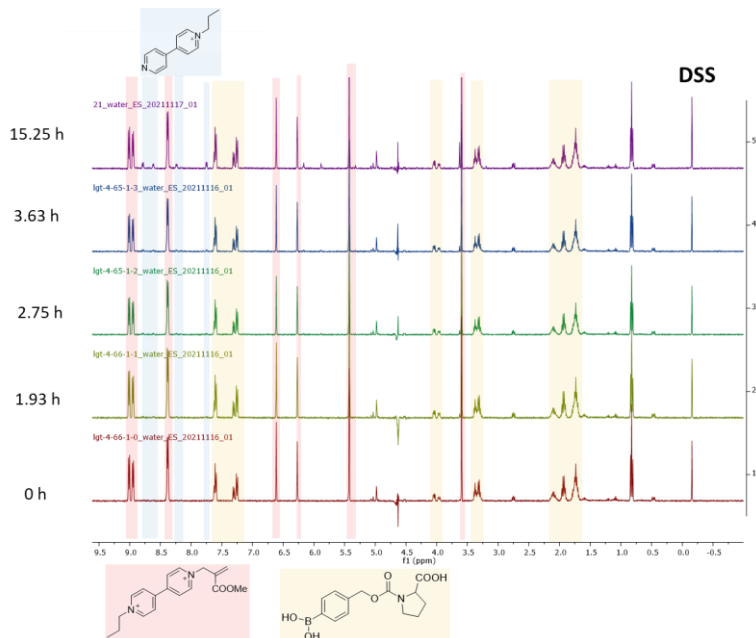
Figure S5.10 ¹H-NMR spectra overlay to follow the reaction of **2²⁺** (2 mM) and **pre-proline** (**5**, 3 mM) over time.
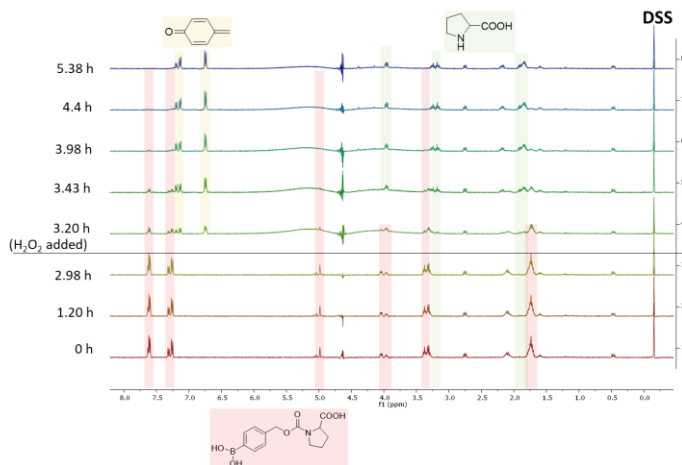
Figure S5.11 ¹H-NMR spectra overlay to follow the reaction of pre-proline (**5**) (3 mM) and H₂O₂ (3 mM) over time. H₂O₂ was added at t = 3 hours.
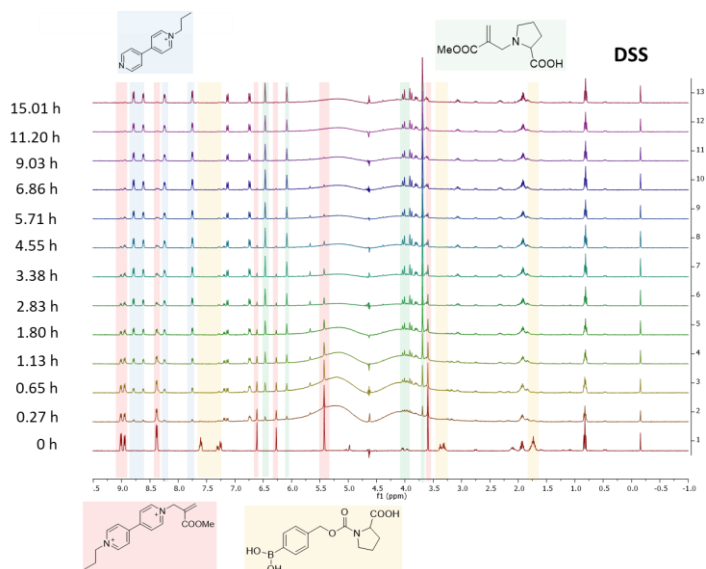
Figure S5.12 ^{1}H-NMR spectra overlay to follow the reaction of **2^{2+}** (2 mM) and **pre-proline** (3 mM), H_2O_2 (3 mM) added at t = 0 h.

5.5.5 Turbidity measurement by Uv-vis

General procedure for turbidity measurement:

Sample solution of 0.3 mM guest molecule and 0.45 mM CB[8] in 50 mM pH=7.4 phosphate buffer solution was prepared by sonicating and heating at 40 °C until complete dissolution, normally taking 30 min. The sample was filtered using a 450 nm syringe filter before measurement. 1.5 mL sample solution was put into a quartz cuvette with 1 cm path length, for which transmittance was measured at 500 nm. At t = 0.5 h, 0.9 mM signal molecule was added into the solution, and we continued measuring for another 9.5 hours.

In the case of pre-proline, pre-proline was mixed first in the solution with 0.3 mM **4^{6+}** and 0.45 mM CB[8] together, while H_2O_2 was added into the solution at t = 0.5 h.
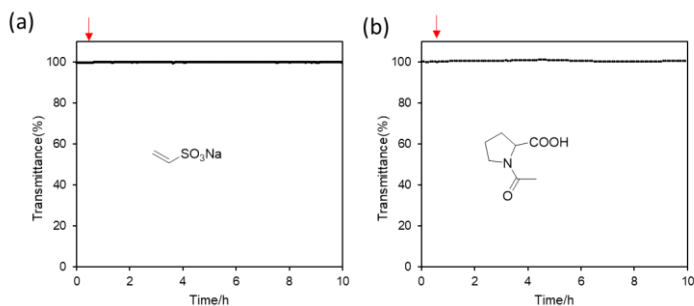
Additional turbidity data:

136

Figure S5.13 Turbidity measurement (transmittance at 500 nm, [4^{6+}] = 0.3 mM, [CB[8]] = 0.45 mM, in 50 mM pH=7.4 sodium phosphate buffer); (a) sodium vinylsulfonate (0.9 mM) (b) acetylproline (0.9 mM) was added at t = 0.5 h.

5.5.6 Analysis of aggregate by NMR

A solution of 4^{6+} (0.8 mM) and CB[8] (1.2 mM) in 50 mM phosphate buffer and 10% D_2O was prepared by heating at 40 °C and sonication until complete dissolution. ^{1}H-NMR was measured for the mixture before and after adding 2-mercaptoethanol (2.4 mM).

The aggregates formed upon adding 2-mercaptoethanol in the NMR tube were isolated by centrifugation. The white precipitate was washed by 1.5 mL water twice and put into NMR tube in D_2O. ^{1}H-NMR was measured again before and after adding *N,N,N*-trimethyl-1-adamantylammonium chloride (24 mM). NMR spectra for each step are shown below.
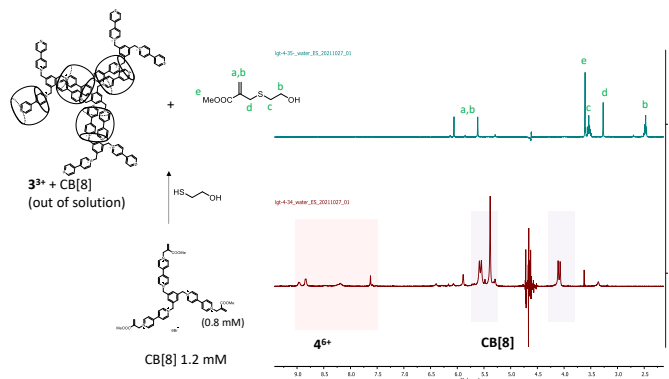

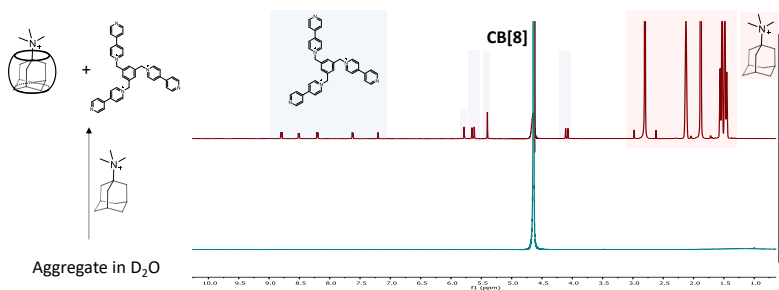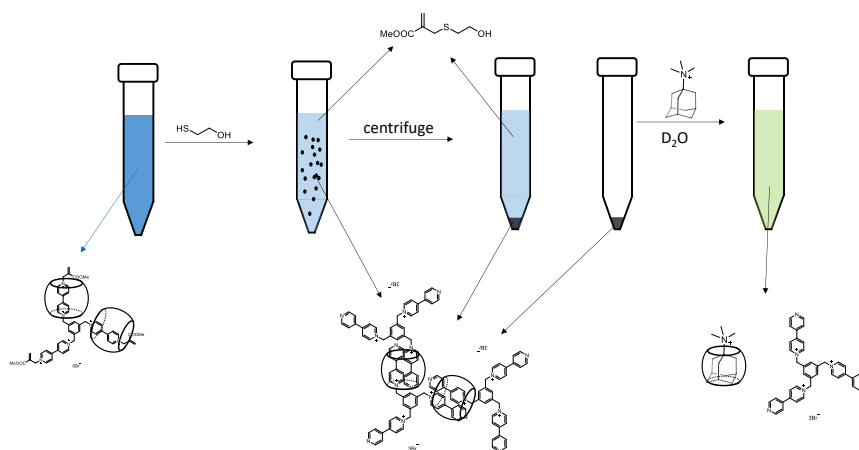**Figure S5.14** ^{1}H-NMR spectra before (bottom) and after (top) adding 2-mercaptoethanol (2.4 mM).

Figure S5.15 ^{1}H-NMR spectra of isolated aggregate in D_2O before (bottom) and after (top) adding *N,N,N*-trimethyl-1-adamantylammonium chloride (24 mM).

Scheme S5.1 Proposed composition of each step in the process.

5.5.7 Dynamic light scattering measurement (DLS)

A sample solution of 0.1 mM **3P^{6+}** and 0.15 mM CB[8] in 50 mM pH = 7.4 phosphate buffer solution was prepared by sonicating and heating at 40 °C until complete dissolution. The solution was filtered using a 200 nm syringe filter before measurement. 0.8 mL solution was measured in a disposable micro cuvette. Signal molecule (0.3 mM) was added at t = 1 hour.
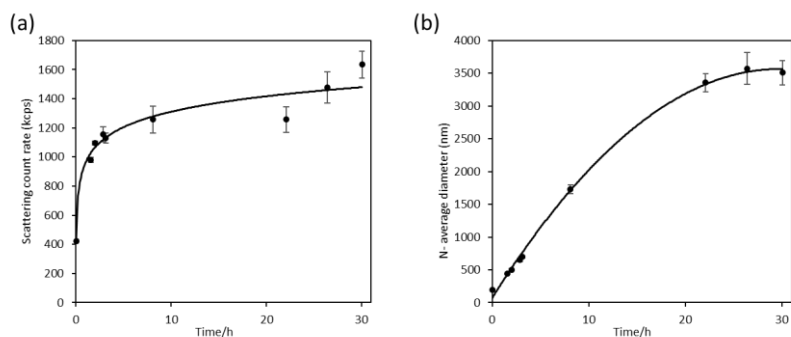
Additional DLS data below:

Figure S5.16 DLS measurement of **3³⁺**(0.1 mM) and CB[8] (0.15 mM) in 50 mM pH=7.4 sodium phosphate buffer. (a) scattering count rate (b) particle size measured as number average diameter.
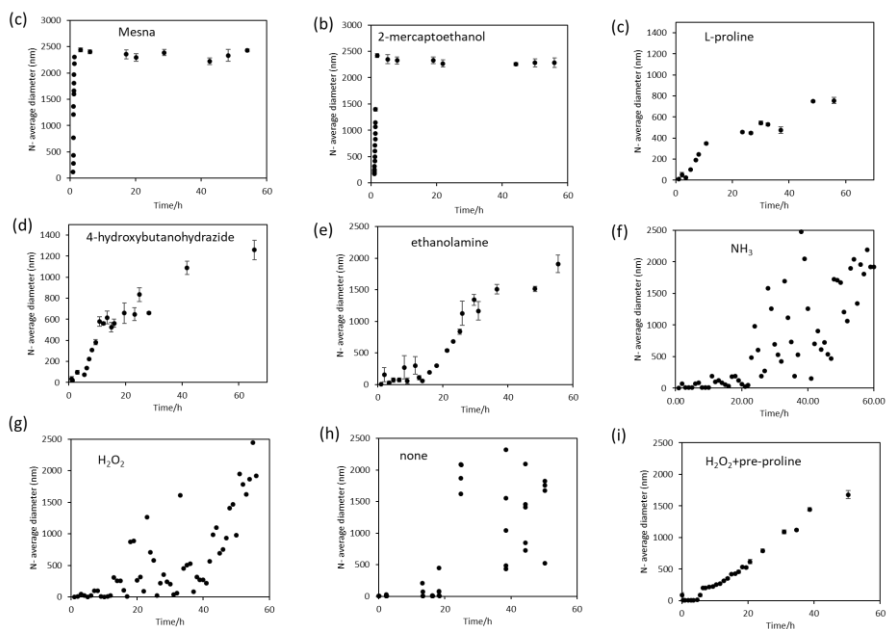

Figure S5.17 Size of aggregates by DLS measurement of **4⁶⁺** (0.1 mM) and CB[8] (0.15 mM) in 50 mM pH=7.4 sodium phosphate buffer after adding signals (0.3 mM).

5.5.8 Avrami analysis

To determine the Avrami coefficient *n*, $\ln(-\ln(1-X))$ was plotted against $\ln(t-t_a)$, with $X = (Abs_t - Abs_a)/(Abs_\infty - Abs_a)$ as a measure of conversion, where t_a is the starting point of

aggregation. The Avrami coefficient is then the slope of the first part of the curve, as this is where the nucleation predominantly occurs.
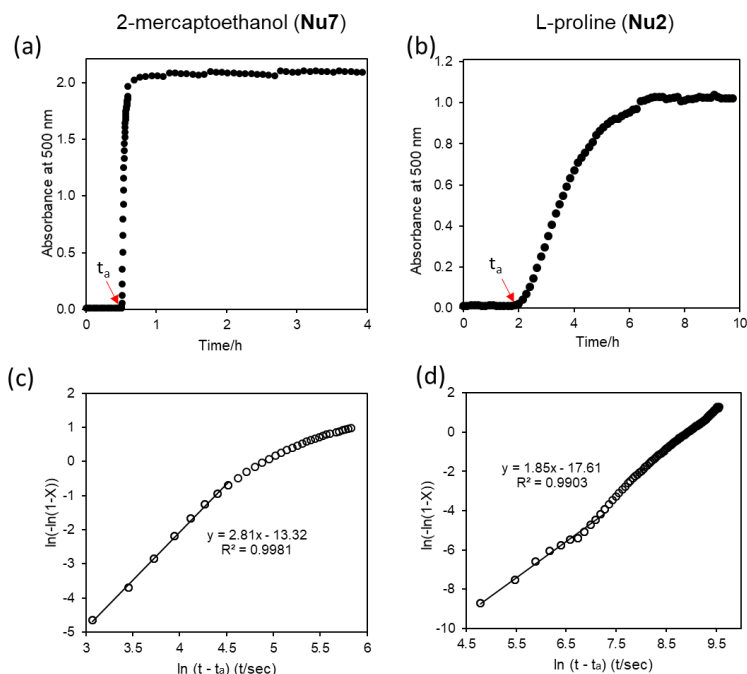

Figure S5.18 Determination of the Avrami coefficient. (a)(b) Time-dependent absorbance of samples during aggregation, [4^{6+}] = 0.3 mM, [CB[8]] = 0.45 mM, [**Nu7**] = 0.9 mM (a), [**Nu2**] = 0.9 mM (b); (c)(d) Derived Avrami plots of aggregation process induced by [**Nu7**] (c) and **Nu2** (d).

5.5.9 Powder X-ray diffraction (PXRD) experiment

To 4 mL solution of 4^{6+} (0.3 mM) and CB[8] (0.45 mM) in 50 mM phosphate buffer was added signal molecules (0.9 mM) of 2-Mercaptoethanol (**Nu7**) or proline (**Nu2**). The formed precipitation was isolated by centrifugation and washed by di-water (1 mL × 3). Sample was loaded in a zero diffraction plates for drying in the air at room temperature for 4 hours and measured by x-ray diffraction afterward.
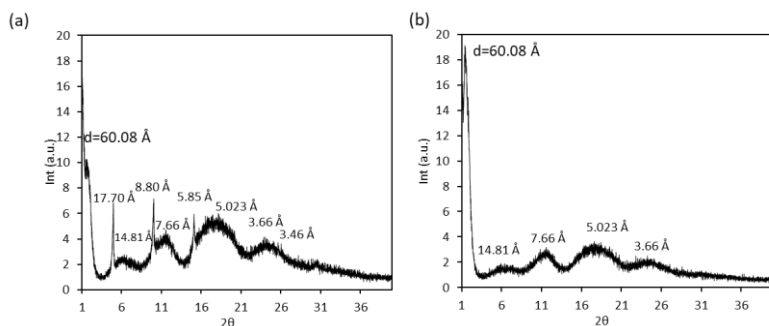
Figure S5.19 PXRD profile of the aggregate formed from **4⁶⁺** (0.3 mM) and CB[8] (0.45 mM) induced by 0.9 mM 2-mercaptoethanol **Nu7** (a) and 0.9 mM proline **Nu2** (b).
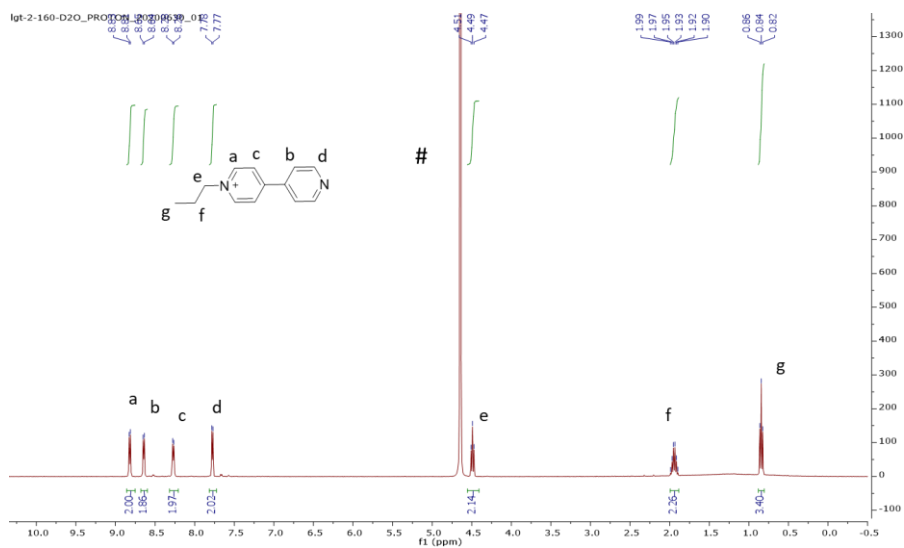
5.5.10 Spectra overview

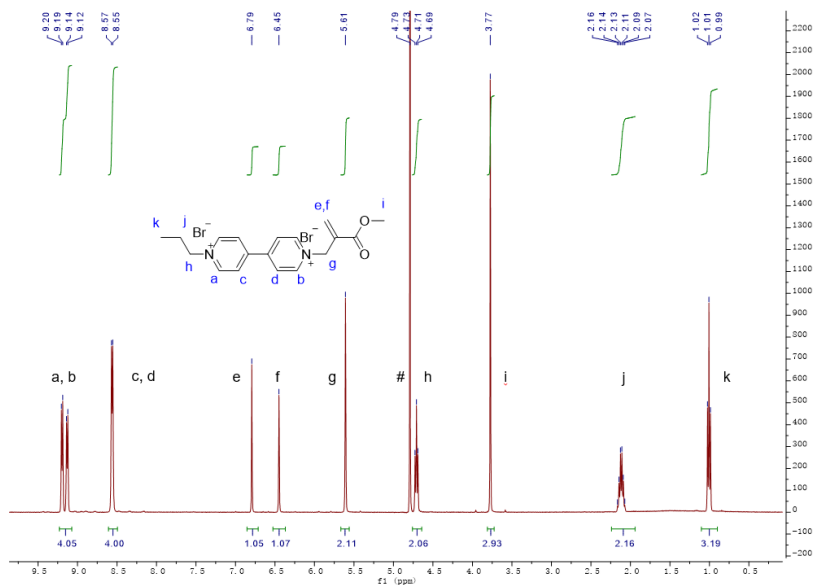**Figure S5.20** ^{1}H-NMR spectrum of guest **1^{1+}** in D$_2$O (marked as #).

Figure S5.21 ^{1}H-NMR spectrum of guest **2^{2+}** in D$_2$O (marked as #).

Figure S5.22 ^{13}C-NMR spectrum of guest **2^{2+}** in D$_2$O (1,4-Dioxane as NMR reference standard, marked as *).

Figure S5.23 ^{1}H-NMR spectrum of guest **3^{3+}** in D$_2$O (marked as #).
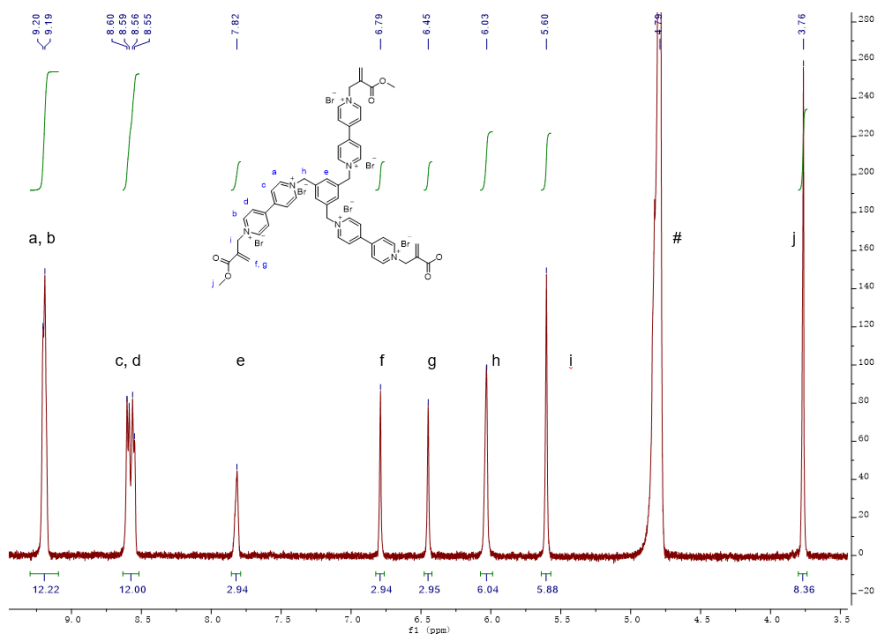
Figure S5.24 ^{1}H-NMR spectrum of guest **4^{6+}** in D$_2$O (marked as #).
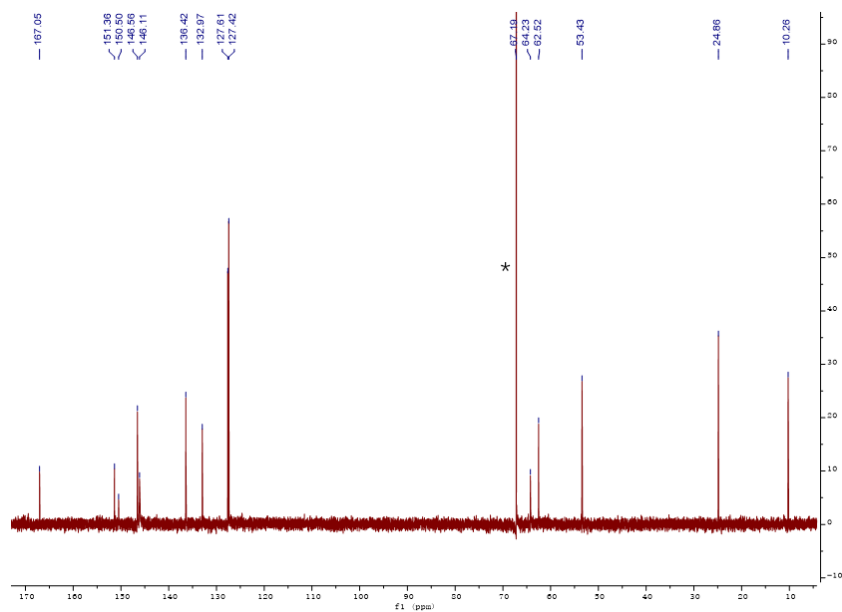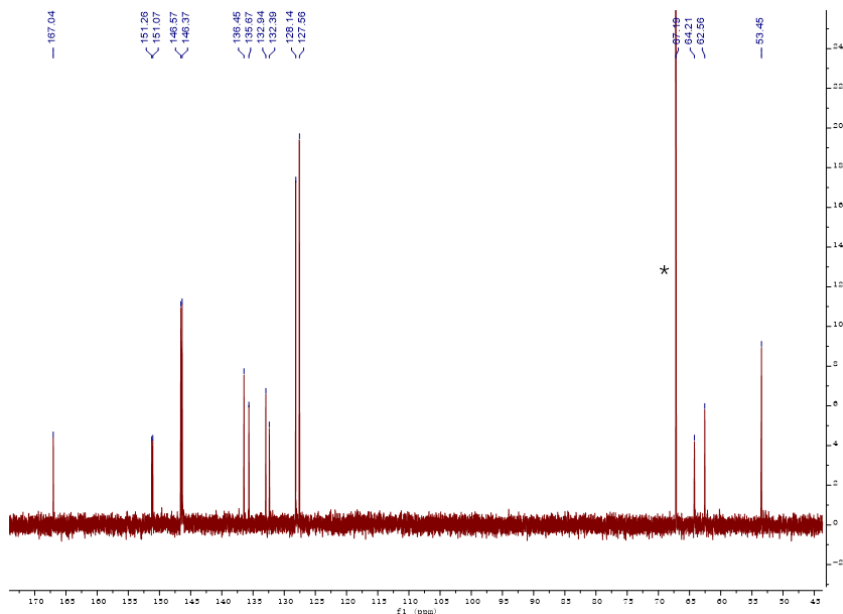
Figure S5.25 ^{13}C-NMR spectrum of guest **4^{6+}** in D$_2$O (1,4-Dioxane as NMR reference standard, marked as *).
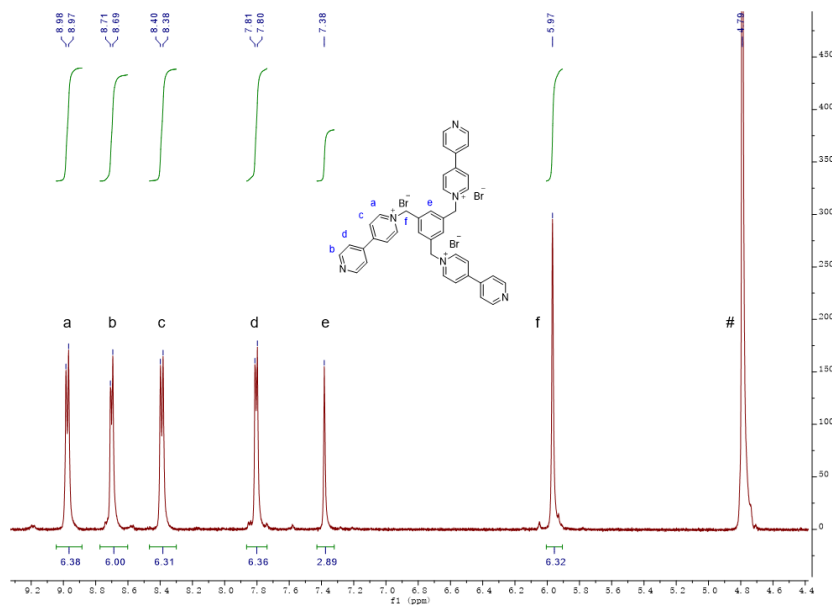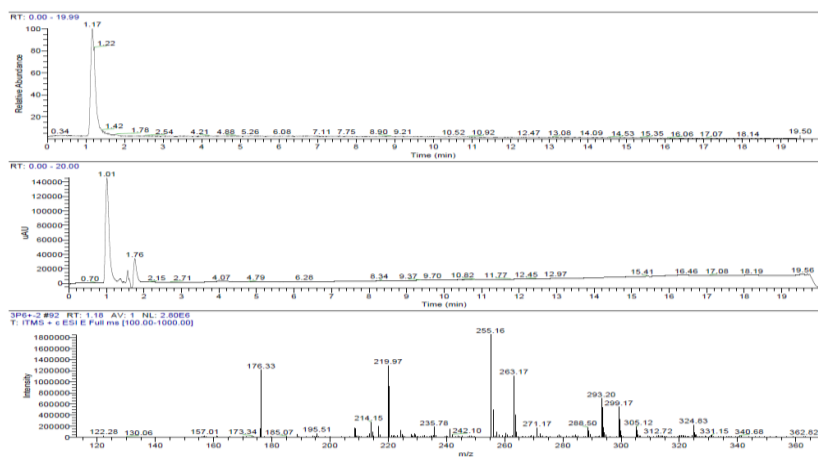

Figure S5.26 LC-MS spectrum of guest molecules **4^{6+}**. MS (ESI Pos) m/z: 176.33 [(M-6Br$^-$)/5]$^+$ (expected m/z = 176.48); m/z: 219.97 [(M-6Br$^-$)/4]$^+$ (expected m/z = 220.60); m/z: 293.20 [(M-6Br$^-$)/3]$^+$ (expected m/z = 294.14).
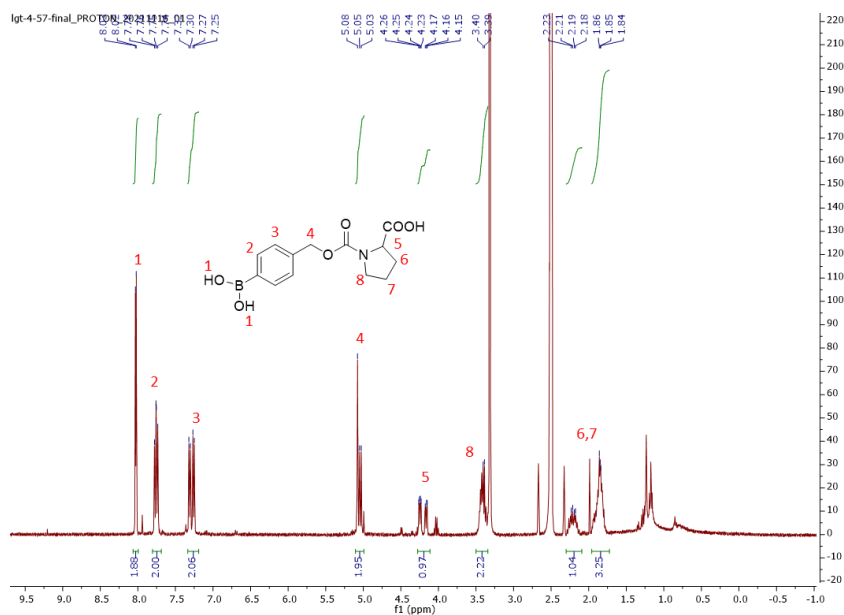
Figure S5.27 ^{1}H-NMR spectrum of guest pre-proline (**5**) in DMSO-d_6.
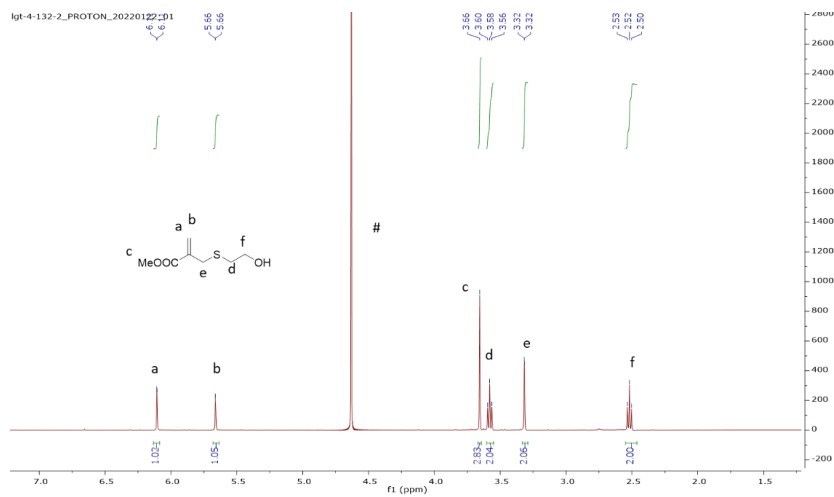
Figure S5.28 ^{1}H-NMR spectrum of waste product from reaction of **2^{2+}** and 2-mercaptoethanol, recorded in D$_2$O (marked as #).
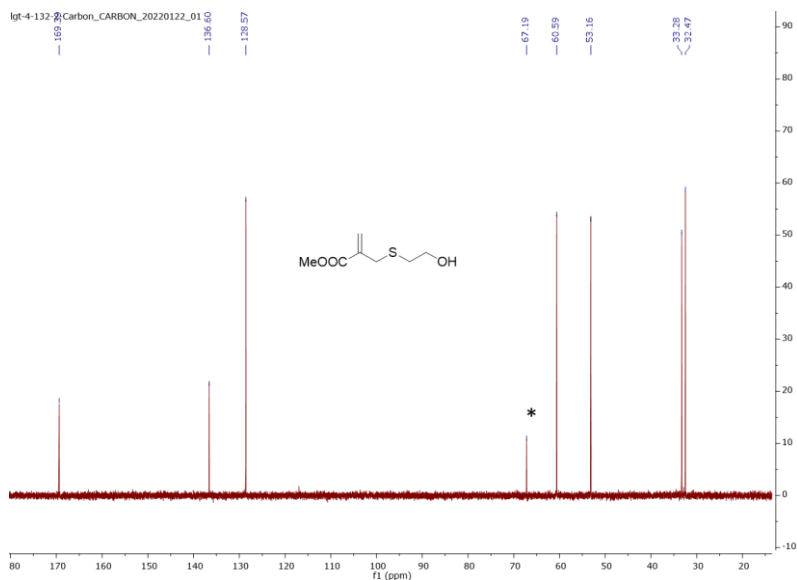
Figure S5.29 ^{13}C-NMR spectrum of waste product from reaction of **2^{2+}** and 2-mercaptoethanol, recorded in D$_2$O (1,4-Dioxane as NMR reference standard, marked as *).
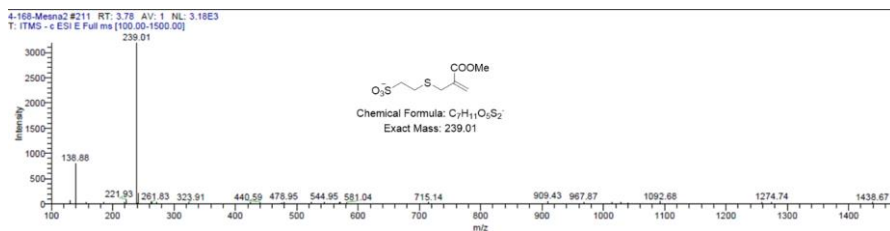
Figure S5.30 Mass spectrum of waste product from reaction of **2^{2+}** and Mesna (**Nu1**), (ESI Neg) m/z: 239.01 [(M-Na)]$^-$ (expected m/z = 239.01).
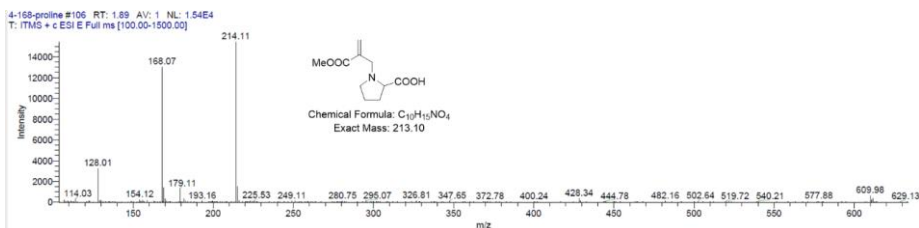
Figure S5.31 Mass spectrum of waste product from reaction of **2^{2+}** and Proline (**Nu2**), (ESI Pos) m/z: 214.11 [(M + H)]$^+$ (expected m/z = 214.10).
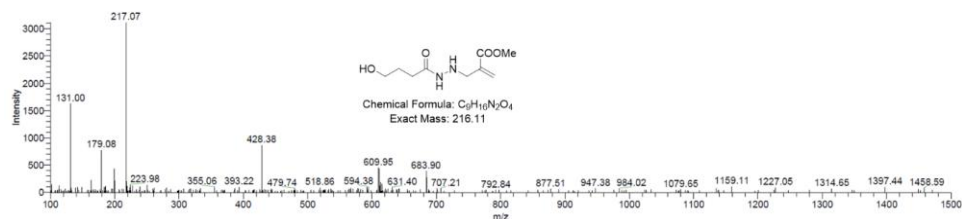
Figure S5.32 Mass spectrum of waste product from reaction of **2²⁺** and 4-hydroxybutanohydrazide (**Nu3**), (ESI Pos) m/z: 217.07 [(M + H)]⁺ (expected m/z = 217.11).
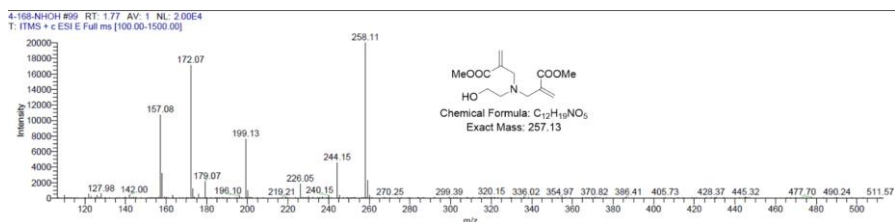
Figure S5.33. Mass spectrum of waste product from reaction of **2²⁺** and ethanolamine (**Nu4**), (ESI Pos) m/z: 258.11 [(M + H)]⁺ (expected m/z = 258.13).
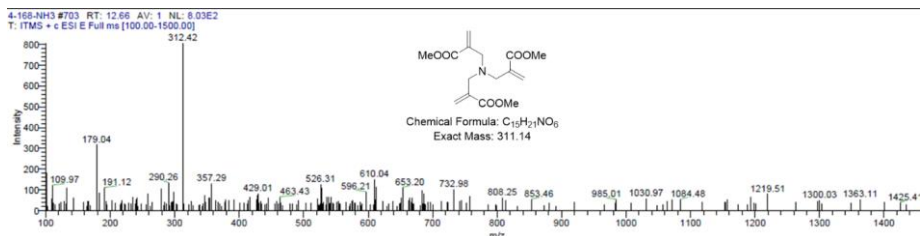
Figure S5.34. Mass spectrum of waste product from reaction of **2²⁺** and NH₃ (**Nu5**), (ESI Pos) m/z: 312.42 [(M + H)]⁺ (expected m/z = 312.14).

5.5.11 Reference

(1)   Wang, Z.; Tsarevsky, N. V. Well-Defined Polymers Containing High Density of Pendant Viologen Groups. *J. Polym. Sci. Part A Polym. Chem.* **2017**, *55* (7), 1173–1182.

(2)   Asaftei, S.; Huskens, D.; Schols, D. HIV-1 X4 Activities of Polycationic Viologen Based Dendrimers by Interaction with the Chemokine Receptor CXCR4: Study of Structure-Activity Relationship. *J. Med. Chem.* **2012**, *55* (23), 10405–10413.

(3)   Li, J.; Lepadatu, A. M.; Zhu, Y.; Ciobanu, M.; Wang, Y.; Asaftei, S. C.; Oupický, D. Examination of Structure-Activity Relationship of Viologen-Based Dendrimers as Cxcr4 Antagonists and Gene Carriers. *Bioconjug. Chem.* **2014**, *25* (5), 907–917.

(4)   Maity, C.; Trausel, F.; Eelkema, R. Selective Activation of Organocatalysts by Specific Signals. *Chem. Sci.* **2018**, *9* (27), 5999–6005.

Chapter 6

Triggered Drug Release from Heteroternary Host-guest Complexes

Abstract Stimuli-responsive drug delivery systems with controlled, local release of drugs are essential for effective therapy, in particular to reduce cytotoxicity to healthy tissues. Host-guest interactions have been widely applied in drug delivery systems to form either dynamic macromolecular materials or the nano-containers of drugs. Analogous to the non-covalent bond, supramolecular materials based on host-guest interaction are inherently stimuli-responsive allowing drug release through material disassembly by external signals. However, host - drug complexes are thermodynamically stable, meaning that encapsulated drugs can only be released by dilution, salt, pH or temperature induced changes in binding affinity, or competitive replacement by another guest molecules. So far, releasing encapsulated drugs triggered by chemical signals remains limited. Heteroternary complexes (1:1:1) formed by CB[8] on the basis of host stabilized charge transfer (HSCT) provide new opportunities to release electron-rich guests by structural changes in the other guest. Previously, this concept was reported using reduction-redox process in viologen guest moieties. However, both the guest structures and the stimulus used for triggering are limited. As we reported previously, host-guest complexes can be switched from 1:1 to 1:2 stoichiometry using chemical reactions triggered by biological signals. In this work, we extend the switch to heteroternary complexes, releasing a guest molecule triggered by biological signals. Starting from the viologen structure as the electron-deficient guest molecule, we found that cationic isoquinoline showed superior performance. Moreover, we demonstrate the system is capable of binding and releasing a wide range of electron-rich heterocyclic compounds, including drugs and natural bioactive compounds. This work offers a novel route to integrate stimuli–responsive disassembly of heteroternary complexes and drug release, which is anticipated to not find application in releasing small molecules but also in the design of new artificial stimuli-responsive materials.

6.1 Introduction

Drug delivery systems can enable more effective therapy by improving solubility and stability of active agents, increasing pharmacological activity and reducing side effects. For these reasons, this field has received much attention and seen great development in the last two decades.[1,2] Stimuli-responsive drug delivery systems with controlled release of drugs into a targeted biological site can further enhance the safety and efficacy by lowering cytotoxicity in healthy tissues.[3,4] The recent development of supramolecular materials provides platforms for the design of new stimuli-responsive drug delivery systems,[5] among which materials based on host-guest interaction are widely used[6]. Macrocyclic molecules find application in drug delivery in constructing self-assembly materials such as micelles[7], liposomes[8], frameworks[9], hydrogels[10,11] and others.[6,12] Moreover, the macrocycle itself can also function as a nano-container to directly encapsulate drug molecules in its cavity, causing changes in properties of the guest molecules, such as solubility, stability, cytotoxicity[13], catalytic activity[14] and others.[15] Once the constructed materials based on host-guest interaction are disassembled in response to an external stimulus, the loaded drugs will be released. Essentially, drugs loaded through direct host-guest encapsulation are usually released by dilution or competitive replacement (Scheme 6.1), or triggered by changing pH[16], light[17], temperature, or redox species[18,19]. Currently, drug release from host-guest complexes by signals-triggered chemical reactions is very rare.

The cucurbituril (CB[*n*]) family are a recently developed, popular group of macrocyclic host molecules.[20] Among the CB family, CB[8] is very interesting due to its unique ability to form diverse complexes with appropriate guests, including binary (1:1; 1 host, 1 guest), homoternary (1:2) and heteroternary (1:1:1) complexes.[21] Among them, the heteroternary complexes (1:1:1) often work through a mechanism of "Host stabilized charge transfer (HSCT)", allowing the binding of two different guest molecules inside: an electron-deficient molecule as the first guest, and an electron-rich one as the second guest.[22] The electron-deficient first guest often has a cationic charge, and their binding with CB[8] through cation-dipole interactions was found to be critical for the formation of heteroternary complexes, since CB[8] typically has low affinity to neutral compounds when interactions are based only on hydrophobicity.[23] Binding of this first, electron deficient guest greatly enhances affinity for a second, electron rich guest where the enhanced affinity is partly caused by charge transfer. Structural changes of the first guest will often impact on the binding behavior of the second guest with CB[8]. A similar strategy was reported to liberate 2,6-dihydroxynaphthalene (second guest) from a ternary complex with CB[8] by reducing methyl viologen (first guest) using sodium dithionite.[16] Our previous work demonstrated a chemically triggered switch of a CB[8] complex from a 1:1 to 1:2 stoichiometry by converting a cationic pyridinium guest through a biological signal triggered chemical reaction.[24] Extending this concept, we hypothesize that CB[8] heteroternary complexes can be disassembled by signal-

triggered neutralization of cationic pyridinium guests leading to release of electron-rich guests including drugs, which we explore in this work.
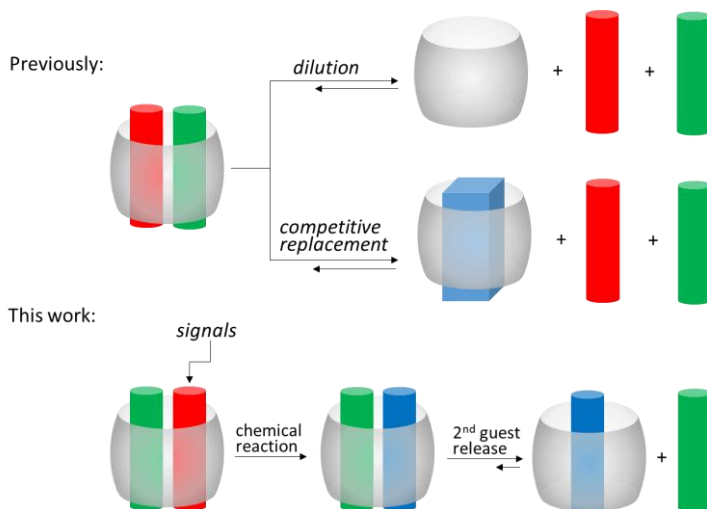
Scheme 6.1 Previous and current strategies for guest release from CB[8] heteroternary complexes.

6.2 Results and discussion

4,4'-Dipyridine (**1a^0**) and its cationic derivative with two removable positive charges (**1a^{2+}**) were chosen as the first guest molecules (Figure 6.1). As a Michael acceptor with an allylic quaternary ammonium leaving group, **1a^{2+}** can react with nucleophiles leading to the removal of cations and generation of **1a^0**.[25–27] For the electron-rich second guest molecule we chose 2,6-naphthalenediol (**2a**), and tested its affinity for CB[8] combined with **1a^{2+}** or **1a^0**, as the combination of dipyridinium derivatives and **2a** are known to give high affinity heteroternary complexes. [28–30] Isothermal titration calorimetry (ITC) indicated a significant difference in the binding constants of 2,6-naphthalenediol (**2a**) to CB[8]/**1a^{2+}** and CB[8]/**1a^0**: K(**2a**⊂(CB[8]/**1a^{2+}**)) = (7.18 ± 0.20) × 10^4 M^{-1} (Figure 6.1b, red line); K(**2a**⊂(CB[8]/**1a^0**)) = (4.63 ± 2.20) × 10^3 M^{-1} (Figure 6.1b, blue line). Meanwhile, without the pyridine derivative first guest molecule, 2,6-naphthalenediol (**2a**) itself does not bind to CB[8] (Figure 6.1b, black line; Table S6.1, entry 1). 2,6-naphthalenediol (**2a**) shows fluorescence in solution, but this fluorescence can be quenched by encapsulation in a CB[8] complex.[31] When CB[8] (20 μM) was added into a **2a** solution ([**2a**]=20 μM, pH 7.4, 10 mM phosphate buffer), only a negligible decrease of fluorescence intensity was observed (Figure 6.1c, black line), indicating only limited complex formation. In contrast, addition of **2a** (20 μM) to a solution of dicationic **1a^{2+}** as the first guest molecule (20 μM) and CB[8] (20 μM), leads to quenching of the fluorescence of 2,6-naphthalenediol by ~60%. The neutral 4,4'-dipyridine (**1a^0**, 20 μM) as first guest molecule also causes ~10%

decrease of fluorescence, indicating that a small portion of **2a** is bound to CB[8]. The fluorescence experiment is in line with the ITC results: the electron-rich second guest molecule strongly binds to the dicationic **1a^{2+}**/CB[8] complex, forming a heteroternary complex, but weakly binds to **1a^0**/CB[8] and even weaker to empty CB[8].

After verifying complex formation and binding characteristics of **1a**/CB[8] complexes with **2a**, we then wanted to test the disassembly of this heteroternary complex in response to charge removal triggered by nucleophilic signals. As reported previously, nucleophilic thiols and primary or secondary amines can react with Michael acceptors with an allylic quaternary ammonium leaving group, leading to elimination of a tertiary amine and the removal of the positive charge.[25,26] In this work, we selected 2-mercaptoethanol (**Nu1**), and L-proline (**Nu2**) as signals as these are strong enough nucleophiles, do not show high affinity for CB[8] and have biological relevance.

Adding **Nu1** (40 µM) into a solution of 20 µM heteroternary complex (CB[8]:**1a^{2+}**:**2a** = 1:1:1) led to a fast recovery of fluorescence, indicating that 2,6-naphthalenediol (**2a**) was released from the complex (Figure 6.1c,d). However, 2,6-naphthalenediol (**2a**) is not stable in sodium phosphate buffer (10 mM, pH 7.4) and its decomposition causes a slow decrease of fluorescence. Combined, these effects led to an incomplete recovery of fluorescence and a decrease on long time scales (Figure 6.1d). For the same reason, when trying the less reactive L-proline (**Nu2**) as a trigger for a slower release, we observed only a decay of fluorescence (SI, Figure S6.5 a,b), because the rate of decomposition of **2a** is much faster than its release. As a control, after adding **Nu1** into a solution of **2a** the fluorescence kept decreasing, indicating the thiol itself is not able to restore the fluorescence of **2a** (SI, Figure S6.5 c,d). As such, we proved that an electron-rich guest molecule can be released from the HSCT heteroternary complex by thiol nucleophile induced chemical reaction.
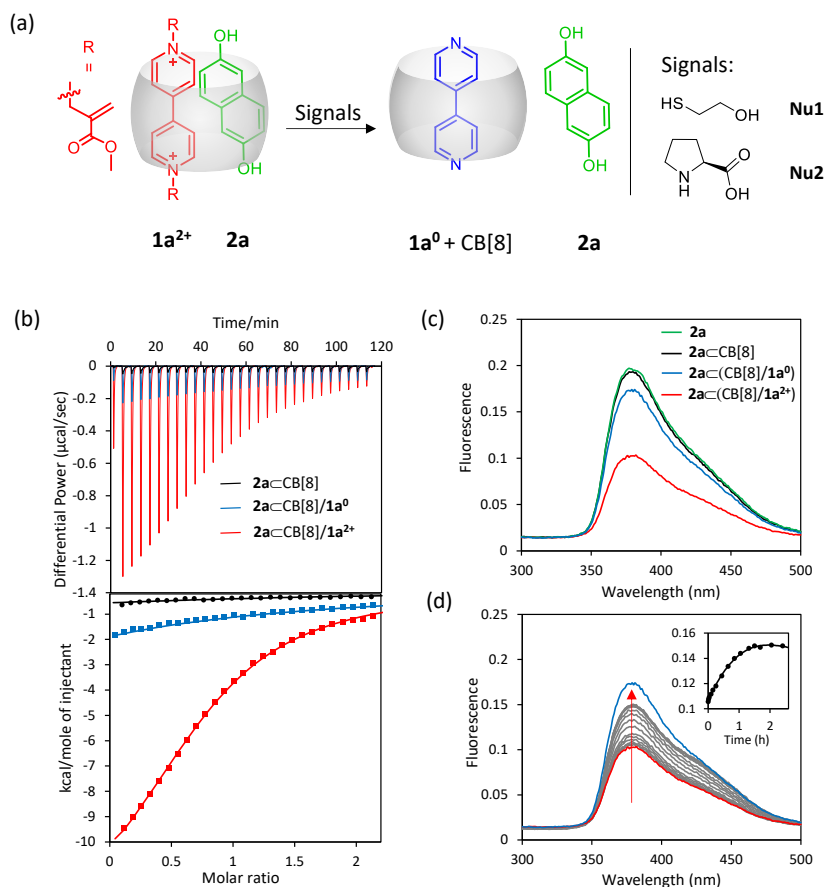
Figure 6.1 Release of an electron-rich guest molecule from a heteroternary complex triggered by chemical signals. (a) Chemical structures and reaction of guest molecules with chemical signals; (b) ITC of complex formation, $K(\textbf{2a} \subset (CB[8]/\textbf{1a}^{2+})) = (7.18 \pm 0.20) \times 10^4$ M^{-1}; $K(\textbf{2a} \subset (CB[8]/\textbf{1a}^0)) = (4.63 \pm 2.20) \times 10^3$ M^{-1}; (c) Fluorescence spectrum comparison, conditions: **2a** (20 μM), CB[8] (20 μM), **1a^0** (20 μM), **1a^{2+}** (20 μM); (d) Fluorescence changes after adding 2-mercaptoethanol (**Nu1**, 40 μM) as compared to **2a**$\subset$(CB[8]/**1a^{2+}** (blue) and **2a**$\subset$(CB[8]/**1a^0** (red), subfigure showing the emission at 376 nm over time (λ_{ex} = 278 nm).

We then aimed to optimize this system using a more stable electron-rich guest molecule. 2-naphthoxyacetic acid (**2b**) was selected because of its stability, water solubility and biological function as a plant growth hormone.[32] Sharing the same electron-rich backbone of naphthalene, **2b** shows similar binding behavior as **2a**, strongly binding to **1a^{2+}**/CB[8] while weakly to **1a^0**/CB[8] and not binding to CB[8] itself (Table 6.1, entries 1-3, Table S6.1, entries 2,5,6). In an NMR titration, addition of CB[8] (0–1 mM) to a
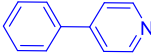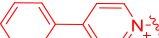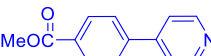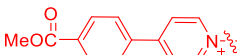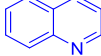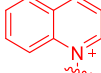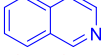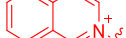
solution of **1a²⁺** (1 mM) and **2b** (1 mM) caused upfield shifts of the proton resonances of the pyridinium group (**1a²⁺**), naphthyl and methylene group (**2b**), and a downfield shift for the allyl and methoxy groups in **1a²⁺**, thereby suggestin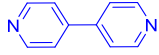g the formation of heteroternary complex where the pyridinium of **1a²⁺** naphthyl and methylene group of **2b** reside in the host cavity of CB[8] (Figure S6.4). Meanwhile, with the increasing concentration of CB[8], the solution of **1a²⁺**, **2b** and CB[8] gradually become purple (Figure S6.1), in line with the previously reported HSCT caused by heteroternary complex formation.[33–35] We subsequently conducted release experiments using nucleophile signal molecules. Adding 2-mercaptoethanol (**Nu1**, 2 mM, 1 eq.) into the solution of the complex ([**1a²⁺**] = 1 mM, [**2b**] = 1 mM, [CB[8]] = 0.6 mM) in sodium phosphate buffer (10 mM, pH 7.4) showed a fast reaction with **1a²⁺**, causing precipitation of CB[8] (Figure S6.2). Simultaneously, in ¹H-NMR broad peaks of **2b** appeared at their original location after ~45 min, showing that part of **2b** was still bound (Figure S6.9). A higher concentration of **Nu1** (4 mM) led to instant CB[8] precipitation and sharp peaks of **2b** were observed in ¹H NMR (15 min), while peaks of **1a⁰** could also be observed (Figure S6.10). Conversely, L-proline (**Nu2**, 4 mM) did not succeed in releasing **2b** as shown in ¹H-NMR, neither causing precipitation nor restoration of the **2b** signals even after 50 hours reaction time (Figure S6.11). Still, the sample color did change from purple to yellow, suggesting a change in the complex structure (Figure S6.2).

So far, these results demonstrate the formation of a ternary complex of an electron-deficient cationic first guest molecule and an electron-rich second guest molecule with CB[8], and its disassembly triggered by nucleophilic signals leading to the release of guest molecules. However, for the purpose of drug delivery or other biomedical applications, the 4,4'-dipyridinium motif is not suitable, as these are generally very toxic and have limited possibilities for further structural modification. With **2b** as the second guest molecule, we performed a series of screening experiments to find a better first guest molecule.

Table 6. 1. Selection of first guest molecules using ITCᵃ.

1a⁺-1f⁺ 2b   **1a⁰-1f⁰ 2b**
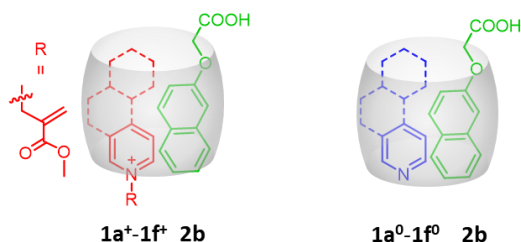
Entry	First Guest	K_a (10³ M⁻¹)	ΔG (kcal/mol)
1	None	-\-ᵇ	-\-

		Structure		
2	**1a^0**		5.04 ± 1.19	-5.05
3	**1a^{2+}**		36.7 ± 3.88	-6.23
4	**1b^0**		-\-	-\-
5	**1b$^+$**		4.84 ± 10.6	-\-
6	**1c^0**		5.29 ± 4.60	-5.08
7	**1c$^+$**		8.36 ± 4.08	-5.34
8	**1d^0**	MeOC	3.83 ± 1.27	-\-
9	**1d$^+$**	MeOC	5.03 ± 1.96	-\-
10	**1e^0**		1.12 ± 64.8	-\-
11	**1e$^+$**		7.14 ± 1.03	-5.25
12	**1f^0**		-\-	-\-
13	**1f$^+$**		30.9 ± 1.39	-6.16

[a] Conditions: in 10 mM sodium phosphate buffer solution, pH 7.4. [b] Measurement errors are too high to calculate a precise value.

As summarized in Table 6.1, compounds with pyridine moieties and their derivatives with a removable cation were tested as the first guest to form heteroternary complexes with **2b** and CB[8]. Pyridine itself in either cationic or neutral form did not show a measurable affinity (Table 6.1, entry 4,5, Table S6.1, entry 7,8), which indicates that a connected aromatic ring is essential. The monocationic phenylpyridinium (**1c$^+$**) can bind with **2b** and CB[8], however, the binding constant is much lower than for **1a^{2+}** but still higher than for **1a^0**. Addition of an electron-withdrawing ester moiety on the phenyl ring (**1d$^+$**) did not improve the affinity (Table 6.1 entry 4). Quinolines (**1d$^+$** and **1d^0**) gave similar results to **1c** and **1d** (Entry 5). To our delight, cationic isoquinoline (**1f$^+$**) shows an affinity comparable with **1a^{2+}** while neutral isoquinoline (**1f^0**) shows very limited capability of forming the complex with (**2b**) and CB[8]. Strikingly, mixing solutions of isoquinoline (**1f^0**) and CB[8] results in a suspension even in a very low concentration (40 µM). A complex appears to come out of solution leading to a lowered possibility of CB[8] to capture the second guest molecule. Noteworthy, under these conditions, both isoquinoline and CB[8] separately are completely soluble (Figure S6.2).

A ^{1}H-NMR titration confirmed the formation of a ternary complex between CB[8], **1f$^+$** and **2b**, with peaks shifting with increasing concentration of CB[8] (0.1 mM–1 mM). The complex of CB[8], **1f$^+$** and **2b** appears a light yellow color compared to that without CB[8] (Figure S6.4). After adding 2-mercaptoethanol (**Nu1**, 2 mM) to the complex solution ([**1f$^+$**] = 1 mM, **2b** = 1 mM, CB[8] = 0.6 mM), a precipitation occurred, and the ^{1}H-NMR peaks of **2b** reappeared within 45 min, indicating a fast release of **2b**. Moreover, unlike in the case of **1a^{2+}**, we did not find the proton resonances of **1f^0** in the spectrum, only **2b** in the aromatic area. We analyzed the precipitate by dissolving it assisted by *N,N,N*-trimethyl-1-adamantylammonium chloride.[36] ^{1}H-NMR showed that the precipitate contains isoquinoline and CB[8] (Figure S6.14). This finding confirms that isoquinoline (**1f^0**) and CB[8] together form insoluble aggregates in sodium phosphate buffer. Remarkably, adding 2 mM L-proline into the solution of CB[8] **1f$^+$** and **2b** also triggered CB[8] precipitation, leading to release of **2b** out in 60 hours (Figure S6.13). Compared to bipyridinium **1a^{2+}**, nucleophile-induced release using **1f$^+$** as first guest molecule requires fewer equivalents of nucleophile, since only one cation has to be removed. Moreover, precipitation of **1f^0** and CB[8] enables facile isolation of pure electron-rich guest molecules. All these together show that the isoquinoline is indeed superior to bipyridine (**1a^0**) as first guest.

2a

$K_a = (6.89 \pm 0.34) \times 10^4\,\text{M}^{-1}$
$\Delta G = -6.66$ kcal/mol

Agomelatine (**2c**)

$K_a = (2.13 \pm 0.17) \times 10^4\,\text{M}^{-1}$
$\Delta G = -6.02$ kcal/mol

2d

$K_a = (3.80 \pm 0.32) \times 10^5\,\text{M}^{-1}$
$\Delta G = -7.64$ kcal/mol

2e

$K_a = (1.11 \pm 0.16) \times 10^6\,\text{M}^{-1}$
$\Delta G = -8.30$ kcal/mol

3-Indolylcarbinol (**2f**)

$K_a = (2.51 \pm 0.25) \times 10^5\,\text{M}^{-1}$
$\Delta G = -7.38$ kcal/mol

Sumatriptan (**2g**)

$K_a = (6.27 \pm 0.11) \times 10^4\,\text{M}^{-1}$
$\Delta G = -6.58$ kcal/mol

2h

$K_a = (2.36 \pm 0.16) \times 10^5\,\text{M}^{-1}$
$\Delta G = -7.32$ kcal/mol

2i

$K_a = (1.78 \pm 0.09) \times 10^4\,\text{M}^{-1}$
$\Delta G = -5.81$ kcal/mol

2j

$K_a = (5.79 \pm 1.18) \times 10^5\,\text{M}^{-1}$
$\Delta G = -7.86$ kcal/mol

2k

$K_a = (1.21 \pm 0.09) \times 10^5\,\text{M}^{-1}$
$\Delta G = -6.94$ kcal/mol

2l

$K_a = (5.22 \pm 0.02) \times 10^5\,\text{M}^{-1}$
$\Delta G = -7.80$ kcal/mol

2m

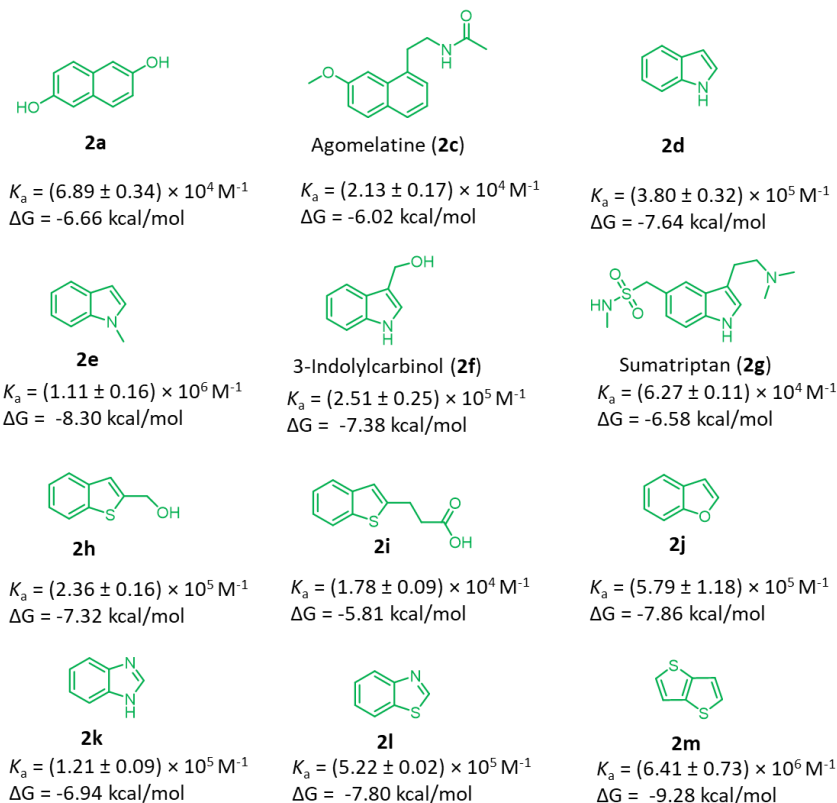$K_a = (6.41 \pm 0.73) \times 10^6\,\text{M}^{-1}$
$\Delta G = -9.28$ kcal/mol

Figure 6.2 Structures of electron-rich second guest molecules and their thermodynamic data for heteroternary complex formation with 1f⁺/CB[8].

We subsequently tested the capability of isoquinoline 1f to form hetereoternary complexes with CB[8] and other electron-rich compounds (Figure 6.2). 2,6-Naphthalenediol **2a** showed a high affinity with the cationic **1f⁺** and low affinity with **1f⁰**. Agomelatine **2c**, a drug molecule with a naphthalene skeleton, has a high binding constant with CB[8]/**1f⁺** ($K = (2.43 \pm 0.1.66) \times 10^4\,\text{M}^{-1}$), but it also has relatively high affinity to CB[8]/**1f⁰** (Table S6.1, entry 19, 20). We then tried other electron-rich heterocyclic compounds: indole, benzofuran, benzothiophene, benzothiazole, benzoimidazole and their derivatives. Such moieties are part of some drugs and bioactive compounds, including Sumatriptan **2g** (a drug for migraines and cluster headaches), indole-3-carbinol[37] **2f** (a metabolite in cruciferous vegetables with anti-cancer effect), and benzothiophene-2-methanol **2h** (a potential CYP2A6 inhibitor[38]). They all show high affinity to CB[8]/**1f⁺**, with binding constants >$10^4\,\text{M}^{-1}$, with thieno[3,2-b]thiophene (**2m**) giving the highest $K = (6.41 \pm 0.73) \times 10^6\,\text{M}^{-1}$. When measuring the affinity to the neutral complex (CB[8]/**1f⁰**) by ITC, guests such as **2c**, **2d** and **2l** also appeared to have high affinity (Table S6.1, entries 20, 22, 38, Table S6.3 entries 19, 21,

37). However, in these ITC measurements the energy release was only observed in the first few injections, and the binding sites (*N*) are unrealistically small. The abnormal ITC curve implies the existence of a small amount of cationic isoquinoline species due to a protonation equilibrium, leading to some binding. We therefore remeasured the binding contants of **2c**, **2d** and **2l** with **1f⁰**/CB[8] in pH 9.8 10 mM Na_2CO_3/$NaHCO_3$ buffer. At pH 9.8, **2c** does not bind to **1f⁰**/CB[8] at all (Table S6.2, entry 1), while for **2d** and **2l** some anomalous injection data appeared in the first three aliquots (Table S6.2, entries 2,3), but they are much lower than at pH 7.4 (Table S6.1, entries 22,32). In addition, the binding sites (*N*) become much smaller at pH 9.8 (Table S6.3). Comparison of ITC data at different pH confirms the protonated isoquinoline inducing a small amount of electron-rich guest molecule binding by CB[8]. Noteworthy, when testing electron-rich guest molecules for their affinity to CB[8] heteroternary complexes, we also found some electron-rich compounds that do not bind to CB[8]/**1f⁺**. These included *N*-acetyl-L-tryptophan, melatonin and nabumetone (Figure S6.15). Therefore, although a wide scope of electron-rich second guest molecules was shown to work in this system, whether a specific molecule is suitable still depends on its particular structure.

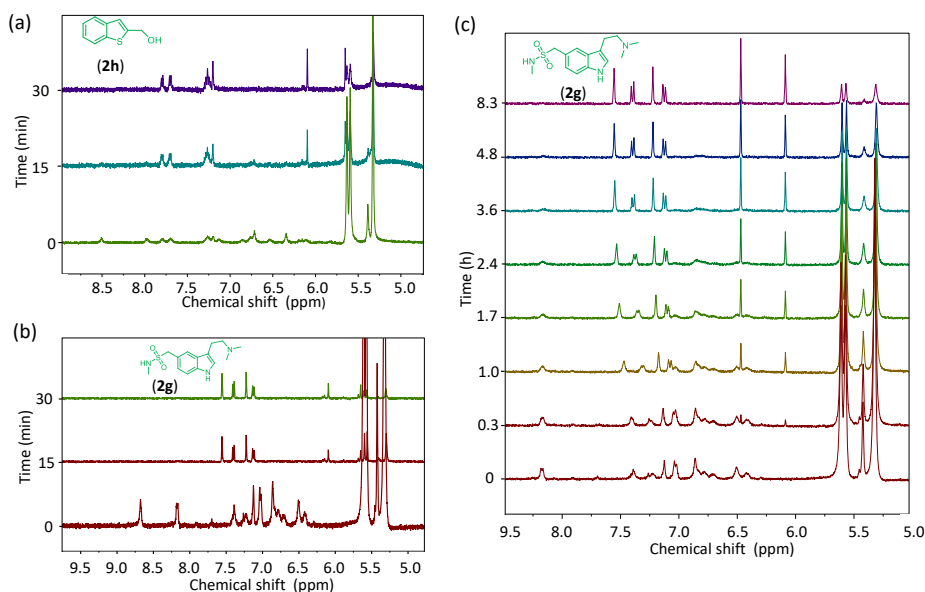**Figure 6.3** Partial ¹H NMR spectra showing release of **2h** and **2g** from **1f⁺**/CB[8] encapsulation after signal addition. (a) [**2h**] = 1 mM, [CB[8]] = 1 mM, [**1f⁺**]= 1 mM, [**Nu1**] = 1 mM; (b) [**2g**] = 1 mM, [CB[8]] = 1 mM, [**1f⁺**]= 1 mM, [**Nu1**] = 1 mM; (c) [**2g**] = 1 mM, [CB[8]] = 1 mM, [**1f⁺**]= 1 mM, [**Nu2**] = 2 mM; in pH 7.4 10 mM phosphate buffer and D_2O (10%) solution (water suppression mode).

We demonstrated release of the naphthalene guest molecules **2a** and **2b** from CB[8]/**1a^{2+}** by reaction with chemical signals (Figure 6.1, Figure S6.9, S6.10). As we subsequently discovered the wide scope of electron-rich heterocyclic compounds with affinity for CB[8]/**1f$^+$**, we tested their potential for signal-induced release. Sumatriptan (**2g**) and benzothiophene-2-methanol (**2h**) were selected for the release experiments considering their solubility and significance. Very similar to the results shown above in naphthalene substrates, encapsulation in CB[8]/**1f$^+$**, led to 1H-NMR peaks of both **2g** and **2h** shifting (Figure 6.3, bottom spectrum). Adding **Nu1** (1 mM) to the solution of CB[8]/**1f$^+$** and **2g** or **2h** induced a drastic decrease of CB[8] peaks within the time to perform one NMR measurement because of its precipitation with **1f^0**, while the peaks of released **2g** and **2h** appeared. After 30 min, no further changes could be observed. In the cases of L-proline **(Nu2**, 2 mM) as release signal, this process is much slower. We can see the gradual decrease of CB[8] peaks, and a slow shift of **2h** peaks to the free species. In all cases of these release experiments, the aromatic areas are clean and sharp. We did not observe the peaks of **1f^0** since precipitated with CB[8] once generated. These experiments demonstrated that this binding-release system can be applied to a wide range of electron-rich compounds.

6.3 Conclusion

In this work, we have demonstrated a new method to release electron rich molecules including certain drugs from molecular hosts, using chemical signal induced reactions. Upon reaction with nucleophilic signals, the cationic charges on an electron-deficient first guest molecule were removed, leading to the disassembly of HSCT heteroternary complex and freeing the electron-rich molecules from the CB[8] cavity. After testing various pyridine derivatives as the first guest molecules, we found that isoquinoline as first molecule gave outstanding performance in this system, where its cationic form (**1f$^+$**) can induce electron-rich guest molecules to bind to the CB[8] cavity forming heteroternary complex and its neutral form (**1f^0**) precipitates with CB[8] to release the guests. As such, switching the isoquinoline moiety from its cationic to neutral form leads to an efficient release of guest molecules. Furthermore, a wide scope of electron-rich molecules are found to be applicable in this system, including derivatives of naphthalene, indole, benzofuran, benzothiophene, benzothiazole, and benzoimidazole, which include FDA approved drugs and bioactive molecules. Our research offers a new route to achieve stimuli–responsive drug release using direct host-guest encapsulation. Moreover, the concept of disassembly of heteroternary complex by reaction with chemical signals will also bring new opportunities to design new stimuli-responsive materials for use in targeted delivery of pharmaceuticals.

6.4 References

(1)   Langer, R. New Methods of Drug Delivery. *Science* **1990**, *249* (4976), 1527–1533.

(2) Li, C.; Wang, J.; Wang, Y.; Gao, H.; Wei, G.; Huang, Y.; Yu, H.; Gan, Y.; Wang, Y.; Mei, L.; Chen, H.; Hu, H.; Zhang, Z.; Jin, Y. Recent Progress in Drug Delivery. *Acta Pharm. Sin. B* **2019**, *9* (6), 1145–1162.

(3) Chountoulesi, M.; Naziris, N.; Pippa, N.; Pispas, S.; Demetzos, C. Stimuli-Responsive Nanocarriers for Drug Delivery. *Nanomater. Clin. Appl.* **2020**, 99–121.

(4) Mura, S.; Nicolas, J.; Couvreur, P. Stimuli-Responsive Nanocarriers for Drug Delivery. *Nat. Mater.* **2013**, *12* (11), 991–1003.

(5) Webber, M. J.; Langer, R. Drug Delivery by Supramolecular Design. *Chem. Soc. Rev.* **2017**, *46* (21), 6600–6620.

(6) Braegelman, A. S.; Webber, M. J. Integrating Stimuli–Responsive Properties in Host–Guest Supramolecular Drug Delivery Systems. *Theranostics* **2019**, *9* (11), 3017–3040.

(7) Zhang, Z.; Ding, J.; Chen, X.; Xiao, C.; He, C.; Zhuang, X.; Chen, L.; Chen, X. Intracellular PH-Sensitive Supramolecular Amphiphiles Based on Host-Guest Recognition between Benzimidazole and β-Cyclodextrin as Potential Drug Delivery Vehicles. *Polym. Chem.* **2013**, *4* (11), 3265–3271.

(8) Wang, X.; Yan, F.; Liu, X.; Wang, P.; Shao, S.; Sun, Y.; Sheng, Z.; Liu, Q.; Lovell, J. F.; Zheng, H. Enhanced Drug Delivery Using Sonoactivatable Liposomes with Membrane-Embedded Porphyrins. *J. Control. Release* **2018**, *286*, 358–368.

(9) Tian, J.; Zhou, T.-Y.; Zhang, S.-C.; Aloni, S.; Altoe, M. V.; Xie, S.-H.; Wang, H.; Zhang, D.-W.; Zhao, X.; Liu, Y.; Li, Z.-T. Three-Dimensional Periodic Supramolecular Organic Framework Ion Sponge in Water and Microcrystals. *Nat. Commun.* **2014**, *5* (1), 5574.

(10) Ding, Y. F.; Sun, T.; Li, S.; Huang, Q.; Yue, L.; Zhu, L.; Wang, R. Oral Colon-Targeted Konjac Glucomannan Hydrogel Constructed through Noncovalent Cross-Linking by Cucurbit[8]Uril for Ulcerative Colitis Therapy. *ACS Appl. Bio Mater.* **2020**, *3* (1), 10–19.

(11) Zou, L.; Braegelman, A. S.; Webber, M. J. Dynamic Supramolecular Hydrogels Spanning an Unprecedented Range of Host-Guest Affinity. *ACS Appl. Mater. Interfaces* **2019**, 8–13.

(12) Geng, W. C.; Sessler, J. L.; Guo, D. S. Supramolecular Prodrugs Based on Host-Guest Interactions. *Chem. Soc. Rev.* **2020**, *49* (8), 2303–2315.

(13) Chen, Y.; Huang, Z.; Xu, J. F.; Sun, Z.; Zhang, X. Cytotoxicity Regulated by Host-Guest Interactions: A Supramolecular Strategy to Realize Controlled Disguise and Exposure. *ACS Appl. Mater. Interfaces* **2016**, *8* (35), 22780–22784.

(14) Li, G.; Trausel, F.; van der Helm, M. P.; Klemm, B.; Brevé, T. G.; van Rossum, S. A. P.; Hartono, M.; Gerlings, H. H. P. J.; Lovrak, M.; van Esch, J. H.; Eelkema, R. Tuneable Control of Organocatalytic Activity through Host–Guest Chemistry. *Angew. Chem. Int. Ed.* **2021**, *60* (25), 14022–14029.

(15) Wang, L.; Li, L. L.; Fan, Y. S.; Wang, H. Host-Guest Supramolecular Nanosystems for Cancer Diagnostics and Therapeutics. *Adv. Mater.* **2013**, *25* (28), 3888–3898.

(16) Mao, D.; Liang, Y.; Liu, Y.; Zhou, X.; Ma, J.; Jiang, B.; Liu, J.; Ma, D. Acid-Labile Acyclic Cucurbit[n]Uril Molecular Containers for Controlled Release. *Angew. Chem. Int. Ed.* **2017**, *56* (41), 12614–12618.

(17) Liu, L. Controlled Release from Cucurbituril. *J. Incl. Phenom. Macrocycl. Chem.*

2017, *87* (1–2), 1–12.

(18)   Jeon, W. S.; Kim, E.; Ko, Y. H.; Hwang, I.; Lee, J. W.; Kim, S.-Y.; Kim, H.-J.; Kim, K. Molecular Loop Lock: A Redox-Driven Molecular Machine Based on a Host-Stabilized Charge-Transfer Complex. *Angew. Chem. Int. Ed.* **2005**, *44* (1), 87–91.

(19)   Appel, E. A.; Loh, X. J.; Jones, S. T.; Biedermann, F.; Dreiss, C. A.; Scherman, O. A. Ultrahigh-Water-Content Supramolecular Hydrogels Exhibiting Multistimuli Responsiveness. *J. Am. Chem. Soc.* **2012**, *134* (28), 11767–11773.

(20)   Barrow, S. J.; Kasera, S.; Rowland, M. J.; Del Barrio, J.; Scherman, O. A. Cucurbituril-Based Molecular Recognition. *Chem. Rev.* **2015**, *115* (22), 12320–12406.

(21)   Pazos, E.; Novo, P.; Peinador, C.; Kaifer, A. E.; García, M. D. Cucurbit[8]Uril (CB[8])-Based Supramolecular Switches. *Angew. Chem. Int. Ed.* **2019**, *58* (2), 403–416.

(22)   Ko, Y. H.; Kim, E.; Hwang, I.; Kim, K. Supramolecular Assemblies Built with Host-Stabilized Charge-Transfer Interactions. *Chem. Commun.* **2007**, No. 13, 1305–1315.

(23)   Biedermann, F.; Uzunova, V. D.; Scherman, O. A.; Nau, W. M.; De Simone, A. Release of High-Energy Water as an Essential Driving Force for the High-Affinity Binding of Cucurbit[n]Urils. *J. Am. Chem. Soc.* **2012**, *134* (37), 15318–15323.

(24)   Li, G.; Wan, Y.; Lewis, R. W.; Fan, B.; Eelkema, R. Signal-Specific Triggering of Supramolecular Aggregate Formation. Unpublished work.

(25)   Lewis, R. W.; Klemm, B.; Macchione, M.; Eelkema, R. Fuel-Driven Macromolecular Coacervation in Complex Coacervate Core Micelles. *Chem. Sci.* **2022**, *13* (16), 4533–4544.

(26)   Zhuang, J.; Zhao, B.; Meng, X.; Schiffman, J. D.; Perry, S. L.; Vachet, R. W.; Thayumanavan, S. A Programmable Chemical Switch Based on Triggerable Michael Acceptors. *Chem. Sci.* **2020**, *11* (8), 2103–2111.

(27)   Klemm, B.; Lewis, R.; Piergentili, I.; Eelkema, R. Temporally Programmed Polymer-Solvent Interactions Using a Chemical Reaction Network. **2021**. ChemRxiv. Cambridge: Cambridge Open Engage.

(28)   jiang, S.; Yang, X.; Yang, C.; Tong, M.; Zou, D.; Wu, Y. Guest-Size Determining the Selective Binding Modes of Cucurbit[8]Uril, Electron-Rich Guests and N-Alkyl-N'-Methyl-4,4'-Bipyridinium. *Tetrahedron Lett.* **2013**, *54* (13), 1638–1644.

(29)   Jiao, D.; Geng, J.; Loh, X. J.; Das, D.; Lee, T. C.; Scherman, O. A. Supramolecular Peptide Amphiphile Vesicles through Host-Guest Complexation. *Angew. Chem. Int. Ed.* **2012**, *51* (38), 9633–9637.

(30)   Kim, H. J.; Heo, J.; Jeon, W. S.; Lee, E.; Kim, J.; Sakamoto, S.; Yamaguchi, K.; Kim, O. Selective Inclusion of a Hetero-Guest Pair in a Molecular Host: Formation of Stable Charge-Transfer Complexes in Cucurbit[8]Uril. *Angew. Chem. Int. Ed.* **2001**, *40* (8), 1526–1529.

(31)   Hashimoto, S.; Thomas, J. K. Fluorescence Study of Pyrene and Naphthalene in Cyclodextrin-Amphiphile Complex Systems. *J. Am. Chem. Soc.* **1985**, *107* (16), 4655–4662.

(32)   Klíma, P.; Laňková, M.; Zažímalová, E. Inhibitors of Plant Hormone Transport. *Protoplasma* **2016**, *253* (6), 1391–1404.

(33)   Biedermann, F.; Scherman, O. A. Cucurbit[8]Uril Mediated Donor-Acceptor Ternary Complexes: A Model System for Studying Charge-Transfer Interactions. *J. Phys. Chem. B* **2012**, *116* (9), 2842–2849.

(34)   Appel, E. A.; Biedermann, F.; Rauwald, U.; Jones, S. T.; Zayed, J. M.; Scherman, O. A. Supramolecular Cross-Linked Networks via Host-Guest Complexation with Cucurbit[8]Uril. *J. Am. Chem. Soc.* **2010**, *132* (40), 14251–14260.

(35)   Liu, Y.; Yu, Y.; Gao, J.; Wang, Z.; Zhang, X. Water-Soluble Supramolecular Polymerization Driven by Multiple Host-Stabilized Charge-Transfer Interactions. *Angew. Chem. Int. Ed.* **2010**, *49* (37), 6576–6579.

(36)   Liu, S.; Ruspic, C.; Mukhopadhyay, P.; Chakrabarti, S.; Zavalij, P. Y.; Isaacs, L. The Cucurbit[n]Uril Family: Prime Components for Self-Sorting Systems. *J. Am. Chem. Soc.* **2005**, *127* (45), 15959–15967.

(37)   Weng, J. R.; Tsai, C. H.; Kulp, S. K.; Chen, C. S. Indole-3-Carbinol as a Chemopreventive and Anti-Cancer Agent. *Cancer Lett.* **2008**, *262* (2), 153–163.

(38)   Tani, N.; Juvonen, R. O.; Raunio, H.; Fashe, M.; Leppänen, J.; Zhao, B.; Tyndale, R. F.; Rahnasto-Rilla, M. Rational Design of Novel CYP2A6 Inhibitors. *Bioorganic Med. Chem.* **2014**, *22* (23), 6655–6664.

6.5 Supplementary information

6.5.1 General information

Methods

NMR spectra were recorded on an Agilent-400 MR DD2 (399.7 MHz for ^{1}H, 100.5 MHz for ^{13}C) at 298 K using residual protonated solvent signals as internal standard (^{13}C in D_2O was referenced to internal 1,4-Dioxane, δ = 67.19). **UV/Vis** spectroscopic measurements were performed on an Analytik Jena Specord 250 spectrophotometer; quartz cuvettes with a path length of 1.0 cm were used. **Isothermal titration calorimetry (ITC)** measurements were carried out at room temperature using a MicroCal VP-ITC. **LC-MS** was performed on a Shimadzu Liquid Chromatograph Mass Spectrometer 2010, LC-8A pump with a diode array detector SPD-M20. The **pH** was recorded with the Consort C830 pH meter. **Fluorescence** spectra were recorded on a JASCO J-815 CD spectrometer (sensitivity 600 Volts, data pitch 1 nm, band width 5 nm, excitation wavelength of 465 nm; black quartz cuvette with a 1 cm path length, volume of 50 μL, at room temperature.

Materials

Sodium phosphate monobasic monohydrate (98%), 2-mercaptoethanol (99.0%), 1-adamantanamine (97%), pyridine (99.8%), 4-phenylpyridine (97%), quinolone (98%), isoquinoline (97%), indol (>99%), 1-methylindole (≥97%), sumatriptan succinate, Indole-3-carbinol, benzothiophene-2-methanol (97%), Benzo[b]thiophene-2-propionic acid (97%), 2,3-Benzofuran (>99%) were purchased from Sigma Aldrich, methyl 2-(bromomethyl)acrylate (>97.0%), 4,4'-bipyridine (>98.0%), *N,N,N*-trimethyl-1-adamantylammonium hydroxide (25% in water), 2,6-dihydroxynaphthalene (>95.0%), benzimidazole (98%), benzothiazole (96%), Thieno[3,2-b]thiophene (>98%) were purchased from TCI Europe. Sodium phosphate dibasic salt (≥99%, analysis grade) was purchased from Acros Organics. Agomelatine (95%), 4-Pyridin-4-yl-benzoic acid methyl ester (95%), deuterium oxide for NMR was purchased from Euriso-top, L-proline (≥99%) was from Fluorochem Ltd. CB[8] was obtained from Professor Oren A. Scherman's group at Cambridge University. Aqueous pH buffers were prepared by mixing the aqueous solution of sodium phosphate monobasic monohydrate salt and sodium phosphate dibasic salt at the same concentration, under the measurement of pH indicator until the required pH is achieved.

6.5.2 Synthesis and characterization

General procedure of Synthesizing first guest molecules[1]

1a⁰-1f⁰   **1a⁺-1f⁺**
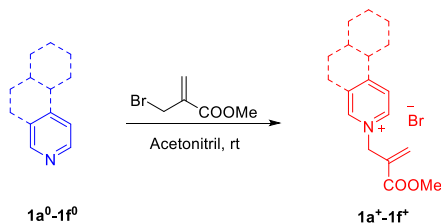
First guest molecules **1a²⁺1f⁺** were synthesized by reacting **1a⁰-1f⁰** with methyl 2-(bromomethyl)acrylate (1.5 eq.) in acetonitrile at room temperature. The solvent and unreacted methyl 2-(bromomethyl)acrylate were removed through rotary evaporation. The resulting solid was washed by ethyl acetate and dried under vacuum to give final pure products with quantitative yield.


1a²⁺
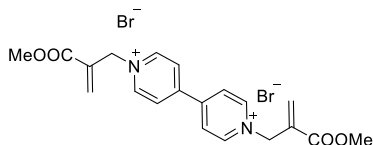
^{1}H NMR (400 MHz, Deuterium Oxide) δ 9.04 (d, *J* = 6.8 Hz, 4H), 8.41 (d, *J* = 6.4 Hz, 4H), 6.64 (s, 2H), 6.30 (s, 2H), 5.46 (s, 4H), 4.63 (s, 2H), 3.62 (s, 6H); ^{13}C NMR (101 MHz, d₂o) δ 167.05, 151.18, 146.58, 136.45, 132.95, 127.49, 62.55, 53.44. **MS** (ESI Pos) m/z: 177.09 [(M-2Br⁻)/2]⁺ (expected m/z = 177.08).

1b⁺
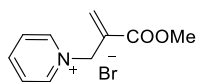
^{1}H NMR (400 MHz, Methanol-*d₄*) δ 9.03 (d, *J* = 6.0 Hz, 2H), 8.61 (t, *J* = 7.8 Hz, 1H), 8.11 (t, *J* = 7.1 Hz, 2H), 6.64 (s, 1H), 6.32 (s, 1H), 5.49 (s, 2H), 3.73 (s, 3H); ^{13}C NMR (101 MHz, Methanol-*d₄*) δ 164.86, 146.13, 145.09, 133.37, 127.89, 61.51, 51.59. **MS** (ESI Pos) m/z: 178.09 [M-Br⁻]⁺ (expected m/z = 178.09).
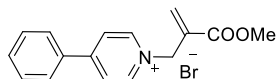
1c⁺

^{1}H NMR (400 MHz, D₂O) δ 8.88 (d, *J* = 7.2 Hz, 2H), 8.33 (d, *J* = 6.8 Hz, 2H), 7.97 (d, *J* = 8.0 Hz, 2H), 7.74 – 7.63 (m, 3H), 6.74 (s, 1H), 6.34 (s, 1H), 5.47 (s, 2H), 3.77 (s, 3H); ^{13}C NMR (100 MHz, D₂O) δ 167.16, 157.48, 145.00, 135.61, 134.12, 133.39, 132.91, 130.29, 128.58, 125.30, 61.31, 53.40. **MS** (ESI Pos) m/z: 254.17 [M-Br⁻]⁺ (expected m/z = 254.12).
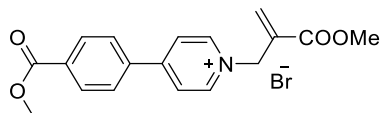
1d⁺

¹H NMR (400 MHz, Methanol-d_4) δ 9.04 (d, J = 6.8 Hz 2H), 8.44 (d, J = 6.8 Hz, 2H), 8.23 (d, J = 8.4 Hz, 2H), 8.09 (d, J = 8.8 Hz, 2H), 6.66 (s, 1H), 6.36 (s, 1H), 5.50 (s, 2H), 3.95 (s, 3H), 3.75 (s, 3H); ¹³C NMR (101 MHz, Methanol-d_4) δ 165.97, 164.94, 145.21, 137.99, 133.52, 133.37, 133.35, 133.06, 130.26, 128.15, 125.14, 60.86, 51.64, 51.62. **MS** (ESI Pos) m/z: 312.20 [M-Br⁻]⁺ (expected m/z = 312.12).
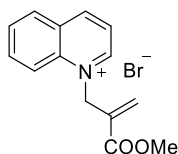
1e⁺

¹H NMR (400 MHz, Methanol-d_4) δ 9.51 (d, J = 5.6 Hz, 1H), 9.27 (d, J = 8.4 Hz, 1H), 8.51-8.44 (m, 2H), 8.28-8.24 (m, 1H), 8.14 (dd, J = 8.4, 6.0 Hz, 1H), 8.06-8.02 (m, 1H), 6.57 (s, 1H), 6.00 (s, 2H), 5.91 (s, 1H), 3.76 (s, 3H); ¹³C NMR (101 MHz, Methanol-d_4) δ 164.79, 150.55, 148.60, 138.32, 136.03, 133.30, 130.82, 130.39, 130.36, 130.33, 129.98, 121.55, 118.60, 57.71, 51.61. **MS** (ESI Pos) m/z: 228.17 [M-Br⁻]⁺ (expected m/z = 228.10).
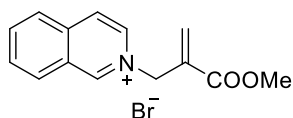
1f⁺

¹H NMR (400 MHz, Deuterium Oxide) δ 9.79 (s, 1H), 8.54 (dd, J = 6.8, 1.2 Hz, 1H), 8.45-8.40 (m, 2H), 8.28–8.18 (m, 2H), 8.06-8.02 (m, 1H), 6.75 (s, 1H), 6.38 (s, 1H), 5.62 (s, 2H), 3.74 (s, 3H). ¹³C NMR (101 MHz, Deuterium Oxide) δ 172.46, 155.71, 143.67, 143.36, 140.79, 139.89, 138.70, 137.34, 136.14, 133.40, 133.10, 132.16, 72.43, 58.61. **MS** (ESI Pos) m/z: 228.12 [M-Br⁻]⁺ (expected m/z = 228.10).

6.5.3 Isothermal titration calorimetry results

General procedure: a solution of guest molecule was titrated to a solution of CB[8] with or without first guest molecule at 25 °C, both in 10 mM sodium phosphate buffer pH 7.4. The first titration point of each ITC measurement was omitted. Binding constants were fitted with Microcal LLC ITC Origin 7 software.

Table S6.1 ITC Spectrum and binding model at pH 7.4.

	Spectrums		Spectrums
1	Condition: 10 mM sodium phosphate buffer pH 7.4, 25 °C, [**2a**] = 0.44 mM, [CB[8]] = 0.044 mM.	2	Condition: 10 mM sodium phosphate buffer pH 7.4, 25 °C, [**2b**] = 0.44 mM, [CB[8]] = 0.044 mM.
3	Condition: 10 mM sodium phosphate buffer pH 7.4, 25 °C, [**2a**] = 0.42 mM, [CB[8]/**1a^0**] = 0.042 mM.	4	Condition: 10 mM sodium phosphate buffer pH 7.4, 25 °C, [**2a**] = 0.47 mM, [CB[8]/**1a^{2+}**] = 0.047 mM.

| 5 |

Condition: 10 mM sodium phosphate buffer pH 7.4, 25 °C, [**2b**] = 0.40 mM, [CB[8]/**1a⁰**] = 0.040 mM. | 6 |

Condition: 10 mM sodium phosphate buffer pH 7.4, 25 °C, [**2b**] = 0.42 mM, [CB[8]/**1a⁺**] = 0.042 mM. |
| 7 |

Condition: 10 mM sodium phosphate buffer pH 7.4, 25 °C, [**2b**] = 0.40 mM, [CB[8]/**1b⁰**] = 0.040 mM. | 8 |

Condition: 10 mM sodium phosphate buffer pH 7.4, 25 °C, [**2b**] = 0.40 mM, [CB[8]/**1b⁰**] = 0.040 mM. |

9	Condition: 10 mM sodium phosphate buffer pH 7.4, 25 °C, [**2b**] = 0.40 mM, [CB[8]/**1c⁺**] = 0.040 mM.	10	Condition: 10 mM sodium phosphate buffer pH 7.4, 25 °C, [**2b**] = 0.40 mM, [CB[8]/**1c⁰**] = 0.040 mM.
11	Condition: 10 mM sodium phosphate buffer pH 7.4, 25 °C, [**2b**] = 0.40 mM, [CB[8]/**1d⁰**] = 0.04 mM.	12	Condition: 10 mM sodium phosphate buffer pH 7.4, 25 °C, [**2b**] = 0.40 mM, [CB[8]/**1d⁺**] = 0.04 mM.

13	 Condition: 10 mM sodium phosphate buffer pH 7.4, 25 °C, [**2b**] = 0.44 mM, [CB[8]]/**1e⁰** = 0.044 mM.	14	 Condition: 10 mM sodium phosphate buffer pH 7.4, 25 °C, [**2b**] = 0.40 mM, [CB[8]]/**1e⁺** = 0.04 mM.
15	 Condition: 10 mM sodium phosphate buffer pH 7.4, 25 °C, [**2b**] = 0.42 mM, [CB[8]]/**1f⁰** = 0.042 mM.	16	 . Condition: 10 mM sodium phosphate buffer pH 7.4, 25 °C, [**2b**] = 0.42 mM, [CB[8]]/**1f⁺** = 0.042 mM.

| 17 |
Condition: 10 mM sodium phosphate buffer pH 7.4, 25 °C, [**2a**] = 0.42 mM, [CB[8]/**1f⁰**] = 0.042 mM. | 18 |
Condition: 10 mM sodium phosphate buffer pH 7.4, 25 °C, [**2a**] = 0.42 mM, [CB[8]/**1f⁺**] = 0.042 mM. |
| 19 |
Condition: 10 mM sodium phosphate buffer pH 7.4, 25 °C, [**2c**] = 0.42 mM, [CB[8]/**1f⁰**] = 0.042 mM. | 20 |
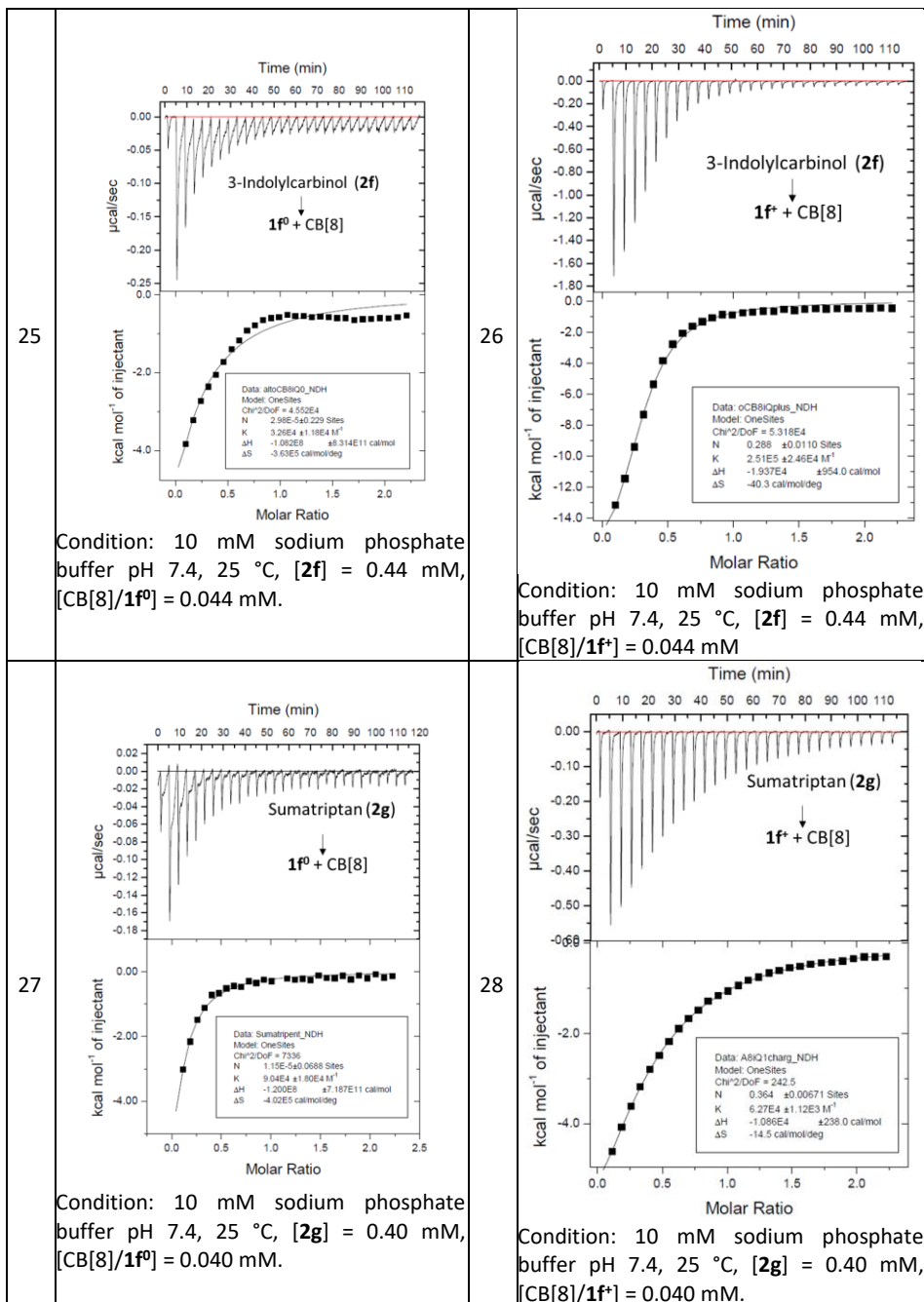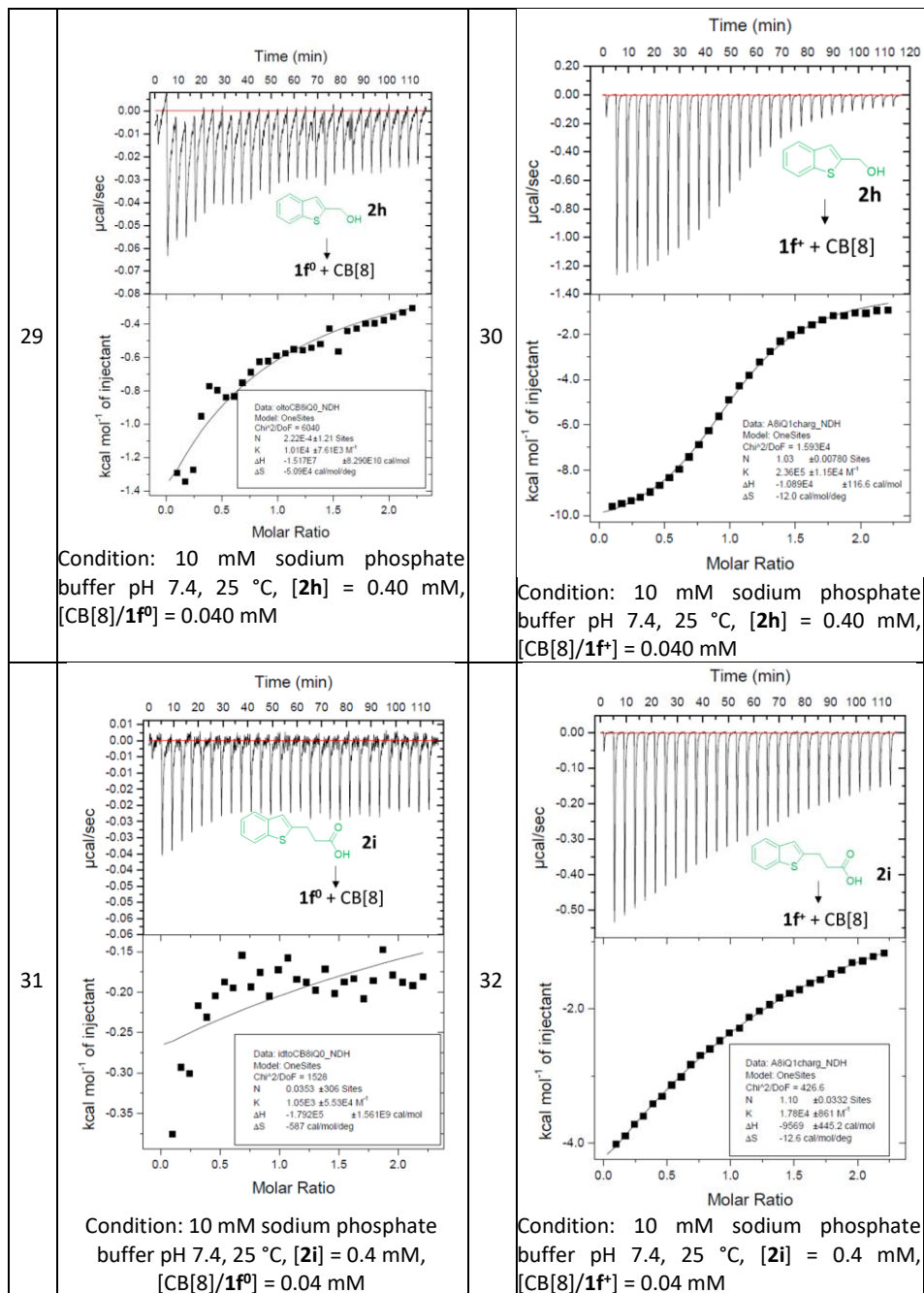Condition: 10 mM sodium phosphate buffer pH 7.4, 25 °C, [**2c**] = 0.42 mM, [CB[8]/**1f⁺**] = 0.042 mM. |
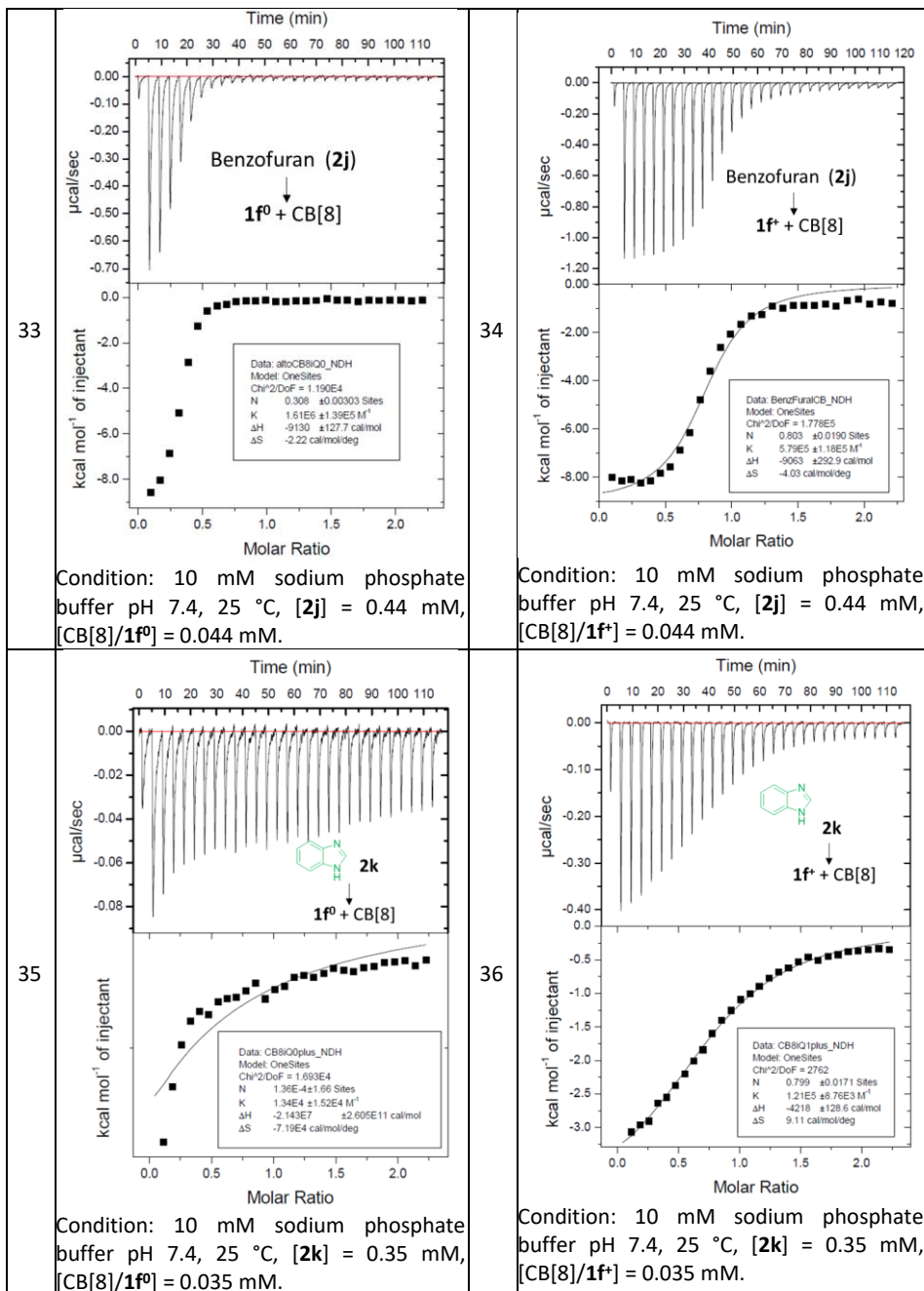
21	Condition: 10 mM sodium phosphate buffer pH 7.4, 25 °C, [**2d**] = 0.40 mM, [CB[8]]/**1f^0** = 0.040 mM.	**22**	
			Condition: 10 mM sodium phosphate buffer pH 7.4, 25 °C, [**2d**] = 0.40 mM, [CB[8]]/**1f$^+$** = 0.040 mM.
23	Condition: 10 mM sodium phosphate buffer pH 7.4, 25 °C, [**2e**] = 0.47 mM, [CB[8]]/**1f^0** = 0.047 mM.	**24**	Condition: 10 mM sodium phosphate buffer pH 7.4, 25 °C, [**2e**] = 0.47 mM, [CB[8]]/**1f$^+$** = 0.047 mM.

25	 Condition: 10 mM sodium phosphate buffer pH 7.4, 25 °C, [**2f**] = 0.44 mM, [CB[8]/**1f⁰**] = 0.044 mM.
26	 Condition: 10 mM sodium phosphate buffer pH 7.4, 25 °C, [**2f**] = 0.44 mM, [CB[8]/**1f⁺**] = 0.044 mM
27	 Condition: 10 mM sodium phosphate buffer pH 7.4, 25 °C, [**2g**] = 0.40 mM, [CB[8]/**1f⁰**] = 0.040 mM.
28	 Condition: 10 mM sodium phosphate buffer pH 7.4, 25 °C, [**2g**] = 0.40 mM, [CB[8]/**1f⁺**] = 0.040 mM.

29	Condition: 10 mM sodium phosphate buffer pH 7.4, 25 °C, [**2h**] = 0.40 mM, [CB[8]]/**1f⁰** = 0.040 mM	30	Condition: 10 mM sodium phosphate buffer pH 7.4, 25 °C, [**2h**] = 0.40 mM, [CB[8]]/**1f⁺** = 0.040 mM
31	Condition: 10 mM sodium phosphate buffer pH 7.4, 25 °C, [**2i**] = 0.4 mM, [CB[8]]/**1f⁰** = 0.04 mM	32	Condition: 10 mM sodium phosphate buffer pH 7.4, 25 °C, [**2i**] = 0.4 mM, [CB[8]]/**1f⁺** = 0.04 mM

| 33 | Condition: 10 mM sodium phosphate buffer pH 7.4, 25 °C, [**2j**] = 0.44 mM, [CB[8]/**1f⁰**] = 0.044 mM. | 34 | Condition: 10 mM sodium phosphate buffer pH 7.4, 25 °C, [**2j**] = 0.44 mM, [CB[8]/**1f⁺**] = 0.044 mM. |
| 35 | Condition: 10 mM sodium phosphate buffer pH 7.4, 25 °C, [**2k**] = 0.35 mM, [CB[8]/**1f⁰**] = 0.035 mM. | 36 | Condition: 10 mM sodium phosphate buffer pH 7.4, 25 °C, [**2k**] = 0.35 mM, [CB[8]/**1f⁺**] = 0.035 mM. |

37	
	Condition: 10 mM sodium phosphate buffer pH 7.4, 25 °C, [**2l**] = 0.35 mM, [CB[8]]/**1f⁰** = 0.035 mM.

Data: CB8iQ0plus_NDH
Model: OneSites
Chi^2/DoF = 4214
N   0.255   ±0.00973 Sites
K   2.45E5 ±1.63E4 M⁻¹
ΔH   -9656 ±458.6 cal/mol
ΔS   -7.73 cal/mol/deg

38	
	Condition: 10 mM sodium phosphate buffer pH 7.4, 25 °C, [**2l**] = 0.35 mM, [CB[8]]/**1f⁺** = 0.035 mM.

Data: CB8iQ1plus_NDH
Model: OneSites
Chi^2/DoF = 1.268E4
N   1.02   ±0.00566 Sites
K   5.22E5 ±2.45E4 M⁻¹
ΔH   -9685 ±74.54 cal/mol
ΔS   -6.32 cal/mol/deg

39	
	Condition: 10 mM sodium phosphate buffer pH 7.4, 25 °C, [**2m**] = 0.4 mM, [CB[8]]/**1f⁰** = 0.04 mM

Data: oltoCB8iQ0_NDH
Model: OneSites
Chi^2/DoF = 6040
N   2.22E-4 ±1.21 Sites
K   1.01E4 ±7.61E3 M⁻¹
ΔH   -1.517E7 ±8.290E10 cal/mol
ΔS   -5.09E4 cal/mol/deg

40	
	Condition: 10 mM sodium phosphate buffer pH 7.4, 25 °C, [**2m**] = 0.4 mM, [CB[8]]/**1f⁺** = 0.04 mM

Data: A8iQ1charg_NDH
Model: OneSites
Chi^2/DoF = 3.696E4
N   1.16   ±0.00437 Sites
K   6.41E6 ±7.28E5 M⁻¹
ΔH   -9222 ±60.99 cal/mol
ΔS   0.218 cal/mol/deg

Table S6.2 ITC Spectrum and binding model in pH 9.8.

Entry	ITC spectrum	Entry	ITC spectrum
1	Condition: 10 mM Na_2CO_3/$NaHCO_3$ buffer pH 9.8, 25 °C, [**2c**] = 0.5 mM, [CB[8]/**1f⁰**] = 0.05 mM	2	Condition: 10 mM Na_2CO_3/$NaHCO_3$ buffer pH 9.8, 25 °C, [**2d**] = 0.5 mM, [CB[8]/**1f⁰**] = 0.05 mM
3	Condition: 10 mM Na_2CO_3/$NaHCO_3$ buffer pH 9.8, 25 °C, [**2I**] = 0.5 mM, [CB[8]/**1f⁰**] = 0.05 mM		

Table S6.3. Overview of the thermodynamic data from ITC.

Entry	Compounds 1st guest	2nd guest	N / (sites)	K_a/ $(10^3)M^{-1}$	ΔH (kcal/mol)	ΔS (kcal/mol/deg)	ΔG (cal/mol)	pH[b]
1		2a	0.00375	1.93 ± 11.7	$-1.73 \times 10^3 \pm 1.17 \times 10^7$	-5.79	-\-[a]	7.4
2		2b	$(1.00 \pm 37300) \times 10^7$	$320 \pm 1.83 \times 10^4$	-0.134 ± 0.0520	0.011	-3.41	7.4
3	1a⁰	2a	$5.64 \times 10^{-4} \pm 1.24$	4.63 ± 2.20	$-1.69 \times 10^4 \pm 3.73 \times 10^7$	-56.8	-\-	7.4
4	1a²⁺	2a	0.791 ± 0.00795	71.8 ± 2.0	-14.2 ± 0.203	-0.0254	-6.63	7.4
5	1a⁰	2b	1.22 ± 0.345	5.04 ± 1.19	-7.11 ± 2.82	-0.00692	-5.05	7.4
6	1a²⁺	2b	1.03 ± 0.0385	36.7 ± 3.88	-10.4 ± 0.636	-0.0140	-6.23	7.4
7	1b⁰	2b	0.00427 ± 12.7	2.14 ± 7.89	$-4.83 \times 10^2 \pm 1.44 \times 10^6$	-1.60	-\-	7.4
8	1b⁺	2b	0.00144 ± 5.29	4.84 ± 10.6	$-1.58 \times 10^3 \pm 5.80 \times 10^6$	-5.27	-\-	7.4
9	1c⁰	2b	1.30 ± 1.31	5.29 ± 4.60	-2.140 ± 3.076	0.00986	-5.08	7.4
10	1c⁺	2b	2.37 ± 0.221	8.36 ± 4.08	-2.296 ± 0.715	0.0102	-5.34	7.4
11	1d⁰	2b	$6.77 \times 10^{-4} \pm 0.789$	3.83 ± 1.27	$-6.75 \times 10^3 \pm 7.88 \times 10^6$	-22.6	-\-	7.4
12	1d⁺	2b	$3.75 \times 10^{-4} \pm 0.794$	5.03 ± 1.96	$-1.03 \times 10^4 \pm 2.18 \times 10^7$	-34.6	-\-	7.4
13	1e⁰	2b	0.00956 ± 317	1.12 ± 64.8	$-3.58 \times 10^2 \pm 1.19 \times 10^7$	-1.19	-\-	7.4
14	1e⁺	2b	0.602 ± 0.188	7.14 ± 1.03	-18.7 ± 6.94	-0.0451	-5.25	7.4
15	1f⁰	2b	$8.15 \times 10^{-5} \pm 0.861$	16.1 ± 13.9	$-9.31 \times 10^3 \pm 9.83 \times 10^7$	-31.2	-\-	7.4
16	1f⁺	2b	0.789 ± 0.0207	30.9 ± 1.39	-10.6 ± 0.383	-0.0149	-6.16	7.4

17	**1f$^+$**	**2a**	$5.81 \times 10^{-4} \pm 3.54$	68.9 ± 3.42	-11.1 ± 0.223	-0.0149	-6.66	7.4
18	**1f^0**	**2a**	1.08 ± 0.0136	9.31 ± 20.0	$-3.33 \times 10^3 \pm 2.03 \times 10^7$	-11.1	-\-	7.4
19	**1f^0**	**2c**	0.140 ± 0.179	24.7 ± 5.56	-29.3 ± 39.4	-0.0780	-6.04	7.4
20	**1f$^+$**	**2c**	0.508 ± 0.0475	24.3 ± 1.66	-11.6 ± 1.31	-0.0187	-6.02	7.4
21	**1f^0**	**2d**	$1.35 \times 10^{-5} \pm 0.0513$	387 ± 49.8	$-7.98 \times 10^4 \pm 3.02 \times 10^8$	-268	-\-	7.4
22	**1f$^+$**	**2d**	0.631 ± 0.00924	380 ± 31.9	-10.8 ± 0.217	-0.0106	-7.64	7.4
23	**1f^0**	**2e**	0.0662 ± 0.0190	947 ± 171	-22.2 ± 8.46	-0.0469	-8.22	7.4
24	**1f$^+$**	**2e**	0.548 ± 0.00776	$(1.11 \pm 0.157) \times 10^3$	-13.4 ± 0.269	-0.0171	-8.30	7.4
25	**1f^0**	**2f**	$2.98 \times 10^{-5} \pm 0.229$	32.6 ± 11.8	$-1.08 \times 10^5 \pm 8.31 \times 10^8$	-363	-\-	7.4
26	**1f$^+$**	**2f**	0.288 ± 0.0110	251 ± 24.6	-19.4 ± 0.954	-0.0403	-7.38	7.4
27	**1f^0**	**2g**	$1.15 \times 10^{-5} \pm 0.0688$	90.4 ± 18.0	$-1.20 \times 10^5 \pm 7.19 \times 10^8$	-402	-\-	7.4
28	**1f$^+$**	**2g**	0.364 ± 0.00671	62.7 ± 1.12	-10.9 ± 0.238	-0.0145	-6.58	7.4
29	**1f^0**	**2h**	$2.22 \times 10^{-4} \pm 1.21$	10.1 ± 7.61	$-1.52 \times 10^4 \pm 8.29 \times 10^7$	-50.9	-\-	7.4
30	**1f$^+$**	**2h**	1.03 ± 0.00780	236 ± 11.5	-10.9 ± 0.117	-0.0120	-7.32	7.4
31	**1f^0**	**2i**	0.0353 ± 306	1.05 ± 5.53	$-1.79 \times 10^2 \pm 1.56 \times 10^6$	-0.587	-\-	7.4
32	**1f$^+$**	**2i**	1.10 ± 0.0332	17.8 ± 0.861	-9.57 ± 0.445	-0.0126	-5.81	7.4
33	**1f^0**	**2j**	0.308 ± 0.00303	$(1.61 \pm 0.139) \times 10^3$	-9.13 ± 0.128	-0.00222	-8.47	7.4
34	**1f$^+$**	**2j**	0.803 ± 0.0190	579 ± 118	-9.06 ± 0.293	-0.00403	-7.86	7.4
35	**1f^0**	**2k**	$1.36 \times 10^{-4} \pm 1.66$	13.4 ± 15.2	$-2.14 \times 10^4 \pm 2.61 \times 10^8$	-71.9	-\-	7.4

36	**1f⁺**	**2k**	0.799 ± 0.0171	121 ± 8.76	-4.22 ± 0.129	0.00911	-6.94	7.4
37	**1f⁰**	**2l**	0.255 ± 0.00973	245 ± 16.3	-9.66 ± 0.459	-0.00773	-7.36	7.4
38	**1f⁺**	**2l**	1.02 ± 0.00566	522 ± 24.5	-9.685 ± 0.0745	-0.00632	-7.80	7.4
39	**1f⁰**	**2m**	$2.22 \times 10^{-4} \pm 1.21$	10.1 ± 7.61	$-1.52 \times 10^4 \pm 8.29 \times 10^7$	-50.9	-\\-	7.4
40	**1f⁺**	**2m**	1.16 ± 0.00437	$(6.41 \pm 7.28) \times 10^3$	-9.22 ± 0.0610	2.18×10^{-4}	-9.28	7.4
41	**1f⁰**	**2c**	$1.19 \times 10^{-28} \pm 1.14 \times 10^{-11}$	1.51 ± 0.00	-0.0772 ± 0.0170	0.0143	-4.34	9.8
42	**1f⁰**	**2d**	$3.00 \times 10^{-5} \pm 0.100$	61.0 ± 15.8	$-2.08 \times 10^4 \pm 6.92 \times 10^7$	-0.00697	-\\-	9.8
43	**1f⁰**	**2l**	$3.73 \times 10^{-5} \pm 0.193$	30.6 ± 9.44	$-1.44 \times 10^4 \pm 7.44 \times 10^7$	-48.2	-\\-	9.8

[a] Measurement errors are too high to calculate a precise value; [b] 10 mM sodium phosphate buffer solution for pH 7.4 solution, 10 mM Na_2CO_3/$NaHCO_3$ buffer for pH 9.8 solution.

6.5.4 Photographs of solutions
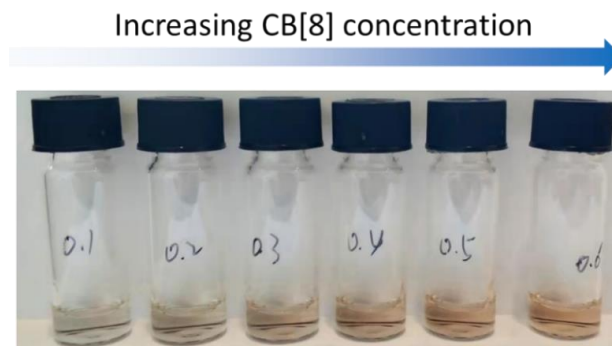
Figure S6.1 Photograph of solutions showing the colours gradually becoming purple with increasing concentration CB[8] (0.1 mM-0.6 mM) to **1a²⁺** (1mM) and **2b** (1 mM).

Figure S6.2 Photographic comparison of solutions of original complex (left, CB[8] = 0.6 mM, [**1a²⁺**] = 1mM, [**2b**] = 1mM), **Nu1** (4 mM) added reacting for 8 hours (middle), and L-proline (**Nu2**, 4 mM) added reacting for 36 h (right).
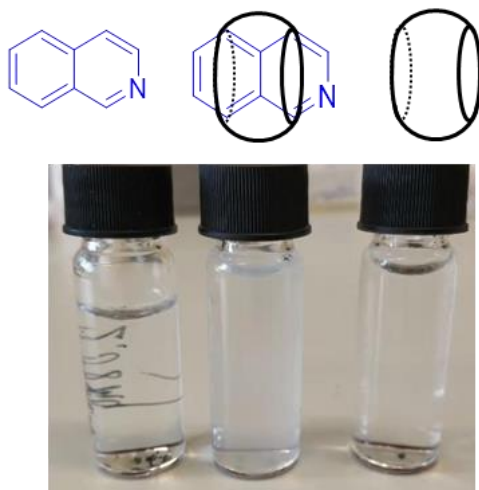
Figure S6.3 Photographic comparison of solutions of 0.04 mM isoquinoline (**1f⁰**, left), mixture of 0.04 mM isoquinoline and 0.04 mM CB[8] (middle), and 0.04 mM CB[8] (right) in pH 7.4 10 mM phosphate buffer solution.
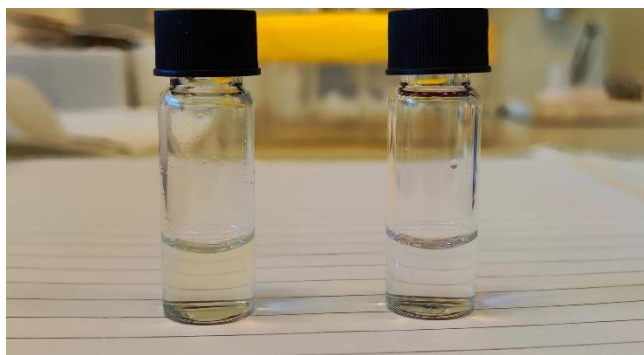
Figure S6.4 Photographic comparison of solutions 1 mM complex (CB[8], **1f⁺**, **2b**, left) and solution of **1f⁺** and **2b** (right) in pH 7.4 10 mM phosphate buffer solution.

6.5.5 Additional fluorescence data
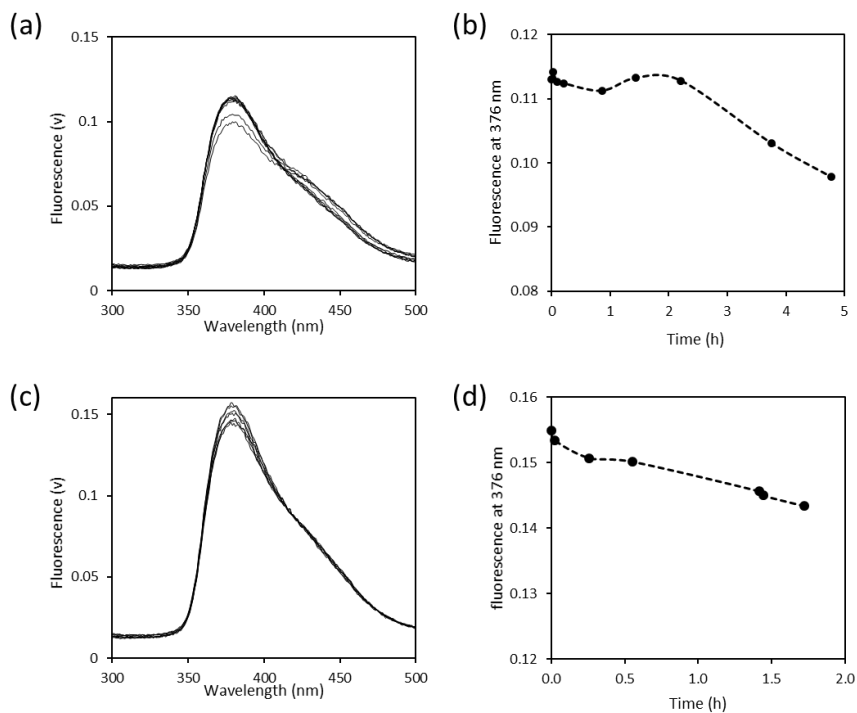
Figure S6.5 Fluorescence changes with time. (a,b) L-proline (20 μM) added into solution of **2a** (10 μM), CB[8] (10 μM) and **1a^{2+}** (10 μM); (c,d) 2-mercaptoethanol (20 μM) added into **2a** (10 μM) and CB[8] (10 μM). All in pH 7.4 10 mM phosphate buffer solution. (λ$_{ex}$ = 278 nm).

6.5.6 ¹H-NMR titration and measurement of releasing by adding signals
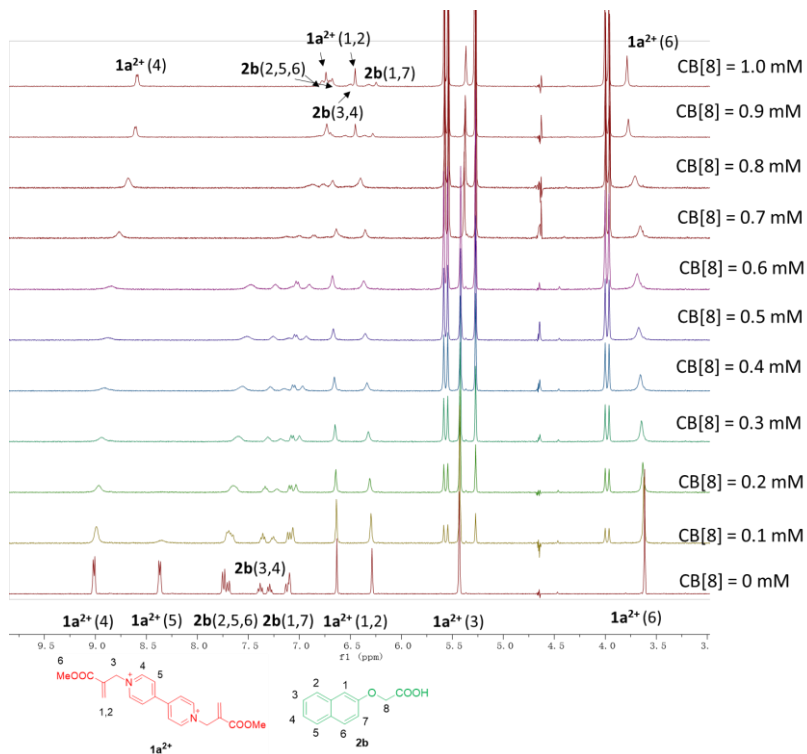
Figure S6.6 ¹H-NMR titration (water suppression mode, in 10 mM pH = 7.4 sodium phosphate buffer) of 1 mM guest molecule $1a^{2+}$ and **2b** with different equivalents of CB[8] (0 to 1mM).
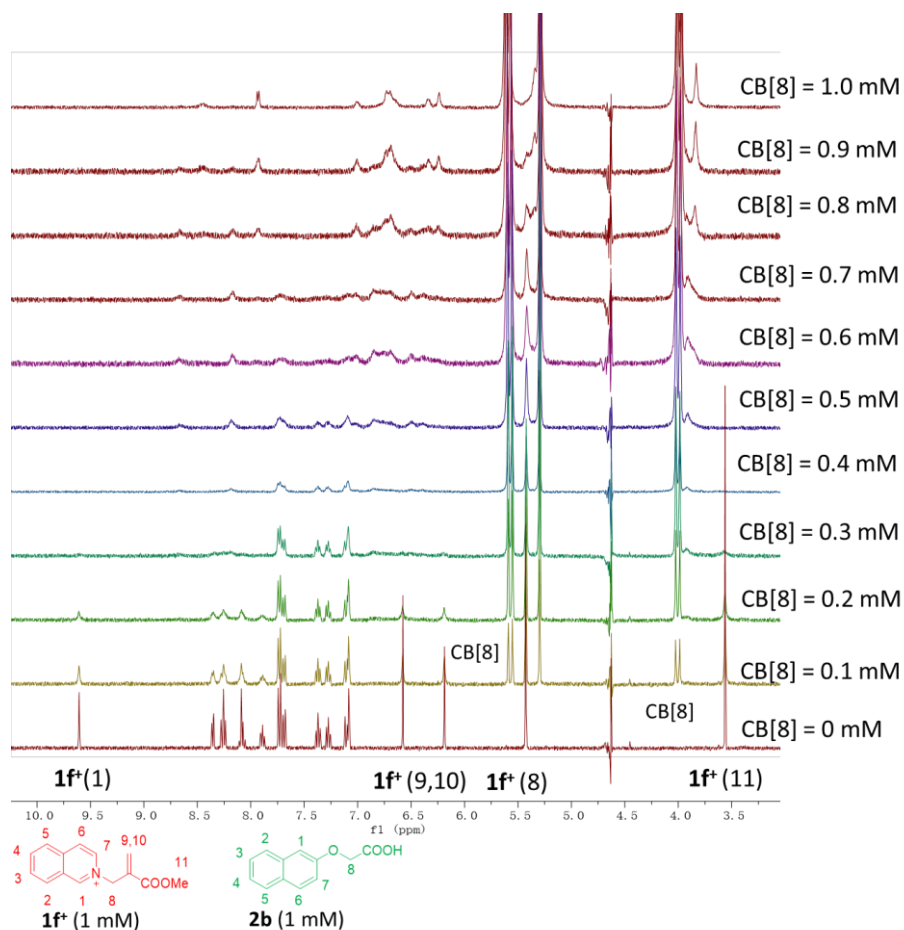
Figure S6.7 ^{1}H-NMR titration (water suppression mode, in 10 mM pH = 7.4 sodium phosphate buffer) of 1 mM guest molecule **1f⁺** and **2b** with different equivalents of CB[8] (0 mM to 1 mM).
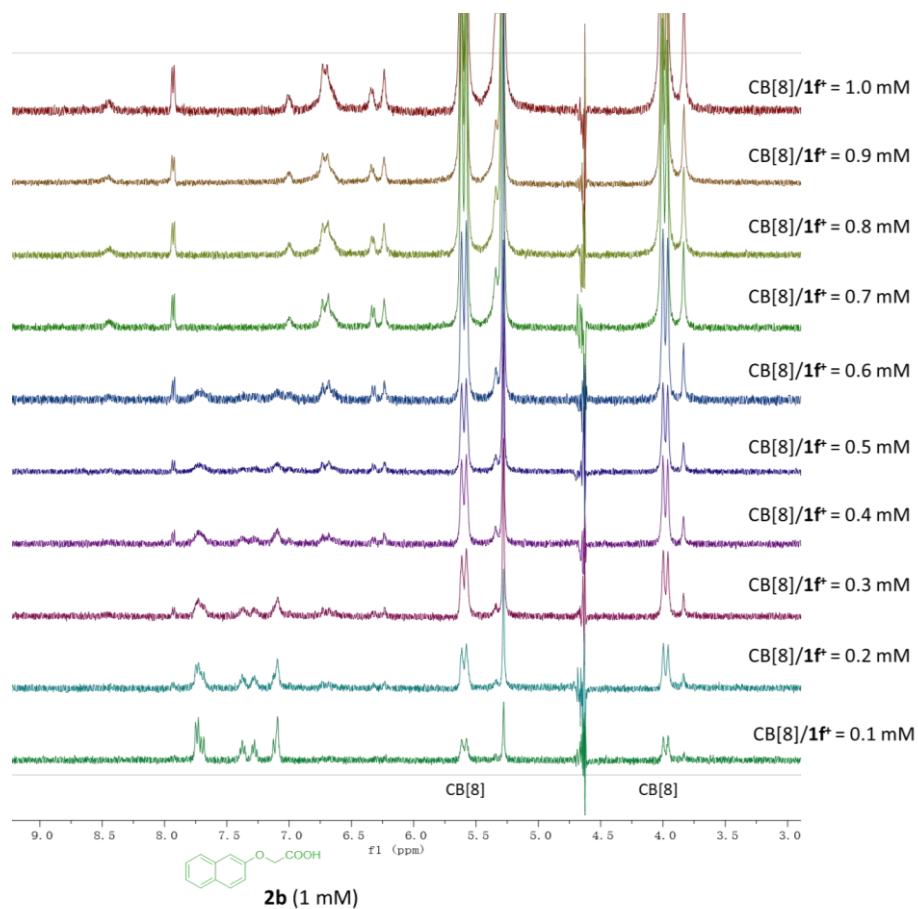
Figure S6.8 ^{1}H-NMR titration (water suppression mode, in 10 mM pH = 7.4 sodium phosphate buffer) of 1 mM guest molecule **1f+** with increasing concentration of CB[8]/**1f+** (from 0.1 mM to 1mM).
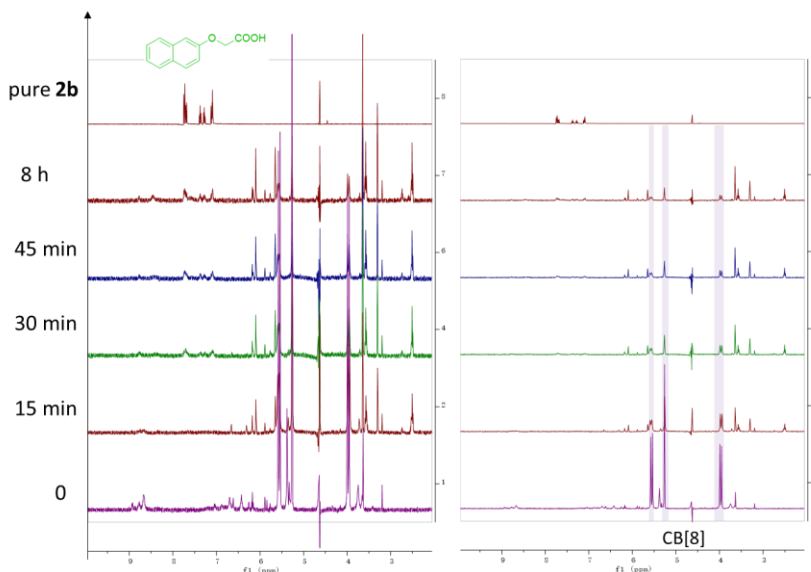
Figure S6.9 ^{1}H NMR spectrums (left: zoom in, right: zoom out) over time to show the releasing of **2b** (1 mM) from CB[8] (0.6 mM), **1a^{2+}** (1 mM) by adding 2-mercaptoethanol (**Nu1**, 2 mM), in pH 7.4 phosphate buffer and D$_2$O (10%) solution (water suppression).
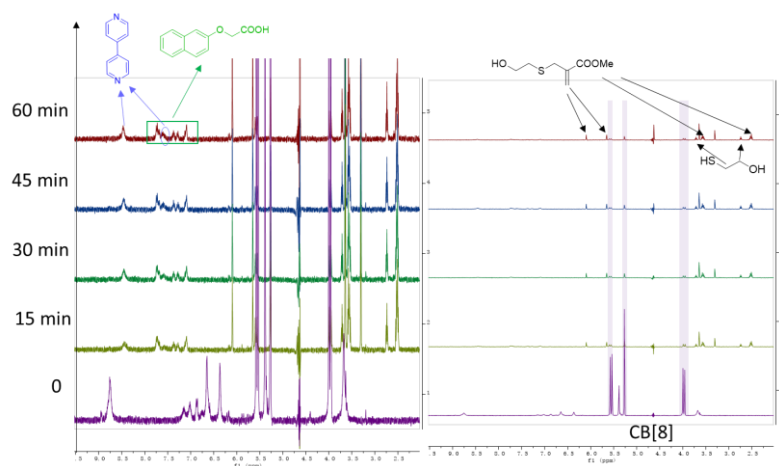
Figure S6.10 ^{1}H NMR spectrums (left: zoom in, right: zoom out) over time to show a fast releasing of **2b** (1 mM) from CB[8] (0.6 mM), **1a^{2+}** (1 mM) by adding 2-mercaptoethanol (**Nu1**, 4 mM), in pH 7.4 phosphate buffer and D$_2$O (10%) solution (water suppression).
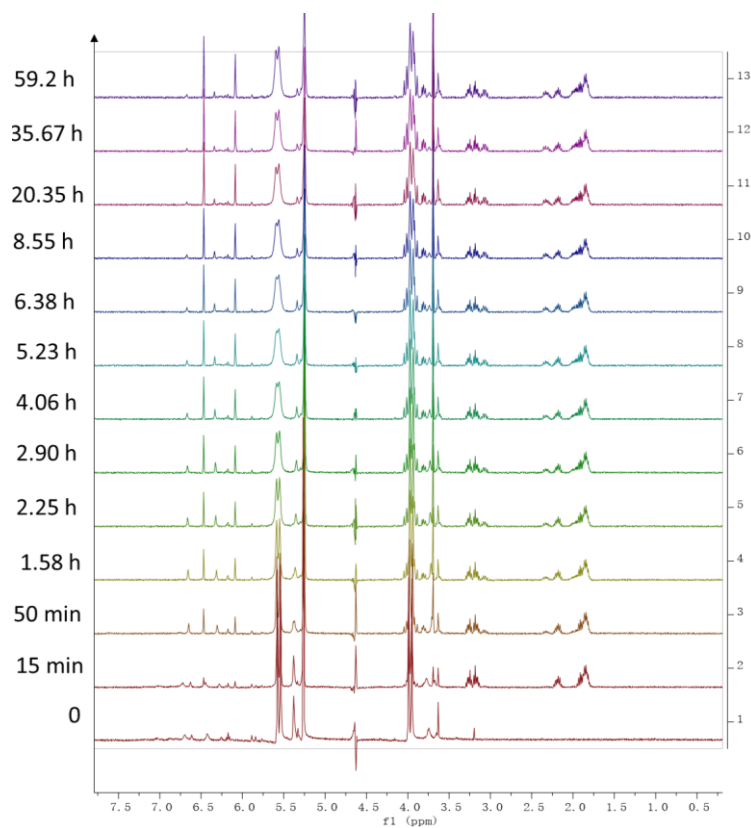
Figure S6.11 ^{1}H NMR spectrums over time of complex([**2b**] = 1 mM, [CB[8]] = 0.6 mM), [**1a²⁺**] = 1 mM) by adding L-proline (**Nu2**, 4 mM), in pH 7.4 phosphate buffer and D$_2$O (10%) solution (water suppression).
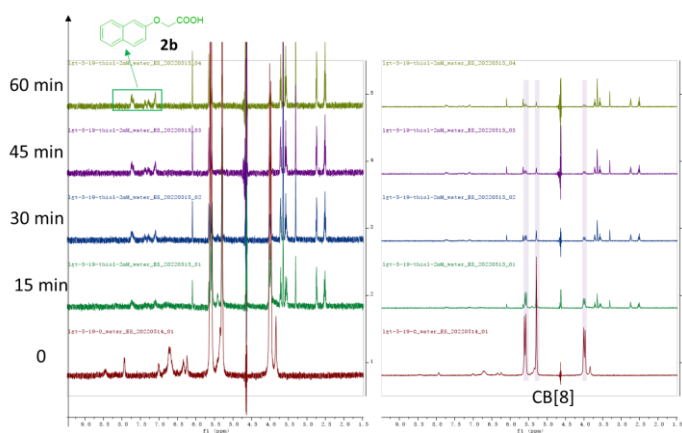
Figure S6.12 ^{1}H NMR spectrums (left: zoom in, right: zoom out) over time to shows a fast releasing of **2b** (1 mM) from CB[8] (0.6 mM), **1f⁺** (1 mM) by adding 2-mercaptoethanol (**Nu1**, 2 mM), in pH 7.4 phosphate buffer and D_2O (10%) solution (water suppression).
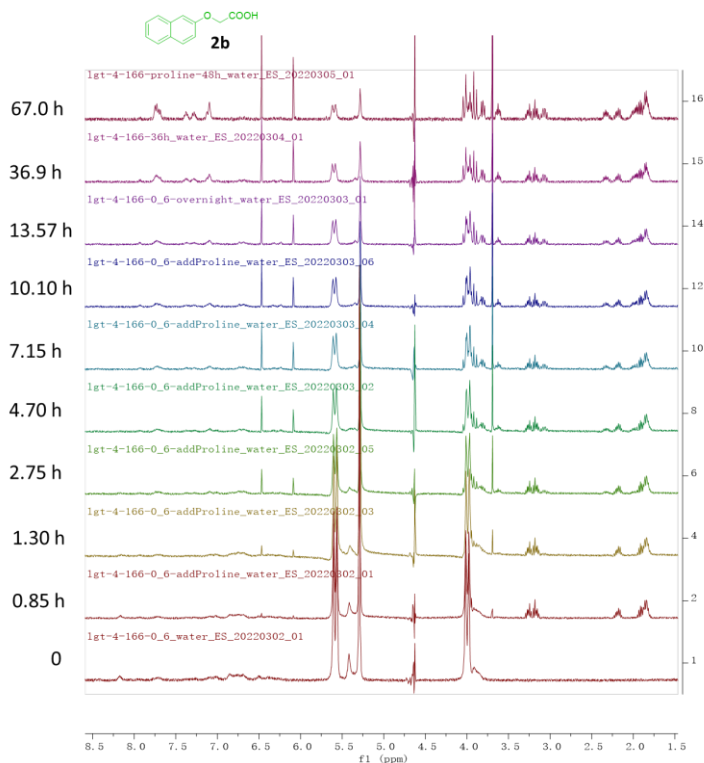
Figure S6.13 ^{1}H NMR spectrums over time to show the releasing of **2b** (1 mM) from CB[8]/**1f⁺** (CB[8] 0.6 mM, **1f⁺** 1 mM) by adding L-proline (**Nu2**, 2 mM) in pH 7.4 phosphate buffer and D_2O (10%) solution (water suppression).

6.5.7 Analysis of precipitation by NMR

Precipitation obtained by adding 2-mercaptoethanol (2 mM) to the solution of **1f⁺** (1 mM), CB[8] (0.6 mM) and **2b** (1 mM), was isolated by centrifugation. The white solid was washed by 1 mL H_2O (×3) and put into NMR tube in D_2O to measure ^{1}H NMR (Figure S6.14b, top). *N,N,N*-Trimethyl-1-adamantylammonium chloride (10 mM) was added in to the NMR tube above. The suspension was dissolved by heating and sonication and measured again by ^{1}H NMR (Figure S6.14b, bottom), showing isoquinoline and CB[8] in the precipitation.
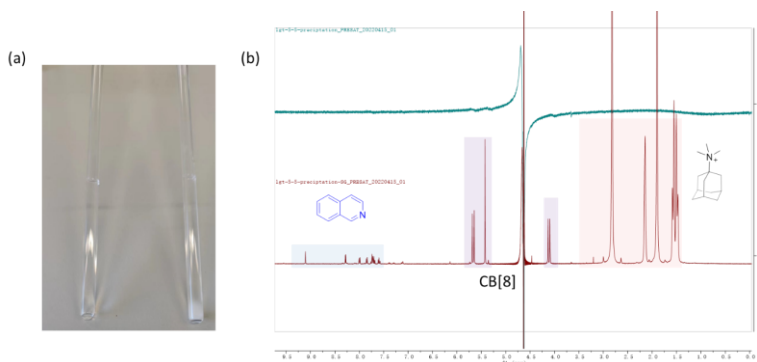
Figure S6.14 Analysis of the precipitation by ^{1}H NMR. (a) Photographic comparison of NMR tubes of a clear solution (left) and precipitation caused by adding signals (right). (b) ^{1}H-NMR overlay of precipitation from centrifuge (top) and solution by adding *N,N,N*-trimethyl-1-adamantylammonium chloride (10 mM). Solution in pH 7.4 10 mM phosphate buffer and 10% D$_2$O.

6.5.8 Additional 2nd electron-rich guest molecules

N-Acetyl-L-tryptophan

Naproxen

Melatonin

Nabumetone

Fluvastatin
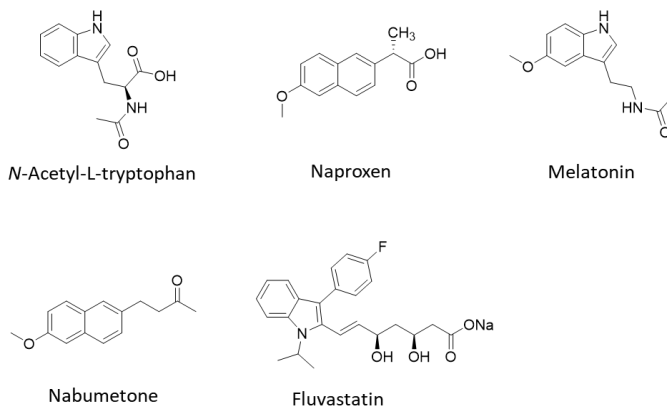
Figure S6.15 Structures of electron-rich chemicals that do not bind with CB[8]/**1f$^+$**

.

6.5.9. Spectra overview
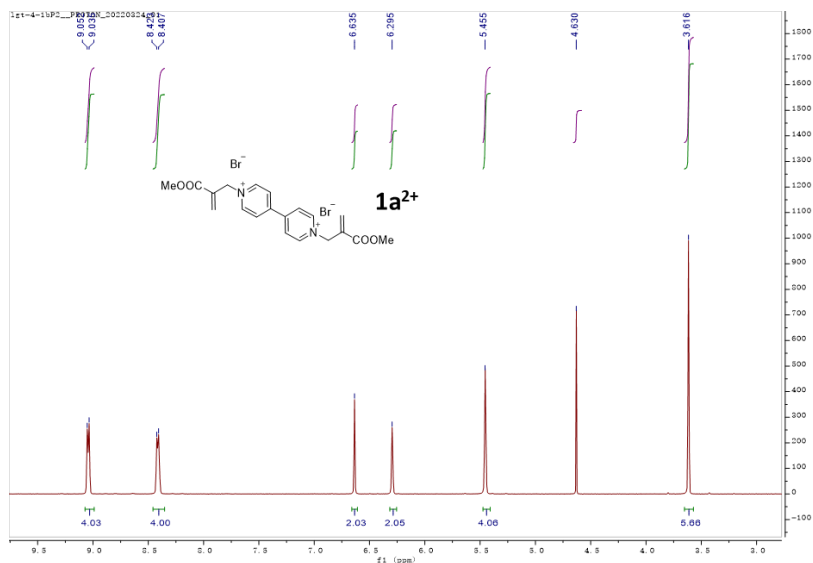
Figure S6.16 ^{1}H-NMR spectrum of guest **1a^{2+}** in D$_2$O.
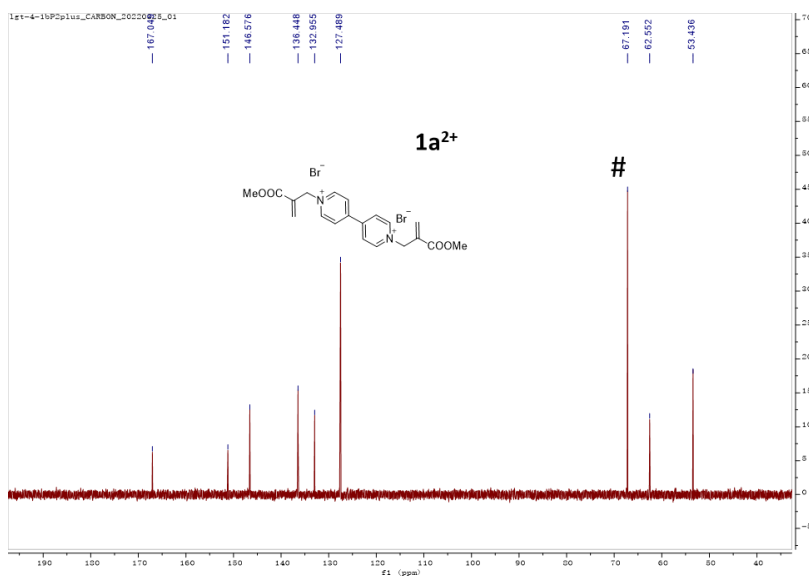
Figure S6.17 ^{13}C-NMR spectrum of guest **1a^{2+}** in D$_2$O. (1,4-Dioxane as NMR reference standard, marked as #).
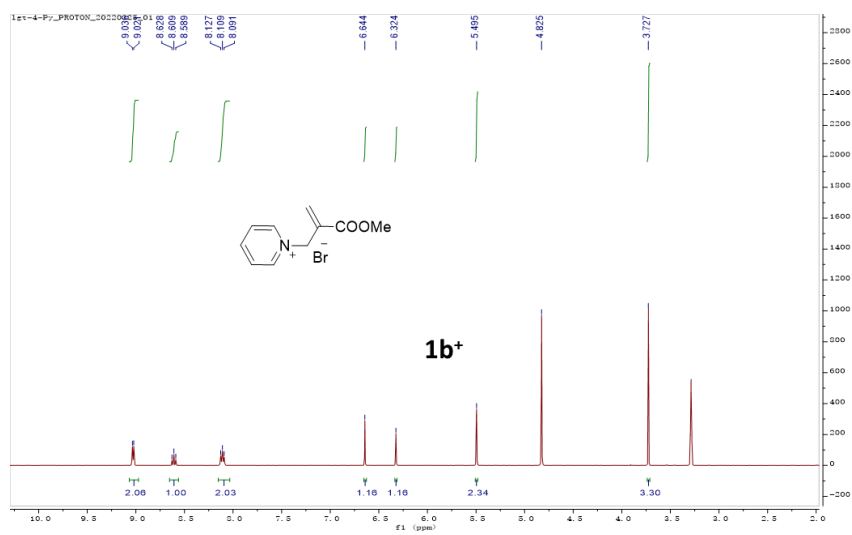
Figure S6.18 ^{1}H-NMR spectrum of guest **1b⁺** in MeOD.
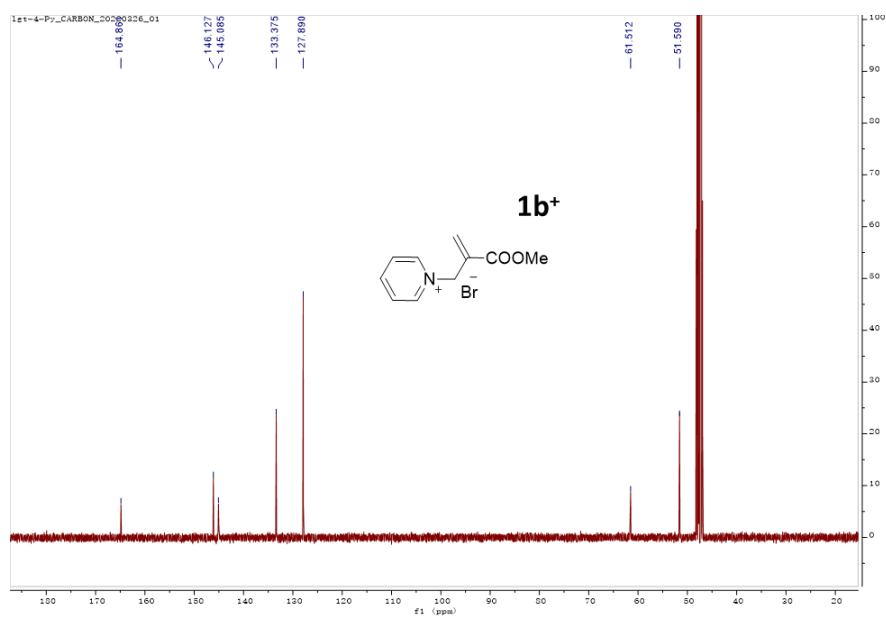
Figure S6.19 ^{13}C-NMR spectrum of guest **1b⁺** in MeOD.
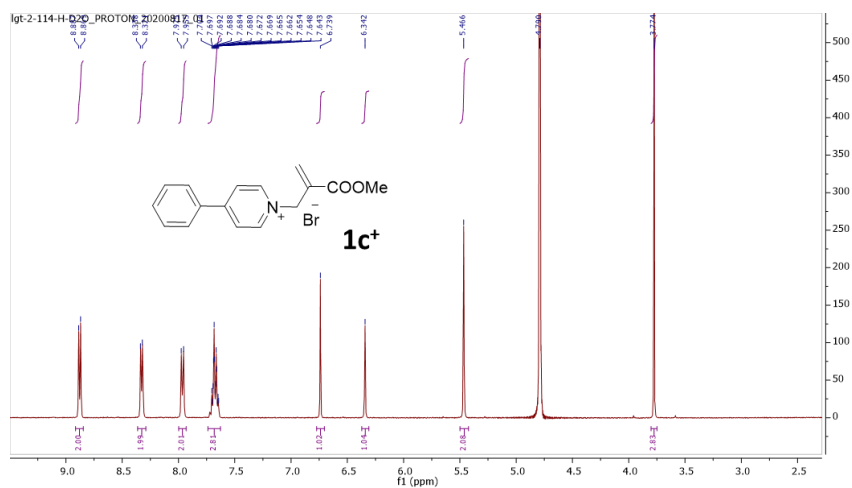
Figure S6.20 ¹H-NMR spectrum of guest **1c⁺** in D₂O.
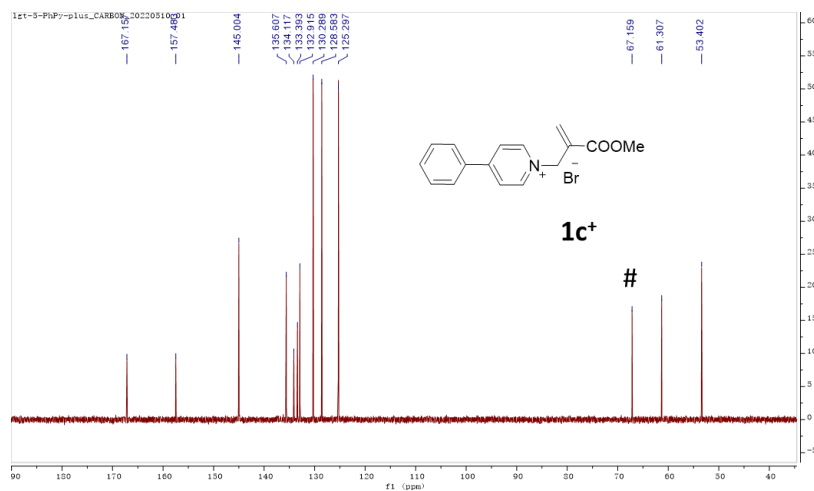
Figure S6.21 ¹³C-NMR spectrum of guest **1c⁺** in D₂O. (1,4-Dioxane as NMR reference standard, marked as #)
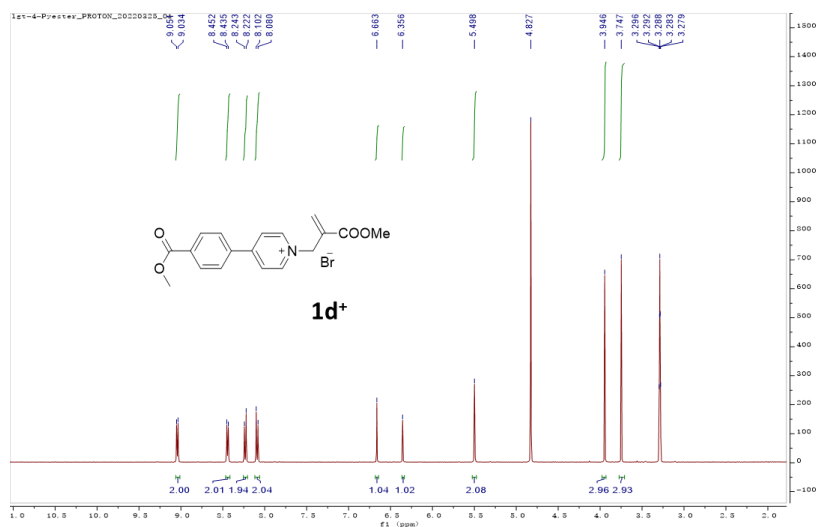
Figure S6.22 ^{1}H-NMR spectrum of guest **1d$^+$** in MeOD.
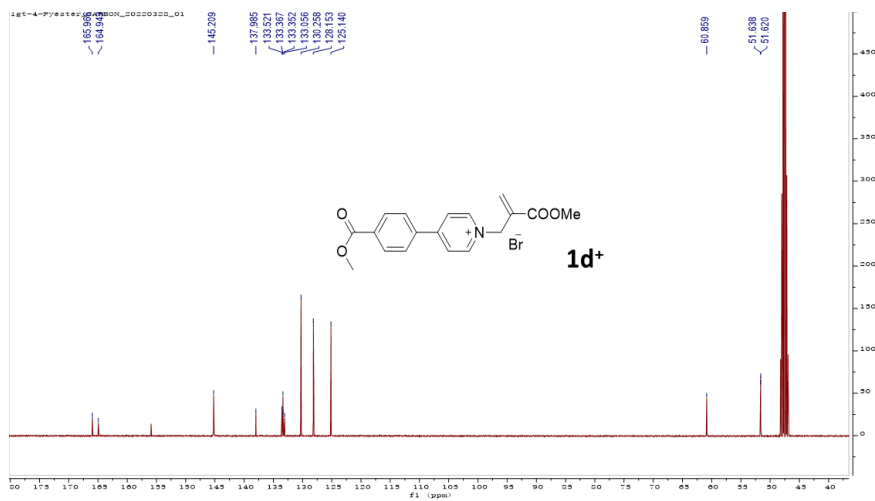
Figure S6.23 ^{1}H-NMR spectrum of guest **1d$^+$** in MeOD.
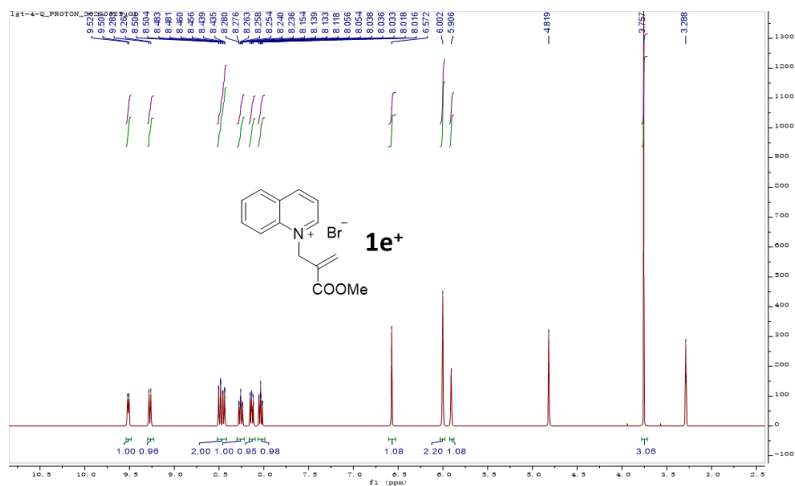
Figure S6.24 ^{1}H-NMR spectrum of guest **1e⁺** in MeOD.
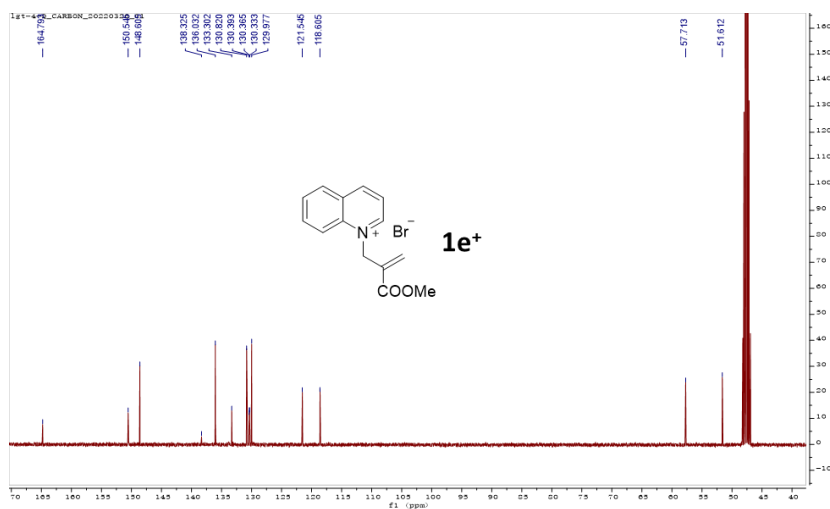
Figure S6.25 ^{1}H-NMR spectrum of guest **1e⁺** in MeOD.
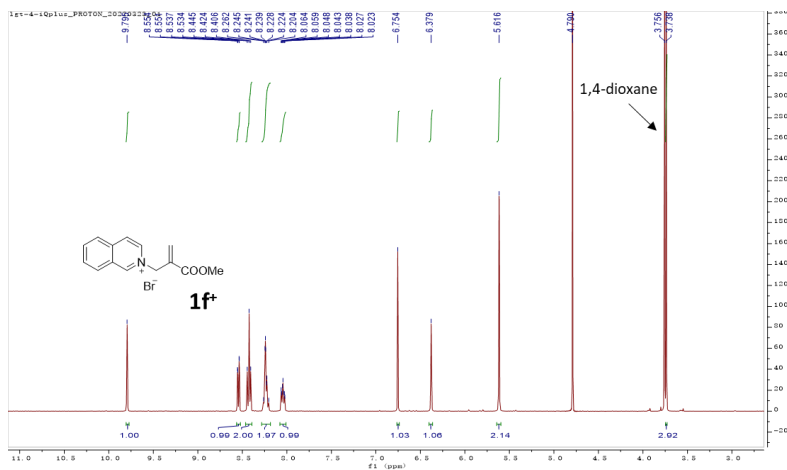
Figure S6.26 ^{1}H-NMR spectrum of guest **1f⁺** in D$_2$O.
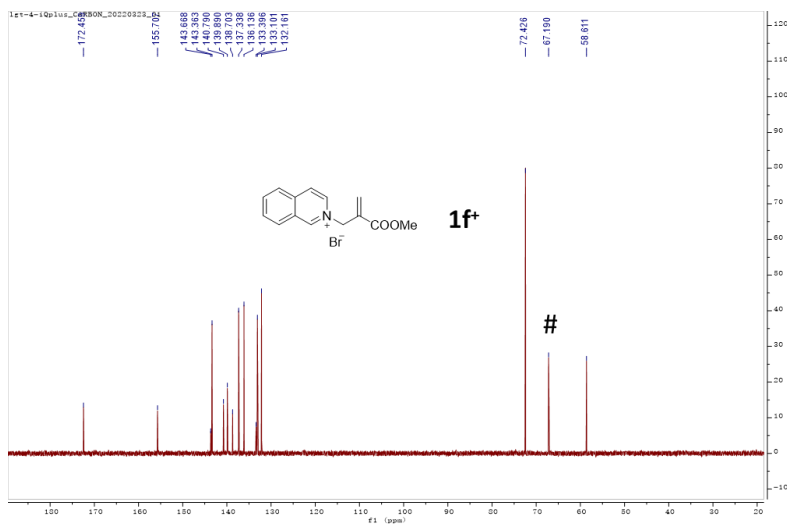
Figure S6.27 ^{1}H-NMR spectrum of guest **1f⁺** in D$_2$O.

6.5.10 Reference

1. Li, G., Wan, Y., Lewis, R. W., Fan, B. & Eelkema, R. Signal-specific triggering of supramolecular aggregate formation. unpublished work.

Summary

Nature has proven to be a great source of inspiration for scientific research and technological innovation in various areas: food, medicine, architecture, chemistry, materials, algorithms, and many other fields. At the basis of sophisticated functions associated with life in nature are all kinds of chemical reactions which are mainly regulated by enzymes through molecular recognition of the substrates. Meanwhile, chemical signals are able to tune the catalytic activities of enzymes through noncovalent bonding or structural modification. Concomitantly, the formation of transient structures that are used temporarily, for instance the mitotic spindle, requires the conversion of energy, mainly in the form of high-energy chemical fuels. All of these phenomena combined endow living systems with high responsivity to various stimuli. Inspired by nature, regulating artificial catalysts in chemical reactions by noncovalent bonding, and controlling formation/deformation of supramolecular materials by chemical reactions are attracting researchers' attention. This thesis integrates chemical reaction networks with host-guest complexation, aiming to bring about some of these advanced properties.

In **chapter 2**, we present a literature overview of out-of-equilibrium assembly systems based on host-guest interactions. We discuss general strategies and recent examples categorized with regards to which component is modulated in the process: hosts, guests and competitive molecules. An outlook is provided on future challenges and research directions.

In **chapter 3**, we show that host-guest encapsulation is a powerful and generic tool to control and tune catalytic activity of organocatalysts. By CB[7] binding, catalytic activities of four catalysts are inhibited in the reactions of hydrazone formation, allylic substitution, aldol reaction and oligomerization of maleimide while for one catalyst the rate of hydrazone formation is enhanced. In most of the cases, addition of a stronger binding signal molecule restores catalytic activity back to the original value. Moreover, these regulation events can be performed *in situ*, leading to an immediate response. In addition, for the reaction of hydrazone, we developed a kinetic model to predict the reaction rate catalysed by aniline or benzimidazole, and regulated by CB[7]. Taken together, we demonstrate that host-guest complexation could be readily applied for signal-responsive control of organocatalyst activity, which is a step forward in the development of man-made chemical reaction networks and cascades capable of responding to chemical changes in the environment.

In **chapter 4**, a chemical reaction network that can control homoternary host-guest complexation driven by chemical fuels was developed. This design was based on the reversible generation of cationic 4-phenylpyridinium, typically forming a 2:1 complex

with CB[8]. We have also developed 2-arm and 4-arm guests with the aim of making out-of-equilibrium supramolecular polymers and networks using this chemistry. Unfortunately, combining these multitopic guests with the reaction network and CB[8] complexation did not work due to precipitation of CB[8] in the presence of the chemical fuel. Still, the results and concept are insightful for a future design and may be applied to control temporary CB[8] solubilisation.

In **chapter 5**, we developed an artificial supramolecular aggregation process that responds to chemical signals. Reacting to a range of biologically relevant nucleophiles such as thiols and amines, positive charges on the bipyridine guest can be regulated, causing the switch of its complex with CB[8] from binary to ternary. Using tripodal bipyridine derivatives we could demonstrate signal induced supramolecular aggregate formation of CB[8]-crosslinked networks. During this process, the rate of aggregation as well as aggregate structure can be controlled with nucleophile strength. Moreover, mimicking the signalling transduction cascades in cellular events, we expanded this concept to weak nucleophiles by developing a signal transducer strategy, enabling supramolecular aggregation triggered by weakly nucleophilic hydrogen peroxide.

Continuing the concept of signal induced host-guest complex switch, in **chapter 6**, we explored a new approach of drugs releasing from direct macrocyclic encapsulation. In this work, upon reaction with nucleophilic signals, positive charges on electron-deficient first guest molecule can be removed, leading to the disassembly of a heteroternary complex with CB[8]. Consequently, the electron-rich second guest molecules are released. While in most of the previous research of heteroternary complex with CB[8], 4,4'-dipyridinium usually acted as the electron-deficient first guest molecule, isoquinolium is found a good alternative to induce electron-rich second guest molecule encapsulation by CB[8]. Furthermore, a wide range of electron-rich molecules have been demonstrated to be applicable for this system: derivatives of naphthalene, indole, benzofuran, benzothiophene, benzothiazole, and benzoimidazole, including FDA approved drugs and anti-cancer natural products. This offers a new route to integrate stimuli-responsive drug release from direct host-guest encapsulation.

In conclusion, our works performed in this thesis show that the combination of chemical reaction networks, chemical signalling and host-guest complexation can be used to design artificial systems with controllable and stimuli-responsive properties, and promising application in catalysis, drug delivery, and molecular sensing. We believe that the contents of this thesis would provide insights of value to future research and design of life-like systems.

Samenvatting

De natuur is een belangrijke inspiratiebron gebleken voor wetenschappelijk onderzoek en technologische innovatie op verschillende gebieden: voeding, medicijnen, architectuur, chemie, materialen, algoritmen en nog vele meer. Aan de basis van de complexe functies die samenhangen met het leven in de natuur, zijn verschillende chemische reacties die voornamelijk worden gereguleerd door enzymen via middel van moleculaire herkenning van substraten. Ondertussen kunnen de chemische signalen zijn in staat om de katalytische activiteiten van enzymen af te stemmen door middel van niet-covalente binding of structurele modificatie. Het tijdelijk vormen van kortstondige structuren (bijvoorbeeld de spoelfiguren bij mitose) maken gebruik van de conversie van energie, voornamelijk in de vorm van hoogenergetische chemische brandstoffen. Al deze combineerde fenomenen geven levende systemen met een hoge responsiviteit op verschillende stimuli. Geïnspireerd door de natuur, het reguleren van kunstmatige katalysatoren in chemische reacties door niet-covalente binding en het beheersen van de vorming/vervorming van supramoleculaire materialen door chemische reacties trekken de aandacht van onderzoekers. Dit proefschrift integreert chemische reactienetwerken met *host-guest* complexatie, met als doel enkele van deze geavanceerde eigenschappen tot stand te brengen.

In hoofdstuk 2 presenteren we een literatuuroverzicht van assemblagesystemen die niet in evenwicht zijn op basis van host-guest interacties. We discussiëren algemene strategieën en recente voorbeelden gecategoriseerd met betrekking tot welke component in het proces wordt gemoduleerd: host, guest en concurrerende moleculen. Er wordt een vooruitblik gegeven op toekomstige uitdagingen en onderzoeksrichtingen.

In hoofdstuk 3 laten we zien dat *host-guest* inkapseling een krachtig en generiek hulpmiddel is om de katalytische activiteit van organocatalysts te controleren en te inregelen. Door CB[7]-binding worden de katalytische activiteiten van vier katalysatoren afgeremd in de reacties van hydrazonvorming, allylische substitutie, aldolreactie en oligomerisatie van maleïmide, terwijl voor één katalysator de snelheid van hydrazonvorming wordt verhoogd. In de meeste gevallen herstelt een toevoeging van sterker bindend signaal molecuul de katalytische activiteit terug naar de oorspronkelijke waarde. Bovendien kan het regelen van deze gebeurtenissen in situ uitgevoerd worden, wat leidt tot een onmiddellijke respons. Als toevoeging is voor de reactie van hydrazone een kinetisch model ontwikkeld om de reactiesnelheid te voorspellen die wordt gekatalyseerd door aniline of benzimidazole en gereguleerd door CB[7]. Alles gecombineerd demonstreert dat *host-guest* -complexering gemakkelijk kan worden toegepast voor signaal responsieve controle van organokatalysator activiteit, wat een stap voorwaarts is in de ontwikkeling van door de niet-biobased chemische reactienetwerken en cascades die in staat zijn om te reageren op chemische veranderingen in de omgeving.

In hoofdstuk 4 laten we zien dat er een chemisch reactienetwerk is ontwikkeld dat homoternaire *host-guest* complexatie aangedreven door chemische brandstoffen kan regelen. Dit constructie was gebaseerd op de reversibele vorming van kationisch 4-

fenylpyridinium, dat typisch een 2:1 complex vormt met CB[8]. We hebben ook 2-armige en 4-armige gasten ontwikkeld met als doel het maken van supramoleculaire polymeren en netwerken die niet in evenwicht zijn met behulp van deze chemie. Helaas werkte het combineren van deze multitopische *hosts* met het reactienetwerk en CB[8]-complexatie niet vanwege op precipitatie van CB[8] in aanwezigheid van de chemische brandstof. Toch zijn de resultaten en het concept inzichtelijk voor een toekomstig ontwerp en kunnen ze worden toegepast om tijdelijke CB[8] oplosbaarheid te controleren.

In hoofdstuk 5 hebben we een kunstmatige supramoleculaire aggregatieproces ontwikkeld dat reageert op chemische signalen. Door te reageren op een reeks biologisch relevante nucleofielen zoals thiolen en aminen, kunnen positieve ladingen op de bipyridine-*host* worden gereguleerd, waardoor het complex met CB[8] van binair naar ternair wordt omgeschakeld. Met behulp van tripodale bipyridine derivaten konden we signaal geïnduceerde supramoleculaire aggregaat vorming van CB[8]-verknoopte netwerken aantonen. Tijdens dit proces kunnen de aggregatiesnelheid en de aggregatiestructuur worden gecontroleerd met nucleofiele sterkte. Bovendien hebben we, door de signaaltransductiecascades in cellulaire gebeurtenissen na te bootsen, dit concept uitgebreid naar zwakke nucleofielen door een signaaltransducerstrategie te ontwikkelen, waardoor supramoleculaire aggregatie mogelijk wordt gemaakt door zwak nucleofiel waterstofperoxide.

Voortbordurend op het concept van signaal-geïnduceerde *host-guest* complex switching, hebben we in Hoofdstuk 6 een nieuwe benadering onderzocht van geneesmiddelafgifte door directe macro-cyclische inkapseling. In dit werk kunnen, na reacties met een nucleofiel signaal, de positieve lading op het elektron-deficiënte eerste-gastmolecuul verwijderd worden, wat leidt tot de dissociatie van het heteroternaire complex met CB[8]. Hierdoor komen de elektronrijke tweede gastmoleculen vrij. Terwijl in het grootste deel van het eerdere onderzoek naar heteroternair complex met CB[8], 4,4'-dipyridinium meestal fungeerde als het elektron-deficiënte eerste-gastmolecuul, wordt isoquinolium een goed alternatief gevonden om elektronrijke tweede-gastmolecuul inkapseling door CB[8] te induceren[8]. Bovendien is voor dit systeem een breed scala aan elektronenrijke molecuulen aangetoond: derivaten van naftaleen, indol, benzofuran, benzothiofeen, benzothiazol en benzimidazol, waaronder door de FDA goedgekeurde geneesmiddelen en natuurlijke producten tegen kanker. Dit biedt een nieuwe route om stimulus-responsieve medicijnafgifte te integreren uit directe inkapseling van gastheer en gast.

In conclusie, onze werken in dit proefschrift laten zien dat de combinatie van chemische reactienetwerken, chemische signalering en *host-guest* complexatie kan worden gebruikt om kunstmatige systemen te ontwerpen met controleerbare en stimuli-responsieve eigenschappen, en veelbelovende toepassing in katalyse, medicijnafgifte en moleculaire detectie. Wij geloven dat de inhoud van dit proefschrift inzichten van grote waarde zou bieden voor toekomstig onderzoek en ontwerp van levensechte systemen.

Acknowledgement

When I decided to start my PhD journey abroad, I thought I've understood the challenge to be faced, but now I know how difficult it is. Luckily, I am in the Netherland, a marvellous experience in my life of studying and working here. And more luckily, with you:

First of all, I am grateful for my promotor and supervisor, **Rienk**. Without you, I don't think I can make it graduation of PhD smoothly. You have not only guided me the right direction of research but also helped in the details of experiments, giving me freedom to try my proposed ideas and correcting me patiently when something wrong. I am used to speak to many people for the same: you are the supervisor that I hope to become in future. Hope to have opportunities to cooperate with you afterward. **Jan**, thanks for being my co-promotor and for your insightful questions in group meeting and my yearly meeting. For the collaborator in Cambridge university, **Oren** and **Zehuang**, thanks for sending me the CB materials and for the useful discussion in the meeting. **Stephen Picken, Wolter, Eduardo, Ger, Laura** thanks for sharing experience and suggestion in ASM group meeting.

Next, I would like to thank the colleagues in ASM group. **Bowen**, you are my deskmate and fumehoodmate for years, and helped me a lot when I started in Delft. We discussed everything about life, experiments, future and more. Thank you and good luck of your postdoc in US. **Benj**, you introduced me in the lab when I came for the interview. Your hard working is impressive and it is always us two in the lab and office. **Tobias**, it is great to talk with you about CB project and more research experience. Thanks for nice BBQ from you. **Irene**, we talked a lot about lab works, graduation pressure, family, Italy and China. Thanks for your listening and sharing. **Reece**, your polymer knowledge is very helpful, and thanks for your help in the master project and measurement in GPC, DLS and TEM. **Suellen**, you are my last year deskmate, thanks for sharing food whenever I need. **Michelle**, we cooperated in Angew and JACS paper. It is great to work with you. Hope you can get your favourite job soon. **Sarah**, thanks for helping in the microscope and for your organizing in the lab dinners. **Benni**, thanks for discussing about the research and experimental details in the project. **Qian**, **Meng**, **Yiming**, **Kai**, **Yongjun**, **Fan** you all helped me a lot when I just started. Your experience and advice shared in life and research is inspiring. It was a good time chatting with you together in the dinner and party. **Qian** and **Meng**, thanks for recommendation of job in Qingdao. **Elmira**, you are my one year officemate. You are a understandable person, and it is a lot of fun talking with you. **Susan** and **Fanny**, you left shortly after my joining, but I always feel warm taking with you. **Huanhuan** and **Juncheng**, thanks for helping me measure my proposed molecules in radiation. We believe we can find something useful. **Yu**, **Nancy**, **Bohang**, **Ying**, thanks for chatting and sharing. **Hendrik**, it is always nice talking with you about

To my friends in China, **Jiahua**, **Yu (Wang)**, **Naibing**, **He**, **Yanjie**, **Qingqing**, **Liuqing** and **Yuying** thanks for the kind accommodation and treatment in the limited occasions back in China, and for the talking, sharing although thousands of miles away.

To my family, **A-Ni** and **Jing**, thanks for your supporting of my PhD and for taking care of father and mother during I am abroad. To mother, sorry for so long time not home. I am coming back soon.

In the end, to my father: I am heartly sorry for not being accompanied in your last stage, which is my life-long pity. I hope you can find your peace and get your memory back in this permanent sleeping.

About the author

Guotai Li was born on 7th December 1988 in Qingdao City, Shandong Province, China. After completing his bachelor degree in Hefei University of Technology (2012), he continued his master study in East China University of Science and Technology, and jointly studied in Shanghai Institute of Organic Chemistry, majoring in Organic Synthesis. After his graduation in 2015, he went to work as an editor for an academic journal *Molecules* for two years. From 2017, he started pursuing his PhD supported by CSC, first in Maastricht University on biobased polymers supervised by Dr. Katrien Bernaerts and Prof. Dr. Stefaan De Wildeman, then to Delft University of Technology in ASM group under the supervision of Dr. Rienk Eelkema from 2018. His works in Tudelft on responsive host-guest complexation regulated by chemical reaction networks are summarized in this thesis as you are reading now.

List of publication

1. **Guotai Li**[#], Fanny Trausel[#], Michelle P. van der Helm, Benjamin Klemm, Tobias G. Brevé, Susan A. P. van Rossum, Muhamad Hartono, Harm H. P. J. Gerlings, Matija Lovrak, Jan H. van Esch, Rienk Eelkema*. Tuneable Control of Organocatalytic Activity through Host–Guest Chemistry, *Angew. Chem. Int. Ed.* 2021, **60**, 14022–14029. (Shared first authors)
2. **Guotai Li**, Kui Yu, Jurrie Noordijk, Monique H. M. Meeusen-Wierts, Bert Gebben, Petra A. M. oude Lohuis, Anton H. M. Schotman, Katrien V. Bernaerts*. Hydrothermal polymerization towards fully biobased polyazomethines *Chem. Commun*. 2020, **56**, 9194–9197.
3. **Guo-Tai Li**, Zhi-Ke Li, Qing Gu and Shu-Li You*, Asymmetric Synthesis of 4-Aryl-3,4-dihydrocoumarins by *N*-Heterocyclic Carbene Catalyzed Annulation of Phenols with Enals. *Org. Lett.* 2017, **19**, 1318–1321.
4. **Guo-Tai Li**, Qing Gu and Shu-Li You*, Enantioselective Annulation of Enals with 2-Naphthols by Tiazolium Slts Drived from L-Penylalanine, *Chem. Sci*. 2015, **6**, 4273–4278.
5. Michelle P. van der Helm[#], **Guotai Li**[#], Muhamad Hartono and Rienk Eelkema*,Transient host-guest complexation to control catalytic activity. *J. Am. Chem. Soc.* 2022, **21**, 9465–9471. (Shared first authors)
6. Bowen Fan, Yongjun Men, Susan A. P. van Rossum, **Guotai Li**, Rienk Eelkema*. A Fuel-Driven Chemical Reaction Network Based on Conjugate Addition and Elimination Chemistry. *ChemSystemsChem*. 2020, **2**, e1900028.
7. Ke-Yin Ye, Ke-Jia Wu, **Guo-Tai Li**, Li-Xin Dai*, Shu-Li You*, Synthesis of Enantioenriched Indolopiperazinones via Iridium(I) *N*-Heterocyclic Carbene Complex Catalyzed Asymmetric Intramolecular Allylic Amination Reaction. *Hetereocycles* 2017, **95**, 304–313.
8. **Patent**: 《Method for Preparations of 3,4-Dihydroisoquinoline Involved Chiral Triazolium Salts and Their Applications》, NO.: CN104558014A